



HAL
open science

Modélisation de l'architecture 4D du blé: identification des patterns dans la morphologie, la sénescence et le positionnement spatial des organes dans une large gamme de situations de croissance

Mariem Abichou

► To cite this version:

Mariem Abichou. Modélisation de l'architecture 4D du blé: identification des patterns dans la morphologie, la sénescence et le positionnement spatial des organes dans une large gamme de situations de croissance. Agronomie. Université Paris Saclay (COMUE), 2016. Français. NNT : 2016SACLA022 . tel-02316154

HAL Id: tel-02316154

<https://theses.hal.science/tel-02316154>

Submitted on 15 Oct 2019

HAL is a multi-disciplinary open access archive for the deposit and dissemination of scientific research documents, whether they are published or not. The documents may come from teaching and research institutions in France or abroad, or from public or private research centers.

L'archive ouverte pluridisciplinaire **HAL**, est destinée au dépôt et à la diffusion de documents scientifiques de niveau recherche, publiés ou non, émanant des établissements d'enseignement et de recherche français ou étrangers, des laboratoires publics ou privés.

NNT : 2016SACLA022

THESE DE DOCTORAT
DE
L'UNIVERSITE PARIS-SACLAY
PREPAREE A
AGROPARISTECH
(L'institut des sciences et industries du vivant et de l'environnement)

ECOLE DOCTORALE N° 581
Agriculture, alimentation, biologie, environnement et santé (ABIES)
Spécialité de doctorat « Sciences agronomiques »

Par

Mme Mariem ABICHOU

Modélisation de l'architecture 4D du blé : identification des patterns dans la morphologie, la sénescence et le positionnement spatial des organes pour une large gamme de situations de croissance.

Thèse présentée et soutenue à l'AgroParisTech à Paris, le 30 novembre 2016 :

Composition du Jury :

M. Thierry DORE	Professeur, AgroParisTech Paris	Président
M. Pierre MARTRE	Directeur de Recherche, INRA Montpellier	Rapporteur
Mme Evelyne COSTES	Directrice de Recherche, INRA Montpellier	Rapporteur
M. Frédéric BARET	Directeur de Recherche, INRA Avignon	Examineur
M. Philippe GATE	Docteur, Arvalis Institut du végétal, Paris	Examineur
M. Bruno ANDRIEU	Directeur de Recherche, INRA Grignon	Directeur de thèse
M. Benoit DE SOLAN	Ingénieur, Arvalis Institut du végétal, Paris	Invité

AVANT PROPOS

J'ai effectué ma thèse au sein de l'Unité Mixte de Recherche Ecologie fonctionnelle et écotoxicologie des agroécosystèmes (EcoSys) à Thiverval-Grignon (Yvelines, France), qui est affiliée à l'INRA (Institut National de la Recherche Agronomique, France) et à AgroParisTech (Institut des sciences et industries du vivant et de l'environnement).

Ma bourse de thèse de trois ans a été financée par une convention CIFRE (Convention Industrielle de Formation par la Recherche) qui a subventionné ARVALIS-Institut du végétal dans le cadre d'une collaboration de recherche avec l'INRA. Des sources complémentaires de financement ont aussi permis de mener à bien mes travaux (financements: INRA et ARVALIS).



Remerciements

En premier lieu, Je tiens à remercier chaleureusement mon directeur de thèse Bruno Andrieu, qui m'a accompagnée quotidiennement dans la réalisation de ce travail. Je salue sa disponibilité permanente, sa générosité et ses qualités scientifiques, pédagogiques et surtout ses qualités humaines. J'ai beaucoup appris à ses côtés pendant ces huit années ; je ne trouverais pas les mots pour lui exprimer ma reconnaissance et mon grand respect.

Je tiens aussi à remercier Arvalis institut de végétal, qui a financé ce travail, et en particulier Benoit De Solan, David Gouache et Philippe Gate qui ont soutenu ce projet.

Je remercie également l'unité Ecosys de l'INRA qui a veillée au bon déroulement des expérimentations. Je remercie l'équipe technique et particulièrement Marc Bidon et Josiane Jean-jacques qui m'ont beaucoup aidé dans les manipes. Je remercie également Camille Chambon et Christian Fournier qui m'ont aidé dans le développement informatique du modèle.

Je suis heureuse que Thierry Doré soit président du jury, il a suivi mon parcours depuis mon master de l'Agro, et m'a toujours encouragée et soutenue dans mes démarches. Je remercie également Pierre Martre et Evelyne Costes pour avoir accepté d'être les rapporteurs de ce travail. Je remercie aussi Frédéric Baret, qui a suivi ce travail en acceptant de participer au comité de pilotage, puis au jury de thèse. Je remercie aussi Delphine Luquet, Vincent Allard et Ela Franc pour avoir accepté d'être membre de mon comité de pilotage, leurs remarques et critiques m'ont été très utiles.

Je remercie tous les scientifiques de l'INRA avec qui j'ai échangé et j'ai appris beaucoup de choses à leurs côtés. Je remercie particulièrement Corine Robert, Romain Barillot, Sebastien Saint jean, Andrée Tuzet, Michaël Chelle, Alexandra Jullien, Amilie Mathieu, Celine Richard, Tiphaine Vidal, Christophe Lercarpentier, Nicolas Mascher et Christophe Gigot. Je tiens aussi à remercier vivement Marina Pavlides, Christine Collin et Claudine Lauransot de leurs accueils toujours chaleureux.

Je remercie également mes profs de l'AgroParisTech (Paris) ainsi que mes profs de l'INAT (Tunis), grâce à leurs formations j'ai pu disposer des outils nécessaires pour mener à bien ce projet.

Dédicace

Je dédie cette thèse :

à mes chers parents Abdel Karim & Mabrouka

à mes sœurs Ikram, Wafa, Blakis et Sirine

*à mon mari Bourhane et ma petite fille Fatma qui ont
participé indirectement à ce travail*

*à mes oncles Mohamed & Fahri Fiaa et Habib & Mansour
Abichou,*

et à ma chère copine Wided Aloui

*Aucun mot ne pourrait exprimer à leur juste valeur la gratitude et
l'amour que je vous porte. Je vous aime fort.*

LISTE DE MES PUBLICATIONS

Articles soumis à des revues impactées à comité de lecture

1. **Abichou M.**, Dornbusch T, Chambon C, Gouache D, de Solan B, Andrieu B. Parametrizing wheat leaf and tiller dynamics for structural plant models. **Submitted in July 2016** to Annals of Botany.
2. Liu S., Baret F., Andrieu B., **Abichou M.**, Allard D., de Solan B., Burger P. Modeling the spatial distribution of plants on the row for wheat crops: Consequences on the green fraction at the canopy level. **Submitted in October 2016** to Computers and Electronics in Agriculture.
3. Liu S., Baret F., **Abichou M.**, Boudon F., Thomas S., Zhao K., Fournier C., Andrieu B., Kamran I., Hemmerlé M., de Solan B. Estimating wheat Green area index from ground-based LiDAR measurement through 3D ADEL-Wheat model. **Submitted in November 2016** to Agriculture and Forest Meteorology.
4. Lecarpentier C., Barillot R., **Abichou M.**, Goldringer I., Enjalbert J., Andrieu B. A 3D wheat model to study competition for light through the prediction of tillering dynamics. **Submitted in October 2016** to Annals of botany.
5. Garin G., Fournier C., **Abichou M.**, Houllès V., Pradal C., Robert C. A plant-pathogen model to explore the race between wheat growth and *Zymoseptoria tritici* epidemics. **Submitted in September 2016** to Phytopathology.

Articles en préparation pour des revues impactées à comité de lecture

6. **Abichou M.**, Dornbusch T., Chambon C., Gouache D., de Solan B., Andrieu B. Parametrizing final organ dimensions and leaf senescence of winter wheat plants. **In prep: submission expected for 2017** to Annals of Botany.
7. **Abichou M.**, De Solan B., Andrieu B. Responses of winter wheat plants to increased row spacing: developmental, morphological and geometrical changes. **In prep: submission expected for 2017** to Annals of Botany.
8. **Abichou M.**, De Solan B., Andrieu B. Dynamics of inclination angle of leaves and stems of winter wheat crop. **In prep: submission expected for 2017** to Annals of Botany.
9. Liu S., Baret F., Buis S., **Abichou M.**, Andrieu B., Kamran I., de Solan B. Extraction of traits from the assimilation of multi-temporal GF measurements into ADEL-Wheat during the early stages. **In prep: submission expected for 2017** to Environmental Modelling and software journal.
10. **Abichou M.**, Chambon C., Andrieu B. Plantgen-ADELwheat: a simplified method to 4D reconstructions of wheat crop from experimental data. **In prep: submission expected for 2017** to Annals of Botany.

Co-auteur de chapitres de manuscrits de thèses

11. Baccar R., Dornbusch T., **Abichou M.**, Bertheloot J., Gate P., Andrieu B. Phyllochron of winter wheat (*Triticum aestivum L.*) for a range of densities and sowing dates. **Chapter 1** of Rim Baccar thesis entitled « *Plasticité de l'architecture du blé d'hiver module par la densité et la date de semis et son effet sur les épidémies de Septoria tritici* ». Defended in juin 2011, AgroParisTech. France.199 p.
12. La référence numéro 4 citée ci-dessus représente le **Chapitre 3** du manuscrit de thèse de Doctorat du Christophe Lecarpentier. Cette thèse de Doctorat est intitulée « *Plasticité de l'architecture aérienne du blé en réponse à la compétition pour la lumière au sein de cultures pures ou d'associations variétales : Caractérisation expérimentale et développement d'un modèle 3D* ». La thèse sera soutenue en Janvier 2017 à University Paris-Saclay (Paris-Sud), Paris, France.214 p.
13. Les références numéros 2,3 et 9 citées ci-dessus représentent respectivement les **Chapitres 2.2, 3 et 4** du manuscrit de thèse de Doctorat du Shouyang Liu. Cette thèse de Doctorat est intitulée « *Phenotyping wheat by combining ADEL-Wheat 4D structure model with proximal remote sensing measurements along the growth cycle* ». La thèse est soutenue le 08 décembre 2016 à Université d'Avignon et des pays de Vaucluse, Avignon, France. 97 p.

Communications orales dans des manifestations scientifiques internationales avec comité de lecture

14. **Abichou M.**, Solan B.D., Andrieu B., 2016. The dynamics of leaf and axes orientation in wheat. In: FSPMA2016, International Conference on Functional-Structural Plant Growth Modeling, Simulation, Visualization and Applications, IEEE, Qingdao (China), 07-11/11/2016, 1 p. (communication orale avec actes).
15. Fournier C., Danthony A., Perriot B., **Abichou M.**, Poidevin S., Da Costa J., Cotteux E., Andrieu B., Saint-Jean S., Robert C., 2016. Simulation of the effects of leaf bending dynamics on fungicide deposit on individual leaves of wheat using a 3D architectural model. In: FSPMA2016, International Conference on Functional-Structural Plant Growth Modeling, Simulation, Visualization and Applications, IEEE, Qingdao (China), 07-11/11/2016, 1 p. (communication orale avec actes).
16. Robert C., Fournier C., **Abichou M.**, Andrieu B., Bancal M.O., Barriuso E., Bedos C., Benoit P., Bergheaud V., Bidon M., Bonicelli B., Chambon C., Chapuis R., Cotteux E., Da Costa J., Durant B., Gagnaire N., Gaudillat D., Gigot C., Girardin G., Gouache D., Jean Jacques J., Mamy L., Ney B., Paveley N., Perriot B., Poidevin S., Pointet S., Pot V., Pradal C., Richard C., Saint-Jean S., Salse J., Sinfort C., Smith J., Ter Halle A., Van Den Berg E., Walker A.S., 2016. ECHAP : un projet pour identifier les possibilités de réduction de l'utilisation des fongicides en utilisant l'architecture des couverts. In: 45e Congrès du Groupe Français des Pesticides "Devenir et impact des pesticides :

verrous à lever et nouveaux enjeux", GFP, INRA, Versailles (FRA), 27-29/05/2015, 62-63. (communication orale, texte intégral avec actes).

17. Robert C., Fournier C., Bedos C., **Abichou M.**, Andrieu B., Bancal M.O., Barriuso E., Benoit P., Bergheaud V., Bidon M., Bonicelli B., Chambon C., Chapuis R., Cotteux E., Da Costa J., Durant B., Gagnaire N., Gaudillat D., Gigot C., Girardin G., Gouache D., Jean Jacques J., Mamy L., Ney B., Paveley N., Perriot B., Poidevin S., Pointet S., Pot V., Pradal C., Richard C., Saint-Jean S., Salse J., Sinfort C., Smith J., Ter Halle A., Van Den Berg E., Walker A.S., 2016. L'architecture des couverts végétaux : un levier pour réduire l'utilisation des fongicides ? In: 45e Congrès du Groupe Français des Pesticides "Devenir et impact des pesticides : verrous à lever et nouveaux enjeux", GFP, INRA, Versailles (FRA), 27-29/05/2015, 122-127. (communication orale, texte intégral avec actes).
18. **Abichou M.**, Fournier C., Dornbusch T., Chambon C., Baccar R., Bertheloot J., Vidal T., Robert C., Gouache D., Andrieu B., 2013. Re-parametrisation of Adel-wheat allows reducing the experimental effort to simulate the 3D development of winter wheat. In: FSPM 2013 Proceedings, 7th International Conference on Functional-Structural Plant Models, Sievänen, R., Nikinmaa, E., Godin, C., Lintunen, A., Nygren, P. (Eds.), Saariselkä (Finland), 09-14/06/2013, 304-306. (communication orale et écrite. avec actes).
19. 20. Fournier C., Pradal C., **Abichou M.**, Andrieu B., Bancal M.O., Bedos C., Benoit P., Chambon C., Chapuis R., Cotteux E., Mamy L., Paveley N., Pot V., Saint-Jean S., Richard C., Sinfort C., Halle A.T., Berg E.V.D., Walker A.S., Robert C., 2013. An integrated and modular model for simulating and evaluating how canopy architecture can help reduce fungicide applications. In: FSPM 2013 Proceedings, 7th International Conference on Functional-Structural Plant Models, Sievänen, R., Nikinmaa, E., Godin, C., Lintunen, A., Nygren, P. (Eds.), Saariselkä (Finland), 09-14/06/2013, 345-347. (communication orale et écrite. avec actes).
20. Bertheloot J., **Abichou M.**, Fournier C., Andrieu B., 2010. Light-nitrogen relationships within plant canopies analysed using in silico reconstruction of wheat crops. In: Proceedings, 6th International Workshop on Functional-Structural Plant Models, DeJong, T., Da Silva, D. (Eds.), University of California, Davis (USA), 12-17/09/2010, 80-82. (communication orale, avec actes).

Communications affichées (Posters) dans des manifestations scientifiques internationales avec comité de lecture

21. Fournier C., Danthony A., Pointet S., Perriot B., **Abichou M.**, Poidevin S., Da Costa J., Cotteux E., Andrieu B., Saint-Jean S., Robert C., 2016. Modeling and simulating the distribution of fungicide among leaves in wheat. In: FSPMA2016, International Conference on Functional-Structural Plant Growth Modeling, Simulation, Visualization and Applications, IEEE, Qingdao (China), 07-11/11/2016, 1 p. (poster abstract, avec actes).

22. Liu S., Baret F., Boudon F., **Abichou M.**, Fournier C., Andrieu B., Hemmerlé M., Solan B.D., 2016. Estimating canopy characteristics from ground-based LiDAR measurement assisted with 3D Adel-Wheat model. In: FSPMA2016, International Conference on Functional-Structural Plant Growth Modeling, Simulation, Visualization and Applications, IEEE, Qingdao (China), 07-11/11/2016, 1 p. (poster abstract avec actes).
23. **Abichou M.**, Fournier C., Dornbusch T., Chambon C., Gouache D., Solan B.D., Andrieu B., 2015. Parameterizing patterns in wheat architecture to simulate the 3D dynamics of wheat crops. In: IWIW2015: International Wheat Innovation Workshop, Legouis, J. (Ed.), Clermont-Ferrand (FRA), 16-17/11/2015, 1 p. (poster abstract).
24. Robert C., **Abichou M.**, *et al*; 2012. The ECHAP project: Reducing fungicide use by associating optimal treatment strategies and canopies promoting disease escape. In: ECA International Conference "Plant and Canopy Architecture Impact on Disease Epidemiology and Pest Development", INRA/Réseau EpiArch - ANR - SFP, Rennes (FRA), 01-05/07/2012, 1 p. (poster, abstract).
25. **Abichou M.**, Bertheloot J., Dornbusch T., Baccar R., Andrieu B., 2010. A simplified measurement to obtain data for the architectural plant model ADEL Wheat to simulate the development of winter wheat in 3D. In: Proceedings of Agro2010, XIth ESA Congress, European Society of Agronomy, Wery, J., Shili-Touzi, I., Perrin, A. (Eds.), Agropolis International Editions, Montpellier (FRA), Montpellier (FRA), 29/08-03/09/2010, 87-88. (poster abstract).
26. Dornbusch T., Baccar R., **Abichou M.**, Fournier C., Andrieu B., 2010. Plasticity of wheat architecture in response to sowing date and plant population density described with the 3D plant model ADEL wheat. In: Proceedings of Agro2010, XIth ESA Congress, European Society of Agronomy, Wery, J., Shili-Touzi, I., Perrin, A. (Eds.), Montpellier (FRA), 29/08-03/09/2010, 465-466. (poster, abstract).
27. Baccar R., Abichou M., Dornbusch T., Gate P. Andrieu B., 2009. Factors affecting leaf emergence rate in winter wheat (*Triticum aestivum*). Poster. In: Society of Experimental Biology Conference, 1 p. (poster, abstract).

Communications orales dans des manifestations scientifiques sans comité de lecture

28. **Abichou M.**, 2014. Spatial foraging of wheat plants: characterization, representation in 3D explicit plant models and implications. Journée école doctorale Abies, Février 2014, Paris, France. (poster)
29. **Abichou M.**, Dornbusch T., Baccar R., Andrieu B., 2012. Simulation 3D de peuplements de blé: finalisation d'une méthode optimisée. Atelier proximité-détection, Avril 2012, Montpellier, France. (communication orale)

Contribution de la recherche au développement : Rapports scientifiques

30. Andrieu B., **Abichou M.**, 2012. Développement d'une application de simulation in silico de peuplements de blé obtenus lors d'expérimentations au champ. **Rapport de fin de contrat Archiblé**, Arvalis-Institut du végétale. France. 35 p.
31. Robert C., **Abichou M.**, Andrieu B., Bancal M.O., Barriuso E., Bedos C., Benoit P., Bergheaud V., Bidon M., Bonicelli B., Chambon C., Cotteux E., Da C., J., Durand B., Fournier C., Gagnaire N., Gaudillat D., Gigot C., Girardin G., Gouache D., Jean-Jacques J., Mamy L., Ney B., Paveley N., Perriot B., Poidevin S., Pot V., Pradal C., Richard C., Saint-Jean S., Salse J., Sinfort C., Smith J., Ter Halle A., Van den Berg E., Walker A.S., 2012. Réduire l'utilisation des fongicides en associant stratégies de traitement optimales et couverts échappants aux maladies (acronyme : ECHAP). Programme Evaluation et réduction des risques liés à l'utilisation des Pesticides - APR 2010 « Changer les pratiques agricoles pour préserver les services écosystémiques », **Rapport intermédiaire** - Juillet 2012, 20 p.

Participation à l'encadrement des étudiants en stage

32. Vidal T., 2013. Simulations 3D de peuplements de blé: évaluation des modèles et propositions d'améliorations. Mémoire de *fin d'étude d'ingénieur*, Ecole Supérieure d'Agriculture d'Angers, France, UMR INRA AgroParisTech Environnement et Grandes Cultures de Grignon, soutenu le 7 janvier 2013, 121 p. Encadrants : Bruno Andrieu et **Mariem Abichou** (UMR EGC Grignon).
33. Renard J., 2013. Caractérisation de l'architecture des couverts de blé. Rapport de stage de *DUT*, Institut Universitaire de Technologie d'Evreux, France, UMR INRA AgroParisTech Environnement et Grandes Cultures de Grignon, soutenu le 21 juin 2013, 43 p.. Encadrante: **Mariem Abichou** (UMR EGC Grignon).
34. Medi T., 2011. Modélisation de l'architecture du blé tendre d'hiver. Rapport de *Licence 2*, spécialité Agronomie, Institut Universitaire de Technologie de Brest, France, UMR INRA AgroParisTech Environnement et Grandes Cultures de Grignon, soutenu le 29 juin 2011, 27 p.. Encadrante: **Mariem Abichou** (UMR EGC Grignon).

Mémoires de fin d'études (master2, ingénieur)

35. **Abichou M.**, 2009. Facteurs affectant le rythme d'apparition foliaire chez le blé d'hiver. Mémoire de *Master 2*, spécialité Agronomie, AgroParisTech, France, UMR INRA AgroParistech Environnement et Grandes Cultures de Grignon, 47 p. Encadrant: Bruno Andrieu (INRA, Grignon).
36. **Abichou M.**, 2008. Etude des risques de la dissémination volontaire de pomme de terre transgénique et élaboration d'un premier modèle de notification pour des essais aux champs. Rapport de *fin d'étude ingénieur*, spécialité production végétale (Option : Biotechnologie et industrie de semences). Institut National Agronomique de Tunisie (INAT). Tunisie. 123 p. Encadrant: Youssef Trifa (INAT, Tunis) & Hazar Belli (MEDD, Tunis).

Table des matières

INTRODUCTION GENERALE.....	1
1. Contexte	3
1.1. Agronomie et modélisation.....	3
1.2. Diversité des modèles, une diversité de questions.....	4
1.3. Les modèles architecturaux: Définition FSPM et SPM.....	6
1.4. Les modèles SPM: quelles applications?	7
1.5. ADELwheat : exemple de modèle SPM pour blé.....	9
2. Objectifs et démarche de la thèse	10
3. Structuration du mémoire.....	11
4. Références bibliographiques	12
CHAPTER 1: Parametrizing wheat leaf and tiller dynamics for structural plant models	15
RESUME	17
ABSTRACT	18
1. INTRODUCTION.....	19
1.1. Phyllochron and Haun stage progress	19
1.2. Final leaf number	20
1.3. Tillering	20
1.4. Objectives	21
2. MATERIALS AND METHODS.....	21
2.1. Experiments	21
2.2. Data analysis	24
2.3. Parameterisation of Haun stage progress.....	26
2.4. Parameterisation of final leaf number on tillers	28
2.5. Parameterisation of dynamics of active tiller population: appearance and mortality.....	28
3. RESULTS.....	29
3.1. Linear or bilinear Haun stage behaviour for fertile axes	29
3.2. Tillers emerged at stable value of main stem Haun stage but their phyllochron did not necessarily equal that of the main stem.....	32
3.3. Final leaf number of tiller highly correlated to that of the main stem	34
3.4. Secondary and higher order tillers emerged at a lower frequency than primary tillers of the same cohort	34
3.5. The start and the end of tiller mortality phase are correlated to plant ontogeny	36
3.6. A stable pattern for tiller mortality phase	36
4. DISCUSSION	36
4.1. Haun stage progress.....	38
4.2. Final leaf number	38
4.3. Tillering	39
5. LITERATURE CITED	41
6. APPENDIX.....	44
7. SUPPLEMENTARY DATA.....	46
CHAPTER 2: Parametrizing final organ dimensions and leaf senescence of winter wheat plants	51
RESUME	53
ABSTRACT	54
1. INTRODUCTION.....	55
1.1. Pattern of final dimension of phytomers	55
1.2. Dynamic of leaf senescence.....	57
1.3. Objectives	57
2. MATERIALS AND METHODS	57
2.1. Experiments and measurements	58
2.2. Sub-model of the final dimensions of phytomers	60

2.3.	<i>Sub-model of the green leaf number</i>	64
2.4.	<i>Models adjustment</i>	66
3.	RESULTS.....	66
3.1.	<i>High variability of phytomers dimensions among different conditions</i>	66
3.2.	<i>The dimensions of tiller phytomers: calibration and evaluation of the submodels</i>	68
3.3.	<i>Change of the dynamics of the green leaf number depending on the ontogeny</i>	73
4.	DISCUSSION.....	77
5.	LITERATURE CITED.....	79
6.	APPENDIX.....	81
7.	SUPPLIMENTARY DATA.....	82
CHAPTER 3: Responses of winter wheat plants to increased row spacing: developmental, morphological and geometrical changes		89
	RESUME	91
	ABSTRACT.....	92
1.	INTRODUCTION.....	93
2.	MATERIALS AND METHODS.....	94
2.1.	<i>Experimental design and treatments</i>	94
2.2.	<i>Measurements at crop level</i>	95
2.3.	<i>Measurements at plant level</i>	95
3.	RESULTS.....	99
3.1.	<i>Tillering and yield</i>	99
3.2.	<i>Ground cover and PAI_g</i>	99
3.3.	<i>Dimension of mature organs of plants</i>	102
3.4.	<i>Geometry of plants</i>	102
4.	DISCUSSION.....	108
5.	Literature cited.....	111
6.	Supplementary data.....	113
CHAPTER 4: Dynamics of the inclination angle of leaves and stems of winter wheat crop		115
	RESUME	117
	ABSTRACT.....	118
1.	INTRODUCTION.....	119
2.	MATERIALS AND METHODS.....	119
2.1.	<i>Experimental design and treatments</i>	119
2.2.	<i>Measurements</i>	120
3.	RESULTS AND DISCUSSION.....	122
3.1.	<i>Dynamic of the inclination angle of stems: similarity of patterns between axes triggered by ontogenic factors</i>	122
3.2.	<i>Dynamic of the inclination angle of leaves: similarity of patterns among leaf ranks</i>	124
4.	CONCLUSION.....	124
5.	Literature cited.....	128
6.	Appendix.....	129
DISCUSSION GENERALE		131
1.	<i>Rappel du contexte et objectifs</i>	133
2.	<i>Axes de travail</i>	134
3.	<i>Synthèse des principaux résultats</i>	135
4.	<i>Conclusion</i>	143
5.	<i>Références bibliographiques</i>	145
ANNEXES		149
1.	<i>Plantgen-ADELwheat : Application permettant la reconstruction à partir d'un protocole de mesure à effort expérimental réduit</i>	151
2.	<i>Documentation « Plantgen-ADELwheat »</i>	162



INTRODUCTION GENERALE

1. Contexte

1.1. Agronomie et modélisation

L'agronomie d'aujourd'hui est confrontée à un défi double qui vise à assurer une production à la fois **compétitive** et **respectueuse de l'environnement** (Papy et Benoît, 1998). L'**agroécologie** est devenue un élément des politiques publiques qui visent à réduire l'utilisation des produits phytosanitaires et préserver les écosystèmes. Elle est définie par Miguel Altieri (1995) comme « *la science de la gestion des ressources naturelles qui porte sur l'accumulation de connaissances sur les fonctionnements des écosystèmes et conduit à la conception, à la création et à l'adaptation sous la forme participative de systèmes de culture complexes productifs et par suite attractifs malgré un milieu défavorable et malgré un recours très faible aux intrants* ». Une des voies pour faire progresser l'agroécologie, c'est d'accroître notre compréhension du fonctionnement des plantes et de leurs interactions avec leur environnement biotique et d'accroître notre capacité à caractériser les systèmes cultivés. Face à la multiplicité des scénarios possibles et à la vitesse de sélection, une des questions qui se pose serait d'avoir des connaissances sur des scénarios sans les essayer expérimentalement. Dans ce contexte, de nombreux efforts de recherche ont été entrepris dans le **développement des modèles** visant à représenter le fonctionnement des systèmes cultivés en interaction avec leur milieu biotique et abiotique. La modélisation est un moyen pour **acquérir des connaissances** en formalisant des idées et des hypothèses scientifiques qu'on évalue en comparant les prédictions des modèles à des données expérimentales. La modélisation ouvre aussi la possibilité d'explorer par simulation des situations nouvelles, et par exemple d'étudier les conséquences de scénarios qui ne pourraient pas être évalués de façon exhaustive par l'expérimentation. Elle peut ainsi fournir des **méthodes et des outils** pour les professionnels afin de mieux gérer les cultures et mieux prédire les risques pour la production et l'environnement.

D'autre part, l'agriculture est touchée par la révolution numérique. On parle aujourd'hui d'une « **agriculture numérique** ». Elle a été définie par Bellon-Maurel et Huyghe (2016) comme étant : « *une agriculture qui utilise les technologies de l'information et de la communication: technologies d'acquisition de données (satellites, capteurs, Lidar, objets connectés, smartphones...), de transfert et de stockage et technologies de traitement embarquées ou déportées (supers calculateurs accessibles par des réseaux de communication très haut débit)* ». Ces technologies peuvent être mises en œuvre à toutes les échelles de la production agricole et de son écosystème, que ce soit au niveau de l'exploitation (optimisation des opérations culturales, de la conduite de troupeau...), dans les services d'accompagnement (nouveaux services de conseil agricole basés sur des données collectées automatiquement), ou à des échelles plus grandes comme dans un territoire (gestion de l'eau) (Bellon-Maurel et Huyghe, 2016). Ces technologies fournissent une masse importante de données qui ne sont que partiellement valorisées actuellement. Les projets visant à développer l'« agriculture numérique » se multiplient.

1.2. Diversité des modèles, une diversité de questions

Un modèle a été défini comme étant « *une représentation mathématique, graphique ou informatique des objets et des relations entre ceux-ci dans un domaine restreint du monde réel, objet d'un questionnement* » (Goffinet *et al.*, 2005). La modélisation des plantes vise à formaliser les relations entre « plante-environnement » pour mieux comprendre le fonctionnement du système et prendre les décisions le concernant.

Les premiers modèles apparus en agronomie pour décrire le système *sol-plante-atmosphère* sont les « **modèles de culture** ». Dans ces modèles la structure de la partie aérienne du couvert végétal est considérée comme un gaz homogène constitué des phytoéléments de très petite taille qui sont répartis aléatoirement dans l'espace (Brisson *et al.*, 1991, Brisson N, 2009; Sinoquet et Caldwell, 1995). Cette représentation simplifiée de la structure a pour parallèle une représentation simplifiée du fonctionnement des plantes et de leurs échanges avec l'environnement. Ces modèles permettent d'estimer des grandeurs agronomiques ou l'impact environnemental du système à partir de calculs dynamiques de flux de matière ou d'information entre les compartiments du système. Ils constituent des outils génériques pour aborder un grand nombre de problèmes rencontrés dans la production agricole comme la **prédiction de la production agricole** et les **flux de matière vers l'environnement**. Ces modèles de culture sont de plus en plus interfacés à d'autres modèles - comme les modèles d'action des agriculteurs, ou les modèles calculant le devenir physico-chimique des produits phytosanitaires ou des modèles socio-économiques- et souvent intégrés dans l'espace ou/et dans le temps (représentation de paysage ; évolution des relations au cours du temps) abordant ainsi des problèmes à des échelles plus larges (exemples: modèle APSIM Keating *et al.*, 2003 ; modèle CERES Gabrielle *et al.*, 1995).

Toutefois, les choix de simplification dans ces modèles limitent la **précision** des calculs et leur capacité à représenter des traits variétaux particuliers. D'autre part, cette approche est fondée sur l'hypothèse d'un milieu homogène, la **validité** de cette hypothèse est remise en question dans le cas des cultures hétérogènes (associées ou en mélanges) pour lesquelles la répartition verticale et horizontale de la surface foliaire est non uniforme.

Pour contourner ces limites, d'autres modèles ont vu le jour depuis une vingtaine d'années adoptant une approche dite « **plantes virtuelle** » qui pose de façon assez spécifique la question de l'intégration des processus entre les différents niveaux d'organisation : à partir de l'organe vers la plante entière et le peuplement (Vos *et al.*, 2010 ; Room *et al.*, 1996). Dans ces modèles, la représentation de la structure des différents organes de la plante est **fidèle à la description botanique** de la plante, et le peuplement est représenté par une population de plantes individuelles (*Fig.1b*, *Fig.2*). De ce fait, ils sont aussi appelés modèles architecturaux. Les modèles architecturaux permettent, par exemple, d'étudier le rôle que joue l'architecture des plantes sur le développement des épidémies et sur le devenir des produits phytosanitaires, ce qui est d'importance majeure en agroécologie. Dans ce travail, on s'est intéressé à cette approche, qui sera présentée d'avantage dans le paragraphe suivant.

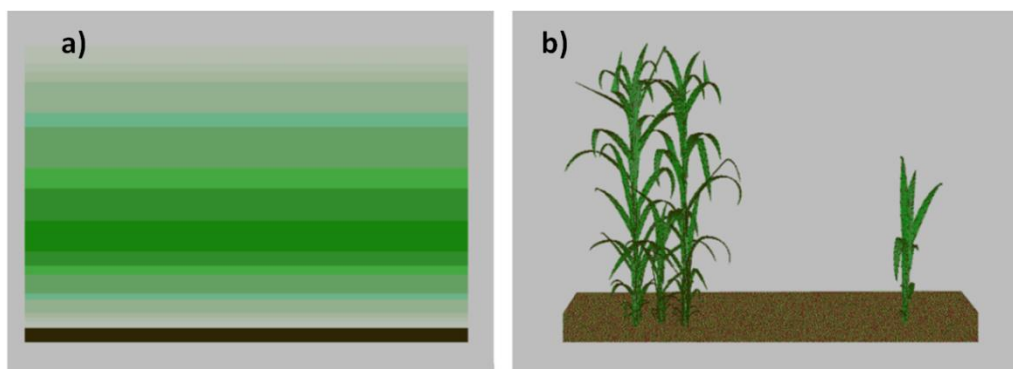


Figure 1 : Représentation d'un couvert végétal dans les modèles : à gauche le modèle « turbid medium » ou modèle de culture et à droite le modèle « plante virtuelle » (Andrieu, 2005).

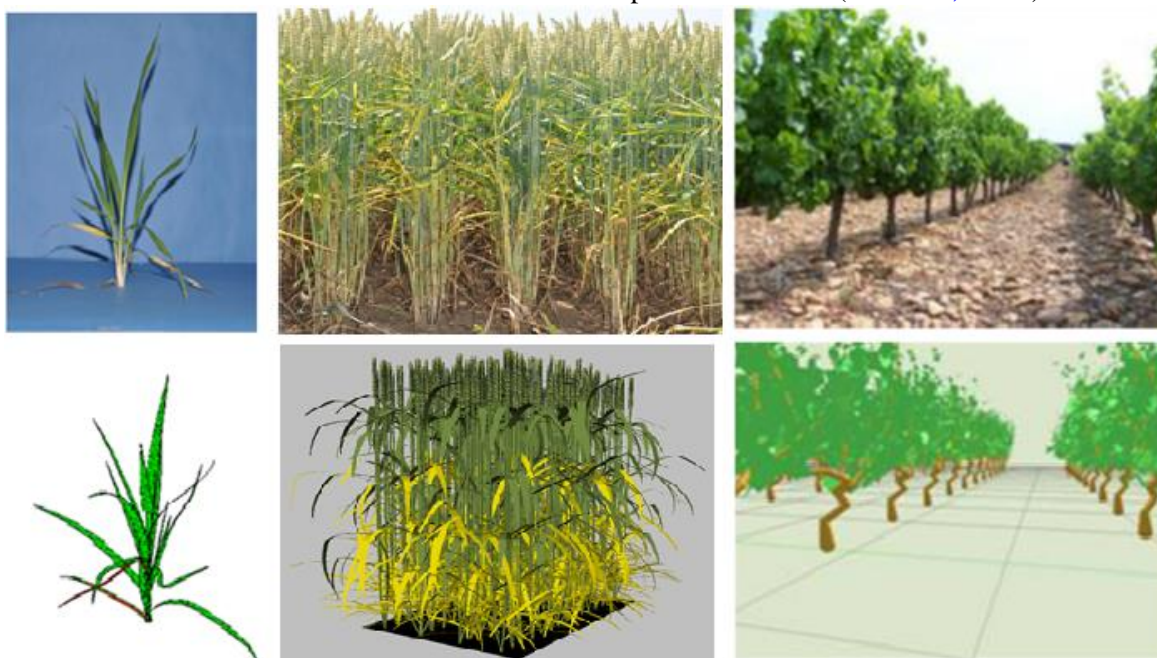


Figure 2 : L'architecture d'une plantule de blé (à gauche), d'un couvert de blé (au milieu) et d'un champ de vigne (à droite). Les figures du haut sont des photographies et celles du bas sont des simulations par un modèle type « plante virtuelle » (Abichou *et al.*, 2013 ; Louarn *et al.*, 2008).

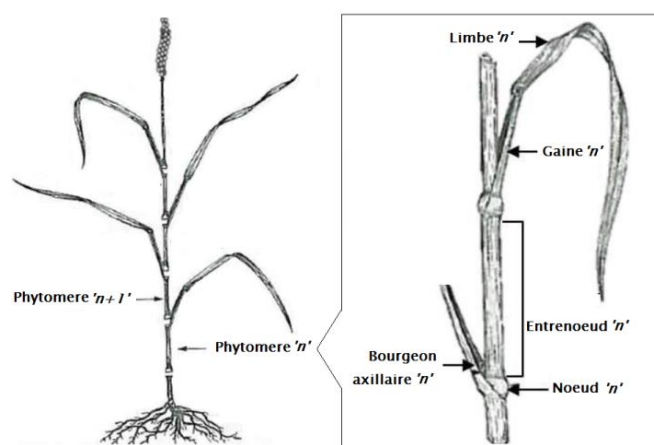


Figure 3 : Anatomie d'une tige de blé avec à gauche une tige, composée de différents phytomères et à droite la description des composants d'un phytomère (Moore and Moser, 1995).

1.3. Les modèles architecturaux: Définition FSPM et SPM

Nous désignons par « **modèles architecturaux** », les modèles qui se fondent sur une représentation explicite et réaliste de l'architecture des plantes. Il y a deux grandes catégories de modèles architecturaux qui sont : (1) les **modèles FSPM** (functional-structural plant model), et (2) les **modèles SPM** (structural plant model) sur lesquelles nous reviendrons par la suite. Ces modèles ont en commun une représentation architecturée de la plante qu'il nous semble utile de définir en se basant sur les aspects suivants:

- **L'identité des phytomères qui composent la plante et leurs dimensions** : la plante est considérée comme un système d'axes, composés d'unités similaires, les phytomères, chaque unité ayant pour principaux composants: un limbe foliaire, une gaine ou un pétiole, un entrenœud et un ou plusieurs bourgeons. Un bourgeon est susceptible de s'activer pour produire une ramification composée de nouveaux phytomères (**Fig.3**).
- **L'agencement de ces phytomères et leur géométrie** : chaque phytomère de la plante doit être défini par sa position, son orientation, sa courbure et forme. Certaines relations doivent être prises en compte dans la description de la géométrie des phytomères successifs (e.g. feuilles alternées chez les céréales).
- **Une description statique ou dynamique de la structure**: l'architecture peut être décrite d'une façon statique, à un instant précis. Plusieurs études caractérisent l'architecture des plantes à floraison sur des couverts purs, en mélange ou en association afin d'étudier les variables d'architecture impactant la répartition de lumière ou la dispersion des spores par éclaboussure des pluies au sein du couvert. L'architecture peut être aussi décrite d'une façon dynamique, pour tout le cycle de culture, ce qui offre la possibilité à d'autres applications que nous détaillerons par la suite (paragraphe 1.3). Dans ce dernier cas, d'autres notions doivent être prises en compte dans la simulation, comme par exemple, les coordinations temporelles entre les organes, la vitesse d'initiation et d'extension de chaque organe, leur durée de vie, les changements de forme géométrique et d'orientation. Des formalismes mathématiques spécifiques ont été développés pour représenter la structure des plantes et l'évolution des composants de l'architecture. Les principaux formalismes sont : les LSystems avec par exemple les logiciels L-studio et L-Py ([Prusinkiewicz et Hanan, 1990](#)) et leurs extensions, comme par exemple GroIMP ([Hemmerling et al., 2008](#)) et puis les graphes multi-échelles MTG ([Godin et Caraglio, 1998](#)).

Comme annoncé au début, deux approches de modèles architecturaux peuvent être distinguées qui correspondent à des finalités différentes:

- **L'approche « structure-fonction »**: les modèles FSPM visent à représenter les interactions entre la structure et les fonctions au sein de la plante ([Godin et Sinoquet, 2005](#), [Vos et al., 2010](#)). Ces modèles fournissent un cadre conceptuel pour représenter et intégrer les processus pour lesquels l'organisation botanique de la plante, sa géométrie et les propriétés individuelles des organes jouent un rôle important. Ces modèles nécessitent souvent un couplage entre des modèles décrivant la structure et des modèles simulant les échanges physiques au sein du couvert. Ce couplage permet de calculer les conditions physiques (rayonnement, température, humidité) perçues par

chacun organe et les mettre en relation avec les processus qui en dépendent (photosynthèse, transpiration, morphogénèse, etc.) et qui en retour affectent la structure des plantes (Fournier et Andrieu, 1998, Verdenal *et al.*, 2008). Les limites des connaissances font que les modèles FSPM sont encore largement exploratoires, ils ne permettent pas de prédire de façon précise la croissance des peuplements dans une large gamme de conditions de milieu.

- ***Une deuxième approche que nous désignerons par SPM*** se focalise sur la « **structure** » et vise à décrire d'une façon réaliste les caractéristiques morphologiques des plantes, et éventuellement leur évolution au cours du cycle. Les modèles SPM s'appuient sur des caractérisations expérimentales des peuplements et sur l'emploi de descripteurs qui sont définies par des fonctions paramétriques, empiriques ou statistiques visant à reproduire au mieux les observations. Ces modèles peuvent être couplés à des modèles simulant les conditions physiques comme le rayonnement, la pluie et les particules. Ces modèles fournissent un outil de reconstruction permettant de retracer la croissance d'un peuplement lors d'une expérimentation et d'accéder à des variables difficiles à mesurer directement, comme par exemple le rayonnement sur chaque étage foliaire et son évolution au cours de la croissance. Ces modèles permettent ainsi de comprendre le rôle que joue l'architecture dans les interactions plante-environnement.

C'est à cette deuxième approche que nous nous sommes intéressés. Nous présentons dans ce qui suit quelques exemples d'applications qui ont motivé mon travail.

1.4. Les modèles SPM: quelles applications?

Les modèles SPM représentent un outil intéressant lorsque la caractérisation des propriétés géométriques à l'échelle fine de l'organe est une clé pour la compréhension des processus d'intérêt. Les exemples d'utilisation de ces modèles *SPM* sont multiples, nous présentons ci-dessous quelques applications en lien avec les thématiques de l'UMR ECOSYS.

- ***La simulation des processus d'interactions avec le couvert.*** Le couplage du modèle SPM avec un « modèle biophysique » ou un « modèle de pathogène » permet de mieux comprendre l'impact de l'architecture sur l'interception de rayonnement, des pesticides ou sur l'épidémie (Calonnec *et al.*, 2013 ; Vidal *et al.*, 2014 ; Saint-Jean *et al.*, 2004). Le principe est de faire varier les valeurs de paramètres de l'architecture et d'analyser comment cela impacte les sorties du modèle couplé. Par exemple, le couplage avec un modèle de « rayonnement » ou de « pesticide » permet d'analyser l'effet de variation des traits d'architecture soit (i) d'une façon globale sur la quantité de rayonnement ou de particules interceptées ; (ii) ou bien d'une façon plus fine, en étudiant l'impact sur la distribution entre les différents rangs foliaires. De même pour le modèle « maladie », le couplage avec un modèle d'épidémie permet d'étudier l'impact global de traits architecturaux en termes d'épidémie ou d'analyser plus finement l'exposition de chaque organe. Il permet aussi 'de décortiquer' une expérience spécifique et de mieux comprendre comment a évolué la maladie au cours du temps. Ces variations d'architecture peuvent viser à simuler précisément la structure de différents géotypes

connus, ou au contraire explorer des architectures potentielles en vue de proposer des ideotypes. *Les applications attendues sont donc de guider le choix des pratiques et des variétés, voire la sélection variétale vers des traits optimisant l'interception du rayonnement, des produits phytosanitaires ou l'échappement à la maladie.*

- ***La simulation des signaux perçus par les capteurs en phénotypage.*** Le couplage de modèles *SPM* avec des modèles qui simulent les signaux perçus par des capteurs (Laser, LiDAR, Caméra, etc.) permet d'étudier comment les traits architecturaux impactent ces signaux. De telles simulations facilitent la mise au point et l'évaluation des méthodes « d'inversion » qui estiment des caractéristiques du peuplement végétal à partir des signaux perçus par le capteur (Lewis *et al.*, 2004, 2005 ; Baret *et al.*, 2010). *Les applications attendues sont ici de mettre au point de nouveaux outils de phénotypage permettant de comparer des variétés, d'évaluer l'effet de traitements, ou de prendre des décisions (irrigation, apport de fertilisants ou de pesticides) dans la conduite des cultures.*

- ***Comprendre les relations entre architectures des plantes et partage de la lumière dans un couvert hétérogène.*** Les modèles *SPM* permettent de représenter des couverts hétérogènes et en particulier des peuplements plurispécifiques. Dans ce cas, le couplage des modèles *SPM* avec un modèle de rayonnement permet d'étudier par simulation la répartition de la ressource lumineuse entre les espèces composant le peuplement. Il est ainsi possible de comprendre comment les traits architecturaux de chaque composante affectent la répartition des ressources dont dépend finalement l'équilibre entre les deux composantes. Par exemple, Barillot (2014) a étudié les traits architecturaux de l'association blé-pois, qui impactent la répartition du rayonnement au sein de chaque espèce, ce qui a permis d'identifier les traits importants qui assurent une meilleure cohabitation. *Les applications attendues des modèles SPM sont donc de guider l'agriculteur vers le choix de meilleures espèces ou le meilleur arrangement spatial qui optimisent l'interception de rayonnement des différentes composantes.*

- ***Evaluer des hypothèses mécanistes.*** Le modèle *SPM* peut être utilisé pour reconstruire une expérimentation bien spécifique et accéder à des variables d'intérêt peu ou non accessibles à la mesure directe. Par exemple, le couplage du modèle *SPM* avec un modèle de rayonnement peut permettre d'analyser les relations entre les propriétés des feuilles et le microclimat qu'elles ont connu au cours de leurs croissances. Ainsi (Bertheloot *et al.*, 2010, Fig.4) a analysé les relations entre la quantité de lumière interceptée par une feuille et sa teneur en azote ; (Evers *et al.*, 2007, Fig.5) a analysé des relations entre la qualité de lumière incidente sur différents organes d'une plante et l'arrêt du tallage. *Les applications attendues sont donc d'avancer nos connaissances sur le fonctionnement des plantes et les lois de réponses. Ainsi, le développement de modèles SPM contribue à faire progresser les modèles mécanistes et notamment les modèles FSPM.*

Les applications des modèles *SPM* pour les questions maladies, pesticides et phénotypage intéressent particulièrement ARVALIS-Institut du végétal qui a financé mes recherches.

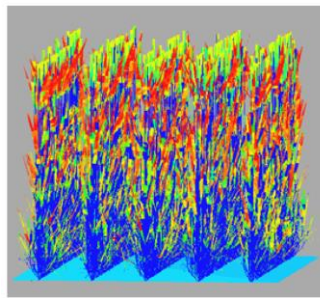


Figure 4: Visualisation de la densité de rayonnement photosynthétique ($J m^{-2} s^{-1}$) au sein d'un peuplement de blé à floraison (Bertheloot *et al.*, 2010). Le peuplement est reconstruit avec le modèle ADELwheat et le rayonnement est calculé avec le modèle Caribu.

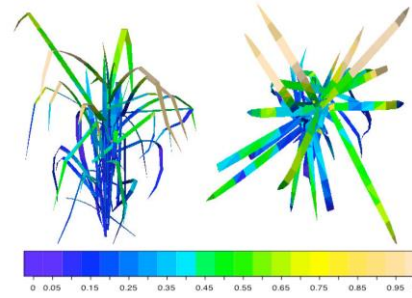


Figure 5: Distribution spatiale du ratio R:FR au sein d'un couvert de blé. Les plantes sont simulées avec le modèle ADELwheat ; le rayonnement est calculé par la méthode de radiosité mixte (Chelle *et al.*, 2007; Evers *et al.*, 2007).

1.5.ADELwheat : exemple de modèle SPM pour blé

Le modèle ADELwheat (Fournier *et al.*, 2003) est un modèle SPM qui permet de générer des représentations 4D de l'architecture aérienne d'un peuplement de blé en se basant sur des mesures réalisées au champ. Il est disponible sur la plateforme Openalea (<http://openalea.gforge.inria.fr>) où il a été couplé à d'autres modèles comme par exemple, le modèle de maladie « septo3D » (Robert *et al.*, 2008) ou le modèle de radiosité « Caribu » (Chelle *et al.*, 2007).

ADELwheat est fondé sur un ensemble de paramétrisations décrivant la dynamique d'apparition et d'extension des organes, leurs dimensions et leurs géométries. La version initiale (Fournier *et al.*, 2003) est fondée sur l'analyse approfondie d'une expérimentation unique, dans laquelle le cultivar Soissons avait été cultivé à deux densités de semis. Depuis 2003, l'équipe plante de l'UMR Ecosys a acquis d'autres données sur l'architecture des peuplements de blé, incluant plusieurs génotypes conduits à des conditions de croissance variées ; des améliorations dans le modèle ont été rajoutées mais sans être véritablement formalisées, évaluées ou documentées.

Finalement, le modèle disponible lorsque j'ai initié mon travail souffrait d'un certain nombre de points faibles :

- les paramétrisations étaient définies sur la base d'un ensemble expérimental réduit. Plusieurs versions coexistaient en fonction des données expérimentales disponibles.
- Il n'y avait pas de formalisation des mesures qui devaient être disponibles pour fournir les entrées nécessaires aux simulations.
- Il manquait une évaluation de la qualité des paramétrisations par rapport aux données expérimentales indépendantes ; il manquait également une évaluation de la qualité de simulation de variables représentatives du peuplement, comme l'indice foliaire ou la couverture du sol.
- la paramétrisation de la géométrie était fondée sur un ensemble restreint de mesures. et ne prenait pas en compte l'évolution du port foliaire après la ligulation de la feuille, ni l'évolution d'inclinaison des tiges au cours du temps.
- Le modèle n'incluait pas de description de la sénescence des feuilles. D'autre part seules les talles se développant jusqu'à former un épi étaient représentées.

2. Objectifs et démarche de la thèse

L'objectif de mon travail de recherche a été de développer un modèle opérationnel qui permette de reproduire par simulation l'architecture 4D d'un peuplement de blé. Les principales caractéristiques recherchées dans le modèle sont :

- (1) Il doit être capable de simuler d'une façon réaliste les caractéristiques du peuplement *spécifique*.
- (2) Il doit pouvoir représenter la plasticité de l'architecture en couvrant une *large gamme de conditions de culture et de géotypes*.
- (3) Il doit générer des reconstructions *dynamiques*, couvrant l'ensemble du cycle de culture, ce qui implique de décrire la dynamique de tallage et l'évolution au cours du temps des propriétés des organes (port foliaire, senescence)
- (4) Il doit avoir un *nombre réduit de paramètres* qui soient faciles à interpréter et à acquérir sur le terrain.
- (5) Il doit présenter une *interface utilisateur*, documentée, simple à gérer et facile à coupler à d'autres modèles (maladie, rayonnement et pluie).

Dans ce travail, nous nous sommes appuyés sur les acquis à l'INRA et à l'INRIA, respectivement le modèle dynamique ADELwheat et la plateforme de simulation OpenAlea. En collaboration avec Christian Fournier, nous avons choisi de définir un outil à interfacier avec ADELwheat et permettant de « piloter » la représentation des plantes par ADELwheat. Cet outil permet de produire « *in silico* » une collection de plantes très proches par leurs caractéristiques morphologiques et dynamiques de plantes réelles. La simulation de ces caractéristiques est fondée sur une approche paramétrique qui s'appuie sur des observations afin de reproduire les caractéristiques spécifiques des peuplements particuliers que l'on se propose de reproduire *in silico*. Un effort important a été consacré à la définition de l'ensemble des fonctions paramétriques permettant de décrire la morphologie des plantes de blé, et son évolution au cours du temps, en s'adaptant à la plasticité de ces caractères en fonction des conditions de croissance. Les principales étapes de travail ont été les suivantes :

Volet expérimentation :

- J'ai analysé une grande base de données avec une gamme large de conditions de croissance et de cultivars. Ces données proviennent d'expérimentations que j'ai personnellement menées au cours de ma thèse (15 traitements), mais également de la compilation de données préexistantes dans l'équipe (36 traitements). Les données décrivent la structure botanique des plantes individuelles avec une description de propriétés de chaque phytomère (nombre, dimensions, état) sur un nombre important de plantes (entre 15 à 60 par traitement). Ces données sont acquises à plusieurs dates, de façon à décrire la dynamique du développement des plantes au cours du temps.
- J'ai mené une expérimentation spécifique dédiée à l'étude du comportement des plantes lié aux changements de l'espacement entre les rangs. Les données acquises caractérisent les dynamiques de développement, les dimensions et la géométrie des plantes.
- J'ai aussi réalisé des expérimentations dédiées au suivi de la dynamique de la géométrie des organes au cours du temps. Les données acquises caractérisent chaque rang foliaire et

chaque tige sur un nombre important de plantes afin d'assurer une bonne représentativité des mesures et d'analyser les gradients en fonction de la position des feuilles sur les axes.

Plusieurs méthodes d'acquisition et d'analyse de données ont été mobilisées: digitalisation 3D (Polhemus digitizer); digitalisation 2D (Popcorn); photographie verticale et inclinée (Satva); photogrammétrie Agisoft PhotoScan (expérimentation de la méthode); suivis non destructifs sur plantes; prélèvements et dépouillement des plantes (mesure directe; scan d'organes; etc.).

Volet modélisation :

- Sur la base des données analysées, j'ai défini un ensemble de fonctions permettant de décrire la dynamique complète de la structure botanique des plantes. Ces fonctions concernent les aspects suivants : (1) la dynamique d'apparition des feuilles ; (2) la dynamique d'apparition et de mortalité des talles; (3) la dynamique du nombre de feuilles vertes et sénescentes le long d'un axe ; (4) le calcul du nombre final de phytomères sur les talles ; (5) les dimensions des organes matures (limbes, gaines, entrenœuds, épis) ; (6) la géométrie des plantes au cours du temps. Sur ce dernier point, je n'ai pas pu aller jusqu'à définir une paramétrisation des aspects géométriques. Ceux-ci seront représentés avec le module géométrique d'ADELwheat.
- J'ai intégré l'ensemble de ces fonctions dans une routine, appelée « Plantgen ». Cette routine est couplée au modèle ADELwheat qui intègre des lois de coordinations temporelles permettant une simulation correcte de l'extension des organes au cours du temps, et effectue la représentation géométrique des plantes en 3D. J'ai développé également des routines de « post-processing » des reconstructions 3D pour calculer des variables caractéristiques à l'échelle du peuplement ; celles-ci ont été utilisées notamment pour évaluer la qualité des peuplements simulés.
- J'ai défini un protocole de mesures assurant l'obtention de l'ensemble des variables nécessaires pour estimer les paramètres de « Plantgen-ADELwheat » avec principalement des mesures à réaliser sur le brin maître.

3. Structuration du mémoire

Ce mémoire s'articule autour de quatre chapitres qui sont rédigés sous forme d'articles scientifiques en anglais, le premier est soumis, les autres sont en cours de finalisation pour la soumission.

- Les deux premiers chapitres définissent des ***fonctions paramétriques décrivant la morphologie et le développement*** des plantes pour tout le cycle de culture. Le premier chapitre est consacré à la dynamique d'apparition des feuilles et à la dynamique de tallage. Le second chapitre porte sur la sénescence foliaire et les dimensions finales des organes. Nos travaux ont permis d'identifier des patterns conservés au travers de la variabilité induite par les conditions de croissance. Les fonctions paramétriques présentées dans ces chapitres représentent une formalisation de ces patterns. Ces fonctions ont été établies en minimisant le nombre de paramètres nécessaires pour la calibration. Ces paramètres sont faciles à mesurer. Ces fonctions ont été implémentées dans une routine permettant de piloter ADELwheat afin de générer des reconstructions

4D des peuplements de blé avec un effort expérimental réduit. La description de la routine, le protocole de mesures et les résultats de l'évaluation globale des reconstructions sont présentés en annexes A1 et A2.

- Le troisième chapitre présente *une analyse expérimentale du comportement* des plantes aux changements de leurs dispositions spatiales. Nous présentons les réponses des plantes en termes de développement, morphologie et géométrie, suite à une augmentation de l'espace d'inter-rangs à densité égale pour une sélection de cultivars.
- Le quatrième chapitre est consacré à une *caractérisation expérimentale de l'évolution de la géométrie* des plantes au cours du temps. Ma recherche s'est plus particulièrement focalisée sur la caractérisation de la dynamique d'inclinaison des feuilles et des tiges qui est très peu documentée.
- La discussion générale *synthétise et discute les principaux résultats* de cette thèse, des perspectives, notamment en termes d'améliorations ou d'applications futures sont proposées. Je présente aussi, deux exemples d'applications qui ont été menées en parallèle à ma thèse dans lesquelles ma méthode de reconstruction a été mise en œuvre.

4. Références bibliographiques

- Abichou M, Fournier C, Dornbusch T, Chambon C, ..., Andrieu B, (2013, June). Re-parametrisation of Adel-wheat allows reducing the experimental effort to simulate the 3D development of winter wheat. In 7th International Conference on Functional-Structural Plant Models (pp. 304-306). Finland.
- Andrieu, B. (avril, 2005). Approche plante virtuelle pour la modélisation des plantes et peuplements cultivés. Ecole interdisciplinaire d'échanges et de formation en biologie, Berder.
- Baret, F., De Solan, B., Lopez-Lozano, R., Ma, K., Weiss, M., 2010. GAI estimates of row crops from downward looking digital photos taken perpendicular to rows at 57.5 zenith angle: Theoretical considerations based on 3D architecture models and application to wheat crops. *Agricultural and Forest Meteorology*, 150(11), 1393-1401.
- Benoît, M., Papy, F., 1998. La place de l'agronomie dans la problématique environnementale. *Les Dossiers de l'environnement de l'INRA*, 17, 53-62.
- Bertheloot, J., Abichou M., Fournier, C., & Andrieu, B. (2010, September). Light-nitrogen relationships within plant canopies analysed using in silico reconstruction of wheat crops. In 6th International Workshop on Functional-Structural Plant Models (pp. 80-82).
- Bellon-Maurel, V., Huyghe, C., 2016. L'innovation technologique dans l'agriculture. *Géoéconomie*, (3), 159-180.
- Brisson N., Delecolle R., 1991. Développement et modèles de simulation de culture. *Agronomie*, 12, 3, 253-263.
- Brisson N, Launay M, Mary B, Beaudoin N. 2009. Conceptual basis, formalisations and parameterization of the STICS crop model. Collection "Update Science and Technologies": Versailles.
- Calonnec, A., Burie, J. B., Langlais, M., Guyader, S., Saint-Jean, S., Sache, I., & Tivoli, B., 2013. Impacts of plant growth and architecture on pathogen processes and their consequences for epidemic behaviour. *European Journal of Plant Pathology*, 135(3), 479-497.
- Edelin C., Moulia B., Tabourel F., 1993. Notions d'analyse architecturale des plantes." *Actes de l'École-Chercheur Inra en Bioclimatologie 1 (1996): 83-106.*

- Fourcaud D., Nicolini E., 1995. Modélisation et simulation de l'architecture des arbres bilan et perspectives. *Reu.For. Fr.* xlviii- n° sp. 1995
- Fournier C., Andrieu B., 1998. A 3D architectural and process-based model of maize development. *Annals of Botany*, 81: 233-250.
- Godin C., Caraglio Y., 1998. A multiscale model of plant topological structures. *Journal of Theoretical Biology*, 191: 1-46.
- Godin C., Sinoquet H., 2005. Functional-structural plant modelling. *New Phytologist*, 166: 705-708.
- Goffinet Bruno et al. 2005. Rôle de la modélisation en tant que démarche de recherche Inra. http://www7.inra.fr/mia/doc/rapport_modelisation_VO.pdf
- Hemmerling, R., Kniermeyer, O., Lanwert, D., Kurth, W., & Buck-Sorlin, G., 2008. The rule-based language XL and the modelling environment GroIMP illustrated with simulated tree competition. *Functional plant biology*, 35(10), 739-750.
- Keating, B. A., Carberry, P. S., Hammer, G. L., Probert, M. E., Robertson, M. J., Holzworth, D., ... , McLean, G., 2003. An overview of APSIM, a model designed for farming systems simulation. *European journal of agronomy*, 18(3), 267-288.
- Lewis, P., Saich, P., Disney, M. I., Andrieu, B., Fournier, C., Macklin, T., Bodley, J. (2004, June). Calibration of an L-system model of winter wheat for remote sensing modelling and inversion. In *Proc. 4th international workshop on functional-structural plant models* (pp. 7-11).
- Lewis, P., Hillier, J., Watt, J., Andrieu, B., Fournier, C., Saich, P., Disney, M. (2005, October). 3D dynamic vegetation modelling of wheat for remote sensing simulation and inversion. In *Proc. 9th Intl. Symp. on Physical Measurements and Signatures in Remote Sensing, Beijing, China* (pp. 17-19).
- Room P., Hanan J., Prusinkiewicz P., 1996. Virtual plants: new perspectives for ecologists, pathologists and agricultural scientists. *Trends in Plant Science*, 1(1), 33-38.
- Saint-Jean, S., Chelle, M., & Huber, L., 2004. Modelling water transfer by rain-splash in a 3D canopy using Monte Carlo integration. *Agricultural and Forest Meteorology*, 121(3), 183-196.
- Sinoquet H, Caldwell MM. 1995. Estimation of light capture and partitioning in intercropping systems. In: Sinoquet H, Cruz P eds. *Ecophysiology of tropical intercropping*. Paris, INRA Editions.
- Sinoquet H, Mouliat B, Gastal F, Bonhomme R, Varlet -Grancher C. 1990. Modeling the radiative balance of the components of a well-mixed canopy: application to a white clover-tall fescue mixture. *Acta Oecologica-International Journal of Ecology*, 11: 469-486.
- Prusinkiewicz, P., & Hanan, J. (1990, January). Visualization of botanical structures and processes using parametric L-systems. In *Scientific visualization and graphics simulation* (pp. 183-201). John Wiley & Sons, Inc.
- Verdenal, A., Combes, D., Escobar-Gutiérrez, A. J., 2008. A study of ryegrass architecture as a self-regulated system, using functional-structural plant modelling. *Functional Plant Biology*, 35(10), 911-924.
- Vos J., 2010. Functional-structural plant modelling: a new versatile tool in crop science. *Journal of Experimental Botany* 61: 2101-2115.
- Vidal, T., Gigot, C., Girardin, C., Robert, C., de Vallavieille, C. P., Suffert, F., ... & Saint-Jean, S. (2014, January). Effet de l'architecture d'un couvert de blé et des caractéristiques pluviométriques sur la dispersion par éclaboussement de *Mycosphaerella graminicola* en conditions contrôlées. In *10es Rencontres de Phytopathologie-Mycologie de la Société Française de Phytopathologie (SFP)* (pp. p-95).



CHAPTER 1: Parametrizing wheat leaf and tiller dynamics for structural plant models

This chapter is based on an article submitted (17 July 2016) in Annals of Botany Journal by:

**Mariam Abichou, Christian Fournier, Tino Dornbusch, Camille Chambon, Benoit de Solan,
David Gouache, Bruno Andrieu**

RESUME

Contexte et Objectifs. Les modèles structuraux 3D des plantes visent à simuler « in silico » le développement des plantes, isolées ou en peuplement, en se fondant sur la caractérisation expérimentale des traits d'architecture. Ces modèles peuvent être couplés avec des modèles physiques pour étudier comment la structure des plantes module leurs interactions avec l'environnement. Les mécanismes qui régulent l'organogenèse ne sont pas pleinement compris, ainsi ils sont souvent décrits par des fonctions paramétriques calées avec des mesures. Une difficulté principale de telles paramétrisations est d'assurer une flexibilité suffisante pour s'adapter à la plasticité liée aux conditions de croissances. Dans ce travail, nous avons défini des fonctions paramétriques qui permettent de décrire la dynamique de l'apparition des feuilles et la dynamique de tallage chez le blé dans une large gamme d'environnement de croissance.

Méthodes. Une large base de données décrivant l'évolution de l'architecture de plantes de blé (*Triticum aestivum*) a été recueillie. Les données représentent 51 traitements expérimentaux, avec une gamme de cultivars, plusieurs années climatiques, des conditions contrastées en termes de date et densité de semis et fertilisation azotée. Sur la base de l'analyse de ces données, des fonctions paramétriques ont été définies pour : décrire le rythme d'émergence des feuilles et représenter la dynamique de l'émergence et de la mortalité de talles.

Principaux résultats. Nous avons pu clarifier les informations contradictoires rapportées dans la bibliographie sur le caractère linéaire ou par phase de la progression du Haun stage en fonction du temps thermique. Les deux comportements ont été observés, sur un même génotype et nos résultats suggèrent que le type de cinétique suivi dépend du nombre total de feuilles formées. Les talles suivent le même type de comportement que le brin maitre, mais peuvent présenter des différences de phyllochrone conduisant à des retards dans la ligulation de la feuille drapeau. Nous avons également montré des relations stables entre le nombre de feuilles formées sur le brin maitres et les talles.

Nous avons par ailleurs précisé les dynamiques d'émergence et la régression des talles. Ainsi l'émergence est coordonnée avec celle des feuilles du brin maitre, comme cela est usuellement rapporté mais nous montrons un décalage dans le temps qui s'accroît régulièrement pour les talles successives et est remarquablement stable vis-à-vis des conditions de croissance. Nous montrons aussi que le début de régression des talles est intervenu à un stade lié au nombre total de feuilles formées et peu ou pas affecté par les conditions de croissance.

Enfin, nous avons pu formaliser les patterns observés par des fonctions paramétriques qui permettent de représenter la dynamique de l'architecture dans les modèles architecturaux de plante.

Conclusions. Cette étude fournit une vue synthétique des patterns d'évolution de l'architecture de plantes de blés. La large gamme de conditions expérimentées a permis de clarifier la robustesse des observations déjà publiés et d'identifier certaines relations, telles que les conditions pour le début de la mortalité des talles, qui méritent une plus grande attention. Ce travail permet de définir les observations nécessaires et un ensemble de relations pour représenter de façon précise dans des modèles le développement des peuplements.

Mots-clés: blé, modèle structure, architecture, feuille, phyllochrone, coordination, tallage.

ABSTRACT

Background and Aims. Structural 3D plant models aim at mimicking the dynamics of plant and crop structure based on experimental data. Such models can be interfaced with physical models to investigate how plants structure modulates their interactions with the environment. Characterizing plant dynamics at phytomer level represents an important aspect in defining structural plant models. The mechanisms that regulate organogenesis are not fully understood so that it is commonly described by descriptive functions adjusted using measurements. One challenge here is to minimize the amount of measurements required to simulate a plot with structural plant models, while keeping sufficient plasticity so the model can be fitted to a wide range of situations. The aim of this work was to define parametric functions that describe the dynamic of leaf appearance and tillering of wheat plants in a wide range of growth conditions.

Methods. A large dataset describing the dynamics of wheat plants architecture was collected. The dataset represents 51 experimental treatments with a range of cultivars, climatic year, sowing date and sowing density, and N fertilisation. On this dataset, the kinetics of Haun stage vs thermal time, and the total number of leaves formed for each category of axe were analysed.

Key Results. Data analysis allowed to precise some contradictory results of the bibliography about the linearity of phasic progress of Haun stage with thermal time: both behaviours existed in our experiments, even on a same genotype. Our results suggest that the behaviour is related to the total number of leaves formed on the stem. Tillers showed a behaviour similar to the main stem, but could differ in their phyllochron, and finally in the time of flag leaf ligulation. Beside, we could define a stable relation between the total number of leaves formed on the main stem and on tillers.

Our work also clarifies some important aspects of tillering dynamics. Tiller emergence was related with leaf emergence, as usually reported but we show that the delay increases with higher tiller position. This increase was remarkably stable, independently of growth conditions. We also consistently observed that the start of tiller regression occurred for values of Haun stage, showing no relation with growth conditions or leaf area index, but correlated to the final leaf number.

Finally, our analyses allowed to define a set of parametric functions that describe the progress of the Haun stage for each axis, derive the final leaf number of all tillers from that of the main stem and describe the emergence and mortality of tillers.

Conclusions. The study provides a comprehensive view of patterns existing in the dynamics of winter wheat plants architectures. The broad range of conditions experimented enabled to clarify the robustness of patterns previously reported and to identify some relations, such as the conditions for the start of mortality that deserve further attention. The functions that we derived make it possible to represent accurately in structural plant models the dynamics of architecture for contrasted growth conditions with a reasonable experimental effort.

Keywords: wheat, Structural Plant Model, architecture, leaf, tiller, phyllochron, phenotype, coordination, tillering

1. INTRODUCTION

Architectural models of crops aim at mimicking the 3D dynamics of a set of plants of which the architecture is explicitly represented. Such models make it possible to simulate the interactions between plants and their environment, such as the interception of light (Chelle and Andrieu, 1998), water (Saint-Jean *et al.*, 2008) or spores (Robert *et al.*, 2008). It is therefore possible to investigate how plant architectural traits modulate these interactions. In architectural models, a shoot is represented as a collection of phytomers, each made of a leaf blade, a sheath and an internode. The interplay between the dynamics of architecture, the dynamics of environmental conditions and the occurrence of events such as rain or agronomic treatments, governs the conditions experimented by each plant component. Simulating a plant implies representing different axes that develop in parallel and may or not complete their development. The patterns of development along and between plant axes are thus important aspects to represent in realistic 3D plant models. Because regulatory mechanisms that define this dynamics are not fully understood, representing it accurately requires using functions adjusted with measurements.

Our general goal was to formalize stable patterns that can be used to minimize the amount of measurements required to simulate the timing of architecture development with structural plant models, while keeping sufficient plasticity so that the model can be fitted to a wide range of situations. In this perspective we studied the following aspects: (i) the rate of appearance of leaves on an axe, (ii) the final number of leaves produced in each axis and (iii) the tillering dynamics (emergence and mortality). In the following paragraph we present an overview of the state of knowledge on these aspects, and define the objectives of the work.

1.1. Phyllochron and Haun stage progress

In wheat and numerous cereals, the progress of vegetative development is often measured by the Haun stage (Haun, 1973), that represents the fractional number of expanding leaves at a given time. The phyllochron is defined as the thermal time required for the Haun stage to progress of one unit. In several models, the rate of the Haun stage is used to drive organ extension of the whole plant (blades, sheaths, internodes) and also the timing of appearance of tillers using co-ordination schemes as presented by Fournier *et al.* (2005). The phyllochron has been extensively investigated in wheat. When the phyllochron is expressed in thermal time, it is often approximated as being constant during plant ontogeny while its value depends on sowing date (Kirby *et al.*, 1985; Baker *et al.*, 1980). In wheat, phyllochron is only slightly affected by abiotic stresses, such as low nitrogen or water availability (McMaster, 1997; Kirby *et al.*, 1985; Cao and Moss, 1991). However, several authors reported ontogenic changes within the course of plant development. Boone *et al.* (1990) provided evidence that such change in the phyllochron may mark the occurrence of an early event related to floral transition of the shoot apical meristem. There has been some debate about whether the change is real or is an artefact caused by difference between soil and air temperature (Jamieson *et al.*, 1995) as the apex first develops in the soil and then emerges with stem extension. The works cited above aimed at representing the crop level and were mainly based on characterizing the main stem behaviour, while structural models address the individual plant level and consider

explicitly all the plant axes. Few parametrisations of the Haun stage patterns have been developed that consider both main stem and tillers. A simple frame, used in Adel-wheat is that tillers emerge in coordination with the leaves on the main stem and then their Haun stage progresses at the same rate as that the main stem (Masle-Meynard, 1982; Klepper *et al.*, 1982, Fournier *et al.*, 2003; Evers *et al.*, 2005). However, these similarities were based on observations of a restricted range of conditions and cultivars and noticeable differences between the phyllochron of main stem and tillers have been reported (Kirby *et al.*, 1985b).

1.2.Final leaf number

The main factors that regulate the floral transition and thus the number of leaves on main stem are the vernalization requirement and day length sensitivity (Miglietta, 1989, 1991; Hay and Kirby, 1991; Kirby, 1992). For tillers that complete their development, the final number of leaves of a tiller at a given rank is strongly related to that of the main stem (Friend 1965), which arises from the quasi-synchrony of their floral transition (Friend 1965; Hay and Kirby 1991). Several authors reported a difference of three leaves between the main stem and the tiller axiled by leaf one (T_1) and then a decrease of one leaf for tillers of successive ranks (Masle-Meynard and Sebillotte, 1981b) however various published results show some departure from this relation (eg Friend, 1965) and we did not find any quantitative assessment based on a large experimental dataset.

1.3.Tillering

During the vegetative phase, each phytomer initiated by the shoot meristems bears a bud. The buds may grow and form tillers or remain dormant. Buds, on phytomers of the main stem, produce first order tillers which produce second order tillers and so on until tillering is stopped. The phase of tiller emergence is followed, immediately or after some delay, by a phase of mortality during which a proportion of tillers die while the others complete their cycle and produce an ear.

A large amount of observations exist that help to build a descriptive model. For winter wheat crop, the lower tiller that appears is most often the tiller emerging in the axil of leaf one (T_1). However in favourable conditions the coleoptile tiller (T_0) may emerge, whereas in unfavourable conditions the first tiller to emerge may be T_2 or T_3 . Once the first tiller has emerged, the next tillers generally appear with a high probability until the end of the tillering phase (Spink *et al.*, 2000; Whaley *et al.*, 2000). The end of tillering generally occurs before competition between plants significantly reduces light availability and it seems that both phytochrome signalling and stem extension are able to trigger the end of tillering (Kirby, 1985; Miralles and Richards, 2000; Sparkes *et al.*, 2006; Vos, 2010). Once tillering has stopped, the number of tillers per plant remains constant until the start of mortality phase. The interval between cessation of tillering and onset of tiller mortality is generally short and the onset of tiller mortality may or not be distinguished from the cessation of tillering. The phase of mortality corresponds to a period of strong competition between plants and among plant axes, which may span until ear emergence (Alzueta *et al.*, 2012). The mortality of tillers in a plant shows a well fixed temporal pattern in which the tiller that dies is often the “last

emerged” or the “less developed” tiller on the plant. The rate of mortality, and thus the number of tillers that complete their cycle is highly influenced by availability of light, water, and nutrients (Alzueta *et al.*, 2012; Davidson and Chevalier, 1990; Fraser 1982; Power, 1978; Sparkes *et al.*, 2006). Within a same plot, plant to plant competition and local heterogeneity in density and resources often results in a large variability of tillering between individual plants (Masle-Meynard and Sébillote, 1981a).

Despite the importance of the dynamic of tillering in wheat, experimental works with detailed characterisation are relatively few and cover a limited range of conditions. A robust empirical model able to describe the tillering dynamics for a wide range of conditions is needed.

1.4. Objectives

In this work, we want to define parametric functions that describe key variables of wheat architecture dynamics required in 3D plant models: (a) the progress of the Haun stage on all plant axes, (b) the correlation in final leaf number between MS and fertile tillers, and (c) the dynamics of tiller emergence and mortality within a population from emergence up to flowering. We aim to define parametrisations that are valid for a wide range of cultivars and growth conditions, that could be adjusted using a reduced number of parameters mostly estimated from main stem measurements, and that are able to simulate the inter-plant variability corresponding to that of the sample set.

There is little data available in the bibliography where wheat plants growing in field conditions have been described following an individual plant approach. That is why our work is based on dedicated experiments that allow investigating the patterns existing at plant level. A large experimental dataset was collected across years and analysed. This dataset guided us to define and to evaluate the parametric functions. Our general approach consisted to parametrize the main stem and to identify similarities between axes so that most parameters are estimated from main stem measurements.

2. MATERIALS AND METHODS

2.1. Experiments

Most experiments were conducted in field conditions, at the INRA campus of Thiverval-Grignon (48°51 N, 1°58 E), with a maritime influenced climate and a deep loamy soil that permits high yields from winter annual crops. Beside, one experiment was conducted in Wageningen (51°58 N, 5°40 E), in containers placed outdoors (Evers *et al.*, 2006). Experiments ranged over ten growing seasons, between 1998/1999 (Y98/99) and 2015/2016 (Y15/16), thus including various meteorological sequences. Agronomical treatments varied from years to years, as summarized in **Table1**; altogether, experiments comprised 12 commercial wheat cultivars *Triticum aestivum* (winter and spring), three plant population densities, three sowing dates and two nitrogen-fertilization treatments (N_+ , N_0). Field plots consisted of nine rows with an inter-row distance of 0.175 m; while the length varied between experiments, with a minimum of 8 meters. Plant population density is referred to as low density (D_1 , ~70p/m²), normal density (D_2 , ~250p/m²), or high density (D_3 , ~500p/m²).

Table 1: Information relative to experimental datasets from E1 to E8 with: (i) growing season; (ii) reference of experiment; (iii) *Triticum aestivum* cultivars; (iv) sowing date: S₁ late September, S₂ mid to late October, S₃ mid-November (the date is given in brackets); (v) sowing density: D₁ low, D₂, normal, D₃ high (number of plants per m⁻² are given in brackets); (vi) nitrogen treatments (N₊: optimal, N₀: no N given); (vii) inter-row spacing (I_S: 17.5cm, I_D: 35 cm); (viii) growth regulators treatments (doses are given in brackets), (ix) the variables analysed (see text and appendix for the definition of the variables); (x) the axes measured ;(xi) the reference for published work in literature by the author group for further experimental details.

Year	Exp.	Cv	Sowing date (jj mm)	Density (pl.m ⁻²)	Nitrogen	Inter-row	Gr. (l.ha ⁻¹)	Variables analysed	Axes measured	Reference
98/99	E1	Soissons	S ₂ (15 Oct.)	D ₁ (70), D ₂ (250)	N ₊	I _S	Gr ₀ (0)	- HS(τ) , τ_0 - N_l	MS MS and primary tillers	Ljutovac (2002)
03/04	E2	Soissons, Caphorn, Apache, Arminda, Isengrain, Thésée, Oratorio, Recital, Florance	S ₂ (16 Oct.)	D ₂ (250)	N ₊	I _S	Gr ₊ (1.5)	- N_l	MS and primary tillers	Watt et al. (2013)
04/05	E3	Soissons , Caphorn	S ₂ (26 Oct.)	D ₂ (250)	N ₊	I _S	Gr ₊ (2.0)	- N_l	MS and primary tillers	Watt et al.(2013)
05/06	E4	Soissons, Caphorn	S ₂ (27 Oct.)	D ₂ (250)	N ₊ , N ₀	I _S	Gr ₊ (2.0)	- HS(τ), N_l - $N_a(\tau)$; N_a^{max} ; N_e - τ_{SM} ; τ_{EM}	MS and primary tillers All axes -	Bertheloot et al. (2008)
05/06	E5	Minaret	S ₄ (1 Marc.)	D ₁ (100), D ₂ (262), D ₃ (508)	N ₊ N ₊ , N ₀ N ₊	I _S	Gr ₊ (2.0)	- $P(T_i)$ - HS(τ) - $N_a(\tau)$; N_a^{max} ; N_e - τ_{SM} ; τ_{EM}	primary tillers MS All plant axes -	Evers et al. (2006)
07/08	E6a	Soissons	S ₁ (25 Sep.)	D ₁ (77), D ₂ (228), D ₃ (514)	N ₊	I _S	Gr ₊ (2.0)	- HS(τ), N_l	MS and primary tillers	Baccar et al. (2011)
07/08	E6b	Soissons	S ₃ (12 Nov.)	D ₁ (77), D ₂ (228), D ₃ (514)	N ₊	I _S	Gr ₊ (2.0)	- HS(τ), N_l	MS and primary tillers	Baccar et al. (2011)
08/09	E7a	Soissons	S ₁ (30 Sep.)	D ₁ (77), D ₃ (514)	N ₊	I _S	Gr ₊ (2.0)	- HS(τ), N_l	MS and primary tillers	Baccar et al. (2011)
08/09	E7b	Soissons	S ₃ (17 Nov.)	D ₁ (77), D ₂ (228), D ₃ (514)	N ₊	I _S	Gr ₊ (2.0)	- HS(τ), N_l	MS and primary tillers	Baccar et al. (2011)
10/11	E8	Maxwell	S ₂ (26 Oct.)	D ₂ (220)	N ₊	I _S	Gr ₀ (0)	- HS(τ), N_l - $N_a(\tau)$; N_a^{max} ; N_e - τ_{SM} , τ_{EM} - $P(T_i)$	MS and primary tillers All axes - primary tillers	
12/13	E9	Maxwell, Soissons, Caphorn, Apache, Renan	S ₂ (02 Oct.)	D ₂ (220)	N ₊	I _S , I _D	Gr ₀ (0)	- HS(τ) - N_a^{max} ; N_e - $P(T_i)$	MS All plant axes primary tillers	
13/14	E10	Caphorn, Apache, Renan Caphorn	S ₂ (30 Oct.)	D ₁ (70), D ₂ (200)	N ₊	I _S	Gr ₀ (0)	- HS(τ) - N_a^{max} ; N_e - $P(T_i)$	MS All plant axes primary tillers	
15/16	E11	Soissons	S ₂ (19 Oct.)	D ₁ (72), D ₂ (170), D ₃ (400)	N ₊ , N ₀ N ₊ , N ₀ N ₊	I _S	Gr ₀ (0)	- HS(τ) - N_a^{max} ; N_e - τ_{SM}	MS All plant axes -	

Sowing dates are referred as early sowing (S_1 , late September) normal sowing (S_2 , mid to late October), late sowing (S_3 , mid-November) for winter wheat; and (S_4 , early March) for spring wheat. N-fertilization followed the standard scheme (N_+) with one dose at tillering stage (late February-early march) and one dose brought shortly before stem elongation (Zadok 3.0, often early April), except in the (N_0) treatment in Y05/06, where no N was supplied. Air temperature at 2 m was recorded from a nearby meteorological station and soil temperature at 3 cm depth was monitored in the experimental plots, using sets of thermocouples that were lined up within rows. Data was recorded every 30 seconds to compute an average hourly value. The apex temperature was estimated based on soil temperature before stem extension and then based on air temperature. In each treatment, between 15 and 60 plants were tagged to perform the architectural measurements described below.

The Haun stage progress of main stems was monitored in 32 treatments (E1, E4-E11) that include five winter cultivars and the full range of growing conditions described above. The average number of fertile axes per plant ranged between 1.5 and 7. The Haun stage progress was monitored for both main stems and first order tillers in 16 treatments (E4, E6-E8). In each case, the number of visible and ligulated leaves and their lengths were noted weekly.

The relation between the final leaf number on main stem and on tillers was analysed in 29 treatments (E1- E4 and E6-E8) that include ten winter cultivars and the full range of growing conditions described above. The total number of leaf produced was recorded for each category of flowering axes.

The probability of emergence of all primary tillers, the number of axes at the plateau of tillering (N_a^{\max}) and the number of ears (N_e) were assessed for 23 treatments (E4, E5 and E8-E10). A tiller was considered as emerged if its first leaf exceeded the collar of the axillant leaf.

The dynamics of the number of active axes were followed weekly from the plant emergence up to flowering on nine treatments (E4, E5 and E8). These treatments include four cultivars (winter and spring), three densities (D_1 , D_2 , D_3) and two nitrogen treatments (N_+ , N_0). A tiller was considered to be non-active, when the youngest leaf had not gained length since the last measurement; the date of death was estimated as halfway between the last time the tiller was recorded as active and the first moment it was recorded as dead.

The starting time of tiller mortality phase was measured on 12 treatments (E4, E5, E8 and E11). This includes six cultivars (winter and spring) and the range of growing conditions described above, excepted that there was no treatment with early sowing date.

In experiments E4, E5 and E8 (14 treatments), the thermal time at the start of tiller mortality phase (τ_{SM}) was measured on 14 treatments from experiments E4, E5 and E8 on tagged plants. It was considered as halfway between the last time for which the median number of active axes was maximum and the first time for which a significant decrease was noted. Alternatively, in experiment E11, frequent destructive samplings were used to estimate the time of start mortality (τ_{SM}), taken as half-way between the last time for which less than 50% of plants had one non-active tiller and the first time for which more than 50% of plants had

one non-active tiller.

The thermal time at the end of tiller mortality phase (τ_{EM}) was estimated in experiments E4, E5 and E8 as halfway between first sampling for which the number of active tillers per m² was equal to the final number of ear per m² and the previous sampling for which a significant difference was noted.

The plant area index (PAI_g, expressed in m² leaf per m² soil) was monitored in some experiments to investigate relations with cessation of tillering. Ground cover photographs with an angle of viewing of 57.5° (Baret *et al.*, 2010) were used to estimate the PAI_g in experiment E8 and E11. Alternatively, in experiment E4, the PAI_g was calculated from scan of plant organs, by cumulating individual organ areas of all axes and taking into account the green fraction of each organ (only organ area of the main stem and primary tillers were measured; the organ size of secondary tillers were supposed equal to that of the primary tiller of the same cohort).

2.2. Data analysis

Thermal time (τ) was computed on an hourly basis, assuming a linear response to temperature with a base temperature of 0°C as widely accepted for wheat (Gallagher *et al.*, 1979; McMaster and Smika, 1988; Baker *et al.*, 1986; Baker *et al.*, 1980).

Haun stage was calculated following equation 1, which slightly differs from the original formulation in (Haun, 1973).

$$HS(\tau) = n + \frac{l}{L} \quad (1)$$

Where n is the number of ligulated leaves at a given time (τ), l and L are respectively the exposed and the final length of the blades of leaf $n+1$.

Representative values for Haun stage, final leaf number and number of active axes were calculated at each sampling date as the mean of measurements on individual plants. Model parameters were estimated using either the least squares fitting methods in R (functions `lm` or `nls`) or Excel 2010 (Solver). Plant emergence was defined from the fitted dynamics of main stem Haun stage vs. thermal time, as the time when fitted Haun stage was null. The Haun stage of main stem at emergence of each tiller was defined by adjusting a linear model between the Haun stage of the tiller and that of main stem as illustrated in supplementary *figureS1*.

We identify tillers according to Kirby *et al.* (1985). T_i is the primary tiller emerging in the axil of leaf i . Secondary tillers are numbered with two indices and $T_{i,j}$ is the tiller emerging from the axil of the j^{th} leaf of T_i . It results from the coordination between leaf and tiller emergence that tillers of various orders can be grouped by cohorts, we refer to cohort N_c as the set of all tillers that emerge at the same time as main stem leaf N_c (see *Table2*).

To select the most efficient model for the dynamics of Haun stage the Akaike Information Criteria (AIC) was calculated for both linear and bilinear model for each experiment.

Table 2: Scheme illustrating potential tillering in wheat under ideal conditions with the nomenclature of tillers used in ADEL-Wheat (adapted from Kirby *et al.*, 1985).

MS: the main stem

T_0 : the coleoptile tiller

T_i : the tiller growing in the axil of the i^{th} leaf of the main stem

$T_{i,j}$: the tiller growing in the axil of the j^{th} leaf of tiller T_i

$T_{i,j,k}$: the tiller growing in the axil of the k^{th} leaf of tiller $T_{i,j}$

N_c is the cohort to which a tiller belongs, that is the rank of the main stem leaf which emerges synchronously with the tiller. For a primary tiller T_i , $N_c = i+3$, for a secondary tiller $T_{i,j}$, $N_c = i+j+5$, for a third order tiller $T_{i,j,k}$, $N_c = i+j+k+7$, etc.

N_c										
1	<i>MS</i>									
2										
3	T_0									
4	-	T_1								
5	$T_{0,0}$	-	T_2							
6	$T_{0,1}$	$T_{1,0}$	-	T_3						
7	$T_{0,2}$	$T_{0,0,0}$	$T_{1,1}$	$T_{2,0}$	-	T_4				
8	$T_{0,3}$	$T_{0,0,1}$	$T_{0,1,0}$	$T_{1,2}$	$T_{1,0,0}$	$T_{2,1}$	$T_{3,0}$	-	T_5	

2.3. Parameterisation of Haun stage progress

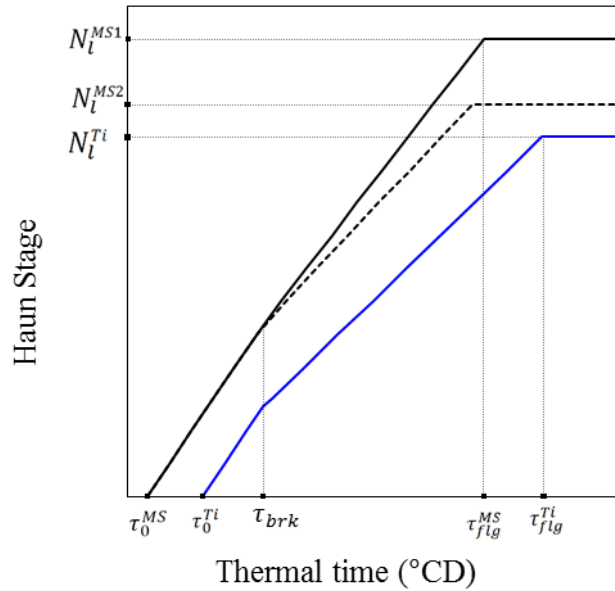
Our parameterisation of Haun stage (HS) of the main stem allows for either a linear or a bilinear model as expressed in Eqn T3.1 and Eqn T3.2 (**Table3**). The **figure1** illustrates the parameterisation of the bilinear behaviour.

We propose also a set of equations to derive the Haun stage of tillers from that of the main stem. The hypotheses on which the equations are founded were elaborated based either on the bibliography or on the observations made on our experimental dataset; they address four questions: when do tillers emerge? how is tiller phyllochron related to that of the main stem? are there differences between fertile and sterile tillers? and are there differences between tillers of a same cohort that differ in their final leaf number? The hypotheses are listed below:

- (i) Each tiller emerges at a given value of Haun stage of the main stem $HS^{MS}(\tau_0^{Ti})$ that depends on tiller position but not of growth conditions. This reflects the report by many authors that the emergence of tillers is synchronized with the emergence of main stem leaves (Friend, 1965; Masle-Meynard and Sebillotte, 1981b; Klepper, 1982; Masle, 1985; Kirby, 1993). To estimate the main stem Haun stage at emergence of each tiller, a linear model was fitted between the Haun stage of tillers and that of main stem before the eventual break point. The time of emergence of a tiller (τ_0^{Ti}) is then defined as the intercept of this model and is expressed in term of Haun stage of the main stem ($HS^{MS}(\tau_0^{Ti})$).
- (ii) When the phyllochron of the main stem is constant over ontogeny, the phyllochron of tillers is taken constant too. In that case the Haun stage dynamics of a tiller is parameterised using the time of tiller emergence (τ_0^{Ti}), the tiller final leaf number, and the thermal time delay (σ_i) at flag ligulation between main stem and tiller (Eqn T3.3 in **Table3**).
- (iii) When the phyllochron of the main stem changes during the cycle, this also occurs for tillers and the break point (τ_{brk}) is the same for all axes. Before the break point, the Haun stage of tillers progresses at the same rate as that of main stem; after the break point, the Haun stage progress may differ between tillers and is parameterised depending on the tiller final leaf number and the delay at flag ligulation between main stem and tiller (**Fig.1**). This is expressed in the equations Eqn T3.4a and Eqn T3.4b in **Table3**.
- (iv) The above description refers to tillers that complete their ontogenic cycle. For sterile tillers, we consider that their development is unaffected until their last leaf emerges, and the extension of the last leaf takes place at a lower rate, approximated as a constant fraction (f) of the rate for previous leaves; this is expressed in equation Eqn T3.6 (**Table3**). The final number of emerged leaves on a sterile tiller is estimated from the tillering sub-model (next paragraph).
- (v) Within a given treatment, main stems of different plants may differ in their final leaf number (N_l); similarly, tillers of a same cohort may differ in final leaf number (**Fig.1**). We assume that there is a constant delay (θ) in the moment of flag leaf ligulation for any supplementary leaf.

Table 3: Equations describing the Haun stage model HS of main stem and tillers and the model of final leaf number of tillers N_l (see Appendix for the definition of symbols).

Axis	Model	Equations	Thermal time interval	N°
Main stem	<i>HS linear model</i>	$HS^{MS}(\tau) = a^{MS}(\tau - \tau_0^{MS})$	$\tau_0^{MS} \leq \tau \leq \tau_{flg}^{MS}$	Eqn T3.1
	<i>HS bilinear model</i>	$HS^{MS}(\tau) = a_1^{MS}(\tau - \tau_0^{MS})$	$\tau_0^{MS} \leq \tau \leq \tau_{brk}$	Eqn T3.2a
		$HS^{MS}(\tau) = a_2^{MS}(\tau - \tau_{brk}) + HS_{brk}^{MS}$; $a_2^{MS} = \frac{N_l^{MS} - HS_{brk}^{MS}}{\tau_{flg}^{MS} - \tau_{brk}}$	$\tau_{brk} < \tau \leq \tau_{flg}^{MS}$	Eqn T3.2b
Fertile tillers	<i>HS linear model</i>	$HS^{Ti}(\tau) = a^{Ti}(\tau - \tau_0^{Ti})$; $a^{Ti} = \frac{N_l^{Ti}}{\tau_{flg}^{Ti} - \tau_0^{Ti}}$; $\tau_0^{Ti} = \tau_0^{MS} - \sigma_i$	$\tau_0^{Ti} \leq \tau \leq \tau_{flg}^{Ti}$	Eqn T3.3
		<i>HS bilinear model</i>	$HS^{Ti}(\tau) = a_1^{MS}(\tau - \tau_0^{Ti})$;	$\tau_0^{Ti} \leq \tau \leq \tau_{brk}$
	$HS^{Ti}(\tau) = a_2^{Ti}(\tau - \tau_{brk}) + HS_{brk}^{Ti}$; $a_2^{Ti} = \frac{N_l^{Ti} - HS_{brk}^{Ti}}{\tau_{flg}^{Ti} - \tau_{brk}}$		$\tau_{brk} < \tau \leq \tau_{flg}^{Ti}$	Eqn T3.4b
	<i>N_l model</i>	$N_l^{Ti} = \alpha N_l^{MS} - \beta N_c^{Ti}$		Eqn T3.5
Sterile tillers	<i>HS model</i>	$HS^{Ti.st}(\tau) = HS^{Ti}(\tau)$;	$0 \leq \tau \leq \tau_s$	Eqn T3.6a
		$HS^{Ti}(\tau_s) = N_l^{Ti.st} - 1$		
		$HS^{Ti.st}(\tau) = f * a^{Ti}(\tau - \tau_s) + (N_l^{Ti.st} - 1)$	$\tau_s < \tau \leq \tau_{flg}^{Ti}$	Eqn T3.6b


Figure 1: Representation of the parameterization of the Haun stage as a function of thermal time. The graph illustrates the case of a bilinear behavior. Black lines represent the HS function for two main stems of the same population having different final leaf number: N_l^{MS1} (solid line) and N_l^{MS2} (dotted line). Blue line represents the HS function for tiller 'i' having a final leaf number N_l^{Ti} . Parameters used in equations Eqn T3.2 and Eqn T3.4 are shown.

Finally, three to five parameters are required to describe the Haun stage progress on the main stem, which should be estimated from experimental data:

- The final leaf number of the main stem (N_l^{MS}), or the distribution;
- The thermal time of plant emergence (τ_0^{MS});
- The thermal time of flag leaf ligulation (τ_{flg}^{MS}),
- The first rate of the Haun stage dynamics if there are two (a^{MS}, a_1^{MS});
- The thermal time of the break point (τ_{brk})

To simulate tillers, the following information is required:

- The delay in thermal time between MS and each tiller at flag ligulation (σ_i), which is expected to be characterized experimentally.
- The Haun stages of the main stem at tillers emergence $HS^{MS}(\tau_0^{Ti})$, which are taken as constants.
- The ratio (f), between the rate of haun stage progress of the last leaf to emerge and that of other leaves, is taken as a constant.
- The final leaf number of each tiller (N_l^{Ti}), which is calculated from main stem leaf number (next section “Parameterisation of final leaf number on tillers”).

Beside, our parameterisation allows representing the variability in Haun stage progress between plants of a same treatment differing in final leaf number. If a distribution of main stem final leaf number is characterized experimentally, the Haun stage progress for different type of plants can be derived from that for the type with the more frequent leaf number.

2.4.Parameterisation of final leaf number on tillers

In our parametrization, we suppose that: (i) tillers of a same cohort produce the same number of leaves (ii) the final leaf number of each cohort is linearly related to that of the main stem as expressed in equation Eqn T3.5 (**Table3**). The final leaf number of the main stem is the only variable that needs to be measured.

2.5.Parameterisation of dynamics of active tiller population: appearance and mortality

Our model use tillering patterns that have been repeatedly reported (Alzueta *et al.*, 2012; Rawson, 1971). It divides the tillering process into four phases as presented in **figure2**: (ϕ_1) the emergence of successive tillers; (ϕ_2) the number of axes is stable (N_a^{max}); (ϕ_3) the number of active axes (N_a) decreases; (ϕ_4) the number of active axes remains constant up to crop maturity. Beside, we use some hypothesis to derive the behaviour of higher order tillers from that of primary tillers using the cohort concept (Masle, 1985). Below, we describe the parametrization of the emergence and regression phases since other phases are plateau.

*Emergence phase (ϕ_1): two keys information are required to describe the emergence process: the moment of emergence of each tiller and the frequency of emergence of each tiller. As seen in section 2.3, the timing of tiller emergence (τ_0^{Ti}) is coordinated with leaf emergence on main stem (Eqn T3.3). Our parametrization implies that the frequency of emergence of primary tillers is given as an input. To calculate the frequency of emergence of higher order tillers, we consider that a high order tiller can be present only if its parent tiller is present and in that case

we assume a constant ratio (k) between the probability of emergence of a high order tiller and that of the primary tiller of the same cohort; for a secondary tiller T_{ij} this is expressed in equation Eqn T4.1 (**Table4**).

*Mortality phase (ϕ_3): based on our observations, we defined the following approximations to describe the mortality phase: (i) the start of tiller mortality occurs for a specific value of Haun stage of the main stem which depends on the final number of leaves produced by the main stem (equation Eqn T4.2, **Table4**), (ii) the end of tiller mortality occurs at the ligulation of the flag leaf of the main stem (equation Eqn T4.3, **Table4**), (iii) During the mortality phase, the number of active axes follows a stable pattern that is scaled according to the duration of the mortality phase and the number of axes that regress (equation Eqn T4.4, **Table4**).

Finally, to simulate the progress of the number of active axes (N_a) at the crop level, the tillering sub-model requires the following parameters:

- The number of plants per square meter (N_p)
- The final number of ears per square meter (N_e)
- The probabilities of appearance of all primary tillers $P(T_k)$
- The final leaf number of the main stem (N_l^{MS})
- The thermal time at the emergence of the each tiller (τ_0^{Ti})

The first four parameters are input data that are expected to be characterized experimentally. The thermal times at tillers emergences (τ_0^{Ti}) are calculated from the Haun Stage sub-model described in the previous section.

To simulate a set of individual plants following the dynamic of active axes described above, we follow a relatively straightforward scheme that we describe only briefly: For each plant, the emergence of a primary tiller is randomly drawn from the probability of emergence of primary tillers. The same process is used to decide for emergence of secondary tillers when a primary tiller exists. For tiller mortality, the dynamic of the number of active tillers determines how many tillers should die at each time step and the tillers that die are taken randomly among the youngest axes in the population of active axes.

3. RESULTS

In the following paragraph we present the results of the dataset analysis and the evaluation of the hypothesis of each sub-model.

3.1. Linear or bilinear Haun stage behaviour for fertile axes

When considering all treatments together, the phyllochron, averaged from emergence to flag leaf ligulation of the main stem, varied from 87 to 126 °Cd and was highly correlated with sowing date ($P < 0.001$). The Haun stage data were fitted separately for each treatment with the linear and the bilinear models and the Akaike Information Criteria (AIC) was used to choose the best model in each case. First, the fit was made for the main stems considering only plants of the most frequent N_l group; then the model with fitted parameters was used to estimate the dynamic of Haun stage for main stems having different N_l .

Table 4: Equations describing the dynamics of tillering (see Appendix for the definition of symbols).

Variable	Equations	N°
frequency of emergence of a secondary tiller	$P(T_{ij}) = k P(T_{i+j+2})$	Eqn T4.1
Timing of start mortality phase	$HS^{MS}(\tau_{SM}) = \rho N_l^{MS} + \mu$	Eqn T4.2
Timing of end mortality phase	$\tau_{EM} = \tau_{flg}^{MS}$	Eqn T4.3
Pattern of mortality phase	$N_a(\tau) = exp\left(\frac{-\theta \tau_n(\tau)}{\delta - \tau_n(\tau)}\right) (N_e - N_a^{max}) + N_e ;$ $\tau_n(\tau) = \frac{\tau - \tau_{SM}}{\tau_{EM} - \tau_{SM}}$	Eqn T4.4

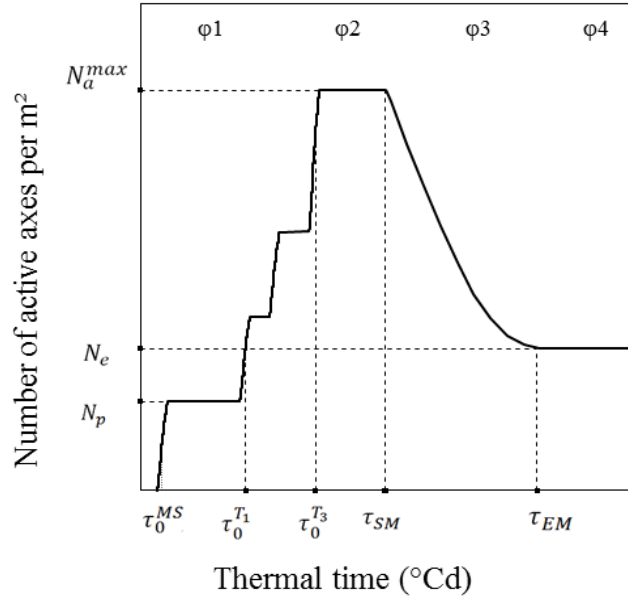


Figure 2: Representation of the parametrization of the number of active axes per m² vs. thermal time. Four phases of tillering are shown: (ϕ_1) tillers emerge in coordination with MS leaf emergence, (ϕ_2) the number of active axe is constant, (ϕ_3) part of the tillers die and (ϕ_4) the number of ears is reached. N_p , N_a^{max} and N_e are respectively the plant number, the maximum number of active axes and the number of ears per m²; τ_0^{MS} , τ_0^{T1} , τ_0^{T3} are the thermal time of emergence of respectively the main stem, tiller 1 and tiller 3; τ_{SM} and τ_{EM} are the thermal time at the start and the end of mortality phase. The full line shows a simulation for a set of plants, with a standard deviation of ± 30 °Cd in the time of plant emergence τ_0^{MS} .

Table 5: The root mean square error of the Haun stage sub-model, calculated separately for the main stems and tillers. Values are measured on 16 treatments from experiments E3 to E6 covering three cultivars sowing under different densities and sowing dates (the total number of HS measurements used for the evaluation is given in brackets).

Haun Stage model	Number of treatments	Main stem		Tillers	Global
		Frequent N_l	Non frequent N_l		
linear	8	0.22 (147)	0.17 (116)	0.25 (375)	0.19 (452)
bilinear	8	0.14 (118)	0.26 (19)	0.23 (273)	0.21 (395)

Table 6: Haun stage of the main stem at the emergence of tiller $HS^{MS}(\tau_0^{Ti})$. Values were estimated on 16 treatments from experiments E3 to E6, covering three cultivars and a range of sowing densities and sowing dates (see [Table S2](#) for more information on agronomic treatments).

Tiller rank	Mean value of $HS^{MS}(\tau_0^{Ti})$	Confidence intervals (95%)	Number of treatments
T ₁	2.5	0.11	12
T ₂	3.2	0.11	16
T ₃	4.3	0.12	14
T ₄	5.5	0.15	12
T ₅	6.9	0.47	2

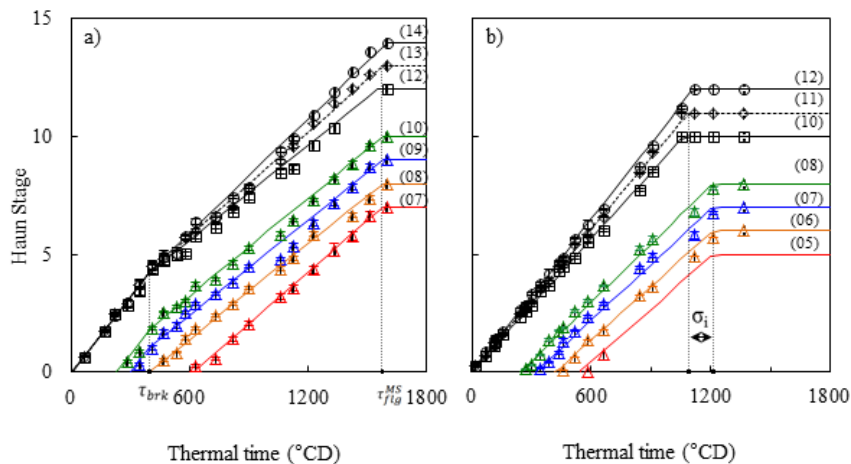


Figure 3: Haun Stage vs. thermal time from plant emergence of individual plant axes: (a) cv Maxwell sown at density 220 p/m² in late October (experiment E8) and (b) cv Soissons sown at density 228p/m² in late September (experiment E6a). Symbols show the mean values observed for main stems having different final leaf number with black symbols, and for tiller 1 (green), tiller 2 (blue), tiller3 (orange) and tiller 4 (red). Only tillers that produced an ear are taken into account. Error bars mark the 95% confidence intervals of mean estimates. Numbers between brackets are the final leaf number of each axis group. Dotted black lines represent the model fitted on main stems having the most frequent N_l^{MS} (11 leaves); solid lines represent model simulation for main stems groups with 10 or 12 leaves in black, and for tiller 1 in green, tiller 2 in blue, tiller3 in orange and tiller 4 in red.

The RMSE were in the range 0.14 - 0.26 (*Table5*) illustrated that the models represented well the data. Parameters values are given in supplementary *TableS1*.

The linear model was appropriate for all cultivars ('Soissons', 'Caphorn', 'Maxwell', 'Renan' and 'Apache') when sown between mid to late October (S_2); the final leaf number was 11 or 12 leaves in these treatments. Changes in phyllochron with ontogeny were observed in the case of either early (late September) or late (mid-November) sowing dates, that is in experimentations E6 and E7 with the cultivar Soissons. There was one case of early sowing (Experiment E7, S_1) for which visual observation of the data suggests a change in phyllochron but the pattern could not be accurately described by a simple bilinear model and in that case the linear model was applied. In early sowings, the final leaf number of the main stems was between 13 and 14 and the phyllochron for higher leaves was longer than for lower leaves (*Fig.3a*). In late sowings, the final leaf number of the main stems was 9 or 10 and the phyllochron for higher leaves was either higher or lower than that of lower leaves depending on the year (see *TableS1*). Altogether, the Haun stage of the main stem at the break point varied between 2.1 to 4 and was highly correlated with final leaf number ($r^2 = 0.6843$). Thus our results confirm that change in phyllochron along ontogeny may occur independently of artefact in the measurement of temperature, and a same genotype may show either a linear or a bilinear behaviour depending on the sowing date or the number of leaves produced.

Plants differing in N_l within a same treatment were nearly synchronous in the date of flag leaf ligulation, with a mean increase of only 21°Cd per additional main stem leaf (*Fig.4*). Consequently, plants with higher N_l had a lower phyllochron. Taking into account this delay of 21°Cd per additional main stem leaf, the dynamics of Haun stage was simulated with an RMSE of 0.17 for main stems with non-frequent N_l .

3.2. Tillers emerged at stable value of main stem Haun stage but their phyllochron did not necessarily equal that of the main stem

Tillers of a same rank emerged at a same value of main stem Haun stage $HS^{MS}(\tau_0^{Ti})$, independently of the treatment or cultivar, the deviation from the mean being generally less than 0.2 leaves (*Table6*). The delay between the emergences of two successive tillers increased markedly with tiller rank (*Fig.5*). On the other hand, the delay at flag leaf ligulation between the main stem and tillers (σ_i , Eqn T3.3) was quite variable depending on treatments: in some treatments there was a synchrony of flag leaf ligulation between MS and all tillers (*Fig.3a*) ; in other treatments flag leaf ligulation was synchronous amongst tillers of all orders, but was significantly delayed compared to the main stem (*Fig.3b*; $\sigma_i = 125^\circ Cd$); finally we observed also cases where main stem, tiller 1 and tiller 2 were nearly synchronous but higher tillers showed a delay that increased with tiller rank. These three behaviours were observed even for the same cultivar Soissons. This justifies that the delays at flag leaf ligulation between the MS and each primary tiller are expected to be characterized experimentally in our parametrisation.

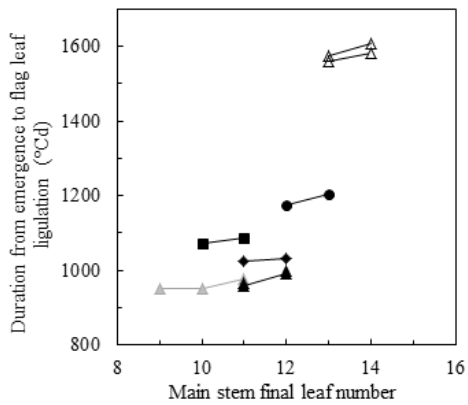


Figure 4: Duration in thermal time from emergence to flag ligulation of the main stem ($\sigma_i = \tau_0^{MS} - \tau_{flg}^{MS}$) vs. final leaf number of main stem for winter wheat Cv. ‘Soissons’ (experiments E6, E7:△, E7:▲, E4:▲), ‘Maxwell’ (E8:■), ‘Renan’ (E10: ●) and ‘Caphorn’ (E4:◆). Cultivars sown in late September (S_1) are putted in empty symbols, those sown in mid-November (S_3) in grey symbols and treatments sown in late October are in black symbols.

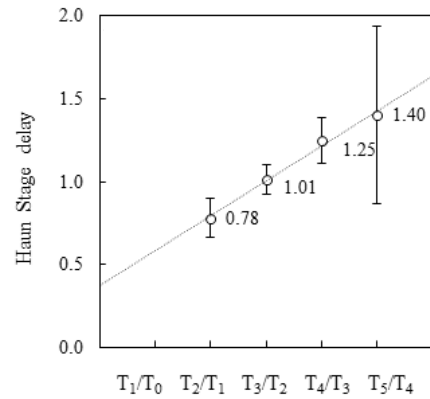


Figure 5: Haun stage delay between the emergences of two successive tillers. Symbols represent the mean value calculated over 16 treatments covering three cultivars of winter wheat (‘Maxwell’, ‘Caphorn’ and ‘Soissons’), different densities (77, 220, 250, 514 p/m²) and sowing dates (experiments E4, E6-E8). Error bars mark the 95% confidence intervals of mean estimates. Line represents the fit of a linear model.

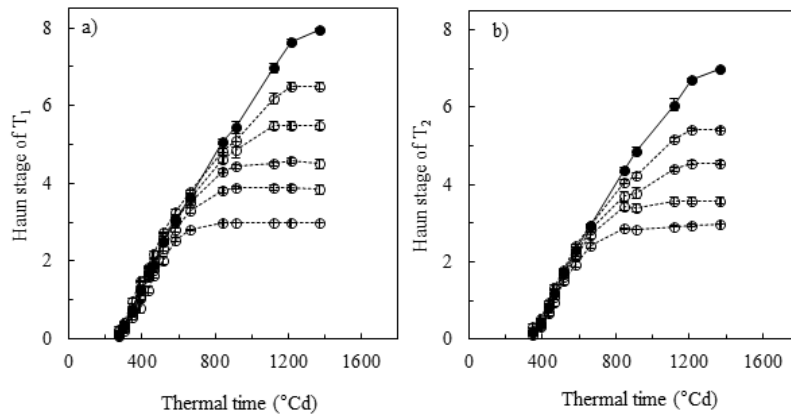


Figure 6: Haun stage vs. thermal time from plant emergence of tiller 1 (a) and tiller 2 (b) measured on cv. ‘Maxwell’ grown in Grignon in 2010/2011 at density 220 p/m² (experiment E8). Symbols represent the mean value of HS measured on the fertile tillers (black circles) and on sterile tillers having different final leaf number (white circles). Error bars mark the 95% confidence intervals of mean estimates.

Using as input the delay in flag leaf ligulation between main stem and each cohort, the Haun stage of tillers was simulated with an RMSE of around 0.24. Note that our parametrisation assumes that if a change of phyllochron occurs on the main stem, this also occurs for tillers, at the same time. This seemed to be the case but could not be statistically tested because the first phase is very short on tillers, so that an accurate estimate of the position break point was not possible for tillers.

A comparison of the rate of Haun stage progress of sterile tillers with that of tillers that completed their development was performed in experiment E8, which was the only one with sufficient data on sterile tillers. As shown in *figure6*, the development was first identical independently of tiller fate, and tillers that would regress showed a reduced rate of development only during extension of the last leaf that emerged. This behaviour was approximated in the model by considering that for sterile tillers, the rate of progress of Haun stage after emergence of that last leaf was reduced by 50%.

3.3.Final leaf number of tiller highly correlated to that of the main stem

The final number of leaves produced on the main stem N_l^{MS} generally differed by one leaf between plants of a same treatment. Between treatments, it varied mainly with the sowing date: from 13 or 14 leaves in early sowings to 9 or 10 leaves in late sowings. The mean value of final leaf number on the main stem N_l^{MS} and on primary tillers N_l^{Ti} in each of the 29 treatments from experiments E1- E4 and E6 to E8, were used to analyse the relation between the final leaf number of main stem and that of tillers. The *figure7* show that N_l^{Ti} was linearly related to N_l^{MS} , with an offset depending on tiller rank i . When the parameters α and β were fitted on these data, Eqn T3.5 predicted satisfactorily the final leaf number of tillers from that on main stem (RMSE = 0.42 leaves). Fitted values were $\alpha = 0.942$, meaning that there was approximately one additional leaf on tillers per additional leaf on main stem and $\beta = -0.623$, meaning that the decrease in final leaf number between successive tillers was significantly less than 1.

3.4.Secondary and higher order tillers emerged at a lower frequency than primary tillers of the same cohort

Averaged over all treatments, the lower tiller to appear was T_1 in 71% of the plants; T_2 in 16%, T_0 in 1%, and 12% of plants didn't produce any tiller. The higher tiller to appear decreased with higher plant density ($P < 0.01$); it was generally T_5 at low density and T_3 at high density. The value of k in equation Eqn T4.1 was adjusted on 23 treatments (experiments E4, E5, E8-E10), for which the maximum number of tillers per plant varied between 3 and 14. When k was fitted ($k=0.60$) the total number of tillers was correctly estimated from the number of primary tillers (RMSE =0.39 axes). Conversely, assuming a probability of emergence of higher order tillers equal to that of primary tillers would have overestimated the number of tillers (*Fig.8*).

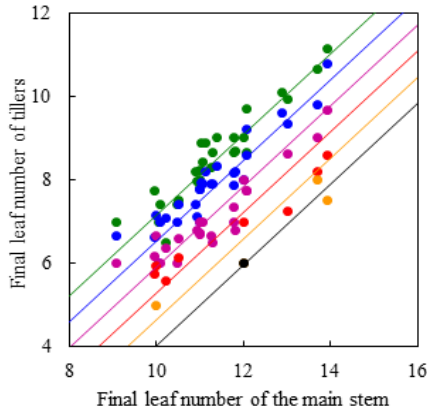


Figure 7: Final leaf number of tiller vs. final leaf number of the main stem. Circles show values from 29 treatments from experiments E1-E4 and E6-E8. In green the T_1 , in blue the tiller, in purple the T_3 , in red the T_4 , in orange T_5 and in black T_6 . Each circle represents the mean value in one treatment. Lines represent the model fitted for each tiller rank and the dotted line represents the line 1:1.

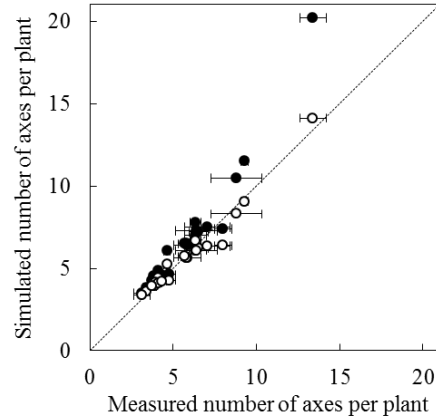


Figure 8: Simulated vs. measured number of axes per plant at the plateau of tillering, for 19 treatments of winter wheat covering five cultivars ('Apache', 'Caphorn', 'Maxwell', 'Renan' and 'Soissons'), two sowing densities (D_1 , D_2) and four seasons (experiments E4, E5, E8-E10). Each circle represents the mean value in one treatment. Error bars show the confidence intervals. Black circles represent simulations considering that probability of emergence of a high order tiller equals to that of the primary tiller of the same cohort ($k= 1$; Eqn T4.1). White circles represent simulations considering a probability of emergence of high order tillers lower than that of primary tillers of the same cohort ($k= 0.60$; Eqn T4.1). The direction 1:1 is shown as dotted line. Detailed information is given in [TableS3](#).

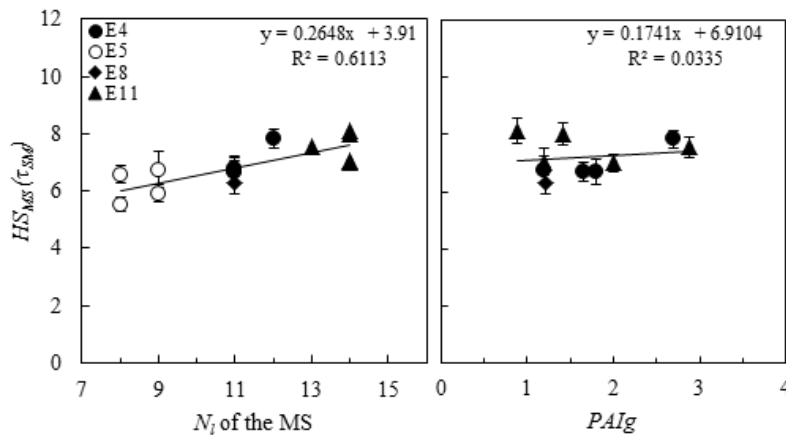


Figure 9: Haun stage of the main stem at start mortality of tillers ($HS^{MS}(\tau_{SM})$) vs. (a) the final leaf number (N_i) of the main stem and (b) plant area index (PAI_g). Symbols show the mean values observed on the 14 treatments from experiments E4 (●), E5 (○), E8 (◆) and E11 (▲) covering: three densities (D_1 , D_2 , D_3); three winter cultivars (black symbols); one spring cultivar (white symbols) and two nitrogen treatments (N_+ , N_0). Error bars mark the 95% confidence intervals of mean estimates and the line show the linear model adjusted.

3.5. The start and the end of tiller mortality phase are correlated to plant ontogeny

The mortality of tiller started for Haun stage of the main stem, $HS^{MS}(\tau_{SM})$, between 5.5 and 8. The **figure9a** shows that $HS^{MS}(\tau_{SM})$, was linearly related to the final leaf number of the main stem ($r^2=0.61$).

So on our dataset covering a large range of plant density and sowing dates, the final leaf number was a good estimator for the plant stage at the start of tiller mortality. On the other hand, the PAI_g at start of tiller mortality was highly variable (between 1 and 3) and was poorly correlated with $HS^{MS}(\tau_{SM})$ (**Fig.9b**, $r^2=0.033$).

The time of end mortality of tillers was also highly correlated to the time of flag leaf ligulation of the main stem ($r^2= 0.78$, **Fig.10**).

3.6.A stable pattern for tiller mortality phase

The dynamic of mortality of tillers was followed on nine treatments from experiments E4, E5, E8 that include four cultivars (Soissons, Caphorn, Maxwell, Minaret), three densities (D_1 : ~70 D_2 :~250 and D_3 :~510) and two nitrogen treatments (N_+ , N_0). The maximum number of axes per plant varied from 4.7 to 13.4 and the number ear varied from 1.4 to 5. The number of ear depended principally on plant density ($P<0.001$), cultivar ($P<0.01$) and N treatment ($P<0.01$).

The pattern of decrease of the number of active axes per square meter was captured by fitting equation Eqn T4.4 using data from eight of the nine available treatments that is excluding the low density treatment from E5. The parameters α and β were adjusted by minimising the difference between the normalized number of active axes observed and simulated on this eight treatments. The result of the fit is presented in **figure11** and the values obtained for θ and δ are respectively 3.32 and 1.77 with an RMSE of 0.10.

In the low density treatment, the start of tiller mortality was correctly predicted from the relation with final leaf number but mortality started with a low rate and the end of tiller mortality occurred 150°Cd after the ligulation of the flag leaf of the main stem.

The good overall behaviour of the parametrisation of tillering dynamics, at the exception of low density treatment, is illustrated in **figure12** that presents the observed and simulated dynamics of active axes for two treatments from experiment E4 and E8.

4. DISCUSSION

In this study we used a large dataset to analyse how to parameterise the development of wheat plants with the objective to formalize stable patterns that can be used to minimize the amount of measurements required to simulate a plot with structural plant models, while keeping sufficient plasticity so the model can be fitted to a wide range of situations.

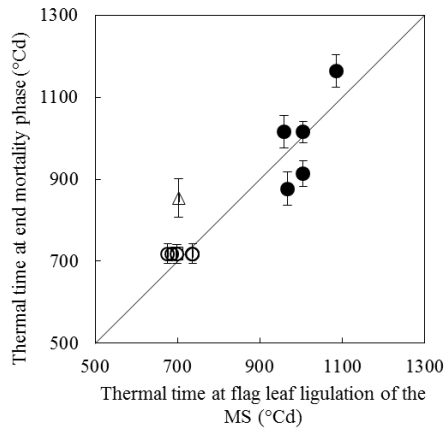


Figure 10: The thermal time at end mortality of tillers (τ_{SM}) vs. the thermal time at flag leaf ligulation of the main stem. Symbols show the mean values observed on the 9 treatments from experiments E4, E5 and E8 covering three sowing densities (D_1 : Δ , D_2 : \circ , \bullet , D_3 : \square), four cultivars ('Soissons', 'Caphorn', 'Maxwell' and 'Minaret') and two nitrogen treatments (N_+ , N_0). Black Symbols refer to values observed on winter wheat cultivars and empty circles represent data of spring wheat cultivar. Error bars mark the 95% confidence intervals of mean estimates and the dotted line represents the line 1:1.

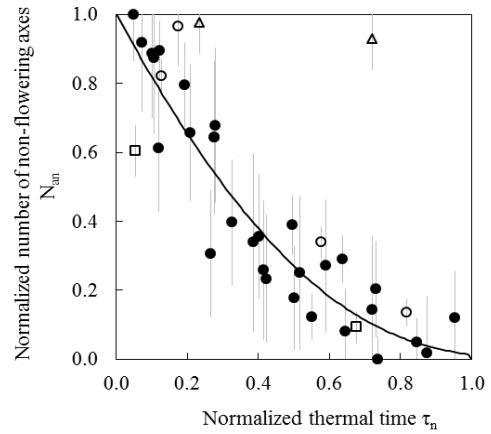


Figure 11: Normalized number of sterile axes (N_{an}) vs. normalized thermal time for nine treatments of winter (full symbol) and spring (empty symbol) wheat corresponding to experiments E4, E5 and E8. Circles represent the mean value measured in each treatment at different times covering three densities (D_1 : Δ , D_2 : \circ , \bullet , D_3 : \square). The triangles show the Soissons N_+ treatment with low density (D_1 : ~ 70) from E5, this treatment was excluded for the fit. The line represents the fitted function (Eqn T4.4). Thermal time is normalized so that $\tau_n=0$ at the start tiller mortality and $\tau_n=1$ at the end tiller mortality. The number of sterile axes N_{an} is normalized so that it is 1 at the plateau of tillering and zero at flowering.

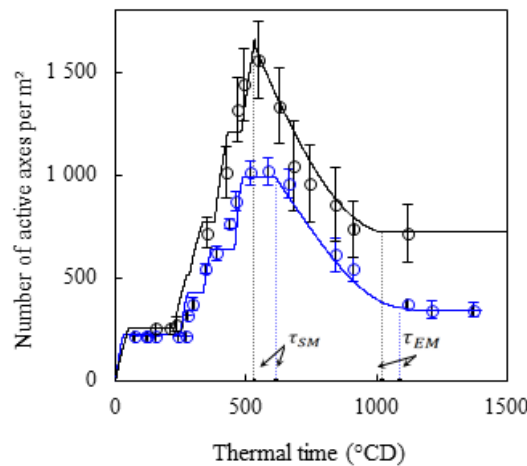


Figure 12: Number of active axes per square meter vs. thermal time from crop emergence for two cultivars of winter wheat. In black cv Soissons grown at density 257p/m² (experiment E4, N_+) and in blue cv 'Maxwell' grown at density 220 p/m² (experiments E8, N_+). Circles represent the mean values measured on 15 plants for experiment E3 and 60 plants for experiment E6. Error bars show the confidence intervals. Lines represent the fitted models. Dotted lines represent respectively the thermal time at the start and the end of tiller mortality phase (τ_{SM} ; τ_{EM}).

1.1. Haun stage progress

Main source of change in phyllochron was sowing date, as reported by various authors. We observed that phyllochron may remain constant during plant development or may change, even for a same genotype. Such changes have been reported by various authors (Cao and Moss, 1991; Calderini *et al.*, 1996; Miralles *et al.*, 2001; Slafer and Rawson, 1997; Miralles and Richards, 2000; Baker *et al.*, 1986; Boone *et al.*, 1990; Hay and Delecolle, 1989) but generally they used air temperature to calculate sum of temperature, so that it has been proposed that such changes may reflect artefact due to the difference between the temperature measured and that sensed by the plants (Jamieson *et al.*, 1995). In our case we used soil temperature when apex was below ground level and air temperature after the start of stem extension so that such artefact did not exist. The Haun stage at the moment of change of phyllochron was correlated with the final leaf number, suggesting a link with phase change at the apex. Changes in phyllochron were most clear for early sowing dates, when plants had 12 leaves or more and in that case the phyllochron at later stage was lower than at early stages. Within a same crop, we observed generally a range of one or rarely two in the total number of leaves produced by main stem of different plants. We consistently observed that the time of flag leaf ligulation was delayed by approximately 21 °Cd per additional main stem leaf, meaning that the phyllochron was significantly reduced in axes with higher leaf number.

We found that significant differences in phyllochron and time of flag leaf ligulation may exist between main stem and tillers, which confirm the variability of results reported in the literature. Here also flag leaf ligulation of early tillers (T₁, T₂) was most frequently only slightly delayed compared to main stem, whereas later tillers were more delayed, but there were significant departures to that frame. Interestingly, such variability in behaviour could be found even for a same genotype, depending on the experiments, so that these differences seem to depend on growth conditions. Finally this justifies that the moment of lag leaf ligulation of tillers is taken as an input if a precise description of tiller development is required. For tillers that die before completing their development, we found negligible difference in their rate of development excepted for the last leaf to emerge. This is consistent with the few data published (Davidson and Chevalier, 1990).

1.2. Final leaf number

In our experiments, the final leaf number of main stems varied with sowing date and to a limited but significant extent, with density. In our work, the final leaf number of the main stem is a key information that is crucial in the parametrisation of others aspects (e.g. start and end of tiller mortality phase) so that we have chosen to directly measure it. In our treatments, difference of one or rarely two leaves could be found between plants of a same plot. A stable relation was found, independently of the treatment, between the final number of leaves of main stem and that of successive tillers, as reported for many species. This decrease was in average 0.6 leaf per higher tiller position, that is less than the previously reported value of one (Masle-Meynard and Sebillotte, 1981b). A value of one would be expected from a perfect synchrony in phyllochron and in floral transition between main stem and tillers. A likely cause for the lower value observed would be a delay in floral transition between successive

tillers, which is consistent with the observed trend of a delay in flag leaf ligulation and in flowering for tillers at higher position.

1.3. Tillering

Our analysis of tiller dynamics followed the scheme in four phases proposed by [Alzueta *et al.* \(2012\)](#): a phase of tiller emergence, a plateau in the number of active tillers, a phase of mortality and a plateau after the final number of reproductive tiller is reached. We did not attempt to predict maximum number of tillers and the number of ears per plant, that are highly dependent on growth condition, but rather to better characterize each phase and to investigate whether the dynamics of tiller population could be simulated from a limited number of measurements, that are the frequency of appearance of primary tillers and the final number of ears.

The phase of tiller emergence is frequently described as the number of tillers following a Fibonacci series ([Porter, 1985](#); [Boone *et al.*, 1990](#); [Miralles and Richards, 2000](#)), assuming from a perfect synchronisation of tiller emergence with leaf emergence, and a probability of appearance independent of tiller position. In our experiments, tiller emergence occurred at stable values of main stem Haun stage, but the interval between emergences of successive tillers did not correspond exactly to one phyllochron. Instead, the delay between successive tillers increased linearly with higher tiller position. This increase was very stable over all treatments and cultivars and our estimates are close to those reported by [Evers *et al.* \(2006\)](#) for spring wheat. A second departure from the classical scheme lied in that the probability of appearance of secondary tillers that were approximately 70% that of primary tillers. This value was derived from a limited number of treatments and is not general, but it suggests that the hypothesis of equal probability may result in significant bias. A count of the total number of tillers at the end of the emergence phase seems required in low density treatments for which the contribution of secondary or higher order tillers is significant.

Given the high coordination of tiller emergence with Haun stage development, the start of the second phase, ie the plateau, is fully defined by the rank of the highest primary tiller that emerges. It has been proposed that cessation of tillering is a response to light quality (red:far-red ratio) rather than to low nutriment availability ([Evers *et al.*, 2006](#); [Alzueta *et al.*, 2012](#)) and that it corresponds to some critical value of LAI reached by the crop, but we did not investigate this hypothesis.

Tiller mortality is often understood as a result of the change in source-sink relations and takes place mostly during stem elongation ([Borràs-Gelonch *et al.*, 2012](#); [Sparkes *et al.*, 2006](#); [Davidson and Chevalier, 1990](#)), however few authors investigated specifically the condition at the onset of tiller mortality and it is not known whether some event specifically triggers the onset mortality phase. [Hay and Kirby \(1991\)](#) reported that the start of mortality phase coincided approximately with terminal spikelet initiation; [Alzueta *et al.* \(2012\)](#) found no correlation between the beginning of tiller mortality and the start of stem elongation and reported that the timing of tiller mortality was independent of nitrogen and sulfur treatments in experiments with both winter wheat and barley cultivars. In our experiments, tiller

mortality started either before (winter cultivars, E3 and E6) or after (spring cultivars, E9) the elongation of the first main stem internode, and showed little relation with sowing density. On the other hand, the Haun stage at the start of mortality phase showed a linear relation with the main stem final leaf number with a high r^2 (0.7 considering all cultivars and treatments pooled together). Finally, this means that the start of the mortality phase could be predicted from final leaf number and the Haun stage model and suggests that ontogeny, rather than sink-source relation, may trigger the beginning of that phase.

[Alzueta *et al.* \(2012\)](#) reported that the number of axes decreased linearly and reached the final ear number at flowering, but the criteria used to identify if a tiller was active or not was not precisely described. In most of our treatments, with the exception of very low sowing densities, the dynamic of the number of active tillers could be quite precisely approximated by considering that the rate of tillering mortality, when normalized by the total number of non-surviving tillers, followed a stable pattern with a rate decreasing from the start of the mortality phase to the ligulation of the flag leaf. This pattern was adjusted by an empirical function (Eqn T4.4). Nevertheless, it will be interesting to check with other data covering different densities and nutrients availability. In low density treatments, the onset of mortality phase was related to the Haun stage as in other treatments, but the period of a high rate of mortality was strongly delayed.

The present study provides a comprehensive view of patterns existing in the architectural dynamics of winter wheat plants. We formalized these patterns in parametric functions that make it possible to represent the dynamics of architecture in structural plant models; The broad range of conditions experimented enabled to clarify the robustness of patterns previously reported and to identify some relations, such as the conditions for the start of mortality, that deserve further attention. Simulating experimental treatments with structural plant models has a large potential to investigate plant-environment interaction, but is hampered by the amount of phenotyping work required to build these models. This study is a step toward reducing the amount of measurements while keeping a high degree of accuracy.

ACKNOWLEDGMENTS

The authors gratefully acknowledge Marc Bidon, Josiane Jean-Jacques, Fabrice Duhamel, Maxime Marques and Rodrigues Julie for their excellent technical assistance in the characterisation of wheat architecture. We thank Jessica Bertheloot, Rim Baccar, Jillian Watt, Jochem Evers and Anne Schneider who made available their data. Mariem Abichou was founded by a CIFRE convention between ARVALIS–Institut du végétal and ANRT. The work was done at INRA, UMR ECOSYS, and was founded by INRA and ARVALIS.

5. LITERATURE CITED

- **Alzueta I, Abeledo LG, Mignone CM, Miralles DJ. 2012.** Differences between wheat and barley in leaf and tillering coordination under contrasting nitrogen and sulfur conditions. *European Journal of Agronomy* **41**:92-102.
- **Baccar R, Fournier C, Dornbusch T, Andrieu B, Gouache D, Robert C. 2011.** Modelling the effect of wheat canopy architecture as affected by sowing density on *Septoria tritici* epidemics using a coupled epidemic-virtual plant model. *Annals of botany* **108**: 1179-1194.
- **Baker CK, Gallagher JN, Monteith JL. 1980.** Daylength change and leaf appearance in winter wheat. *Plant, Cell and Environment* **3**: 285-287.
- **Baker JT, Pinter PJ, Reginato RJ, Kanemasu ET. 1986.** Effects of temperature on leaf appearance in spring and winter wheat cultivars. *Agronomy Journal* **78**: 605-613.
- **Baret F, de Solan B, Lopez-Lozano R, Ma K, Weiss M. 2010** GAI estimates of row crops from downward looking digital photos taken perpendicular to rows at 57.5° zenith angle: Theoretical considerations based on 3D architecture models and application to wheat crops. *Agricultural and Forest Meteorology* **150**:1393-1401
- **Bertheloot J, Andrieu B, Fournier C, Martre P. 2008.** A process-based model to simulate nitrogen distribution in wheat (*Triticum aestivum*) during grain-filling. *Functional Plant Biology* **35**: 781-796.
- **Boone MYL, Rickman RW, Whisler FD. 1990.** Leaf appearance rates of two winter wheat cultivars under high carbon dioxide conditions. *Agronomy Journal* **82**: 718-724.
- **Borràs-Gelonch G, Rebetzke GJ, Richards RA, Romagosa I. 2012.** Genetic control of duration of pre-anthesis phases in wheat (*Triticum aestivum* L.) and relationships to leaf appearance, tillering, and dry matter accumulation. *Journal of Experimental Botany* **63** : 69-89.
- **Cao WX, Moss DN. 1991.** Phyllochron change in winter wheat with planting date and environmental changes. *Agronomy Journal*, **83**: 396-401.
- **Chelle M, Andrieu B. 1998.** The nested radiosity model for the distribution of light within plant canopies. *Ecological Modelling* **111**: 75-9.
- **Davidson DJ and Chevalier PM. 1990.** Preanthesis tiller mortality in spring wheat. *Crop Science* **30**: 832-836.
- **Evers JB, Vos J, Andrieu B, Struik PC. 2006.** Cessation of tillering in spring wheat in relation to light interception and red:far-red ratio. *Annals of Botany* **97**: 649-658.
- **Evers JB, Vos J, Chelle M, Andrieu B, Fournier C, Struik PC. 2007a.** Simulating the effects of localized red:far-red ratio on tillering in spring wheat (*Triticum aestivum*) using a three-dimensional virtual plant model. *New Phytology* **176**: 325-336.
- **Evers JB, Vos J, Fournier C, Andrieu B, Chelle M, Struik PC. 2007b.** An architectural model of spring wheat: evaluation of the effects of population density and shading on model cohort parameterisation and performance. *Ecological Modelling* **200**: 308-320.
- **Fournier C, Andrieu B, Ljutovac S, Saint-Jean S. 2003.** ADEL-wheat: A 3D architectural model of wheat development. In: Hu BG, Jaeger M. eds. *Plant Growth Modelling and Applications*, Proceedings of 2003 International Symposium on plant growth modelling, simulation, visualization and their applications. Tsinghua University Press: Springer Verlag, Beijing, China: 54-63.
- **Friend DJC. 1965** Tillering and leaf production in wheat as affected by temperature and light intensity. *Canadian Journal of Botany* **43**:1063-1076.
- **Gallagher JN. 1979.** Field studies of cereal leaf growth. I. Initiation and expansion in relation to temperature and ontogeny. *Journal of Experimental Botany* **30**: 625-636.

- **Haun J. 1973.** Visual quantification of wheat development. *Agronomy Journal* **65**: 116-119.
- **Hay RKM, Delecolle R. 1989.** The setting of rates of development of wheat plants at crop emergence: influence of the environment on rates of leaf appearance. *Annals of Applied Biology* **115**: 333-341.
- **Hay RKM, Kirby EJM. 1991.** Convergence and synchrony-a review of the coordination of development in wheat. *Australian Journal of Agricultural Research* **42**: 661-700.
- **Jamieson PD, Brooking IR, Porter JR, Wilson DR. 1995.** Prediction of leaf appearance in wheat: a question of temperature. *Field Crops Research* **41**: 35-44.
- **Kirby EJM, Appleyard M, Fellowes G. 1985a.** Effect of sowing date and variety on main shoot leaf emergence and number of leaves of barley and wheat. *Agronomie* **5**: 117-126.
- **Kirby EJM, Appleyard M, Fellowes G. 1985b.** Leaf emergence and tillering in barley and wheat. *Agronomie* **5**: 193-200.
- **Kirby EJM. 1992.** A field study of the number of main shoot leaves in wheat in relation to vernalization and photoperiod. *Journal of Agricultural Science* **118**: 271-278.
- **Kirby EJM. 1993.** Effect of sowing depth on seedling emergence, growth and development in barley and wheat. *Field Crops Research* **39**: 101-111.
- **Kirby EJM, Siddique KHM, Perry MW, Kaesehagen D, Stern WR. 1989.** Variation in spikelet initiation and ear development of old and modern Australian wheat varieties. *Field Crops Research* **20**: 113-128.
- **Klepper B, Rickman RW, Peterson CM. 1982.** Quantitative characterization of vegetative development in small cereal grains. *Agronomy Journal* **74**:789-792
- **Ljutovac S. 2002.** Coordination dans l'extension des organes aériens et conséquences pour les relations entre les dimensions finales des organes chez le blé. PhD Thesis, Institut National Agronomique Paris-Grignon, Paris, France.
- **Masle-Meynard J, Sebillotte M. 1981a.** Étude de l'hétérogénéité d'un peuplement de blé d'hiver. I.-Notion de structure du peuplement. *Agronomie* **1**: 207-216.
- **Masle-Meynard J, Sebillotte M. 1981b.** Étude de l'hétérogénéité d'un peuplement de blé d'hiver. II. Origine des différentes catégories d'individus du peuplement; éléments de description de sa structure. *Agronomie* **1**: 217-224.
- **Masle J., 1985.** Competition among tillers in winter wheat: consequences for growth and development of the crop. In *Wheat growth and modelling* (pp. 33-54). Springer US.
- **Masle-Meynard J. 1982.** Elaboration du nombre d'épis d'un peuplement de blé d'hiver en situation de compétition pour l'azote. II. Modélisation du nombre d'épis. *Agronomie* **2**:17-24.
- **Matsuba K. 1988.** Morphological studies on the regularity of shoots development in rice plants. II. Regularity in tillering termination and the maximum number of tillers. *Japanese Journal of Crop Science* **57**: 599-607.
- **McMaster GS, Smika DE. 1988.** Estimation and evaluation of winter wheat phenology in the central Great Plains. *Agricultural and Forest Meteorology* **43**: 1-18.
- **Miglietta F. 1989.** Effect of photoperiod and temperature on leaf initiation rates in wheat (*Triticum* spp.). *Field Crops Research* **21**: 121-130.
- **Miglietta F. 1991.** Simulation of wheat ontogenesis. II. Predicting dates of ear emergence and main stem final leaf number. *Climate Research* **1**: 151-160.

- **Miralles DJ, Richards RA. 2000.** Responses of leaf and tiller emergence and primordium initiation in wheat and barley to interchanged photoperiod. *Annals of Botany* **85**: 655-663.
- **Miralles DJ, Ferro BC, Slafer GA. 2001.** Developmental responses to sowing date in wheat, barley and rapeseed. *Field Crops Research* **71**: 211-223.
- **Porter JR. 1985.** Approaches to modelling canopy development in wheat. In: Day W, Atkin RK. eds *Wheat growth and modelling*. Plenum Press: New York, 69-81.
- **Rawson H.M. 1971.** Tillering patterns in wheat with special reference to the shoot at the coleoptile node. *Australian Journal of Biological Sciences* **24**:829-841.
- **Robert C, Fournier C, Andrieu B, Ney B. 2008.** Coupling a 3D virtual wheat (*Triticum aestivum*) plant model with a *Septoria tritici* epidemic model (Septo3D): a new approach to investigate plant-pathogen interactions linked to canopy architecture. *Functional Plant Biology* **35**: 997-1013.
- **Saint-Jean S, Kerhornou B, Derbali F, Leconte M, de Vallavieille-Pope C, Huber L. 2008.** Role of rain-splash in the progress of *Septoria* leaf blotch within a winter wheat variety mixture. *Aspects of Applied Biology* **89**: 49–54.
- **Slafer GA, Rawson HM. 1995.** Development in wheat as affected by timing and length of exposure to long photoperiod. *Journal of Experimental Botany* **46**: 1877-1886.
- **Slafer GA, Rawson HM. 1997.** Phyllochron in wheat as affected by photoperiod under two temperature regimes. *Australian Journal of Plant Physiology* **24**: 151-158.
- **Sparkes DL, Holme SJ, Gaju O. 2006.** Does light quality initiate tiller death in wheat? *European Journal of Agronomy* **24**: 212–217.
- **Spink JH, Semere T, Sparkes DL, Whaley JM, Foulkes MJ, Clare RW, Scott RK. 2000.** Effect of sowing date on the optimum plant density of winter wheat. *Annals of Applied Biology* **137**: 179-188.
- **Vos J. 2010.** Functional-structural plant modelling: a new versatile tool in crop science. *Journal of Experimental Botany* **61**: 2101-2115.
- **Whaley JM, Sparkes DL, Foulkes MJ, Spink JH, Semere T, Scott RK. 2000.** The physiological response of winter wheat to reductions in plant density. *Annals of Applied Biology* **137**: 165-177.

6. APPENDIX

list of notations and Abbreviations

Symbols	Explanation	status	Unit
MS	Main stem	Abbreviation	-
T_i	Tiller rank i	Abbreviation	-
n	The number of ligulated leaves at a given time	Abbreviation	-
l, L	The exposed and the final length of the blade	Abbreviation	cm
σ_i	Delay in thermal time at flag ligulation between MS and a primary tiller T_i	Abbreviation	°Cd
N_c^{Ti}	Cohort number of a tiller T_i (e.g. $N_c^{T0} = 3$ and $N_c^{T1} = 4$;see Table2)	Abbreviation	-
$HS(\tau)$	Haun stage at thermal time (τ)	Output variable of HS model	-
τ_s	The time when the last leaf of a sterile tiller ligulates	Internal variable of HS model	°Cd
τ_0^{Ti}	Thermal time at the emergence of the tiller T_i	Internal variable of HS model	°Cd
a^{Ti}	The rate of leaf appearance of tiller i for the HS linear model	Parameter of HS model	(°Cd) ⁻¹
a_1^{MS}, a_2^{MS}	The first and second rate of leaf appearance of the main stem for the HS bilinear model	Parameter of HS model	(°Cd) ⁻¹
a_1^{Ti}, a_2^{Ti}	The first and second rate of leaf appearance of a tiller T_i for the HS bilinear model	Parameter of HS model	(°Cd) ⁻¹
$HS_{brk}^{MS}, HS_{brk}^{Ti}$	Haun stage at the break point of the main stem and a tiller T_i	Parameter of HS model	-
τ_{brk}	Thermal time of the break point for the HS bilinear model	Parameter of HS model	°Cd
τ_0^{MS}	Thermal time at the emergence of the main stem	Parameter of HS model	°Cd
$\tau_{flg}^{MS}, \tau_{flg}^{Ti}$	Thermal time of flag leaf ligulation of the main stem and tiller T_i	Parameter of HS model	°Cd
N_l^{MS}	Final number of phytomers of the main stem	Parameter of HS model and Input variable of N_l model	-

N_l^{Ti}	Final number of phytomers of a fertile tiller T_i	Parameter of HS model Output variable of N_l model	-
$N_l^{Ti.st}$	Final number of phytomers of a sterile tiller T_i	Parameter of HS model and Output variable of tillering model	-
$HS^{MS}(\tau_0^{Ti})$	The haun stage of the main stem at the emergence of tiller T_i	Constant of HS model	-
f	See equation Eqn T3.6b	Constant of HS model	%
α, β	See equation Eqn T3.5	Constant of N_l model	-
N_a	Number of active axes per square meter	Output variable of tillering model	-
N_a^{max}	The number of axes (MS and tillers) at the plateau of tillering	Output variable of tillering model	-
$P(T_{ij})$	The probabilities of emergence of secondary tiller T_{ij} (see Table2 for tillers nomenclature)	Output variable of tillering model	%
N_p	Plant number per square meter	Input variable of tillering model	plt.m ⁻²
N_e	Ear number per square meter	Input variable of tillering model	ear.m ⁻²
N_{an}	The normalized number of sterile axes; N_{an} is 1 at the plateau of tillering and 0 at flowering	Internal variable of tillering model	-
$\tau_{SM}; \tau_{EM}$	Thermal time at the start and the end of the tiller mortality phase	Internal variable of tillering model	°Cd
τ_n	The normalized thermal time during the phase of tiller mortality. It is 0 at the start of mortality phase and 1 at the end of mortality phase.	Internal variable of tillering model	-
$P(T_i)$	The probabilities of emergence of primary tiller	Parameters of tillering model	%
$k, \rho, \mu, \delta, \theta$	See equations Eqn T4.1-4	Constants of tillering model	-

7. SUPPLEMENTARY DATA

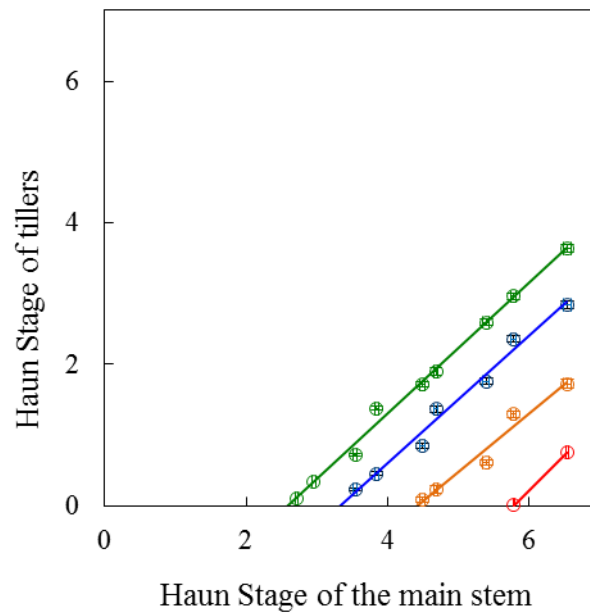


Figure S1: Haun stage of tillers vs. Haun stage of the main stem for winter wheat *cv.* 'Maxwell' at density 220 p/m² sown in late October (experiment E8, N₊). Symbols show the mean values for tiller 1 (green), tiller 2 in (blue), tiller 3 (orange) and tiller 4 (red). Lines show the linear models adjusted. Error bars mark the 95% confidence intervals of mean estimates.

Supplementary Table S1: Information relative to the parameters of the Haun stage model fitted for each treatment with: (i) the experiment number, (ii) *T. aestivum* cultivars, (iii) sowing date: S₁ late September, S₂ mid to late October, S₃ mid-November (the date is given in brackets); (iv) sowing density: D₁ low, D₂ normal, D₃ high, (v) nitrogen treatments (N₊: optimal, N₀: no N given); (vi) inter-row spacing (I_S: 17.5 cm, I_D: 35 cm); (vii) the frequent final leaf number of the main stems N_l^{MS} (frequency is given in brackets); (viii) the Haun stage model applied having a lower AIC (L for linear and BL for bilinear); (ix) the phyllochron of the first phase before the break point if there is one ($\frac{1}{a1^{MS}}$, unit : °Cd); (x) the phyllochron of the second phase after the break point if there is one ($\frac{1}{a2^{MS}}$, unit : °Cd); (xi) the thermal time at emergence of plant (τ_0^{MS} , unit: °Cd); (xii) the thermal time at the break point (τ_{brk} , unit: °Cd); (xiii) the thermal time at flag ligulation of the main stem (τ_{flg}^{MS} , unit: °Cd); (xiv) the thermal time from emergence to flag ligulation ($\tau_{flg}^{MS} - \tau_0^{MS}$), unit : °Cd ; (xv) the root mean square error (RMSE) calculated between simulated and the observed values (observed values represent the mean value of the N_l^{MS} group) and (xvi) the number of Haun stage measurement used for the fit (n.mes), it represent the number of dates of field measurements.

Exp.	Cv.	Sowing date	Density	Nitrogen	Inter-row	N_l^{MS} (freq.)	HS model	$\frac{1}{a1^{MS}}$	$\frac{1}{a2^{MS}}$	τ_0^{MS}	τ_{brk}	τ_{flg}^{MS}	HS_{brk}^{MS}	$\tau_{flg}^{MS} - \tau_0^{MS}$	RMSE	n.mes
E1	‘Soissons’	S ₂	D ₂	N ₊	I _S	11 (0.8)	L	110	NA	0	NA	1213		1213	NA	12
		S ₂	D ₁	N ₊	I _S	12 (0.8)	L	97	NA	0	NA	1164		1164	NA	12
E4	‘Caphorn’	S ₂	D ₂	N ₊	I _S	12 (0.87)	L	84	NA	0	NA	1005		1005	0.19	17
		S ₂	D ₂	N ₀	I _S	11 (0.60)	L	88	NA	37	NA	1006		969	0.24	19
E6	‘Soissons’	S ₂	D ₂	N ₊	I _S	11 (0.60)	L	88	NA	4	NA	967		963	0.16	16
			D ₂	N ₀	I _S	11 (0.67)	L	87	NA	0	NA	959		959	0.16	18
		S ₁	D ₁	N ₊	I _S	14 (0.86)	BL	89	123	20	376	1603	4.0	1583	0.18	19
			D ₂	N ₊	I _S	13 (0.80)	BL	93	132	8	367	1568	3.9	1560	0.21	19
			D ₃	N ₊	I _S	13 (0.64)	BL	94	135	5	373	1605	3.9	1600	0.15	18
			D ₁	N ₊	I _S	10 (0.94)	BL	161	95	-17	331	1077	2.2	1094	0.12	10
S ₃	D ₂	N ₊	I _S	10 (0.79)	BL	153	97	-9	318	1077	2.1	1086	0.11	10		
	D ₃	N ₊	I _S	10 (0.95)	BL	159	99	-25	323	1096	2.2	1120	0.15	16		
E7	‘Soissons’	S ₁	D ₁	N ₊	I _S	14 (0.67)	L	115	NA	-18	-18	1589		1607	0.38	17
			D ₃	N ₊	I _S	13 (0.88)	L	121	NA	-18	-18	1557		1575	0.30	19
		S ₃	D ₁	N ₊	I _S	10 (0.54)	BL	77	104	130	394	1076	3.4	946	0.07	16
			D ₂	N ₊	I _S	10 (0.72)	BL	74	104	136	362	1085	3.1	949	0.10	16
			D ₃	N ₊	I _S	9 (0.79)	L	115	NA	43	43	1074		1032	0.07	18
E8	‘Maxwell’	S ₂	D ₂	N ₊	I _S	11 (0.82)	L	99	NA	0	0	1086		1086	0.07	23
E9	‘Apache’	S ₂	D ₂	N ₊	I _D	11(0.50)	L	95	NA	136	NA	1180		1044	0.27	5
		S ₂	D ₂	N ₊	I _S	10 (0.70)	L	103	NA	136	NA	1165		1029	0.02	6
	‘Caphorn’	S ₂	D ₂	N ₊	I _D	11 (0.80)	L	96	NA	126	NA	1178		1051	0.08	5
		S ₂	D ₂	N ₊	I _S	11 (0.60)	L	95	NA	126	NA	1174		1048	0.22	6
	‘Maxwell’	S ₂	D ₂	N ₊	I _D	11 (0.40)	L	98	NA	130	NA	1213		1083	0.10	4
		S ₂	D ₂	N ₊	I _S	11 (0.70)	L	100	NA	132	NA	1233		1100	0.05	6

E10	'Renan'	S ₂	D ₂	N ₊	I _D	11 (0.60)	L	95	NA	125	NA	1165	1040	0.21	5
		S ₂	D ₂	N ₊	I _S	11 (0.90)	L	97	NA	128	NA	1193	1065	0.02	6
	'Soissons'	S ₂	D ₂	N ₊	I _D	12 (0.70)	L	88	NA	117	NA	1175	1058	0.18	5
		S ₂	D ₂	N ₊	I _S	11 (0.70)	L	92	NA	122	NA	1138	1016	0.11	5
	'Apache'	S ₃	D ₁	N ₊	I _S	11 (0.81)	L	106	NA	3	NA	1171	1168	0.28	15
	'Caphorn'	S ₃	D ₁	N ₊	I _S	12 (0.87)	L	97	NA	0	NA	1166	1166	0.20	15
		S ₃	D ₂	N ₊	I _S	11 (0.69)	L	108	NA	-6	NA	1177	1183	0.24	15
	'Renan'	S ₃	D ₁	N ₊	I _S	12 (0.5)	L	96	NA	29	NA	1175	1147	0.17	15

Supplementary Table S2: Haun stage of the main stem at the emergence of a tiller T_i ($HS^{MS}(\tau_0^{Ti})$) estimated on 16 treatments from experiments E3 to E6 that covering three cultivars ('Soissons', 'Caphorn', 'Maxwell') sowing in different dates (S₁ late September, S₂ mid to late October, S₃ mid-November), under different densities (D₁ low, D₂ normal, D₃ high) and with or without nitrogen fertilization (N₊: optimal, N₀: no N given).

Exp.	Cultivar	Sowing date	Density	Nitrogen	$HS^{MS}(\tau_0^{Ti})$ for each tiller rank				
					T ₁	T ₂	T ₃	T ₄	T ₅
E4	'Caphorn'	S ₂	D ₂	N ₀	2.01	3.24	4.34	5.12	
			D ₂	N ₊	2.36	3.44	4.27	5.38	
E6	'Soissons'	S ₂	D ₂	N ₀	2.48	3.13	4.46	5.45	
			D ₂	N ₊	2.57	3.22	4.04	5.32	
		S ₁	D ₁	N ₊	2.62	3.28	4.41	5.70	6.67
			D ₂	N ₊	2.30	2.97	4.17	5.67	
			D ₃	N ₊	2.58	3.33	4.37		
		S ₃	D ₁	N ₊		3.69	4.40	5.92	
			D ₂	N ₊		3.25	4.38	5.56	
E7	'Soissons'	S ₃	D ₃	N ₊		2.63	3.69		
			D ₁	N ₊	2.47	3.12	4.03	5.64	7.15
		S ₁	D ₃	N ₊	2.22	3.20			
			D ₁	N ₊		3.27	4.35	5.37	
		S ₃	D ₂	N ₊	2.69	3.28	4.08	5.11	
			D ₃	N ₊	2.67	3.36			
E8	'Maxwell'	S ₂	D ₂	N ₊	2.52	3.42	4.56	5.81	
			<i>Mean of estimated values of $HS^{MS}(\tau_0^{Ti})$</i>					2.46	3.24
<i>Number of treatments</i>					12	16	14	12	2
<i>Standard deviation</i>					0.20	0.23	0.23	0.26	0.34
<i>Confidence interval (95%)</i>					0.11	0.11	0.12	0.15	0.47

Supplementary Table S3: Number of axes per plant at the plateau of tillering (N_a^{\max}), for 19 treatments of winter wheat with: (i) the experiment number (E3, E6, E7 and E8), (ii) *T. aestivum* cultivars, (iii) sowing date: S_2 mid to late October; (iv) sowing density: D_1 low (70 plt.m⁻²), D_2 normal (200-250 plt.m⁻²) (v) nitrogen treatments (N_+ : optimal, N_0 : no N given); (vi) inter-row spacing (I_S : 17.5cm, I_D : 35 cm); (v) measured mean value of N_a^{\max} ; (vi) number of plant measured; (vii) the confidence intervals (95%); (viii) simulated value of N_a^{\max} considering that probability of emergence of a high order tiller equals to that of the primary tiller of the same cohort ($k=1$; Eq. 8); (ix) simulated value of N_a^{\max} considering a probability of emergence of high order tillers lower than that of primary tillers of the same cohort ($k=0.60$; Eq. 8)

Exp.	Cultivar	Sowing date	Density	Nitrogen	Inter-row	Measured N_a^{\max}			Simulated N_a^{\max}	Simulated N_a^{\max}
						mean	n.plant	CI	($k=1$)	($k=0.60$)
E3	Minaret	S_4	D_2	N_0	I_S	8		0.54	7.40	6.38
	Minaret	S_4	D_2	N_+	I_S	9.3		0.21	11.50	9.07
	Minaret	S_4	D_3	N_+	I_S	5.7		0.40	6.50	5.72
	Minaret	S_4	D_1	N_+	I_S	13.4		0.78	20.20	14.12
E4	Caphorn	S_2	D_2	N_0	I_S	6.33	15	0.65	7.00	6.22
	Soissons	S_2	D_2	N_0	I_S	5.87	15	0.83	6.40	5.75
	Soissons	S_2	D_2	N_+	I_S	6.53	15	0.57	7.20	6.37
	Caphorn	S_2	D_2	N_+	I_S	6.33	15	0.31	7.80	6.84
E8	Maxwell	S_2	D_2	N_+	I_S	4.75	60	0.38	4.63	4.33
E9	Renan	S_2	D_2	N_+	I_D	3.83	30	0.23	4.51	4.19
	Renan	S_2	D_2	N_+	I_S	4.13	30	0.16	4.89	4.50
	Soissons	S_2	D_2	N_+	I_D	4.64	30	0.18	6.05	5.34
	Soissons	S_2	D_2	N_+	I_S	5.78	30	0.20	6.50	5.77
	Caphorn	S_2	D_2	N_+	I_D	3.38	30	0.19	3.82	3.61
	Caphorn	S_2	D_2	N_+	I_S	3.96	30	0.20	4.47	4.17
	Apache	S_2	D_2	N_+	I_D	3.88	30	0.13	4.26	3.97
	Apache	S_2	D_2	N_+	I_S	4.09	30	0.22	4.46	4.16
	Maxwell	S_2	D_2	N_+	I_D	3.75	30	0.17	4.28	3.99
	Maxwell	S_2	D_2	N_+	I_S	4.35	30	0.24	4.61	4.28
E10	Caphorn	S_2	D_2	N_+	I_S	3.13	16	0.50	3.51	3.38
	Apache	S_2	D_1	N_+	I_S	6.38	16	1.25	7.29	6.24
	Caphorn	S_2	D_1	N_+	I_S	7.06	16	1.34	7.50	6.50
	'Renan'	S_2	D_1	N_+	I_S	8.80	16	1.54	10.47	8.60



CHAPTER 2: Parametrizing final organ dimensions and leaf senescence of winter wheat plants

This chapter is the base of a journal paper by:

Mariam Abichou, Tino Dornbusch, Camille Chambon, Benoit de Solan, Bruno Andrieu

RESUME

Contexte et objectifs. Les modèles structuraux 3D des plantes visent à simuler « *in silico* » le développement des plantes, isolées ou en peuplement, en se fondant sur la caractérisation expérimentale des traits d'architecture. Ces modèles peuvent être couplés avec des modèles physiques pour étudier comment la structure des plantes module leurs interactions avec l'environnement. Dans le chapitre 1 nous avons analysé comment représenter le développement des axes par des fonctions paramétriques. Ce travail complète le précédent par l'analyse des dimensions des organes matures et de la sénescence foliaire au sein de l'architecture.

Méthodes. Une large base de données décrivant les propriétés de chaque phytomère de plantes de blé a été collectée et analysée. Les données représentent 34 traitements expérimentaux, avec une gamme de cultivars, plusieurs années climatiques, des conditions contrastées en termes de date et densité de semis et fertilisation azotée. Sur la base de l'analyse de ces données, nous avons étudié comment décrire les patterns de dimension ainsi que l'évolution du nombre de feuilles vertes et sénescentes au cours du temps.

Résultats. La séquence de dimensions des organes successifs sur le brin maître présente une forte dépendance aux conditions de croissance, ce qui nous a conduit à représenter explicitement cette séquence plutôt que d'en rechercher une représentation paramétrique. Nous avons alors précisé les conditions de validité du concept de « numéro relatif de phytomère » pour déduire les dimensions des organes sur les talles à partir de celles sur le brin maître, en considérant un « shift décimal » dont la valeur dépend de la position botanique de la talle. Nous montrons que cette approche permet de bien estimer les longueurs des limbes, gaines et entrenœuds pour les phytomères supérieurs. En outre des valeurs de « shift » uniques ont pu être prises en compte : identiques pour ces trois composants du phytomère et indépendantes des conditions de croissances ou du cultivar. La méthode toutefois ne convient pas pour les premiers phytomères des talles, portés par des entrenœuds courts. Elle ne permet pas non plus d'estimer les largeurs des limbes et les diamètres des gaines et des entrenœuds. Pour ces dimensions, nous avons établi des formulations qui remplacent ou complètent l'utilisation de la notion de phytomère relatif.

Nous avons analysé la cinétique du nombre de feuille verte (G_l) le long des différents axes de la plante. Sur l'ensemble de nos traitements, cette cinétique suit un même pattern avec des moments de rupture qui correspondent à des stades du développement de la plante et n'apparaissent pas dépendre des conditions de croissance. Nous montrons que les talles suivent une dynamique analogue à celle du brin maître. Ces observations ont permis de définir un ensemble de fonctions paramétriques pour représenter la dynamique de sénescence au sein de l'architecture avec des paramètres qui ont une interprétation simple et qui peuvent être estimés avec un effort expérimental raisonnable

Conclusion. Cette étude fournit une vue synthétique des patterns caractérisant les dimensions finales des organes et la dynamique de sénescence au sein de l'architecture d'une plante de blé. Les fonctions paramétriques permettent de les représenter dans des modèles architecturés à partir de caractérisation expérimentales portant principalement sur le brin maître.

Mots clés. Sénescence, dimension, longueur, largeur, diamètre, limbe, gaine, entrenœud, blé.

ABSTRACT

Background and Aims. 3D structural models of plants are designed to simulate "*in silico*" the development of plants or plant populations, based on the experimental characterization of architectural features. These models can be coupled with physical models to study how plant structure modulates the interactions with the environment. In chapter 1, we presented how to represent the development of plant axes by parametric functions. This work complements the previous by analysing the size of mature organs and the progress of leaf senescence over the crop cycle.

Methods. A large database describing the properties of each phytomer of wheat plants was collected and analysed. Data represent 34 experimental treatments, with a range of cultivars, several climatic years, and contrasting conditions in terms of sowing date, seed density and nitrogen fertilization. Based on the analysis of these data, we studied how to describe the dimension of patterns and the evolution of the number of green and senescent leaves over time.

Key Results. The sequence of the dimension of successive organs on the main stem has a high dependency to the growth conditions, which led us to explicitly represent this sequence rather than define a parametric representation. Then, we specified the conditions of validity of the concept of "relative phytomer number" used to derive the dimensions of all tillers organs from that of the main stem, assuming a "decimal shift value" that depends on the botanical position the tiller. We show that this approach can properly estimate the lengths of blades, sheaths and internodes for upper phytomers. Moreover, unique values of "shift" could be used, identical for these three components of phytomer and independent from growth conditions and cultivars. However, the method is not suitable for the first phytomers of tillers, ie those having short internodes. It does not allow either to estimate the widths of blades and the diameters of sheaths and internodes. For these dimensions, we could establish formulations that substitute to or complement the use of the relative phytomer concept.

We analysed also the kinetic of the green leaf number along the different plant axes. On all our treatments, this kinetic follows the same pattern with break points corresponding to precise stages of plant development that didn't show dependency to growing conditions. We show that tillers follow patterns similar to those of the main stem. These analyses have led to identify a set of parametric functions that represent the dynamics of leaf senescence, with parameters that have a simple interpretation and can be estimated with a reasonable experimental effort.

Conclusions. This study provides an overview of the patterns characterizing the final dimensions of organs and the senescence dynamics describing the architecture of wheat plants. These parametric functions could be used in SPM models using experimental measurements focusing on main stem.

Keywords. Senescence, dimension, length, width, diameter, blade, sheath, internode, wheat.

1. INTRODUCTION

Structural 3D plant models, interfaced with physical models, are increasingly used to investigate how the structure of plants modulates their interactions with the environment (Saint-Jean *et al.*, 2008; Robert *et al.*, 2008; Evers *et al.*, 2007). Important efforts are required to obtain faithful description of individual plant organ that represent the traits produced by specific experimental conditions. In a previous paper (Abichou *et al.*, 2016), we described a parametrisation of the dynamics of leaf and tiller appearances that can be used to drive the dynamics of appearance of phytomers of wheat plants. To get a complete description of the plant structure, in this work, we present a parametrisation of the size of mature phytomers and their lifespan. Together with the previous work, the aim is to provide a reconstruction of the dynamics of the architecture of plants during the full crop cycle, with sufficient flexibility so that it can be fitted to a wide range of situations, while parameters are easy to measure and having a clear botanical interpretation. In the following sections, we present an overview of the state of knowledge concerning the pattern of final dimension of phytomers and the dynamic of leaf senescence; and then we specify our objectives concerning each aspect.

1.1. Pattern of final dimension of phytomers

A grass plant is composed of axes, with a main stem and tillers. Each axis is composed of phytomers which are in turn composed of blades, sheaths, internodes and buds. To analyse the pattern of final size of phytomers, it is useful to consider two aspects: (i) pattern along an axis (over phytomer ranks), and (ii) pattern among axes (over tiller ranks).

Patterns along an axe

Several factors contribute to shape the size of the phytomer that build an axe:

A main source of patterning is the ontogenic changes that occur during plant life. In wheat as in other cereals, lower phytomers are characterized by non-elongated internodes and short blade. Upper phytomers have elongated internodes and longer blade. Internal changes connected with the floral transition are responsible for these differences (Dwyer and Steward, 1986; Borrill, 1959; Kirby and Faris, 1972; Gallagher, 1979). Another major ontogenic feature is the decrease in size occurring for the topmost blade, the rank of the longest blade is at some position below the flag leaf, frequently one rank below but sometimes more in wheat. This reduction in length has sometime been interpreted as resulting from competition for resources with the growing ear; on the other hand Andrieu *et al.* (2006) presented evidences in favour of a developmental control reducing the duration of extension of upper blades.

A second source of modulation is the environmental conditions (light and temperature) and the availability of resources such as water and nitrogen. Seasonal trends and the increasing competition between plants during crop development contribute to shape the pattern of size of successive phytomers, with variability linked to the specific environmental conditions (Hotsonname and Hunt, 1997; Dornbusch *et al.*, 2011).

Finally a third source of patterning is the “whorl size effect”. Each leaf first grows within the pseudostem cylinder (whorl) made by sheaths of previously emerged leaves (Klepper *et al.*, 1982). The length of this whorl impacts the size of the growth zone - and ultimately the mature size - of the leaves that grows within. The size of the whorl also determines when the growing leaf starts perceiving external stimuli. Finally the whorl can be seen as a

“dimensional reference system” that produces slightly longer sheaths and blades compared to it resulting in an increase in length with increasing phytomer ranks (Fiorani *et al.*, 2000; Arredondo and Schnyder, 2003; Yu *et al.*, 1975; Fournier, 2000; Ljutovac, 2002; Davies *et al.*, 1983; Wilson and Laidlaw, 1985; Casey *et al.*, 1999). Such “size reference system” also modulates how stresses impact leaf size, buffering the impact of short stress while propagating the impact of longer stresses even to phytomers that grow after the period of stress (Louarn *et al.*, 2010). Changes in dimension over phytomer ranks are gradual, with high correlations between the sizes of successive phytomers (Evers *et al.*, 2005). These correlations result from the whorl effect described above and also from the similarity in the environment perceived, as there is a large recovering in the periods of growth of successive phytomers. These correlations however vanish as the distance – in terms of position on the stem – increases. Dornbusch *et al.* (2011) observed that the size of adult leaves of winter wheat showed very little correlation with that of juvenile leaves. Fournier *et al.* (2003) parametrized the pattern of size along the shoot in winter wheat for blades, sheaths and internodes, using broken line functions, in which the break points related to ontogenetic change, and parameters allow to adapt the size to cultivar and growth conditions. The model of Fournier *et al.* (2003) produced realistic patterns that are frequently found, but showed limits to simulate a wide range of conditions (personnel communication).

Similarities between axes

Tillers of grass species present high similarities in their morphology with the main stem and, from a botanical perspective, can be seen as reiterates of the main stem (Mouliat, 1999). From an ecophysiological perspective, these similarities can be expected as the processes that build the axes are the same, and take place in similar conditions. A tiller emerges in the same whorl as the axillary leaf, so that whorl effect propagates to it; besides, the synchrony of emergence of the tiller leaves with those of the main stem implies that they undergo the same environmental conditions (Friend, 1965; Masle-Meynard and Sebillotte, 1981; Klepper, 1982; Masle, 1985; Kirby, 1993). Finally, convergence in floral development between main stem and tillers results in similarities in the ontogenetic component of the patterning (Evers *et al.*, 2005).

In wheat, rice and barley, several authors observed that the size of upper phytomers of tillers matched nearly exactly that of main stem phytomers when a shift (depending on tiller position) was added to their phytomer rank (Fournier *et al.* 2003; Evers *et al.* 2005; Tivet *et al.* 2001). The values calculated for the shift of a tiller were equal to the difference in leaf number between main stem and the tiller. Thus the method amounts to consider that, when counting basipetally from the topmost phytomer, the sequence of size of phytomers is the same on all axes (Kemp, 1981; Tivet *et al.*, 2001). Other authors considered a decimal value for the shift, which was fit to ensure the best match of dimensional patterns on all axes (Fournier *et al.*, 2003; Evers *et al.*, 2005; Vos *et al.*, 2010, Tivet *et al.*, 2001). The use of a decimal value makes sense if one considers that the delay between leaf emergence and tiller emergence increases is not constant but increases slightly with successive phytomer ranks (Abichou *et al.*, 2016).

Finally the use of a decimal phytomer shift to derive the length of upper phytomer of tillers is simple, generic of over a range of species and proved to be accurate in the conditions in which it was tested. The questions that we will address here is whether it works for a broad range of

growth conditions, and for other dimensions than length and how to address the case of the lower phytomers.

1.2. Dynamic of leaf senescence

We define here senescence as the irreversible change of state of tissues from turgid to necrotic and dried. The senescence is the ultimate fate of all photosynthetic tissues (blades, sheaths and internodes) and depends on regulations that are only partly understood (Lim *et al.*, 2007; Thomas and Stoddart, 1980). In cereals, the senescence progresses within plant architecture following an acropetal order and our aim was to describe the kinetics of this progress with a flexible and parsimonious parametrization. Our work focussed on blades, which represent most of green tissues.

When a leaf senesces, the necrotic area progresses from the tip to the base of blade. McMaster *et al.* (1991) proposed a model in which this progress occurs over one phyllochron, and leaves senesce in an acropetal sequence in which the completion of senescence at one rank coincides with the start of senescence on the rank above. In this view there is only one leaf senescing at any time and the life span is the same at all phytomer positions. Hillier *et al.*, 2007 and Baccar *et al.*, 2011 reported a more complex behavior in which the sequence described by McMaster *et al.* (1991) occurs for the lower phytomers but the progress of senescence is slower for leaves on elongated internodes, resulting in a progressively longer life span and a significant overlap in the senescence of upper leaves. An interesting outcome of their study was that senescence of successive blades are highly coordinated so that the progress of the senescence of individual leaves can be deduced from the progress of the (decimal) number of senesced leaves on the shoot.

1.3. Objectives

In this work, we focussed on establishing parametric functions that: (i) define the final dimensions (length and width/diameter) of phytomer components (blade, sheath and internode) for all leaf ranks and all tiller ranks from those of the main stem, and (ii) describe the progress with thermal time of the green leaf number (G_l) for both main stem and tillers. We aim to define parametrisations that were valid for a wide range of cultivars and growth conditions and could be adjusted using a reduced number of parameters mostly estimated from main stem measurements.

2. MATERIALS AND METHODS

A large experimental dataset of winter wheat crop (*Triticum aestivum* L.) that describes properties of individual plant phytomers were collected and analysed. This dataset includes experimental data from published works (see reference in **Table 1**) and data acquired for this study. This dataset was used to define and evaluate the models for final dimension and for senescence. Our general approach consisted to identify similarities between main stem and tillers in order to define parametrization with most parameters estimated from main stem measurements. We will not present the exploratory work that led us to define the parametrizations: we will describe the choices that we made, and that will be evaluated in the result section. As a prerequisite, we suppose that dynamic of the Haun stage of all axes (MS

and tillers), their final leaf number (N_1^{MS}, N_1^{Ti}) and most dimensions of the main stem phytomers are known. In this work, the Haun stage and the final leaf number of all axes were measured for the main stem and estimated for tillers following [Abichou *et al.* \(2016\)](#). We identified tillers as follow: T_i is the primary tiller emerging in the axil of leaf i . Tillers of various orders that emerge at the same time as main stem leaf are grouped by cohorts N_c . All variables and model parameters are listed in the appendix.

2.1. Experiments and measurements

The dataset includes eight experiments conducted between 1998/1999 and 2013/2014, thus including various meteorological sequences. Experiments ([Table 1](#)) are numbered E1 to E8 and correspond to those presented in [Abichou *et al.* \(2016\)](#). Most experiments were conducted in field conditions, at the INRA campus of Thiverval-Grignon (48°51 N, 1°58 E), with a maritime influenced climate and a deep loamy soil allowing high yields from winter annual crops. Beside, one experiment (E8) was conducted in outdoors containers. Plots of experiments E1 to E7 consisted of nine rows with an inter-row distance of 0.175 m; besides, five treatments in E7 had an inter-row distance of 0.35 m; plot length varied between experiments, with a minimum of 8 meters. In experiment (E8), five outdoors containers (length 1.82m; width 1.12m; depth 1.2m) were placed next to each other and each container included ten rows with an inter-row distance of 0.175 m. Altogether, experiments represented 34 treatments, with 11 commercial winter wheat cultivars, three plant population densities, three sowing dates and two nitrogen-fertilization. Plant population density is referred to as low density (D1, ~70p/m²), normal density (D2, ~250p/m²), or high density (D3, ~500p/m²). Sowing dates are referred as early sowing (S1, late September) normal sowing (S2, mid to late October), late sowing (S3, mid-November). N-fertilization followed the standard scheme with one dose between late February and early March and one dose brought early to mid-April, except in the N0 treatments from experiment E3, where no N was supplied. Air temperature at 2 m was recorded hourly from a nearby meteorological station and soil temperature at 3 cm depth was monitored in the experimental plots. The apex temperature was assumed to be soil temperature before stem extension and then air temperature. The thermal time τ was computed from plant emergence, on an hourly basis, assuming a linear response to temperature with a base temperature of 0°.

The dimensions of mature phytomers on both main stems and primary tillers were measured on 17 treatments from experiments E1-E6. These treatments included ten cultivars, three sowing dates, three densities and two levels of fertilization (see [Table 1](#)). For each axis, the length and maximum width of blades, and the length and diameter of sheaths and internodes were measured. Four to six samplings per treatment were carried out during the crop cycle. In each sampling, 15 to 60 tagged plants were collected and their dimensions were measured with a ruler or by image processing of scans. Leaf senescence was monitored for nine treatments, covering five genotypes, one sowing date (S2), two densities (D₁ and D₂) and two levels of fertilization (N₊, N₀). Senescence was measured on the main stem in the nine treatments (E3, E6, E8) and on primary tillers in five treatments (E3 and E6).

Table 1: information relative to experimental datasets from E1 to E8 with: (i) growing season; (ii) reference of experiment; (iii) *Triticum aestivum* cultivars; (iv) sowing date: S₁ late September, S₂ mid to late October, S₃ mid-November (the date is given in brackets); (v) sowing density: D₁ low, D₂, normal, D₃ high (number of plants per m⁻² are given in brackets); (vi) nitrogen treatments (N₊: optimal, N₀: no N given); (vii) inter-row spacing (I_S: 17.5cm, I_D: 35 cm); (viii) growth regulators treatments (doses are given in brackets), (ix) the variables analysed (see appendix for the definition of the variables); (x) the axes measured (MS: main stem; T_i: primary tillers) ;(xi) the reference for published work in literature by the author group for further experimental details.

Year	Exp.	Cv	Sowing date (jj mm)	Density (pl.m ⁻²)	N.trt	Inter -row	Gr. (1.ha ⁻¹)	Variables analysed	Axes measured	Reference
98/99	E1	Soissons	S ₂ (15 Oct.)	D₁(70), D₂(250)	N ₊	I _S	Gr ₀ (0)	- L _b , L _S , L _i , W _b , D _i	MS and T _i	Ljutovac (2002)
03/04	E2	Soissons, Caphorn, Apache, Arminda, Isengrain, Thésée, Oratorio, Recital, Florance	S ₂ (16 Oct.)	D ₂ (250)	N ₊	I _S	Gr ₊ (1.5)	- L _b , L _S , L _i , W _b	MS and T _i	Watt et al. (2013)
04/05	E3	Soissons, Caphorn	S ₂ (27 Oct.)	D ₂ (250)	N₊, N₀	I _S	Gr ₊ (2.0)	- L _b , L _S , L _i , W _b , D _S , D _i - G _l (τ)	MS and T _i MS and T _i	Bertheloot et al. (2008)
07/08	E4	Soissons	S ₁ (25 Sep.),	D ₂ (228),	N ₊	I _S	Gr ₊ (2.0)	- L _b , L _S , L _i , W _b	MS	Baccar et al. (2011)
08/09	E5	Soissons	S ₃ (17 Nov.)	D₁(77), D₂(228), D₃(514)	N ₊	I _S	Gr ₊ (2.0)	- L _b , L _S , L _i , W _b , D _S , D _i	MS and T _i	Baccar et al. (2011)
10/11	E6	Maxwell	S ₂ (26 Oct.)	D ₂ (220)	N ₊	I _S	Gr ₀ (0)	- L _b , L _S , L _i , W _b , D _S , D _i - G _l (τ)	MS and T _i MS and T _i	
12/13	E7	Maxwell, Soissons, Caphorn, Apache, Renan	S ₂ (02 Oct.)	D ₂ (220)	N ₊	I_S, I_D	Gr ₀ (0)	- L _b , L _S , L _i , W _b , D _S	MS	
13/14	E8	Caphorn, Apache, Renan Caphorn	S ₂ (3 Nov.)	D ₁ (70), D ₂ (200)	N ₊	I _S	Gr ₀ (0)	- L _b , W _b - G _l (τ)	MS MS	

Between 15 and 60 tagged plants per treatment were tagged and the green and total length of all ligulated leaves plus the emerged length of the growing leaf were measured at weekly intervals. We computed the green leaf number G_l^{axis} and the Haun stage HS^{axis} of each axis using equations (Eqn.1) and (Eqn.2). The difference $HS^{axis} - G_l^{axis}$ represents the fractional number of senescent leaves, S_l^{axis} (Eqn.3).

$$HS^{axis}(\tau) = n_l + \frac{l_e^{n_l+1}}{L_f^{n_l+1}} \quad (\text{Eqn. 1})$$

$$G_l^{axis}(\tau) = \sum_{x=1}^{n_l+1} \frac{L_g^x}{L_f^x} \quad (\text{Eqn. 2})$$

$$S_l^{axis}(\tau) = HS^{axis}(\tau) - G_l^{axis}(\tau) \quad (\text{Eqn. 3})$$

Where n_l is the number of ligulated blades on an axis at thermal time τ ; l_e and L_f are the length of the non ligulated leaf (n_l+1) at thermal time τ and after ligulation; l_f^x and L_g^x are the total length and the green length of a blade x at thermal time τ .

2.2. Sub-model of the final dimensions of phytomers

A set of parametric functions were defined to describe the dimensions of mature phytomers for all plant axes from those of main stem. These parametric functions describe the length of blades L_b , sheaths L_s , internodes L_i , the maximum width of blades W_b , the diameter of sheaths D_s and the diameter of internodes D_i . The final leaf number of the main stem N_l^{MS} is supposed to be measured and those of tillers N_l^{Ti} are estimated following [Abichou et al. \(2016\)](#).

We defined continuous functions to fit the measured dimensions of main stem phytomers vs phytomer position. Even if all dimensions are known, fitting a continuous function is required to estimate the shift between main stem and tillers; besides, it allow for interpolating in case some values are missing for the main stem. We used ‘‘ad hoc’’ functions, with a sufficient degree of freedom so that they could be fitted without notable deviation from measured data. Equations that describe these functions are presented in [Table 2](#). Excepted when specified below, parameters were fitted independently for each treatment.

- For length of blades, sheath and internode, we used a polynomial function of order 4 (Eqn T2.1, Eqn T2.2, Eqn T2.3).
- For width of blades, we used a polynomial function of order 3 (Eqn T2.4).
- For diameter of internodes, we used a polynomial function of order 2 (Eqn T2.6). Here a fixed shape was considered so that only one parameter, ie d_{i2} , the mean diameter of elongated internodes is fitted for each treatment.
- For diameters of sheaths, we used a linear-plateau function, in which the break point corresponds to the position of the lower elongated internode (Eqn T2.5ab). The diameter of sheath 1, d_{s1} is considered as constant so only one parameter, d_{s2} , representing the diameter for sheaths of upper phytomers for each treatment is fitted for each treatment.

To describe the dimensions of the mature phytomers of a given tiller, we consider two aspects their cohort number and their state (fertile or sterile). We assume that:

- All fertile axes (producing ears) of the same cohort N_c have the same pattern of phytomer dimension. We derived the dimensions of the phytomers of all fertile tillers from that of the main stem by applying the concept of “shifted phytomer number”. This concept is presented below.
- All sterile axes (that die before producing ears) have reduced area for all their leaves compared to fertile tillers of the same cohort N_c . The reduction concerns both the length and width or diameter of phytomers with constants reduction factors: k_l^{st} for length and k_w^{st} for width (Eqn T2.13 to Eqn T2.18). So, we estimate the dimensions of sterile tillers from that of fertile tillers.

As a general approach, we assume that patterns of dimensions of fertile tillers follow the same pattern as main stem, once the concept of “shifted phytomer number” was used. This concept is used to estimate most dimensions ($L_b^{Ti}, L_s^{Ti}, L_i^{Ti}, D_s^{Ti}, D_i^{Ti}$), except the maximum width of blades W_b^{Ti} for which the use of the shift was not suitable. The shifts values were estimated separately for each dimension (blades length, sheaths length and internodes length). The adjustment of the shifts values s^{Ti} was made by minimizing the RMSE on the 17 treatments (from experiments E1-E3, E5 and E6).

For the lengths patterns of blades, sheaths and of internodes ($L_b^{Ti}, L_s^{Ti}, L_i^{Ti}$), we applied the same polynomial functions as the main stem (Eqn T2.7b, Eqn T2.8, Eqn T2.9). An exception was made on the length of tiller blades of early leaves that have a non-elongated internode. For these leaves, we suppose that their pattern increases linearly from the first emerged leaf (l_{b1}) to the first leaf of the main stem having an elongated internode ($L_b^{MS}(r)$) (Eqn T2.7a, **Fig1**). We suppose that the length of the first leaves of all the tillers (l_{b1}) are constants. The length of the leaf having the first elongated internode is deduced from the function of the main stem (Eqn T2.1).

For the diameters of sheaths and internodes of tillers (D_s^{Ti}, D_i^{Ti}), we suppose that they follow reduced patterns compared to that of the main stem. A reduction factor (k^o) depending to the relative position of the tiller in the plant was used (Eqn T2.11, Eqn T2.12)

For the maximum blade width of tillers (W_b^{Ti}), as mentioned above, the use of shifts was not suitable. The blade width pattern is different to that of the main stem. It follows a linear model from the first leaf to the flag leaf (Eqn T2.10). We suppose that the first leaf on a tiller $W_b^{Ti}(1)$ is reduced compared to that of the main stem $W_b^{MS}(1)$ and a reduction factor k_w is applied; and so on for the flag leaf. The value of the reduction factor k_w was adjusted on the 17 treatments by minimizing the RMSE of the W_b^{Ti} model.

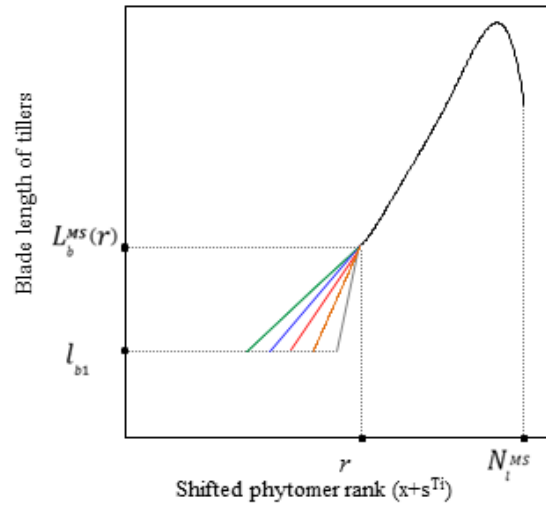


Figure 1: Representation of the parametrization of the blade length of tillers vs. shifted phytomer rank. The black line represents the pattern of upper leaves common to all tillers ranks and the main stem. The coloured lines represent the pattern of lower leaves with non-elongated internodes, which differs between tillers: green for T_1 , blue for T_2 , red for T_3 , orange for T_4 , and grey for T_5 .

Table 2: Equations defining the final dimension of blades, sheaths and internodes.

Axis	phytomer dimension	Equations	Phytomer rank interval	N° of Eqn
Main stem	blade length	$L_b^{MS}(\mathbf{x}) = \sum_{k=0}^4 b_k * (\mathbf{x})^k$	$r - 1 \leq x \leq N_l^{MS}$	T2.1
	sheath length	$L_s^{MS}(\mathbf{x}) = \sum_{k=0}^4 s_k * (\mathbf{x})^k$	$1 \leq x \leq N_l^{MS}$	T2.2
	internode length	$L_i^{MS}(\mathbf{x}) = \sum_{k=0}^4 i_k * (\mathbf{x})^k$	$r - 1 \leq x \leq N_l^{MS}$	T2.3
	maximum blade width	$W_b^{MS}(\mathbf{x}) = \sum_{k=0}^3 d_k * (\mathbf{x})^k$	$1 \leq x \leq N_l^{MS}$	T2.4
	sheath diameter	$D_s^{MS}(\mathbf{x}) = \frac{d_{s2} - d_{s1}}{r - 1} * (\mathbf{x} - 1) + d_{s1}$	$1 \leq x \leq r$	T2.5a
		$D_s^{MS}(\mathbf{x}) = d_{s2}$	$r < x \leq N_l^{MS}$	T2.5b
	internode diameter	$D_i^{MS}(\mathbf{x}) = d_{i2} * \sum_{k=0}^2 c_k * \left(\frac{\mathbf{x}}{N_l^{MS}}\right)^k$	$r < x \leq N_l^{MS}$	T2.6
Fertile tiller	blade length	$L_b^{Ti}(\mathbf{x}) = \frac{L_b^{MS}(r) - l_{b1}}{(r - s^{Ti}) - 1} * (\mathbf{x} - 1) + l_{b1}$	$1 \leq x < r - s^{Ti}$	T2.7a
		$L_b^{Ti}(\mathbf{x}) = L_b^{MS}(\mathbf{x} - s^{Ti})$	$r - s^{Ti} \leq x \leq N_l^{Ti}$	T2.7b
	sheath length	$L_s^{Ti}(\mathbf{x}) = L_s^{MS}(\mathbf{x} - s^{Ti})$	$1 \leq x \leq N_l^{Ti}$	T2.8
	internode length	$L_i^{Ti}(\mathbf{x}) = L_i^{MS}(\mathbf{x} - s^{Ti})$	$r - s^{Ti} \leq x \leq N_l^{Ti}$	T2.9
	maximum blade width	$W_b^{Ti}(\mathbf{x}) = \frac{k_w * (w_{bflg}^{MS} - w_{b1}^{MS})}{N_l^{Ti} - 1} * (\mathbf{x} - 1) + k_w * w_{b1}^{MS}$	$1 \leq x \leq N_l^{Ti}$	T2.10
	sheath diameter	$D_s^{Ti}(\mathbf{x}) = k^o * D_s^{MS}(\mathbf{x} - s^{Ti}) ;$	$1 \leq x \leq N_l^{Ti}$	T2.11
	internode diameter	$D_i^{Ti}(\mathbf{x}) = k^o * D_i^{MS}(\mathbf{x} - s^{Ti}) ;$	$r - s^{Ti} \leq x < N_l^{Ti}$	T2.12
Sterile tiller	blade length	$L_b^{Ti.st}(\mathbf{x}) = k_l^{st} * L_b^{Ti}(\mathbf{x})$	$1 \leq x \leq N_l^{Ti.st}$	T2.13
	sheath length	$L_s^{Ti.st}(\mathbf{x}) = k_l^{st} * L_s^{Ti}(\mathbf{x})$	$1 \leq x \leq N_l^{Ti.st}$	T2.14
	internode length	$L_i^{Ti.st}(\mathbf{x}) = k_l^{st} * L_i^{Ti}(\mathbf{x})$	$1 \leq x \leq N_l^{Ti.st}$	T2.15
	maximum blade width	$W_b^{Ti.st}(\mathbf{x}) = k_w^{st} * W_b^{Ti}(\mathbf{x})$	$1 \leq x \leq N_l^{Ti.st}$	T2.16
	sheath diameter	$D_s^{Ti.st}(\mathbf{x}) = k_w^{st} * D_s^{Ti}(\mathbf{x})$	$1 \leq x \leq N_l^{Ti.st}$	T2.17
	internode diameter	$D_i^{Ti.st}(\mathbf{x}) = k_w^{st} * D_i^{Ti}(\mathbf{x})$	$1 \leq x \leq N_l^{Ti.st}$	T2.18

2.3. Sub-model of the green leaf number

The parameterisation of the dynamics of the green leaf number G_l was first defined for main stems; then we analysed how it could be transposed to tillers. Below we present successively the two cases.

For the main stem, the green leaf number G_l^{MS} showed a pattern with four phases, illustrated in **figure 2a**. The four phases are as follow (**Table 3**):

- **(ϕ_1)**: a phase in which G_l^{MS} is equal to the Haun stage HS^{MS} since senescence has not begun (Eqn T3.1);
- **(ϕ_2)**: a phase in which G_l^{MS} decreases linearly from the moment of start senescence (τ_1^{MS}, g_1^{MS}) to the ligulation of the leaf ($N_l^{MS} - 4$), i.e. the fourth leaf from the top (τ_2^{MS}, g_2^{MS}) (Eqn T3.2);
- **(ϕ_3)**: a phase in which the G_l^{MS} increases linearly from (τ_2^{MS}, g_2^{MS}) to reach a maximum at the ligulation of the flag leaf (τ_3^{MS}, g_3^{MS}) (Eqn T3.3);
- **(ϕ_4)**: a phase in which the G_l^{MS} decreases following a polynomial pattern until the full senescence at τ_4^{MS} corresponding to the monocarpic senescence (Eqn T3.4).

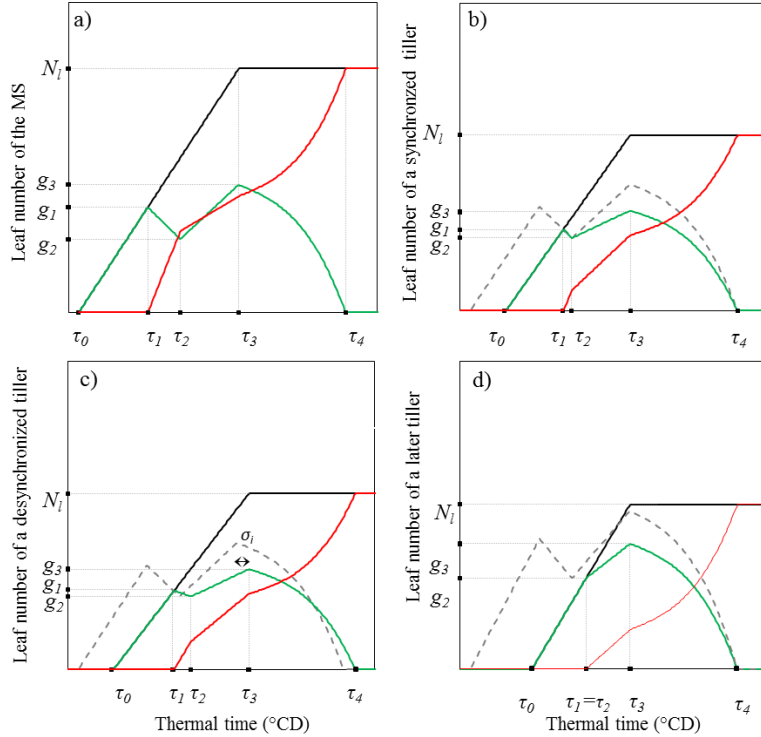
For tillers, we assume that all axes of a same cohort N_c follow the same dynamics of green leaf number G_l^{Ti} . We assume that the progress of senescence S_l^{Ti} of tillers is independent of their fates (flowering or regressing). For early tillers, green leaf number follows four phases similar to that of the main stem (**Fig. 2b,c**). For late tillers, they are only three phases (**Fig. 2d**) as two phases merge:

- **(ϕ_1)**: a phase in which G_l^{Ti} is equal to the Haun stage HS^{Ti} (Eqn T3.5);
- **(ϕ_2)**: a phase in which the senescence of the tiller progresses linearly. The start of the phase 2 depends to the tiller order. For early tillers (T_1 and T_2), senescence starts when their number of green leaves reaches that of the main stem (**Fig 2b,c**); the green leaf number G_l^{Ti} decreases during phase 2, to reach the same minimum than the main stem g_2^{MS} . This minimum is reached at ligulation of the fourth leaf from the top τ_2^{Ti} (Eqn T3.6). For later tillers (higher than T_3 or T_4), phase 2 vanishes because HS^{Ti} does not reach G_l^{MS} before stem elongation (**Fig. 2d**); thus late tillers start to senesce during phase 3.
- **(ϕ_3)**: a phase in which the G_l^{Ti} increases linearly to reach a maximum g_3^{Ti} at time τ_3^{Ti} , which is the ligulation the flag leaf. This maximum g_3^{Ti} is supposed to be the same for all tillers but may be lower compared to that of the main stem g_3^{MS} . We note $\partial = g_3^{Ti} / g_3^{MS}$ (Eqn T3.7).
- **(ϕ_4)**: after the ligulation of the flag leaf, the green leaf number of the tiller follows the same pattern than that of the main stem, but scaled by the factor ∂ (Eqn T3.8). If the ligulation of the tiller flag leaf is delayed compared to the main stem, all the phase 4 on tiller is similarly delayed (**Fig 2c**).

As mentioned above, the dynamic Haun stage, the final leaf number and the timing of major events of all axes (MS and tillers) are supposed to be known. Here, the Haun stage progress, the final leaf number N_l and the timing of the major events (e.g. axis emergence " τ_0 ", ligulation of leaves " $\tau_2; \tau_3$ ",) are obtained from the models presented in [Abichou et al. \(2016\)](#).

Table 3: Equations describing the dynamics of green leaf number for main stem and tillers (see Appendix for the definition of each symbol).

Axis	Phase	Equations	Thermal time interval	N° of Eqn
Main stem	φ_1	$G_l^{MS}(\tau) = HS^{MS}(\tau)$	$\tau_0^{MS} \leq \tau \leq \tau_1^{MS}$	T3.1
	φ_2	$G_l^{MS}(\tau) = \frac{(g_2^{MS} - g_1^{MS})(\tau - \tau_1^{MS})}{\tau_2^{MS} - \tau_1^{MS}} + g_1^{MS}$; $HS^{MS}(\tau_2^{MS}) = N_l^{MS} - 4$	$\tau_1^{MS} \leq \tau \leq \tau_2^{MS}$	T3.2
	φ_3	$G_l^{MS}(\tau) = \frac{(g_3^{MS} - g_2^{MS})(\tau - \tau_2^{MS})}{\tau_3^{MS} - \tau_2^{MS}} + g_2^{MS}$	$\tau_2^{MS} \leq \tau \leq \tau_3^{MS}$	T3.3
	φ_4	$G_l^{MS}(\tau) = \alpha(\tau - \tau_3^{MS})^3 + \beta(\tau - \tau_3^{MS}) + g_3^{MS}$	$\tau_3^{MS} \leq \tau \leq \tau_4^{MS}$	T3.4
Tillers	φ_1	$G_l^{Ti}(\tau) = HS^{Ti}(\tau)$	$\tau_0^{Ti} \leq \tau \leq \tau_1^{Ti}$	T3.5
	φ_2	$G_l^{Ti}(\tau) = \frac{(g_2^{Ti} - g_1^{Ti})(\tau - \tau_1^{Ti})}{\tau_2^{Ti} - \tau_1^{Ti}} + g_1^{Ti}$; $HS^{Ti}(\tau_2^{Ti}) = N_l^{Ti} - 4$	$\tau_1^{Ti} < \tau \leq \tau_2^{Ti}$	T3.6
	φ_3	$G_l^{Ti}(\tau) = \frac{(g_3^{Ti} - g_2^{Ti})(\tau - \tau_2^{Ti})}{\tau_3^{Ti} - \tau_2^{Ti}} + g_2^{Ti}$	$\tau_2^{Ti} < \tau \leq \tau_3^{Ti}$	T3.7
	φ_4	$G_l^{Ti}(\tau) = \partial(\alpha(\tau - \tau_3^{Ti})^3 + \beta(\tau - \tau_3^{Ti}) + g_3^{Ti})$; $\tau_3^{Ti} = \tau_3^{MS} + \sigma_i$	$\tau_3^{Ti} < \tau \leq \tau_4^{Ti}$	T3.8


Figure 2: Representation of the parametrization of the green leaf number (G_l) and the senescent leaf number (S_l) vs. thermal time of: the main stem (a), an early tiller senescing before the stem elongation (b), an early tiller for which the ligulation of the flag leaf is delayed compared to that of the main stem (c) a late tiller starting senescing after the stem elongation (d). Black, green and red solid lines represent respectively the Haun stage (HS), the green leaf number (G_l) and the senescent shoot index (S_l). Dotted grey line in figures (b), (c) and (d) represents the green leaf number (G_l) of the main stem. The green leaf number at transition times τ_1 , τ_2 and τ_3 are respectively g_1 , g_2 and g_3 (see appendix for the definition of variables).

The parameters that need to be estimated for the green leaf sub-model are: (i) the thermal time at start senescence of the main stem τ_1^{MS} (ii) the green leaf number at the ligulation of the fourth leaf from the top g_2^{MS} and the flag leaf g_3^{MS} of the main stem (iii) the green leaf number of the main stem at least on two times after flowering and before full senescence (vi) the ratio of green leaf number between tillers and main stem at flowering ∂ , (v) the delay σ_i between ligulation of flag leaf on main stem and on tillers.

2.4. Models adjustment

To measure the deviation between measured and simulated values, we used the root mean squared error (RMSE) or the mean absolute percentage error (MAPE). Model parameters were estimated using fitting methods in R or Excel 2010 solver to minimize MAPE or RMSE.

$$RMSE = \sqrt{\frac{\sum_{j=1}^n (Y_j^{obs} - Y_j^{sim})^2}{n}}; \quad MAPE = \frac{1}{n} \sum_{j=1}^n \frac{|Y_j^{obs} - Y_j^{sim}|}{Y_j^{obs}}$$

3. RESULTS

We will first present the major observations resulting from the analysis of the experimental data and then the evaluation of each sub-model.

3.1. High variability of phytomers dimensions among different conditions

The range of variability observed for the cultivar ‘‘Soissons’’ in term of final dimensions patterns of main stem phytomers are shown in **figure 3**. The figure 3 illustrates data from 15 treatments from experiments E1-E5 and E7, covering three sowing dates (S_1 - S_3), three densities (D_1 - D_3) and two nitrogen treatments (N_+ - N_0). The figure shows the patterns as a function of inversed phytomer rank (computed from the top with the flag leaf being number 1). The final leaf number varied from 8 to 14 leaves.

The typical profile of blade length shows an increase with phytomer rank up to the penultimate leaf blade (or the blade below in some treatments), with the flag leaf being shorter (**Fig.3a**). The typical profile of sheath length shows of slow increase for the lower leaves then a high increase for the elongated leaves (**Fig.3b**). The typical profile of internode length shows an increase from the first elongated phytomer up to the internode of the flag leaf with generally 4 to 5 elongated internodes (**Fig.3c**). The typical profile of maximum blade width shows a pattern similar TO that of sheath length. The sheath diameter shows a complex pattern with a larger diameter this may be explained by the difficulty of the measurement when the ear grows inside the pseudo-stem. The pattern of internode diameter shows an increase for the two first elongated internodes then a quasi-stable diameter for the upper internodes. The variations of phytomer dimensions among environmental condition were higher than that observed among the range of commercial cultivars investigated here (data not shown). For example, the length of the larger phytomer varied among treatments: from 18 to 30 cm for blade and from 14 to 20 cm for sheath.

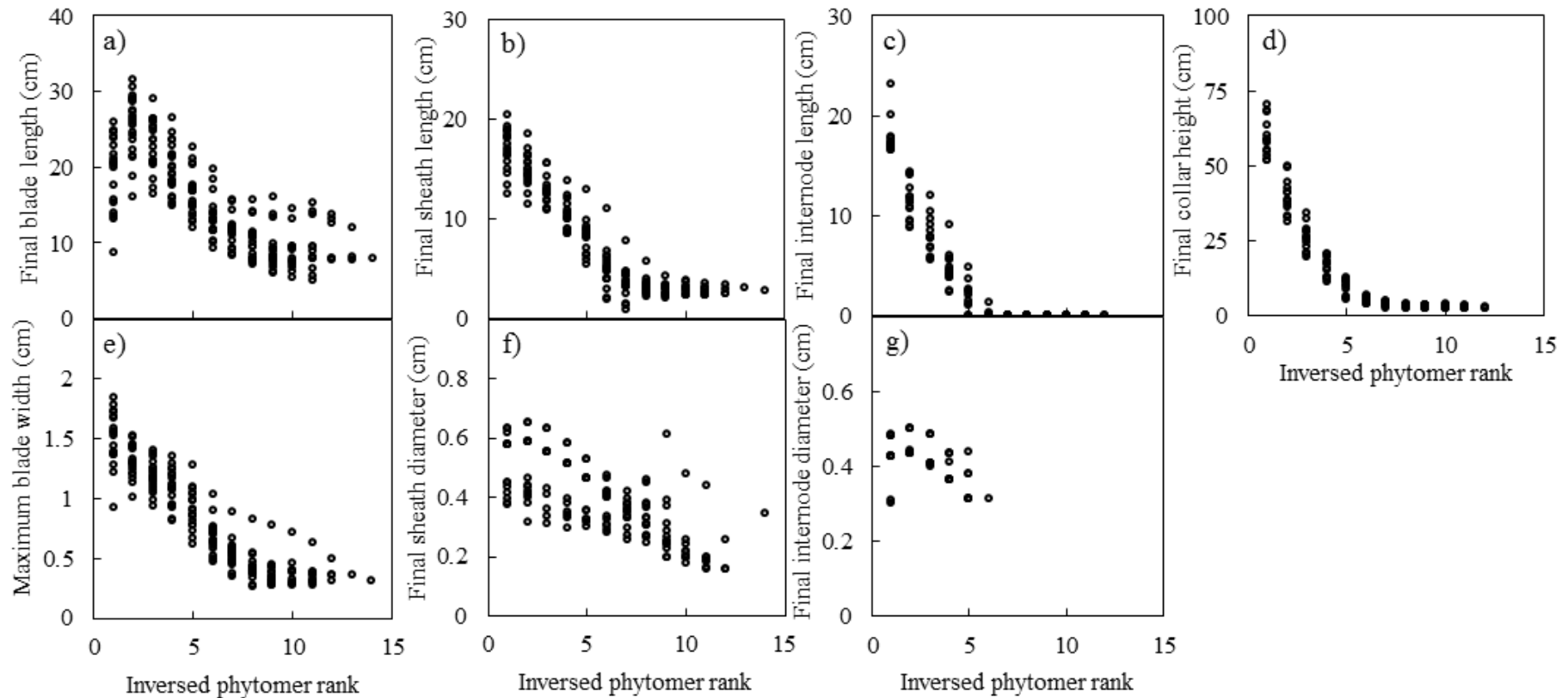


Figure 3: Final dimensions of main stem phytomer vs. the inversed phytomer rank (flag leaf is number 1) of the cultivar “Soissons” growing under different conditions in the Paris region. The figures show 15 treatments from experiments E1-E5 and E7 covering two sowing dates (S_1 - S_3), three densities (D_1 - D_3) and two nitrogen treatments (N_+ , N_0). Figures present: (a) the final length of blade, (b) the final length of sheath, (c) the final length of internode, (d) the final height of collar (distance between the base of axis and the collar of leaf rank x ; the geometry and inclination of the axis are not considered), (e) the maximum width of blade, (f) the diameter of sheath, (g) and the diameter of internode. Each circle represents the mean value of a leaf rank for one treatment.

The correlation between the dimensions of successive phytomers was analysed from 20 treatments from experiments E1-E3 and E5-E8. The dimension of a phytomer was highly correlated to that of the previous phytomer with a global R^2 of 0.9 (for more details see *Fig.S1*). However, the correlation weakened when considering more distant phytomers. For example, the correlation between the penultimate phytomer and the fourth phytomer (counted from the base) was low with respectively an R^2 of 0.3 and 0.04 for blades length and sheaths length (for more details see *Fig.S2*). So, the patterns could not be described using a simple function.

The dimensional patterns of MS varied highly with environmental condition. It seem possible to propose a parametrization of the MS patterns, in that case, at least three measurement dates are needed to the calibration. Three dates are also sufficient to get directly to the dimension on all the MS phytomers so that we preferred to measure directly all dimensions and we used polynomial approximation. This choice ensured a good description of patterns for all treatments and it is useful to estimate by interpolation dimensions if the dimension one or two ranks is missing.

3.2.The dimensions of tiller phytomers: calibration and evaluation of the submodels

Most dimensions of tiller phytomers are derived from that of the main stem after applying the concept of “shifted phytomer rank”. The shift values s^{Ti} of each tiller rank were estimated globally by minimizing the cumulated RMSEs of blade length, sheath length and internode length on the 17 treatments analyzed. The shift values obtained were: 2.76, 3.43, 4.09, 4.59, 4.90 and 5.32 respectively for tiller T1 to T6 (*Fig.S3*).

Results of using the shift values mentioned above for matching the length of blades, sheath and internode on main stem and tillers are exemplified in Figure 8 for two contrasted treatments. Other treatments yield similar results. As shown in Figure 8, the pattern of blades, sheaths and internode lengths per shifted phytomer rank were similar on all axes, except for the length of the lower blades: Blades of lower phytomers in tillers, ie phytomers with non-elongated internodes, were smaller than predicted. On the other hand, the length flag leaf blade on tillers was generally well predicted from the pattern of main stem blade length. This is of special interest as the processes that lead to the shorter flag leaf blade are not understood.

Finally we used the concept of phytomer shift, with the fixed values given above, to estimate length of internodes, sheaths and upper blades on tillers from that on main stem. For blades of lower tiller phytomers, ie those with short internodes, we considered a linear progress of length with phytomer rank (Eqn T2.7a). This progress is fully defined by considering a constant blade length size for the first phytomer, and a blade length equal to that predicted by phytomer shift for the first phytomer with elongated internode.

Patterns of maximum blade width and of sheath or internode diameter on tillers (W_b^{Ti} , D_s^{Ti} and D_i^{Ti}) presented differences compared to that of the main. The *figure5* shows examples for a selection of treatments. Maximum blade widths on tillers generally increased linearly with phytomer rank (*figure5a*), which was not the case on main stems, so the use of a shift was

not appropriate to derive blade widths of tillers from those of main stem. Instead our parameterization is based on the linear progression of blade width with phytomer rank. Besides the width of the first blade was similar on all axes (*figure6*). The widths of the flag leaves blade of all tillers were similar and ~12% smaller compared to main stem (*figure6*). Consequently, in our parametrization, we used of a constant reduction of flag leaf width of tillers ($k_w=0.88$).

When plotted vs the shifted phytomer rank (*Figure5b,c*), the diameter of sheaths and internodes of the tillers showed patterns similar to that of the main stem, but scaled by a factor k^o depending on the position of the tiller.

The normalized pattern of internode diameter vs shifted phytomer rank was relatively stable in all treatments, and could be fitted by equation T2.6. *Figure7* shows the result of this adjustment.

Table4 summarizes the adjusted values of all constants of the phytomer final dimensions sub-models.

Globally, we observed a good adjustment of our parametrizations of dimensions. The RMSE values for each sub model are presented in the *Table6*. The mean relative error (MAPE) was generally less than 15%, except for sheath diameters.

- Blade area, collar height and sheath diameter define most of the apparent dimensions of an axe so they can be considered as synthetic variables to evaluate the quality of the simulations. A comparison between simulated and measured blade area, collar height and sheath diameter is shown in *figure8*. Blade area and leaf insertion height were generally correctly estimated and the dispersion observed (*Fig.8a,b*) represents few points. Most of them correspond to tillers for which the measured final number of leaf did not match that predicted from the number of main stem leaves. This occurred mainly in cases where there were some uncertainties in identifications of tillers rank and likely was partly due to measurements errors.
- For sheath diameters (Fig. 12 c) the estimates were less accurate. One source of difficulty was that sheath diameter enlarges when the ear grows inside the sheaths and some residual deformation remains after. So an accurate representation of the stem would have required a more complex model than the approximation by a cylinder. On the other hand, Figure 12c shows little bias so that we expect that the approximation is sufficient for most applications. The results of the comparison of the other phytomer dimensions were also acceptable (*Fig.S4*).

The result described above concern fertile tillers. The *figure9* shows a comparison of dimensions (blade length and width and sheath length) between fertile and sterile tillers of the same tiller rank. It illustrates that sterile tillers had smaller leaves compared to fertile tillers of the same cohort with a mean reduction of 20% on blade area.

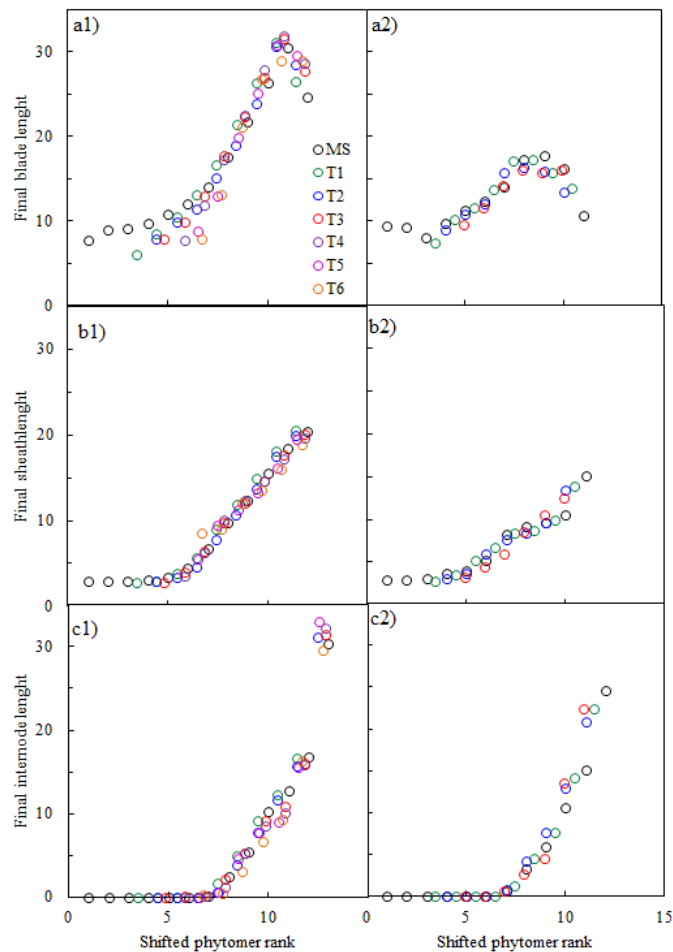


Figure 4: Measured final length of blades (a), of sheaths (b) and internodes (c) vs. shifted phytomer rank. Symbols show the median values observed for two cultivars: “Soissons” (D_1, N_+) from experiment E1 in the left and “Maxwell” (D_2, N_+) from experiment E6 in the right. Each color represents an axis as indicated in figure a1.

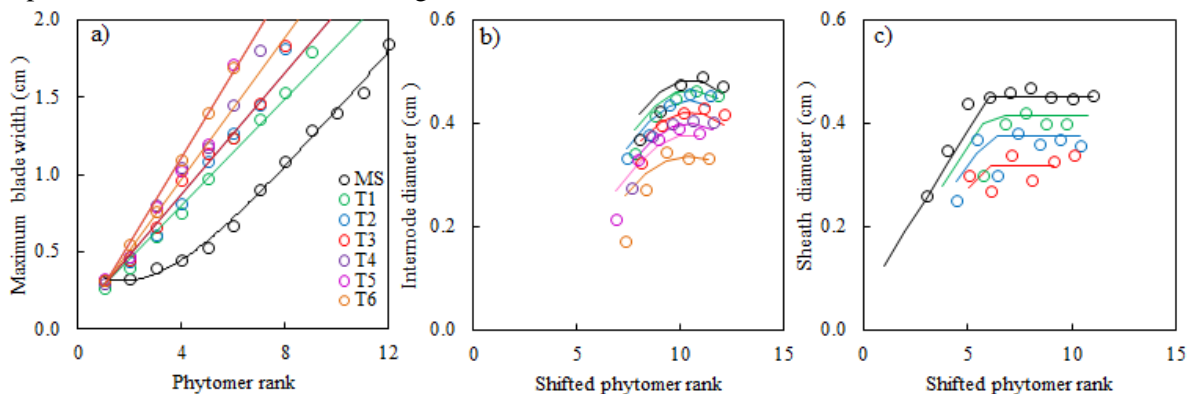


Figure 5: The width or diameter of phytomers of main stem and tillers vs. phytomer rank. Figure a shows the maximum blade width vs. phytomer rank, figure b shows the internode diameter vs. shifted phytomer rank and figure c shows the sheath diameter vs. shifted phytomer rank. Figure a and b show data of cv “Soissons” in experiment E1 (D_1/ N_+); figure c show data of cv Maxwell in experiment E6 (D_2/ N_+). Symbols show the median values observed and the lines represent the fitted model. Each color represents an axis as indicated in fig.a.

Table 4: adjusted values of the constants of the dimensions sub-models and their unit (see appendix for the definition of the constants).

Constant	Value	Unit
s^{T1}	2.755	-
s^{T2}	3.427	-
s^{T3}	4.091	-
s^{T4}	4.588	-
s^{T5}	4.899	-
s^{T6}	5.322	-
l_{b1}	7.023	cm
d_{s1}	0.124	cm
c_2	-0.014	-
c_1	0.290	-
c_0	-0.526	-
ρ_1	-0.265	-
ρ_2	1.007	-
ρ_3	0.702	%
k_w	0.877	%
k_i^{st}	0.885	%
k_w^{st}	0.906	%

Table 5: The root mean square Error (RMSE), the mean absolute percentage error (MAPE) and the number of measurement (n) relative to phytomer dimension sub-models calculated from the 17 treatments from experiments E1-E6.

Variable	RMSE (cm)	MAPE (%)	n
Blade length	3.627	12%	496
Sheath length	3.675	11%	493
Internode length	2.007	16%	306
Maximum Blade width	0.119	13%	335
Sheath diameter	0.067	18%	362
Internode diameter	0.0361	8%	166
Leaf insertion height	4.449	14%	378

Table 6: values of fitted parameter ∂ (Eqn T3.7) defining the reduction of on the green leaf number of tillers at flag ligulation compared to that of the main stem

Exp.	Cv	Sowing date	Density	N.trt	∂
E3	Soissons	S ₂	D ₂	N+	96%
E3	Soissons	S ₂	D ₂	N-	100%
E3	Caphorn	S ₂	D ₂	N+	85%
E3	Caphorn	S ₂	D ₂	N-	96%
E4	Maxwell	S ₂	D ₂	N+	79%

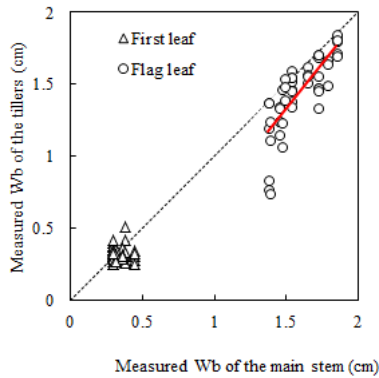


Figure 6: The maximum width of blade of tillers vs. the maximum blade of the main stem. The triangles show the data relative to the first leaf and circles shows data for the flag leaf. Data are from experiments E1-E3 and E5-E6. Each symbol represents the mean value measured for one tiller in one treatment.

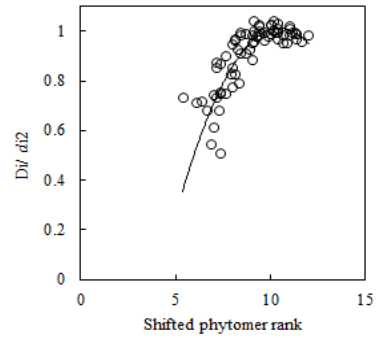


Figure 7: Normalized internode diameter vs. shifted phytomer rank of main stem and tillers. Data are from six treatments from experiments E1, E5 and E6. The normalized internode diameter was calculated as the ratio between the internode diameter of each phytomer and the mean internode diameter of the 3 upper phytomers of the axis. Each symbol represents the mean measurement on a phytomer rank of an axis for one treatment (see also Fig.S6).

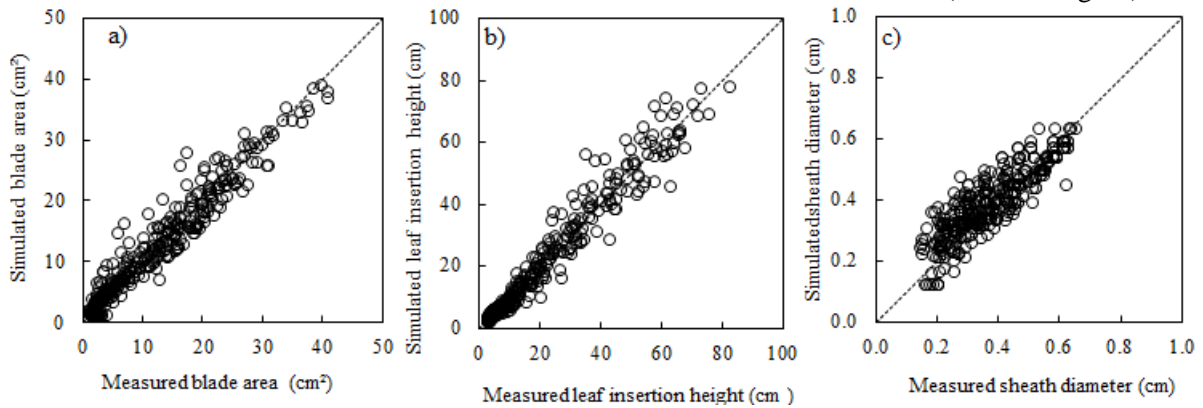


Figure 8: Simulated vs. measured final blade area (a), leaf insertion eight (b) and sheath diameter . Data are from the 17 treatments (experiment E1-E4 and E5-E6). The dotted line is the line 1:1.

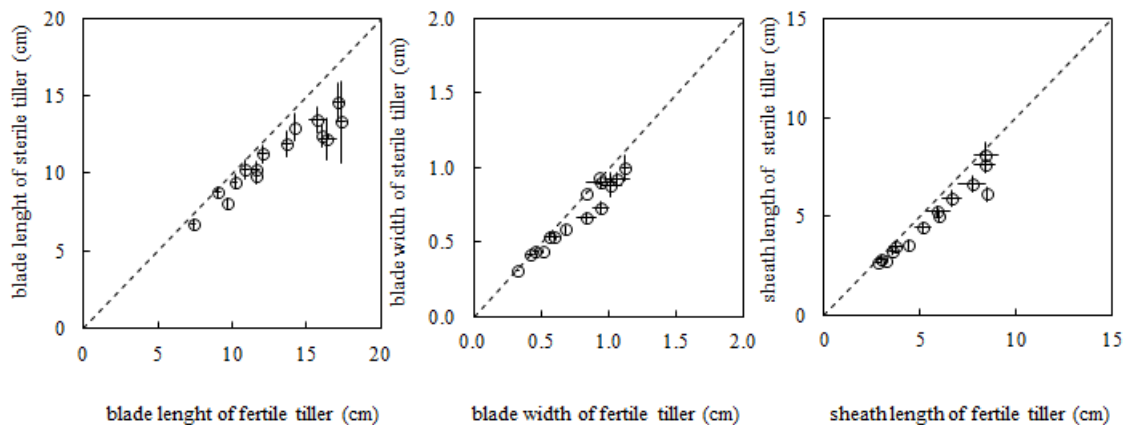


Figure 9: Phytomer dimension of sterile tiller vs. fertile tiller of the same tiller rank. Figures (a), (b) and (c) show respectively the blade length, the maximum blade width, and sheath length. Data are from experiment E6. Symbols represent the mean values measured on both tillers T_1 , T_2 and T_3 . Error bars mark the 95% confidence intervals of mean estimates.

3.3. Change of the dynamics of the green leaf number depending on the ontogeny

The dynamics of the green leaf number on the main stem G_l^{MS} was monitored in nine treatments from experiments E3, E6, E8 covering five genotypes, one sowing date (S2), two densities (D_1 and D_2) and two levels of fertilization (N_+ , N_0). For these treatments, the final leaf number of the main stem was either 11 or 12, and the phyllochron varied from 84 to 108 °Cd (data not shown). The **figure 10** shows that the dynamics of green leaf number G_l followed four phases. In this figure, the simulated curves were obtained by adjusting the G_l pattern while leaving free the choice of the break points.

- The first break point (τ_1, g_1) corresponds to the start of senescence of the main stem. For the treatments investigated here, this occurred when the Haun stage of the main stem HS^{MS} was between 3.9 and 5.4 leaves; τ_1 was highly correlated to the thermal time of flag leaf ligulation. (**Fig.S7b**; $R^2=0.732$).
- The second break point (τ_2, g_2) corresponds to the green leaf number G_l reaching a minimum value; g_2 varied between 2.6 and 4.2 leaves. The time τ_2 was reached when the Haun stage of the main stem HS^{MS} was around 7.5 leaves (standard deviation=0.7), that is close to the ligulation of the 4th leaf from the top. Despite varying in a limited range, the Haun stage at time τ_2 was highly correlated to the phyllochron ($R^2=0.819$, **Fig.S7a**). Besides, the thermal time at τ_2 was correlated to the time of start senescence τ_1 ($R^2=0.621$, **Fig.S7b**): the later the senescence starter, the sooner the minimum was reached. The thermal time at τ_2 was also correlated to the thermal time of flag leaf ligulation. (**Fig.S7c**; $R^2=0.582$).
- The third break point (τ_3, g_3) corresponded to a clear maximum of the green leaf number. The thermal time τ_3 and the thermal time at the flag leaf ligulation τ_{flg} were estimated separately and their values were very close (**Fig.S2d**; $R^2=0.956$). This was expected because the number of green leaf can only decrease after flag leaf ligulation. The green leaf number g_3 varied between 4.0 and 6.5 leaves, and was slightly higher than g_1 , except in one case (**Figure 10b**: experiment E3/Soissons).

To summarize, in all the treatments investigated here, representing contrasted sowing densities, nitrogen fertilisation and 3 cultivars, the dynamics of green leaf number G_l of the main stem presented similar phases during the crop cycle; the change of phases occurred at specific values of Haun stage that could be related to the final leaf number and the phyllochron of the treatment. We have not a simple interpretation of all relations shown, but that they exist for a range of treatments supports the idea of an ontogenic determinism.

The green leaf number of both the main stem and primary tillers G_l^{MS} and G_l^{Ti} were monitored in five treatments from experiments E3 and E6. These treatments included three cultivars (Caphorn, Soissons and Maxwell), two nitrogen treatments (N_+ and N_0) and one sowing density of 250-220 plant/m². The **figure11** shows the measured and simulated dynamics of the green leaf number G_l and the senescent leaf number S_l on main stem and primary tillers for three representative treatments. Simulations correspond to our parametrization, with τ_2 and τ_3 being the thermal times of the ligulation of the 4th leaf from the top and of the ligulation the flag leaf on each axis. The **figure11** shows that the green leaf number G_l of

tillers was generally lower than that of the main stem and its dynamic followed either four or three phases as described in the parametrization: tillers T1 and T2 had generally four phases and T3 had three phases. *Fig.11a1*, and *Fig.11b1*, show results from experiment E3 in which the ligulation of the 4th leaf from the top and of the flag leaf was synchronous on main stem and tillers so τ_2 and τ_3 were the same between axes. *Fig.11c1* show results from experiments E6 in which the development of tillers was delayed compared to that of the main stem. In all cases the minimum green leaf number g_2 was almost identical for main stem and tillers. The green leaf number of tillers g_3 was always similar between tillers, but in some of the treatments was lower compared to that of the main stem: the cultivar Caphorn/ N_+ and Maxwell/ N_+ presented respectively a reduction of 16% and 21% (*Fig.11a1,c1*), while no reduction was observed for the Soissons/ N_+ , Soissons/ N_0 and Caphorn/ N_0 (*Fig.11b1*). Finally, *figure11a2-c2* illustrate that in all these cases our parametrization allowed an accurate description of the dynamics of the decimal number of senescent leaf S_l , which is the output driving the representation of the progress of senescence.

The results presented above corresponded to the fertile tillers that produced ears. The progress of senescence on sterile tillers was monitored in experiment E6. The *figure12* shows that progress of senescence versus thermal time was similar for sterile and fertile tillers.

Finally *figure13* shows the scatter plot of the simulated vs measured senescent leaf number S_l for main stem and primary tillers in the nine treatments investigated. There was no systematic bias and the overall RMSE was 0.32 leaves for the main stems and 0.35 leaves for tillers.

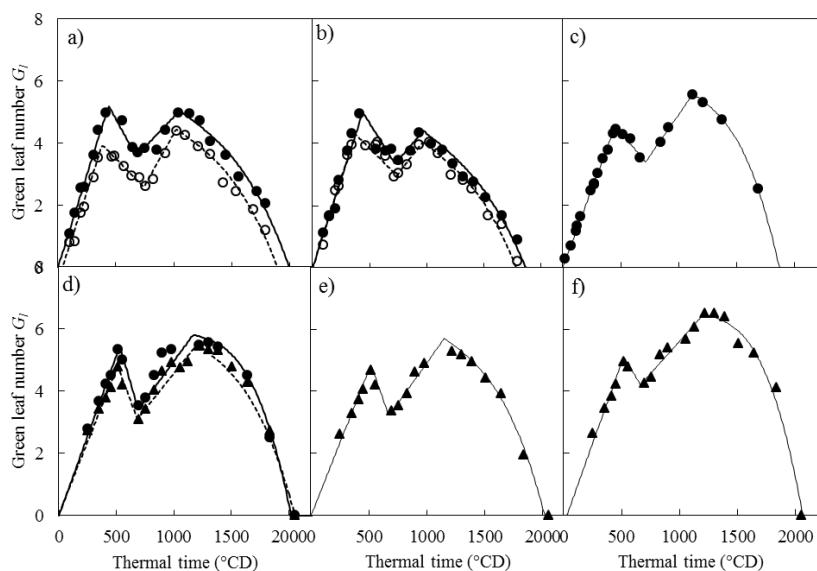


Figure 10: The green leaf number (G_l) of the main stem vs. thermal time from emergence for nine treatments from experiments E3, E6 and E8. Figures (a) and (b) show respectively Caphorn and Soissons cultivars grown at density D_2 (experiment E3). Figure (c) represents Maxwell cultivar grown at density D_2 (experiment E6; N_+). The figure (d) shows the cultivar Caphorn grown at density D_1 and D_2 (experiment E8, N_+). The figures (e) and (f) represent the cultivars Apache and Renan sowing under low density D_1 (experiment E8, N_+). Circles represent treatments sowing under standard density D_2 and triangles represent treatments sowing under low density D_1 . Full symbols refer to treatments with standard fertilisation N_+ and empty symbols for treatments without fertilization N_0 . Symbols show the median values observed and lines represented the result of model calibration keeping free the choice of the breaking points.

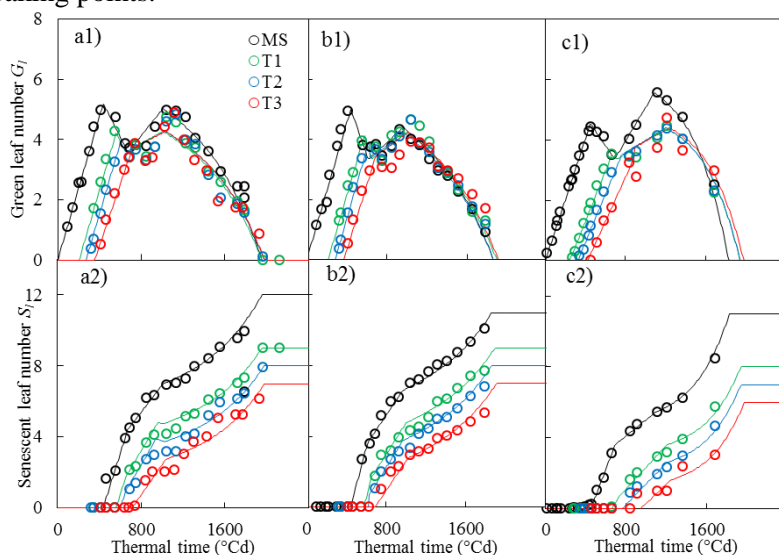


Figure 11: Green leaf number and senescent leaf number vs. thermal time from emergence to full maturity. The figures represent three cultivars: Caphorn in the left (a1-2), Soissons in the middle (b1-2) and Maxwell in the right (c1-2). The treatments are from experiment E3 and E6 sowing under standard density D_2 (~ 250 plant/m 2) with standard nitrogen treatment (N_+). Symbols show the median values measured in plants and lines show the model simulation (the choice of τ_2 and τ_3 is not free). Each colour represents an axis as indicated in figure a1. The figures a, b and c refer to the same experiments presented in the [figure 10](#).

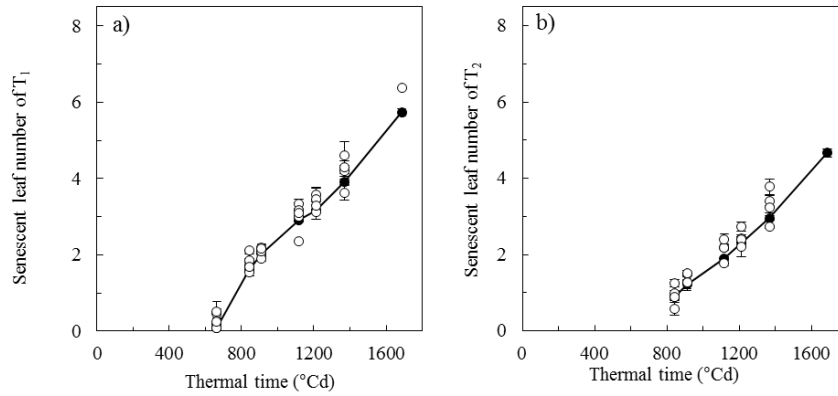


Figure 12: senescent leaf number (S_l) vs. thermal time of tiller 1 (a) and tiller 2 (b) measured on cv. ‘Maxwell’ grown in Grignon in 2010/2011 at density 220 p/m² (experiment E6). Symbols represent the mean value measured on the flowering tillers (black circles) and on regressing tillers having different final leaf number (white circles). Error bars mark the 95% confidence intervals of mean estimates.

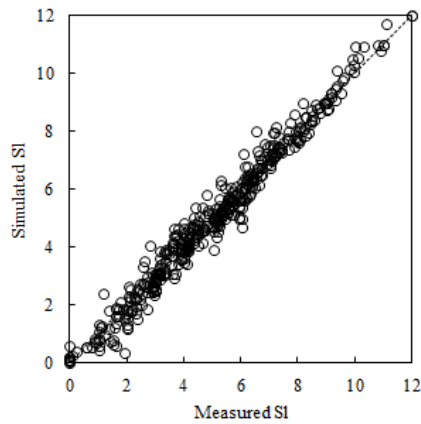


Figure 13: Simulated vs. measured senescent leaf number (S_l) for both main stem and primary tillers. Data are from the treatments from experiments E3, E6 and E8.

4. DISCUSSION

In our experiments, the range of experimental conditions resulted in large variation in the size, with a ratio ~2:1 for similar phytomers of a same genotype in different conditions. This environmental plasticity was larger than differences observed between genotypes grown in the same conditions. Some ontogenic patterns were generally conserved within this range of conditions as seen in [figure7](#) for the main stem, but our objective to represent faithfully any of the experiments, implies that quite a high number of measurement are required. On the other hand, a full description of the size of mature phytomer on main stem can be obtain by tagging plant and dissecting plants at 2 dates along the crop cycle, typically at the five leaf stage and at flowering. There is few correlation between the size of lower and upper phytomer so that no parametrisation could avoid acquiring field information representing each of these periods. Thus we found our representation on an explicit description of main stem dimension.

Given that changes in dimensions are progressive, with high correlations in the size of successive phytomers, a polynomial approximation allows to estimate by interpolation dimensions in case such protocol misses one or two ranks. Thus our work focussed more on the possibility of estimating tiller characteristics from that of main stem. Our results confirm that the use of a decimal phytomer shift is an accurate way to derive length of upper phytomer in tillers from that of the main stem.

The phytomer shift was efficient in the case of growth condition with water or nitrogen stress and enabled to represent detailed patterns, such as the reduced length of the flag leaf. Moreover we found that the shift was identical for blade, sheath or internode, and a same value could be taken for all cultivar and treatments. This value, estimated from the pattern of organ size was close to the Haun stage delay between main stem and tillers that had been independently estimated in [Abichou et al. \(2016\)](#); leaves or internode that grow simultaneously reaches the same dimension.

The phytomer shift was not appropriate or not sufficient to derive dimension such as blade width and stem diameter. Blades of successive leaves in tiller show a pattern that differs significantly from that of main stem. On the other hand, considering that the width of the largest leaf is the same for all axes and a linear increase of blade width with phytomer rank allowed to represent width of tiller blade with a good accuracy. Sheath and internode diameter also show a more complex pattern than length, following that of the main stem, but scaled depending on tiller position.

Few works have attempted to describe precisely the progress of senescence in grass and for wheat, and based on the analysis of a large dataset, our work bring original information. One striking feature is the “M” shape pattern followed by the dynamics of the number of green leaves on the main stem. In our experiments senescence of the first leaf occurred when the Haun stage was ~5, which is before plant development results in significant shadowing between plants. In our parameterization we kept the Haun stage at the onset of senescence as a parameter to be measured. A novel feature that comes out from our experiments is that there is a phase of decrease in the number of green leaves, that precedes a phase of increase until

flag leaf ligulation. In our experiments, the total number of leaves formed on the main stem was 11 or 12, and the Haun stage when the minimum number of green leaves was reached varied between 7 and 8, that is approximately the start of stem extension. Surprisingly, despite this short range of variation, the Haun stage at τ_3 precisely correlated to the phyllochron. It would be of high interest to extend the analyse to treatments with a wider range of final leaf number in order to evaluate the generality of this relation. Finally the period following ligulation of flag leaf, which is dominated by monocarpic senescence, is mainly characterized by a progressive increase of the decimal number of senescing leaves that was in all cases well fitted by a second order polynomial.

The progress of senescence on tillers could be satisfactorily described by transposing to tillers the parameterisation developed on the main stem. Practically, this requires that two kinds of information is measured on tillers (i) the time of flag leaf ligulation, which is to be specified for all tillers and (ii): the number of green leaves at flag leaf ligulation, which showed little variation between tillers in our experiments.

5. LITERATURE CITED

- **Andrieu B., Hillier J., Birch C., 2006.** Onset of sheath extension and duration of lamina extension are major determinants of the response of maize lamina length to plant density. *Annals of Botany*, 98(5), 1005-1016.
- **Baccar R, Fournier C, Dornbusch T, Andrieu B, Gouache D, Robert C. 2011.** Modelling the effect of wheat canopy architecture as affected by sowing density on *Septoria tritici* epidemics using a coupled epidemic-virtual plant model. *Annals of botany* **108**: 1179-1194.
- **Bertheloot J., Andrieu B., Fournier C., Martre P., 2008.** A process-based model to simulate nitrogen distribution in wheat (*Triticum aestivum*) during grain-filling. *Functional Plant Biology* 35: 781-796.
- **Bertheloot J., 2009.** Distribution de l'azote chez le blé (*Triticum aestivum* L.) après la floraison : un modèle dynamique fondé sur une approche structure-fonction. Phd thesis, Paris, Agoparitech.
- **Bos HJ, Neuteboom JH. 1998.** Growth of individual leaves of spring wheat (*Triticum aestivum* L.) as influenced by temperature and light intensity. *Annals of Botany* 81: 141-149.
- **Evers J. B., Vos J., Fournier C., Andrieu B., Chelle M., Struik P. C., 2005.** Towards a generic architectural model of tillering in Gramineae, as exemplified by spring wheat (*Triticum aestivum*). *New Phytologist*, 166(3), 801-812.
- **Evers, J.B., Vos, J., Fournier, C., Andrieu, B., Chelle, M., Struik, P.C., 2007.** An architectural model of spring wheat: evaluation of the effects of population density and shading on model parameterization and performance. *Ecol. Model.* 200, 308–320.
- **Fournier C, Andrieu B, Ljutovac S, Saint-Jean S. 2003.** ADEL-wheat: A 3D architectural model of wheat development. In: Hu BG, Jaeger M. eds. *Plant Growth Modelling and Applications*, Proceedings of 2003 International Symposium on plant growth modelling, simulation, visualization and their applications. Tsinghua University Press: Springer Verlag, Beijing, China: 54-63.
- **Hillier J, Watt J, Bertheloot J, Lewis P, Fournier C, Andrieu B. 2007.** Modelling the time course of senescence in winter wheat at the individual leaf and whole plant level. In: Horticulture and Food Research Institute of New Zealand, Proceedings of 2007 International Workshop on Functional-Structural Plant Models. Napier, France:33.
- **Kemp, D. R. (1981).** Comparison of growth rates and sugar and protein concentrations of the extension zone of main shoot and tiller leaves of wheat. *Journal of Experimental Botany*, 32(1), 151-158.
- **Louarn G, Andrieu A, Giauffret C. 2010.** A size-mediated effect can compensate for transient chilling stress affecting maize (*Zea mays*) leaf extension. *New Phytologist*, 187:106-118.
- **Lim P. O., Kim H. J., Gil Nam H., 2007.** Leaf senescence. *Annu. Rev. Plant Biol.*, 58, 115-136.
- **Gallagher, J.N., 1979.** Field studies of cereal leaf growth. I. Initiation and expansion in relation to temperature and ontogeny. *J. Exp. Bot.* 30, 625–636.
- **Masle J., 1985.** Competition among tillers in winter wheat: consequences for growth and development of the crop. In *Wheat growth and modelling* (pp. 33-54). Springer US.
- **Moullia B., Loup C., Chartier M., Allirand J. M., Edelin C., 1999.** Dynamics of architectural development of isolated plants of maize (*Zea mays* L.), in a non-limiting environment: the branching potential of modern maize. *Annals of Botany*, 84(5), 645-656.
- **Thomas H., Stoddart J. L., 1980.** Leaf senescence. *Annual review of plant physiology*, 31(1), 83-111.

- **Klepper B, Rickman RW, Peterson CM. 1982.** Quantitative characterization of vegetative development in small cereal grains. *Agronomy Journal* **74**:789-792
- **McMaster, G. S., Klepper, B., Rickman, R. W., Wilhelm, W. W., & Willis, W. O. (1991).** Simulation of shoot vegetative development and growth of unstressed winter wheat. *Ecological Modelling*, 53, 189-204.
- **Masle J., 1985.** Competition among tillers in winter wheat: consequences for growth and development of the crop. In *Wheat growth and modelling* (pp. 33-54). Springer US.
- **Kirby EJM. 1993.** Effect of sowing depth on seedling emergence, growth and development in barley and wheat. *Field Crops Research* **39**: 101-111.
- **Tivet, F., Pinheiro, B. D. S., Raïssac, M. D., & Dingkuhn, M., 2001.** Leaf blade dimensions of rice (*Oryza sativa* L. and *Oryza glaberrima* Steud.). Relationships between tillers and the main stem. *Annals of botany*, 88(3), 507-511.
- **Vos J. 2010.** Functional-structural plant modelling: a new versatile tool in crop science. *Journal of Experimental Botany* **61**: 2101-2115.
-

6. APPENDIX

Description and status of model variables

Symbols	Description	status
MS	Main stem	-
T_i	Fertile tiller rank i	-
$T_{i.st}$	Sterile tiller rank i	-
x	Absolute rank according to the chronological order of appearance	-
r	Absolute phytomer rank of the first elongated internode on the MS.	Input
N_l	Final number of leaves on the axis.	Input
s^{Ti}	Corrector shift of phytomer rank relative to T_i	Constant
τ	Thermal time from plant emergence	-
τ_0	Thermal time at the emergence the axis.	Input
τ_1	Thermal time at the start senescence of the axis.	Parameter
τ_2	Thermal time at the ligulation of the 4 th leaf from the top on the axis.	Parameter
τ_3	Thermal time at the ligulation of the flag leaf of the axis.	Parameter
τ_4	Thermal time at the full senescence of all leaves on the axe (time of end filling)	Parameter
σ_i	Delay in thermal time at flag ligulation between the MS and T_i	Input
$HS^{axis}(\tau)$	Haun stage of the axis at the thermal time τ .	Input
$G_l^{axis}(\tau)$	Green leaf number on the axis at the thermal time τ .	-
$S_l^{axis}(\tau)$	Senescent leaf number on the axis at the thermal time τ .	-
$L_b(x)$	Final length of blade of the phytomer rank x on the axis.	-
$L_s(x)$	Final length of sheath of the phytomer rank x on the axis.	-
$L_i(x)$	Final length of internode of the phytomer rank x on the axis.	-
$W_b(x)$	Maximum width of blade of the phytomer rank x on the axis.	-
$D_s(x)$	Final diameter of sheath of the phytomer rank x on the axis.	-
$D_i(x)$	Final diameter of internode of the phytomer rank x on the axis.	-
l_{b1}	Final length of the first blade of the tiller taken as a constant for all tiller rank	Constant
w_{b1}^{MS}	Maximum width of the first blade of the MS	Input
w_{bflg}^{MS}	Maximum width of the flag blade of the MS	Input
d_{s1}	Sheath diameter of the first leaf on the main stem	Constant
d_{s2}	Mean sheath diameters of the upper leaf of the MS	Input
d_{i2}	Mean internode diameters of the upper leaf of the MS (peduncle not included)	Input
α, β	Coefficient of the polynomial function of the green leaf number (G_l)	Parameter
b_{0-4}	Coefficient of the polynomial function of final blade length	Parameter
s_{0-4}	Coefficient of the polynomial function of final sheath length	Parameter
i_{0-4}	Coefficient of the polynomial function of final internode length	Parameter
d_{0-4}	Coefficient of the polynomial function of maximum blade width	Parameter
c_{0-2}	Coefficient of the polynomial function of final internode diameter	Constant
$k_f; k_l$	Reduction factors for maximum width of respectively the first and the last blade of fertile tillers compared to that of the MS	Constant ≤ 1
p^{Ti}	The relative order of appearance of the tiller T_i in the plant (tiller rank/total number of tiller in the plant)	Input
k^o	Reduction factors for diameter of sheaths and internodes of a given tiller. This factor depend to the position of the tiller in the plant; if the tiller is last emerged tiler then $k^o = \rho_3$, if else $k^o = \{\rho_1 * p^{Ti} + \rho_2; \rho_3\}$ with p^{Ti} is the relative position of the tiller in the plant. (e.i.the relative position is defined as the ratio between the rank of the tiller and the total number of tillers in the plant)	Parameter
ρ_{1-3}	Coefficient of reduction for diameter of sheaths and internodes of a tiller	Constant
$k_i^{st}; k_w^{st}$	Reduction factors of final phytomer dimensions for sterile tillers compared to fertile tillers	Constant ≤ 1
g_1^{MS}	Number of green leaf on the main stem at start senescence.	Input
g_2^{MS}	Minimum green leaf number on the main stem	Input
g_3^{MS}	Green leaf number on the main stem at the flag ligulation	Input
g_4^{MS}	Green leaf number on the main stem just after flowering	Input
g_5^{MS}	Green leaf number on the main stem just before full senescence	Input
g_1^{Ti}	Number of green leaf on the tiller (T_i) at start senescence.	Parameter
g_2^{Ti}	Minimum green leaf number on the tiller (T_i)	Parameter
g_3^{Ti}	Green leaf number on the tiller (T_i) at the flag ligulation	Parameter
∂	Ratio between the number of green leaf on the MS and tillers ($\partial = g_3^{Ti}/g_3^{MS}$)	Input

7. SUPPLEMENTARY DATA

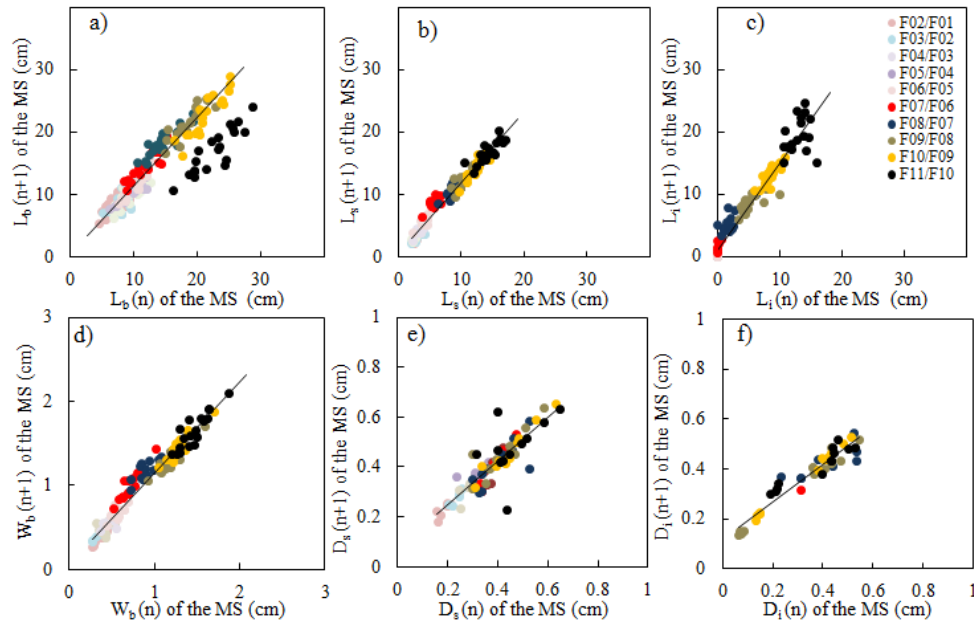


Figure S1: final dimension of the phytomer (n+1) vs final dimension of the previous phytomer (n) of main stems having eleven leaves. Data are from 20 treatments from experiments E1-E3 and E5-E8 including 9 commercial cultivars, two sowing densities (D_1 and D_2) and two sowing date (S_2 and S_3). Each symbol represents the mean value of a treatment and the different colors represent a couple of phytomer rank as indicated in the figure in the right. The line represent the fitted linear regression model for all phytomer ranks except in figure a for which data relative to the flag leaf (in black) was excluded for the fit. Each color represents a couple of leaf ranks as indicated in figure c and lines represent the fitted linear model. A caption of equation and R^2 are shown in right bottom of each figure.

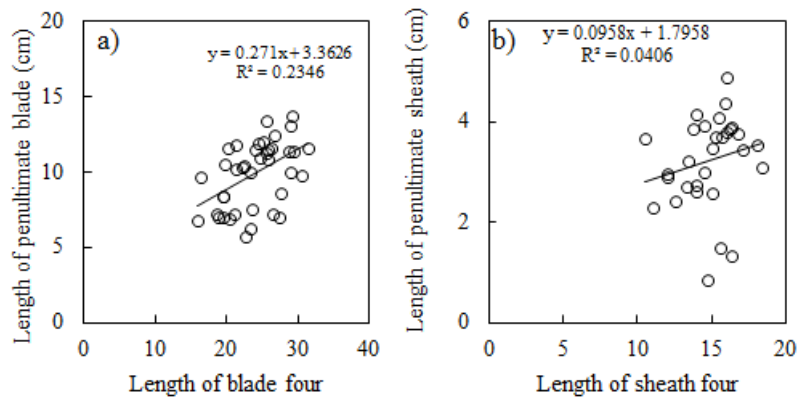


Figure S2: final length of the penultimate phytomer vs. final length of the 4th emerged phytomer of the main stem. Data are from 39 treatments from experiments E1-E8 including 10 commercial cultivars; three sowing densities (D_1 - D_3) and three sowing date (S_1 - S_3). Each symbol represents the mean value of a treatment. The line represents the fitted linear regression model and equation and R^2 are captured in each figure.

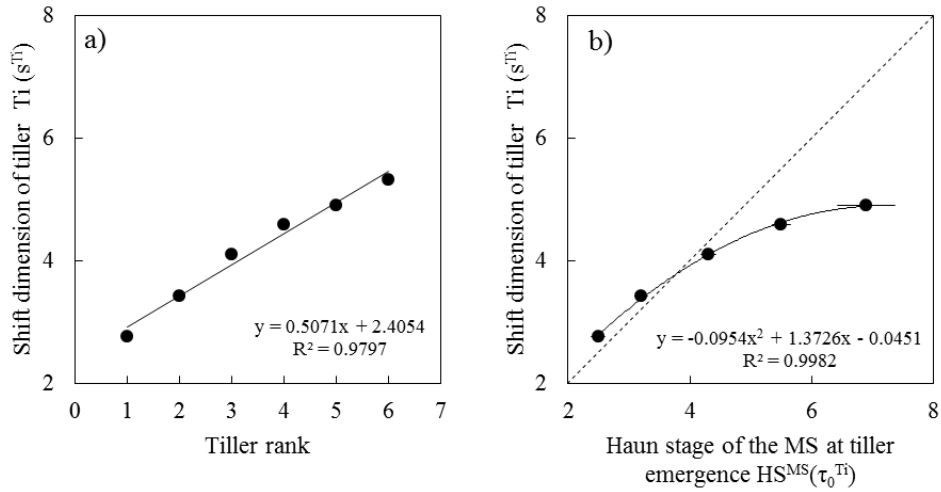


Figure S3: The adjusted shift values s^{Ti} vs. the tiller rank in figure a and vs. the haun stage of the main stem at tiller emergence $HS^{MS}(\tau_0^{Ti})$ estimated by *Abichou et al. (2016)* in figure b. Figure b shows that for the three first tillers, the adjusted shift values s^{Ti} were close to the Haun stage of the main stem at tiller emergence $HS^{MS}(\tau_0^{Ti})$ suggesting that leaves grown in the same time have the same length, but this is not the case for tiller 4 and 5.

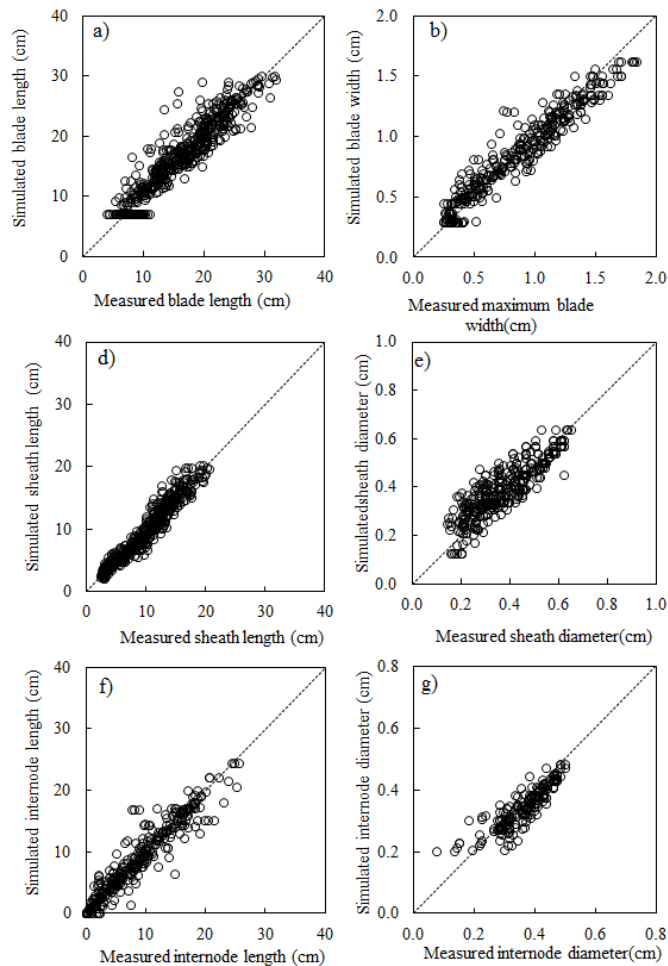


Figure S4: simulated vs. measured phytomers dimensions. Data are from the 17 treatments from experiment E1-E4 and E5-E6. The figures a, b, c, d,e and f are respectively for blade length, maximum blade width, sheath length, sheath diameter, internode length and internode diameter. The dotted line is the line 1:1.

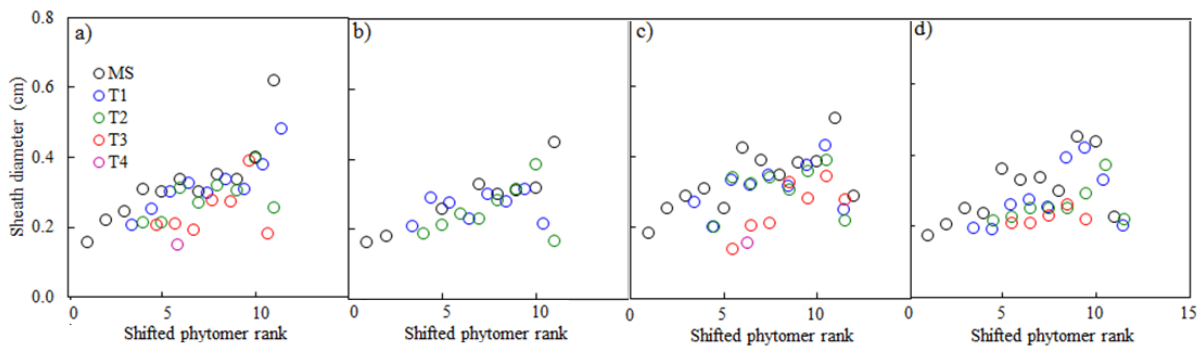


Figure S5: sheath diameter vs. shifted phytomer rank of main stem and primary tillers. Data are from five treatments from experiment E3. Symbols represent the mean measurement of each axis. Colors represent the different axes as indicated in figure(a). Figures a and b show data of Soissons cultivar, respectively with nitrogen treatment N_+ and N_0 . Figures c and d show data for Caphorn cultivar, respectively with nitrogen treatment N_+ and N_0 .

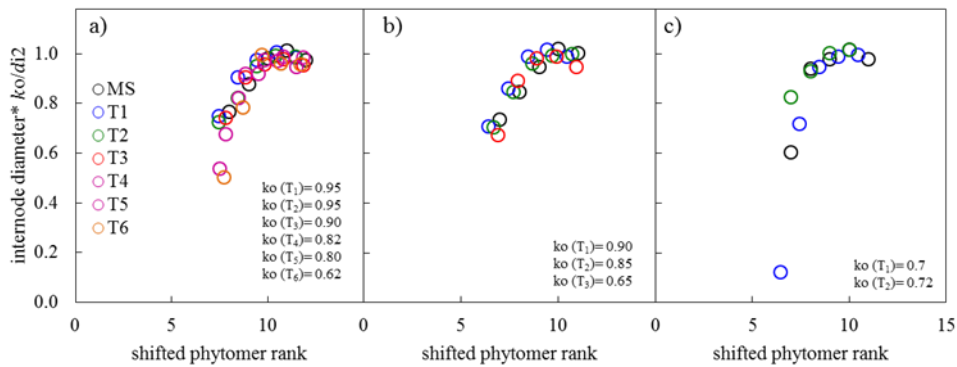


Figure S6: normalized internode diameter vs. shifted phytomer rank of main stem and primary tillers. Data are from five treatments from experiments E1 (figures a, b) and E6 (figure c). Symbols represent the mean measurement of each axis. Colors represent the different axes as indicated in figure a. Figures a and b show data of Soissons cultivar, respectively with density D1 and D2. Figure c shows data for Maxwell cultivar with density D2. The values of fitted scale factor k^0 relative to each tiller (T_i) are noted in the right bottom of each figure.

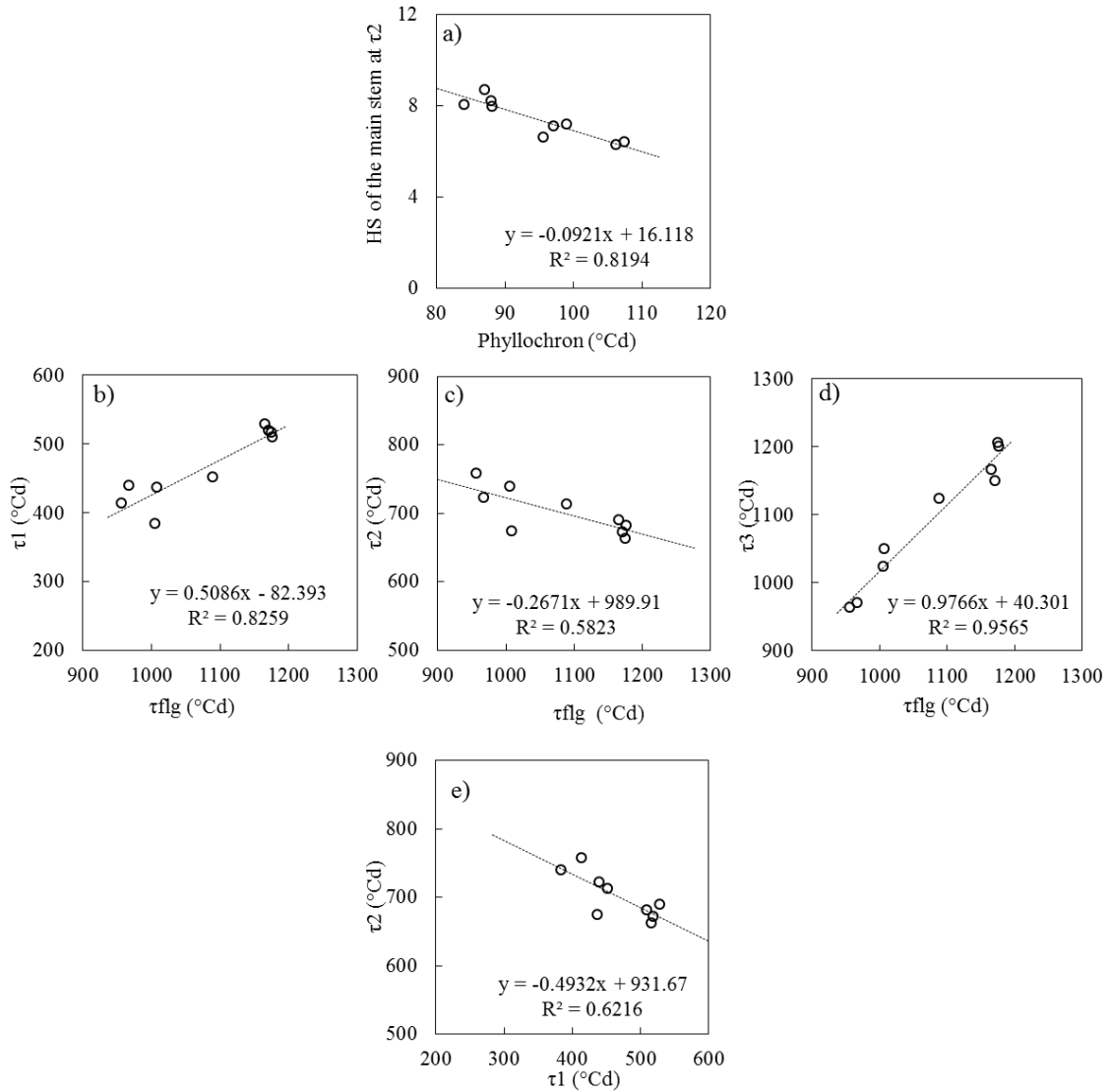


Figure S7: correlation between variables of the green leaf number G_l of the main stem. Symbols represent the adjusted parameters of the nine treatments from experiments E3, E6 and E8. The figure a represents the haun stage of the main stem at the minimum of green leaf (τ_2) vs. their phyllochron ($R^2 = 0.819$). Figure b shows the relation between thermal time at the start of senescence (τ_1) and the thermal time at flag leaf ligulation. Figure c shows the relation between thermal time at the minimum of green leaf (τ_2) and the thermal time at flag ligulation. Figure d shows the the thermal time at the maximum of green leaf number (τ_3) and the the thermal time at flag ligulation. Figure e shows the relation between thermal time at the minimum of green leaf (τ_2) and the thermal time at the start of senescence (τ_1)

Table S1: fitted parameters of the of green leaf number model for the nine treatments with: (i) the experiment number, (ii) cultivars, (iii) sowing density: (D₁:low, D₂:normal), (iv) nitrogen treatments (N₊: optimal, N₀: no N given); (v) cohort number (MS:1, T₁:4, T₂:5); (vi) the mean phyllochron (unit :°Cd); (vii) the final leaf number; (viii) the green leaf number at the start of senescence; (x) the minimum of green leaf number; (xi) the maximum of green leaf number; (xii) the thermal time at start senescence; (xiii) the thermal time at the ligulation of the 4th leaf from the top; (xiv) (xiii) the thermal time at the ligulation of the flag leaf ;(xv) the root mean square error (RMSE) calculated between simulated and the observed values.

Exp.	Cv.	Density	Sowing Date	N.trt	axis	phyllochron	N ₁	g1	g2	g3	τ ₁	τ ₂	τ ₃	α	β	RMSE
E3	Caphorn	D2	S2	N0	MS	88	11	4.0	2.6	4.5	389	653	1006	-3.2E-09	-2.7E-03	0.26
					T ₁	88	9	3.4	2.6	4.5	520	660	1006	-3.2E-09	-2.7E-03	0.42
					T ₂	88	8	2.9	2.6	4.5	590	687	1046	-3.2E-09	-2.7E-03	0.33
E3	Caphorn	D2	S2	N+	MS	84	12	5.2	3.6	5.2	437	672	1008	-2.9E-09	-2.7E-03	0.34
					T ₁	84	9	4.1	3.6	4.7	570	651	1008	-2.6E-09	-2.4E-03	0.33
					T ₂	84	8	4.0	3.6	4.7	590	651	1030	-2.6E-09	-2.4E-03	0.46
					T ₂	84	9	4.8	3.6	4.7	665	681	1009	-2.6E-09	-2.4E-03	0.36
					T ₃	84	7	3.6	3.6	4.7	701	701	1034	-2.6E-09	-2.4E-03	0.52
E3	Soisson	D2	S2	N0	MS	87	11	4.5	2.8	4.1	392	609	957	-3.3E-09	-2.7E-03	0.45
					T ₁	89	9	3.5	2.8	4.1	525	659	1017	-3.3E-09	-2.7E-03	0.22
					T ₁	103	8	3.0	2.8	4.1	525	625	1038	-3.3E-09	-2.7E-03	0.59
					T ₂	86	8	3.3	2.8	4.1	560	623	966	-3.3E-09	-2.7E-03	0.38
					T ₂	74	9	3.8	2.8	4.1	560	649	944	-3.3E-09	-2.7E-03	0.42
E3	Soisson	D2	S2	N+	MS	88	11	5.0	3.3	4.4	440	616	968	-3.0E-09	-2.7E-03	0.25
					T ₁	87	9	3.8	3.3	4.3	550	651	999	-3.0E-09	-2.7E-03	0.33
					T ₁	101	8	3.3	3.3	4.3	550	618	1021	-3.0E-09	-2.7E-03	0.36
					T ₂	85	8	3.6	3.3	4.3	590	626	968	-3.0E-09	-2.7E-03	0.32
					T ₃	92	7	3.3	3.3	4.3	676	676	1017	-3.0E-09	-2.7E-03	0.46
E6	Maxwell	D2	S2	N1	MS	99	11	4.7	3.3	5.8	470	693	1089	-8.8E-09	-2.7E-03	0.12
					T ₁	120	8	3.6	3.3	4.8	670	722	1203	-7.3E-09	-2.2E-03	0.21
					T ₁	104	9	4.1	3.3	4.8	670	762	1178	-7.3E-09	-2.2E-03	0.18
					T ₂	126	7	3.3	3.3	4.8	738	738	1203	-7.3E-09	-2.2E-03	0.18
					T ₂	107	8	3.9	3.3	4.8	738	749	1178	-7.3E-09	-2.2E-03	0.10
					T ₃	137	6	3.3	3.3	4.8	872	872	1239	-7.3E-09	-2.2E-03	0.22
E8	Caphorn	D1	S2	N+	MS	97	12	5.4	3.4	5.7	529	680	1166	-8.0E-09	-1.0E-03	0.27
					MS	108	11	4.8	3.1	5.7	510	747	1177	-5.2E-09	-2.7E-03	0.29
					MS	106	11	4.9	3.2	5.5	519	746	1171	-5.2E-09	-2.7E-03	0.29
					MS	96	12	5.1	4.2	6.6	517	698	1175	-9.0E-09	-1.0E-03	0.23
					MS	96	12	5.1	4.2	6.6	517	698	1175	-9.0E-09	-1.0E-03	0.23

Table S2: fitted parameters of the phytomer dimensions sub-models for the 17 treatments with: (i) the experiment number, (ii) cultivars, (iii) sowing date (S2: normal, S3: late), (iv) density: (D₁:low, D₂:normal), (v) nitrogen treatments (N₊: optimal, N₀: no N given); (vi-x) the coefficients b_0 to b_4 of the polynomial function of final blade length; (xi-xv) the coefficients s_0 to s_4 of the polynomial function of final sheath length; (xvi-ixx) the coefficients i_0 to i_3 of the polynomial function of final internode length; (xx) the rank of the last non elongated internode, (xxi) the final leaf number of the main stem N_1^{MS} ; (xxii-xxiii) the mean diameter of the three upper sheaths (d_{s2}) and internodes (d_{i2}) and (xxiv-xxx) the RMSE values for each sub-models.

Exp.	Cv.	Sowing Date	Density	N.trt	b_0	b_1	b_2	b_3	b_4	s_0	s_1	s_2	s_3	s_4	i_0	i_1	i_2	i_3	r-l	N_1^{MS}	d_{s2}	d_{i2}	RMSE L_b	RMS L_s	RMSE L_i	RMSE W_b	RMSE D_s	RMSE D_i
E1	Soissons	S2	D1	N+	-422.8	220	-41.8	3.5	-0.11	2.20	1.34	-0.69	0.12	-0.01	44.3	-18.0	2.2	-0.1	6	12	-	0.49	7.16	6.69	1.02	0.08	-	0.03
E1	Soissons	S2	D2	N+	-262.0	157	-33.8	3.2	-0.11	2.93	0.49	-0.43	0.11	-0.01	68.9	-29.1	3.8	-0.1	5	11	-	0.42	5.73	5.54	1.21	0.08	-	0.03
E2	CapHorn	S2	D2	N+	-94.4	65	-15.4	1.6	-0.06	4.01	0.50	-0.45	0.10	-0.01	-29.1	8.6	-0.9	0.0	5	11	-	-	1.62	0.69	1.76	-	-	-
E2	Florence	S2	D2	N+	2585.5	-1311	247.0	-20.3	0.62	4.87	-2.20	0.93	-0.11	0.01	86.3	-37.6	5.0	-0.2	6	10	-	-	2.93	1.20	3.58	-	-	-
E2	Isengrain	S2	D2	N+	-570.8	293	-55.5	4.7	-0.15	2.04	1.68	-0.78	0.15	-0.01	74.7	-37.1	5.5	-0.2	6	11	-	-	1.73	0.88	2.17	-	-	-
E2	Oratorio	S2	D2	N+	-66.8	63	-17.0	1.9	-0.07	1.30	2.98	-1.37	0.23	-0.01	9.5	-6.3	0.9	0.0	6	11	-	-	2.04	1.86	1.85	-	-	-
E2	Recital	S2	D2	N+	-629.2	326	-61.6	5.1	-0.16	2.90	-0.27	-0.02	0.04	0.00	-337.9	116.0	-13.3	0.5	6	11	-	-	1.40	1.60	1.91	-	-	-
E2	Soissons	S2	D2	N+	-353.1	202	-41.7	3.8	-0.13	2.22	1.50	-0.63	0.11	0.00	-306.5	105.8	-12.2	0.5	6	11	-	-	1.36	1.35	1.10	-	-	-
E2	Theese	S2	D2	N+	-117.5	88	-20.9	2.1	-0.08	4.63	-2.27	0.68	-0.05	0.00	-492.6	161.9	-17.8	0.7	7	11	-	-	1.64	1.15	1.34	-	-	-
E3	Caphorn	S2	D2	N+	-769.9	361	-62.4	4.8	-0.14	2.81	-0.09	-0.22	0.07	0.00	-165.4	47.7	-4.7	0.2	7	12	0.40	0.23	2.91	3.45	0.00	0.17	0.06	0.08
E3	Soissons	S2	D2	N+	-2919.9	1360	-236.1	18.2	-0.52	2.99	-0.51	-0.01	0.04	0.00	-498.2	159.3	-17.0	0.6	7	11	0.45	0.21	1.84	3.11	0.00	0.08	0.10	0.07
E3	Caphorn	S2	D2	N0	-1610.9	750	-130.2	10.1	-0.29	3.00	-0.57	0.05	0.03	0.00	-313.0	98.7	-10.5	0.4	7	11	0.37	0.24	1.62	4.01	0.00	0.15	0.07	0.07
E3	Soissons	S2	D2	N0	-2367.3	1109	-193.2	14.9	-0.43	1.85	1.06	-0.63	0.12	-0.01	-90.7	27.6	-2.9	0.1	7	11	0.36	0.22	1.50	2.72	0.00	0.15	0.06	0.08
E5	Soissons	S3	D1	N+	-1171.7	644	-131.1	11.8	-0.39	1.35	2.64	-1.21	0.21	-0.01	-411.9	152.8	-18.9	0.8	6	10	0.64	0.49	3.81	1.66	2.10	0.09	0.06	0.04
E5	Soissons	S3	D2	N+	-362.3	228	-52.0	5.2	-0.19	3.15	0.39	-0.50	0.14	-0.01	-143.3	56.3	-7.4	0.3	5	10	0.54	0.39	2.52	1.26	1.90	0.10	0.08	0.04
E5	Soissons	S3	D3	N+	-1024.6	647	-150.1	15.3	-0.58	3.09	0.43	-0.48	0.15	-0.01	-130.5	58.6	-8.7	0.4	5	9	0.54	0.39	3.98	6.81	4.63	0.16	0.06	0.08
E6	Maxwell	S2	D2	N+	282.7	-132	23.2	-1.7	0.04	5.78	-3.61	1.22	-0.13	0.01	7.1	-3.7	0.4	0.0	6	11	0.45	0.38	2.69	0.82	1.08	0.14	0.04	0.04

CHAPTER 3: Responses of winter wheat plants to increased row spacing: developmental, morphological and geometrical changes

This chapter is the base of a journal paper by:

Mariam Abichou, Benoit de Solan, Bruno Andrieu

RESUME

Contexte et objectifs. Le choix de la densité de semis et de l'écartement entre les rangs sont deux techniques de gestion de culture qui influencent fortement l'architecture des plantes. Il est bien connu que les plantes sont capables de détecter la présence de leurs voisines et d'adapter leurs architectures afin de mieux explorer les ressources. Les réactions d'adaptation les plus étudiées concernent les réponses à la densité. Un effet moins connu est lié à la sensibilité des plantes à l'emplacement exact de leurs voisines. Il y a encore un manque d'études qui analysent les réponses, morphologiques et géométriques des plantes de blé, sous un changement d'espace entre les rangs. Ce travail vise à étudier comment les plantes adaptent leurs développements, morphologies et géométries lorsque l'espacement entre rangs double tout en maintenant une même densité au m².

Méthodes. Nous avons mesuré des variables à l'échelle de la plante et à l'échelle du couvert pendant toute la phase végétative. Les variables analysées sont: la dynamique de tallage, le rendement, la dynamique de couverture du sol en visée verticale *GC*, l'indice foliaire *PAI_f*, le rythme d'apparition des feuilles, le nombre et la dimension finale des organes, les angles d'azimut des feuilles et des tiges et leur espacement à partir de la base de la plante.

Résultats. Les principales différences de l'architecture des plantes sous un espacement large entre les rangs *WI* comparée à un espacement étroit *NI*, sont les suivantes: (i) une réduction du nombre de talles, (ii) une légère augmentation du rendement en grain, (iii) un développement avancé, (iv) une couverture du sol à la verticale similaire à *NI*, (v) augmentation de la surface des limbes de dernières feuilles, (vi) augmentation de la distance horizontale entre les axes et la base des plantes à la floraison avec une légère tendance d'une orientation vers l'espace libre entre les rangs et (vii) mise en évidence des différences entre les cultivars.

Conclusion. Cette étude est particulièrement intéressante du fait qu'elle a permis d'identifier les stratégies que les plantes mettent en jeu pour s'adapter au changement de son environnement local en soulevant les degrés de libertés de leurs traits architecturaux.

ABSTRACT

Background and Aims. The adjustment of the density and the row spacing are among the crop management techniques that most influence plant architecture. Plants are able to detect the presence of their neighbours and adapt their architecture to better explore resources. In crops, the most studied adaptation reactions concerns the responses to plant density. A less known aspect is how plants adapt to the exact location of their neighbours. This work aimed to study how wheat plants adapt their development, morphology and geometry under increasing the row spacing, at constant population density.

Methods. Measurements of up-ground variables at plant and at crop scale were carried out during the vegetative phase. The variables investigated were: dynamic of tillering, yield, dynamic of vertical ground cover, plant area index *PAI_g*, rate of leaf appearance, number and final dimension of organs, azimuth angles of leaves and stems and their spacing from the plant base.

Results. The major differences in plant architecture under wide row spacing *WI* compared to narrow row spacing *NI*, were the following: (i) a reduction of the number of tillers, (ii) a slight increase of grain yield, (iii) an advanced development with higher final leaf number, (iv) a similar vertical ground cover, (v) increase of blade area of upper leaves, (vi) increase of the horizontal distance between axes and the base of plants at flowering with a slight trend to an orientation towards the free space between the rows and (vii) results pointed to differences among cultivars.

Conclusion. Plant responses in the first stages of growth, suggest that in wide inter-rows, plants reacted mainly to a higher perception of competition, due to the lower distance with their closest neighbours. However, they show no trend to avoid specifically their closest neighbours and prospect the inter-row space. In the later stages of growth, plants in the wide inter row showed traits characteristic of a lower level of competition, than in normal inter row; indeed they compensated the reduced number of ears by a higher yield per ear. At this stage, some cultivars, but not all, show a trend to prospect more specifically the inter-row space.

1. INTRODUCTION

It is well known that plants are able to detect the presence of their neighbours and adapt their architecture to avoid shading and to better explore the resources. The most studied responses of plant adaptation concerns the change in density. Density effect was often related to resources (Alzueta *et al.*, 2012; Kirby and Faris, 1972) and to phytochrome signalling. It was shown that red:far-red ratio acted as an early signal for plant to avoid competition (Ballaré and Casal, 2000; Evers *et al.*, 2006;). A less known aspect is the sensitivity of plants to the exact location of their neighbours. For crops, the choice of row spacing is generally a compromise between the search for homogeneity of crop, to reduce interplant competition, and practical constraints, as the mechanical weed control in organic farming or the conservation of soil moisture in mulch-till and no-till farming. Therefore, the question of managing the row spacing at constant density is of major interest. In conventionally grown wheat crops, the row spacing varies from 12 to 18 cm, whereas it varies from 35 and 50 cm, in organic farming conditions. Several studies investigated the impact of changing the row spacing on grain yield and weed control. For wheat, several researches have recorded higher grain yields (from +8 to +13%) with reduction of row spacing from 23 to 8 cm. This yield increase was associated with a higher number of ears per square meter and was interpreted as narrow row spacing allowing a more efficient capture of resources (Joseph *et al.*, 1985; Epplin *et al.*, 1992, Johnson *et al.*, 1988). However, other works shown no yield advantages with reduced row spacing (Marshall and Ohm, 1987; Teich *et al.*, 1992; Freeze and Bacon, 1990) interpreted by an increase of resource-use efficiency. Studies aiming at design organic or no tillage farming investigated the effect of increasing rows spacing, from 17 to 24-40 cm. Most authors reported that wide row spacing resulted in yields similar to those in conventional spacing (Crabtree and Rupp, 1980; Teich *et al.*, 1993; Lafond 1994; Lafond and Gan, 1999; Hiltbrunner *et al.*, 2005). In general wide row spacing produced a lower density of ears, but this was compensated as the number of kernels per ear and the thousand kernel weight were higher (Lafond, 1994; Hiltbrunner *et al.*, 2005, Johnson, 1988). Some works even reported an increase on grain protein content (~ +12%) under wide row spacing (Hiltbrunner *et al.*, 2005).

The work cited above focused on the effect of row spacing on yield without investigating the adaptations in plant architecture. Many studies on maize showed that the azimuthal positioning of the leaves react significantly to the presence of neighbours and plants tended to align their leaves perpendicularly to the row direction under rectangular plantings patterns (Maddonni *et al.*, 2001; Drouet and Moulia, 1997) which increase light capture. To our knowledge, there is a lack of studies that

analysed the morphological and geometrical responses of wheat plants under change of row spacing. Addressing these questions may help to identify or even design cultivar trait the more adapted to new management techniques.

The aim of this work is to study how plants adapt their development, architecture and geometry under increasing the row spacing, at constant population density. We addressed two principal questions: (i) Are there differences in plant development, tillering and organ dimension? (ii) Are there adaptations in the spatial disposition of organs?

2. MATERIALS AND METHODS

Measurements of above ground variables at plant and at crop scale were carried out during the vegetative phase in treatments with contrasted row spacing. Measurements aimed to characterize the development, architecture and geometry of winter wheat plants. The variables investigated here are: density of axes (maximum and final), the yield, the vertical ground cover, the plant area index, the light extinction coefficient, the rate of leaf appearance (phyllochron), the number and dimension of organs, angles of leaves and stems (zenith, azimuth) and their spacing from the row. Measurements were carried out on five commercial winter wheat cultivars that had been selected regarding to their difference in leaf curvature (planophyll to erectophyll).

1.1. Experimental design and treatments

The experiment was conducted in 2012/2013 in field conditions, at the INRA campus of Thiverval-Grignon (48°51 N, 1°58 E), with a maritime influenced climate and a deep loamy soil. Five cultivars of winter wheat *Triticum aestivum* (Maxwell, Apache, Caphorn, Renan, and Soissons) were sown at a density of 200 seeds m⁻² on 02 October 2012. The distance between rows was either the conventional distance in the region, 17.5 cm (narrow row spacing, *NI*), or 35 cm (wide row spacing, *WI*). The mean interplant distances on the row were 2.9 cm in *NI* treatments and 1.4 cm in *WI* treatments. Field plots consisted of two blocs (15 m x 1.75 m) per treatment. Nitrogen fertilization followed the standard scheme with one dose at tillering stage and one dose brought shortly before stem elongation. Weeds were controlled by herbicide application at sowing and during the crop cycle. Air temperature at 2 m was recorded from a nearby meteorological station and soil temperature at 3 cm depth was measured in the experimental plots. Thermal time was computed from plant emergence on an hourly basis, assuming a linear response to temperature with a base temperature of 0°C.

1.2. Measurements at crop level

The density of axes (axes.m²) was measured five times during the crop cycle at 590, 795, 934, 1333, 1630 °Cd after plant emergence. Measurements were conducted on 10 to 50 plants per treatment. Plants were collected in the field and brought to the laboratory. Axes having at least one green leaf were recorded. At the end of the cycle, the grain yield (t.ha⁻¹) was measured on an area of 10 m².

Vertical ground cover $GC(0^\circ)$ was monitored weekly from ligulation of the 4th leaf to flag leaf ligulation (from 08/02/2013 to 24/05/2013). Six down-looking photographs were taken at constant locations in each treatment. We used a NIKON camera D90, with a sensor size =23.6x15.8 mm and a focal length of 50 mm which defines a field of view of $\pm 13.5^\circ$ around the optical axis. Photographs were taken from a 2.215 m height and covered an area of 1.05m x 0.70m. Synchronously with *vertical photographs*, oblique photographs with a direction of view at 57.5° from the vertical were acquired to monitor oblique ground cover $GC(57.5^\circ)$. $GC(57.5)$ was used to estimate the green plant area index PAI_g (m² leaf per m² soil), following (Baret *et al.*, 2010):

$$PAI_g = \frac{-\cos(57.5^\circ) \cdot \log(1 - GC(57.5^\circ))}{0.5}$$

Photographs (0° and 57°) were processed using the SATVA software (<https://www6.paca.inra.fr/emmah/Production-Documentation/Outils-et-modeles/>) to determine the proportion of vegetation pixels, which corresponds to ground cover. Beside, PAI_g was directly measured at flowering by dissecting 45 plants per treatment and scanning all phytoelements.

1.3. Measurements at plant level

The number and length of individual leaves of the main stems were measured six times during the crop cycle on 10 tagged plants per treatment to characterise the Haun stage as described in Abichou *et al.* (2016). The phyllochron was defined by adjusting a linear model between the Haun stage and the thermal time.

The length of the pseudostem l_{stem} and the apex l_{apex} of the main stems were measured by ruler on 30 tagged plants from destructive measurement, at 960 °Cd after emergence (i.e. Haun stage~8.7).

The dimensions of the individual mature organs of the main stems were measured on 30 tagged plants to determine: (i) the blade length l_{blade} , (ii) the blade area a_{blade} and (iii) the collar height $l_{col(i)}$ (e.i. distance from the plant base to the collar position) of individual leaf rank. Plants were dissected and blade images were obtained with a flat-bed scanner and were processed using the program Lamina2Shape (Dornbusch and

Andrieu, 2010).

The leaf curvature and the angle of insertion of leaves i_{leaf} at each position on the main stem were collected weekly from the start of stem elongation (960°Cd; Haun stage~8.7) to full senescence (2009°Cd) on 20 main stems per treatment. Stems with their attached leaves were photographed following the silhouette method then photographs were analysed with the POPCORN software (Weiss and de Solan, <https://www6.paca.inra.fr/emmah/Production-Documentation/Outils-et-modeles/>), to register the coordinates of point along the stem and the leaf midribs.

Three D digitization was conducted to ensure a comprehensive characterization of 3D geometry of plants at 795°Cd (Haun stage~7), and at 1333°Cd (1.8 phyllochron after flag leaf ligulation). Two segments of rows per treatment (40 cm length), were collected and measured in each treatment. A segment was collected as an intact bloc, including the soil and root to a depth of ~ 15 cm. There were ~15 plants in *NI* treatments and ~30 plants in *WI* treatments. Row segments were transplanted in pots, photographed and leaves and stems of all plants of the rows segment were digitized in the lab (see **Fig.1**). We used a Polhemus digitizer to register in 3D all plant components (i.e. stems and midrib of leaves for main stem and all tillers). From digitalization, the following variables were calculated (for more details see **Fig.2**):

- β_{stem} : inclination angle of the stem or the pseudostem of the main stem (angle relative to the vertical direction)
- d_{stem} : horizontal distance between the plant base and the upper collar on each axis,
- d_{leaf} : horizontal distance between the plant base and the tip of leaf on each axis,
- θ_{leaf} : azimuth angle of the midrib relative to the row direction
- θ_{stem} : azimuth angle of the pseudostem of an axis relative to the row direction (e.i. the pseudostem direction was defined as the line between the base of the plant and the upper collar of that axis).

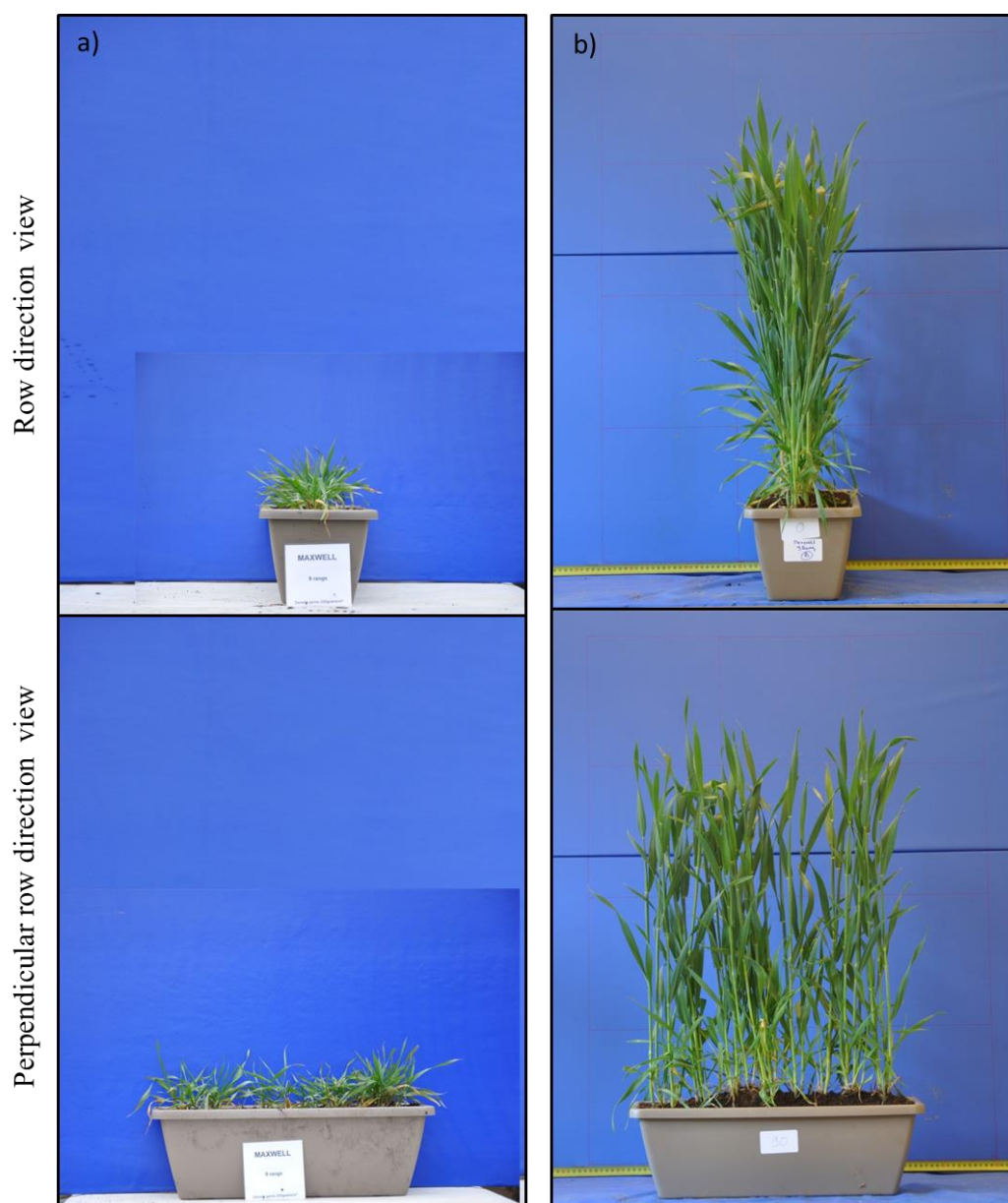


Figure 1: Photographs of segments of rows (wheat *cv.* Maxwell, NI treatment), collected from field and transplanted in pots. Samplings were conducted at 795°Cd (left) and at 1333°Cd (right) after plant emergence.

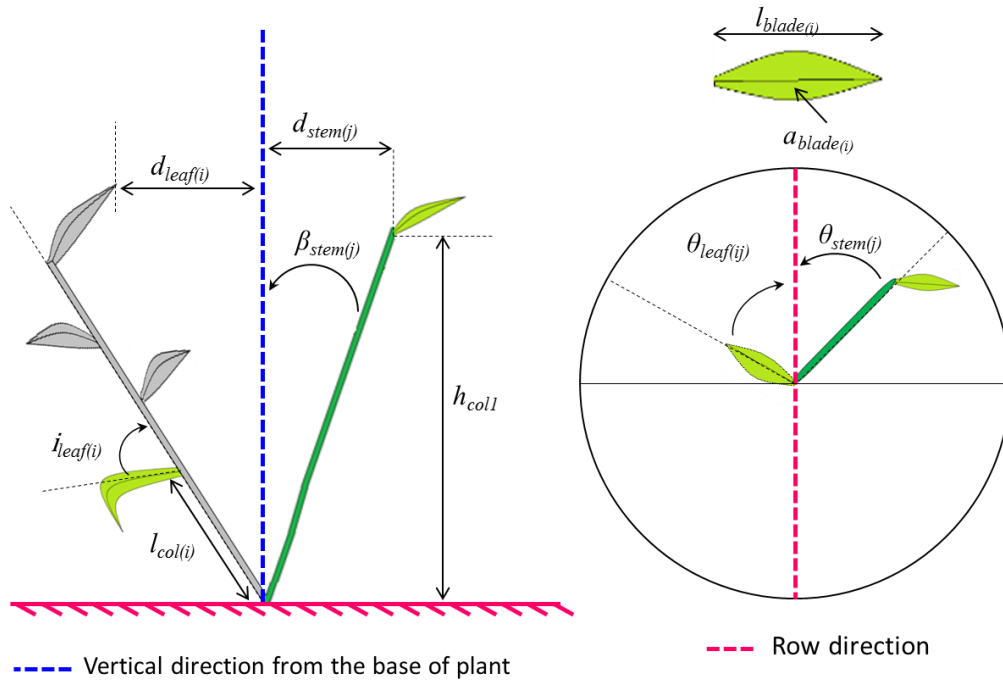


Figure 2: Scheme illustrating the architectural plant variables analyzed:

a) on main stems:

$l_{blade(i)}$: The final blade length of leaf rank 'i' of the main stem.

$a_{leaf(i)}$: The final area of leaf rank 'i' of the main stem.

$l_{col(i)}$: The length between the base of the plant and the collar of leaf 'i' of the main stem.

h_{coll} : The height (vertical distance) between the base of the plant and the upper collar of the main stem

$i_{leaf(i)}$: The angle of insertion of leaf rank 'i' of the main stem, the angle is relative to the direction of the bearing axis.

$\beta_{stem(1)}$: The inclination angle of the pseudostem of the main stem relative to the vertical direction. The pseudostem was defined as the line between the base of the plant and the upper collar of that axis.

b) on both main stems and tillers:

$d_{stem(j)}$: The horizontal distance between the base of plant and the upper collar on the axis 'j'.

$d_{leaf(ij)}$: The horizontal distance between the tip of leaf rank 'i' of an axis 'j' and the base of plant

$\theta_{leaf(ij)}$: The azimuth angle of the midrib of leaf rank 'i' of an axis 'j' and the row direction.

$\theta_{stem(j)}$: The azimuth angle of the pseudostem of the axis 'j' relative to the row direction. The pseudostem was defined as the line between the base of the plant and the upper collar of that axis.

3. RESULTS

3.1. Tillering and yield

Increasing row spacing impacted tillering. The dynamic of the number of axes from 590°Cd after emergence (Haun stage~4.8) to 451°Cd after flag ligulation is shown in *figure3*. For all the cultivars, the number of axes in *WI* treatments was lower than that in *NI* treatments and this was true along the cycle; It is noticeable that this occurred despite the rate of leaf appearance and the final leaf number were either unchanged or higher in *WI* treatments (see next section 3.3.). At the maximum of tillering, the tiller number in *WI* treatment ranged between -13% and -20% below that in *NI* treatment. The difference decreased during the mortality phase, and the density of ear in *WI* treatments ranged from -3% to -10% below that in *NI* treatments. Despite the lower ear density, the grain yield was slightly higher in *WI* in (+2% to +4%) excepted for Apache (-6%) (*Table1*).

3.2. Ground cover and *PAIg*

A comparison of the vertical ground cover $GC(0^\circ)$ between *WI* and *NI* treatments, during the full crop cycle, is shown in *figure4*. For Caphorn and Renan, the points are very close to the bisect line, meaning that increasing row spacing did not impact ground cover during the full crop cycle. For other cultivars, the ground cover was slightly reduced in *WI* treatments and the difference varied along the cycle to reach a maximum around start stem elongation (HS~7.8). The vertical ground cover $GC(0^\circ)$ depends on the plant area index *PAIg* and the plant geometry.

A comparison of the Plant area index *PAIg*, between *WI* and *NI* treatments, during the crop cycle, is shown in the *figure5*. During the early phases of crop cycle, and despite the higher rate of leaf appearance in *WI* (see section 3.3.), the *PAIg* estimated for *WI* treatments was lower compared to *NI* treatments with a mean difference of ~30%. This is consistent with the lower tillering observed in *WI* treatments. However, the accuracy of this estimate is uncertain because the method of estimation is in principle valid for homogeneous crop, and the marked row disposition in the *WI* treatments may present a limit especially at early stages of crop. At flowering, the *PAIg* was measure directly; *PAIg* in *WI* treatments was similar to that in *NI* treatments, despite a lower ear density in *WI* treatments. This is consistent with the larger size of upper leaves blades (*see next section 3.4.*).

Table 1 : Grain yield of five wheat cultivars sown with row spacing of 17.5cm (NI) or 35 cm (WI)

Cultivar	Yield (t ha ⁻¹) of NI	Yield (t ha ⁻¹) in WI
Apache	5.4	5.1
Maxwell	5.4	5.5
Caphorn	4.5	4.7
Soissons	4.3	4.4
Renan	3.8	3.8

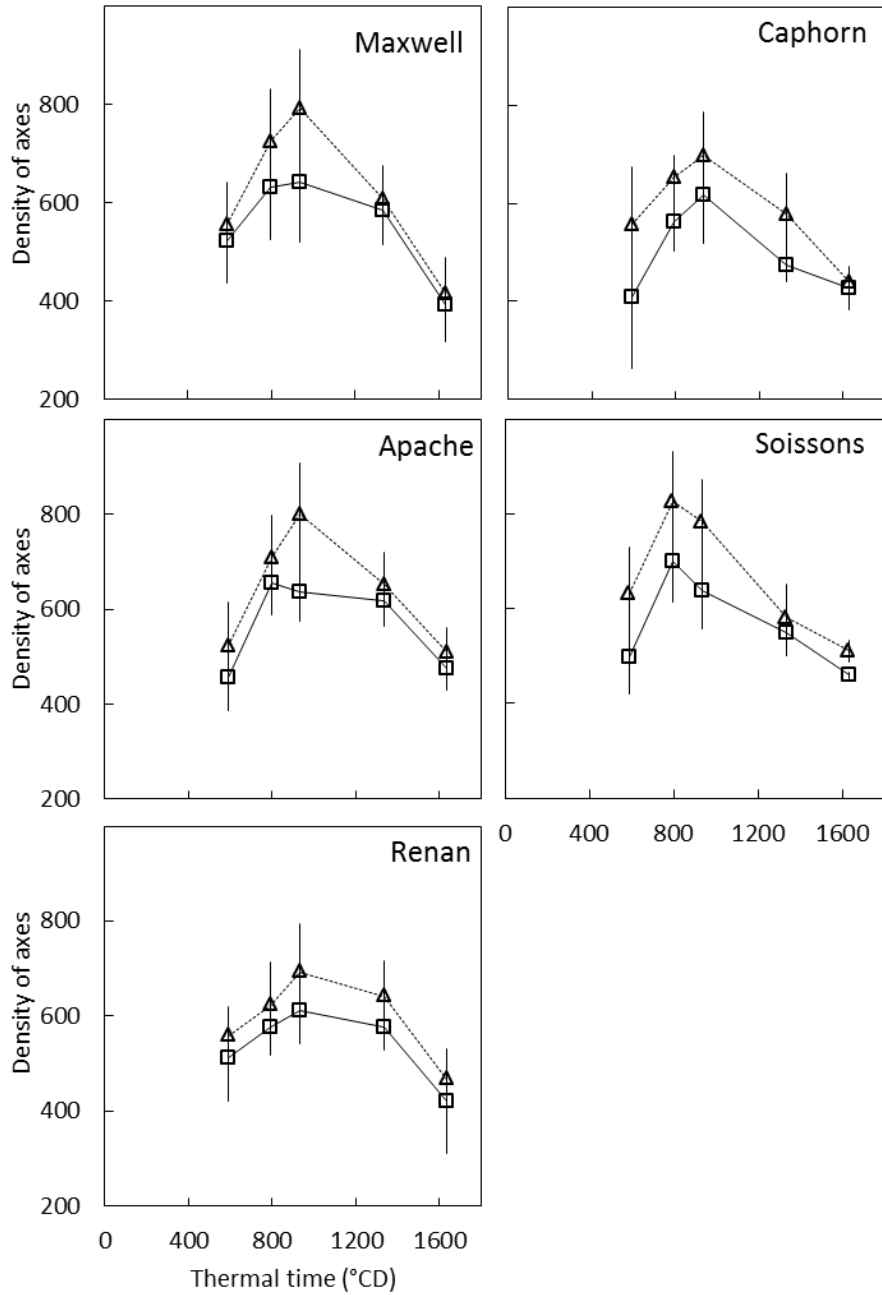


Figure 3: The density of axes per square meter vs. the thermal time from emergence for the five cultivars. Symbols represent the mean values measured on 10 to 50 plants per treatment. Squares and solid lines represent the WI treatment and triangles and dotted lines represent the NI treatment. Each Error bars marks the 95% confidence intervals of mean estimates.

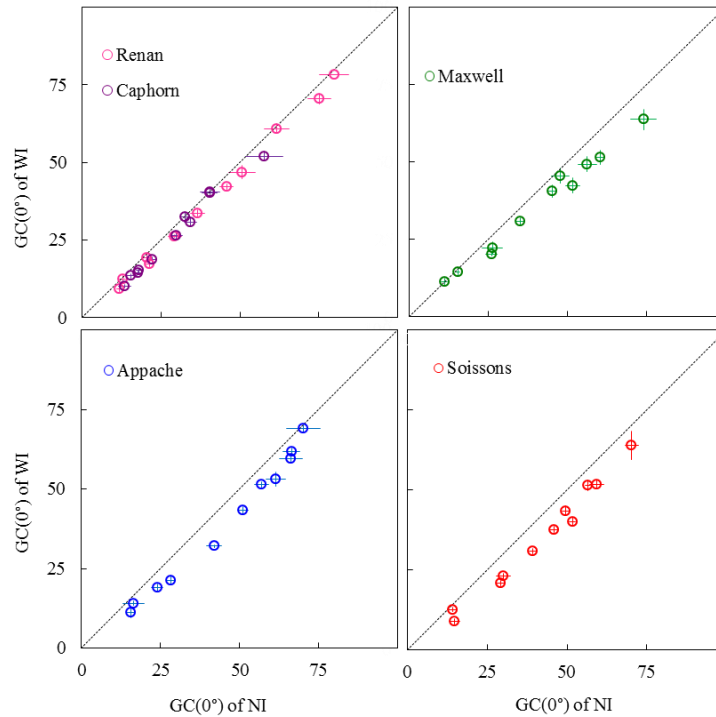


Figure 4: The vertical ground cover $GC(0^\circ)$ of the wide row spacing treatment WI vs. the narrow row spacing treatment NI. The ground cover was measured 12 times from 08/02/2013 to 24/05/2013. Each color represent a cultivar as shown in the legend of figures and each symbol shows the mean values from the analyze of six photographs taken at constant locations (each photograph covered an area of 0.73 m²). Error bars marks the 95% confidence intervals of mean estimates. The dotted line represents the line 1:1.

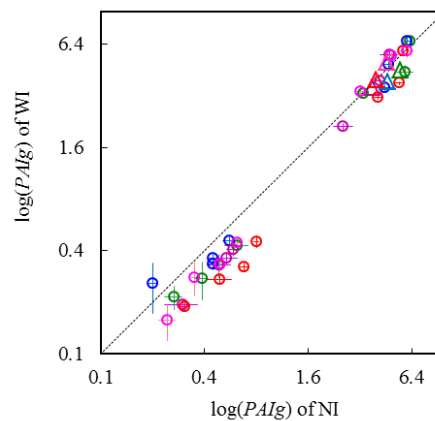


Figure 5: The green plant area index $PAIg$ of the wide row spacing treatments WI vs. that in narrow row spacing treatments NI. Triangles shows the $PAIg$ measured at flowering from scans of leaves and stems. Circles shows the $PAIg$ estimated from photographs with an angle of viewing of 57°, monitored seven times from 18/02/2013 to 17/06/2013. Each color represents a cultivar as follow: red for Soissons, blue for Apache, green for Maxwell, purple for Caphorn, pink for Renan. Each circles shows the mean values from the analyze of three photographs taken at constant locations (each photograph covered an area of 2.03 m²). Error bars mark the 95% confidence intervals of mean estimates. The dotted line represents the line 1:1.

3.3.Plant development

A comparison of the phyllochron of the main stem between *WI* and *NI* treatments is shown in the **figure 6a**. The phyllochron was lower (i.e. leaf appearance rate was higher) under wide row spacing for Apache and Soissons cultivars with a reduction of 11% to 14% respectively. For other cultivars, the phyllochron was almost equal in *WI* and *NI* treatments. In the other hand, increasing row spacing resulted on a slight increase of the final leaf number of about 0.5 leaves for all the cultivars, except Caphorn which showed a decrease of 0.5 leaves under wide row spacing (see **Fig.6b**).

A comparison of the length of the pseudostem l_{stem} and the length of apex l_{apex} of the main stem at 960°Cd after emergence, between *WI* and *NI* treatments is shown in the **figure7**. Both l_{stem} and l_{apex} was higher under *WI* treatments compared to *NI* treatments. Given that the final lengths of collars were similar in *WI* and *NI* treatments (see **Fig.8**), the higher length of l_{stem} and l_{apex} at 960°Cd indicates an advanced stage of development of plants grown under *WI* treatments.

3.4.Dimension of mature organs of plants

The patterns of final blade length, final blade area and final collar height on the main stem are shown in **figure 8**. For all cultivars, blades of lower leaves had almost equal length in *WI* and *NI* treatments but blade of upper leaves (ranks 8-11) were longer in *WI*. Upper leaves blades were also wider in *WI* treatments (not shown) so that upper blade areas were larger (**Fig.8b**). Considering all cultivars together, the cumulated area of the 4 upper blades was 10% higher in *WI* than in *NI*. On the other hand, collar height was not impacted by the inter row distance (**Fig.8c**), meaning that the vertical distribution of leaf insertions was unaffected.

3.5.Geometry of plants

The change over time of the angle of insertion i_{leaf} of main stem leaves from 960°Cd to 2008°Cd (i.e. from Haun stage ~8.7 to the full senescence of leaves) is presented in **figure 9**. For Maxwell, Apache and Soissons cultivars, this angle i_{leaf} was larger in *WI* treatments compared to *NI* treatments and difference increased over time. The i_{leaf} of the Caphorn cultivar was similar in *WI* and *NI* treatments (Renan data are not presented here, analysis is ongoing). The distances and orientation of leaves and stems are presented in **figure10** for the two key stages: at start stem elongation (795°Cd) and close to flowering (1333°Cd).

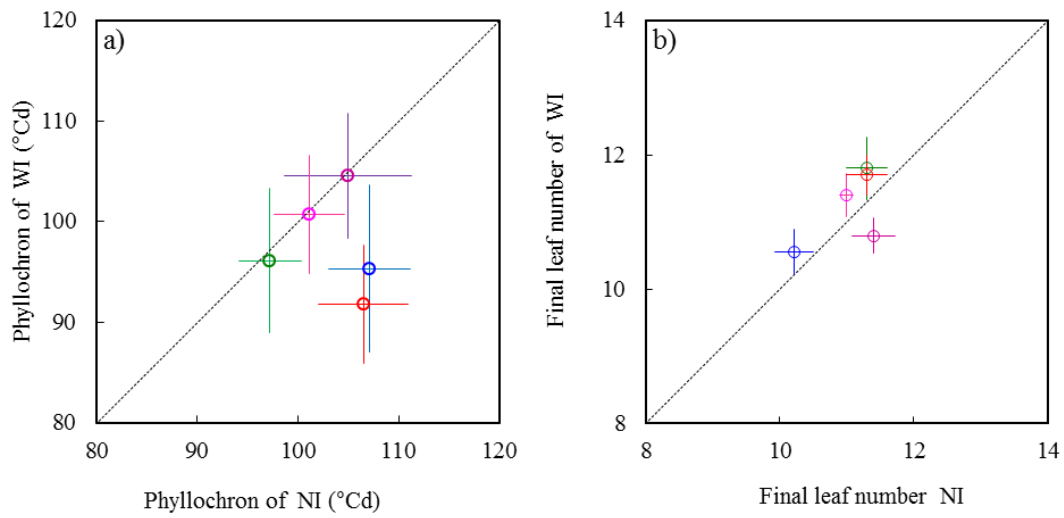


Figure 6: The phyllochron (a) and the final leaf number (b) of the main stem in wide row spacing treatment *WI* vs. those in narrow row spacing treatments *NI*. Each color represents a cultivar as follow: red for Soissons, blue for Apache, green for Maxwell, purple for Caphorn, pink for Renan. Each symbol shows the mean of values measured on 10 to 15 tagged plants. Error bars marks the 95% confidence intervals of mean estimates. The dotted line represents the line 1:1.

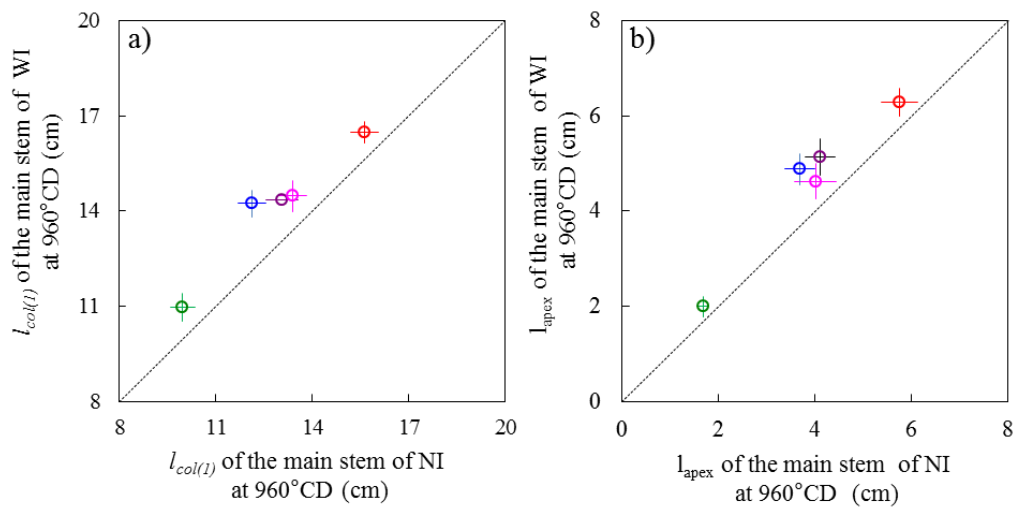


Figure 7: (a) Collar height of the last ligulated leaf l_{col} and (b) apex length l_{apex} of *WI* treatment vs. *NI* treatment. Each symbol represents the mean of values measured on 30 tagged main stems at 960°Cd after emergence. Each color represents a cultivar as follow: red for Soissons, blue for Apache, green for Maxwell, purple for Caphorn, pink for Renan. Error bars mark the 95% confidence intervals of mean estimates. The dotted line represents the line 1:1.

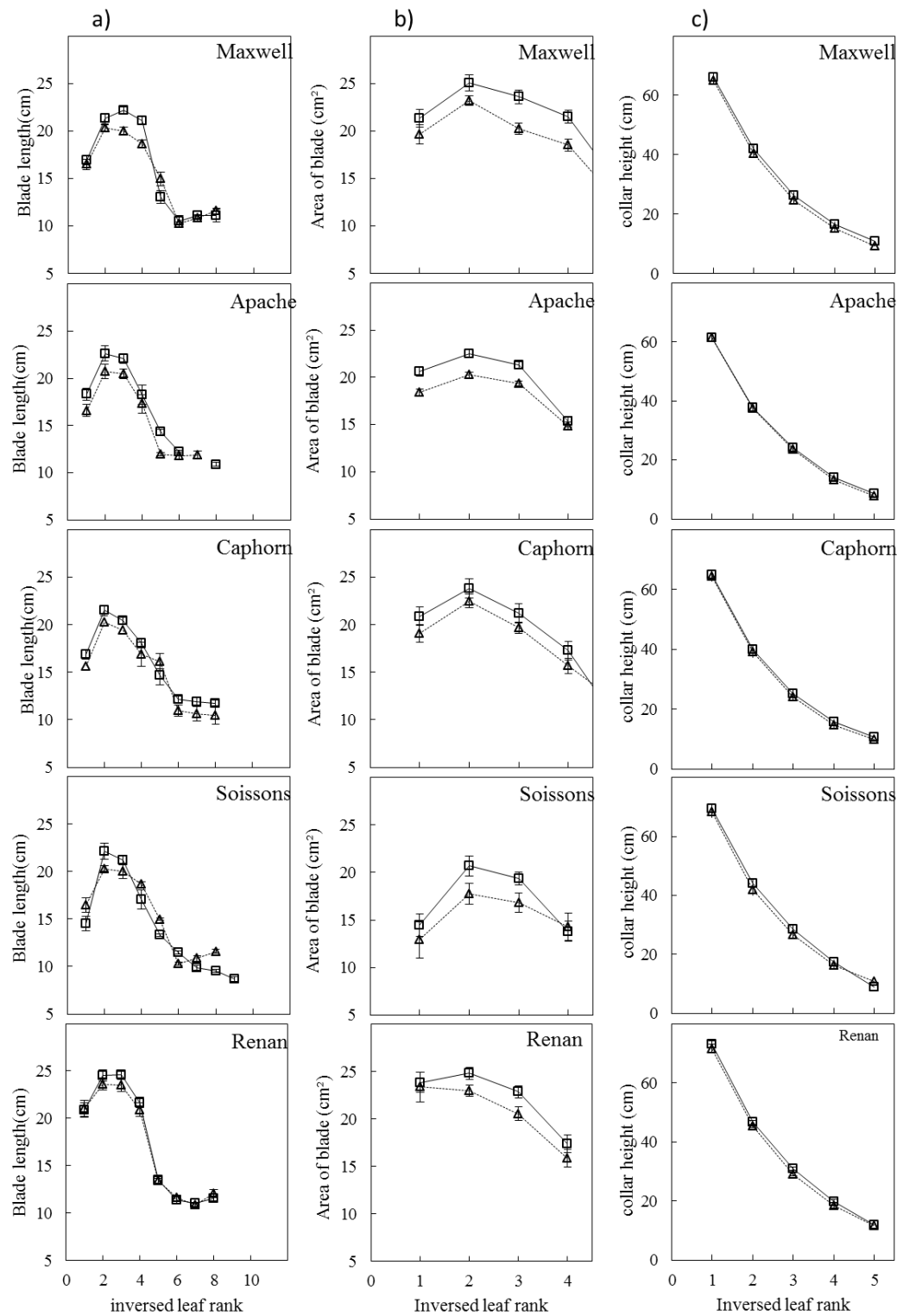


Figure 8: The final dimensions of main stem leaves vs. the inverted leaf rank for the five cultivars. We counted phytomer rank from the top (e.i. basipetally) where $n = 1$ represents the rank of the flag leaf. Figures represent in: (a) the blade length of all leaves, (b) the blade area of upper leaves and (c) the height of collar of upper leaves. Symbols represent the mean of values measured on 10 to 30 tagged plants per treatment. Squares and solid lines represent the WI treatments and triangles and dotted lines represent the NI treatments. Error bars mark the 95% confidence intervals of mean estimates.

The notable features observed at the start stem elongation (at 795°Cd) are:

- The mean horizontal distance d_{stem} between the top of the pseudostem and the base of a plant was 15% - 21% lower in *WI* treatments compared to *NI* treatments for Maxwell, Renan and Soissons (**Fig.10a1**), meaning that pseudo stems in *WI* treatments were more erect. Apache and Caphorn cultivars did not show this behaviour and had similar d_{stem} on *WI* and *NI* treatments.
- The mean horizontal distance of leaf tips, d_{leaf} , differed markedly between interrow spacing treatments only for in cultivars Soissons and Renan (**Fig.10a2**). In Soissons d_{leaf} was 8% lower in *WI* treatment suggesting that plants limited their horizontal propection. Renan showed an opposite behaviour with an increase of + 7% in d_{leaf} .
- The mean azimuth angle of pseudo stems relative to the row direction θ_{stem} was about 45° in all cultivars (**Fig.10a3**), meaning that there was not a general trend to orientate axes relatively to row direction. In the *WI* treatment however, θ_{stem} in Renan was lower (35°), meaning that this cultivar orientated more axes along the row direction. To a lesser extend, Caphorn in *WI* tended to orientate more axes toward the interrow. The mean azimuth angle of leaves relative to the row direction θ_{leaf} was close to 45°, meaning that there was not a general trend to orientate leaves relatively to the row direction. Our data do not show any clear difference between *NI* and *WI* treatments (**Fig.10a4**).

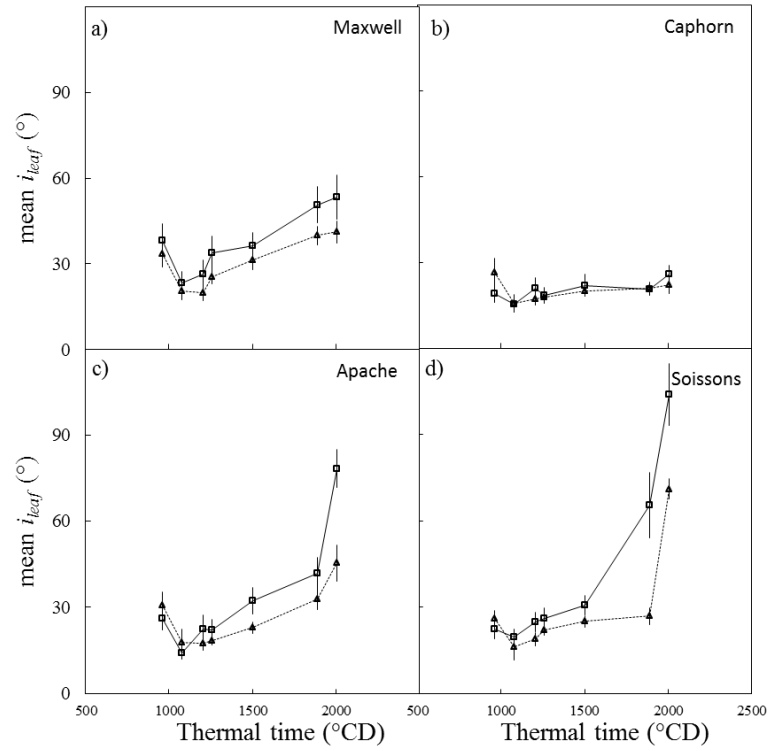


Figure 9: The mean angle of insertion of main stem leaves (i_{leaf}) vs. thermal time from emergence. Each symbol represents the mean values of the upper 4 to 5 leaves of the main stem measured on 30 tagged plants per treatment. Squares and solid lines represent the WI treatment and triangles and dotted lines represent the NI treatment. Each Error bars marks the 95% confidence intervals of mean estimates. The data of Renan cultivar is not available.

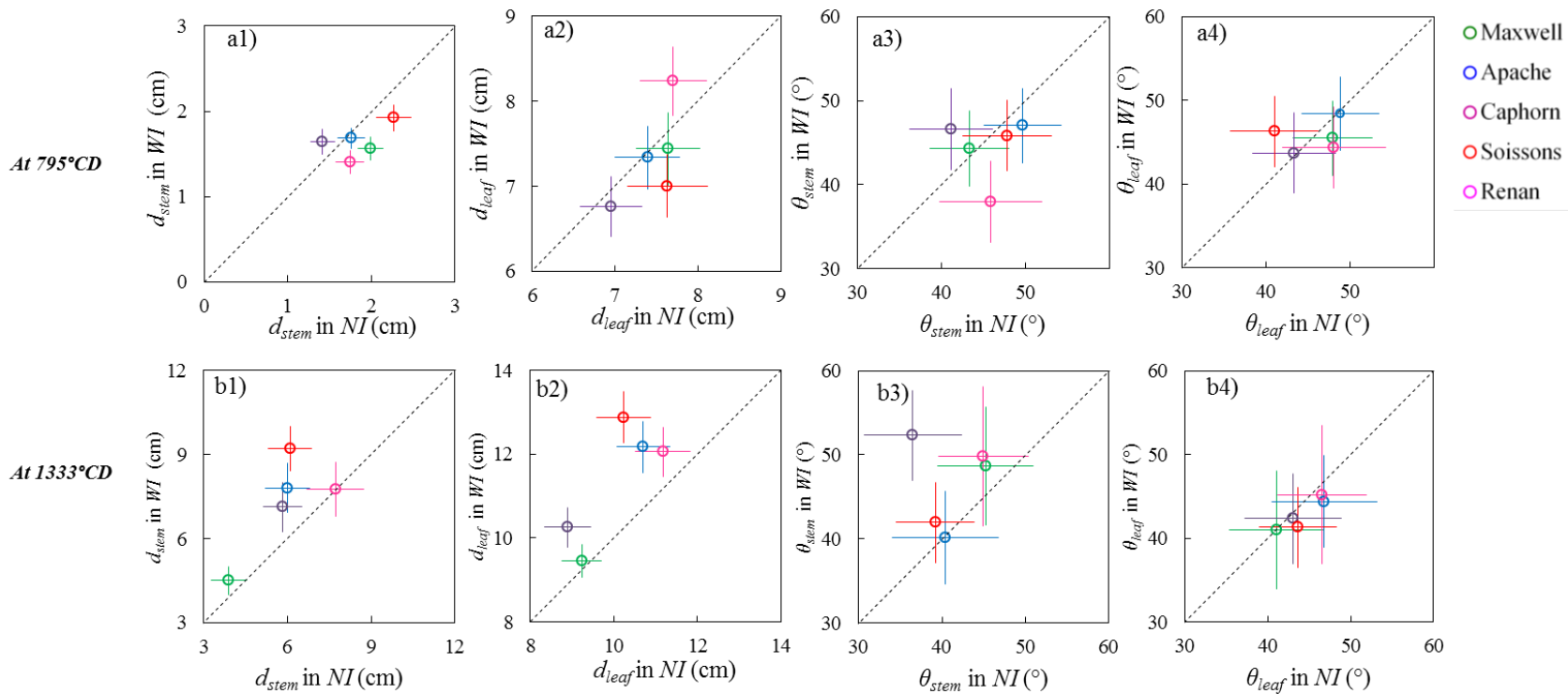


Figure 10: Characterization of stems and leaves horizontal distance from the base of the plant and their azimuth angle from the row direction at two major stages: at start stem elongation in the left 795°Cd and close to flowering in the right 1333°Cd. Each figure shows a comparison of the variable of wide row space treatment (*WI*) vs. the narrow row space treatment (*NI*) (see figure 1 for the definition of the variables). Figures (a1-b1) show the horizontal distance between the top of an axis and the base of the plant d_{stem} . Figures (a2-b2) show the horizontal distance between the tip of a leaf and the base of plant d_{leaf} . Figures (a3,b3) show the azimuth angle of stems or pseudostem (angle relative to the row direction). Figures (a4,b4) show the azimuth angle of the leaf (angle relative to the row direction). Symbols represent the mean values measured on all axes (MS and tillers) from 45 to 55 tagged plants per treatment. Each color represents a cultivar as follow: red for Soissons, blue for Apache, green for Maxwell, purple for Caphorn, pink for Renan. Each Error bars marks the 95% confidence intervals of mean estimates. The dotted line represents the line 1:1.

The notable features observed at the start stem elongation (at 1333°Cd) are:

- The mean horizontal distance d_{stem} differed markedly between cultivars, in the range of 3cm for Maxwell to 8-9 cm for Soissons (**Fig.10b1**). In *WI* treatments d_{stem} was in general higher than in *NI* treatment, but cultivars differed in their response, ranging from no difference for Renan to an increase of 51 % in Soissons. Since plant height was not affected by row spacing (see previous section), this higher value of d_{stem} in *WI* treatment indicates that plant axes were more inclined compared to that in *NI* treatment.
- The mean azimuth angle θ_{stem} was close to 45° in *NI* treatment, meaning that there was no dominant axis orientation in this treatment (**Fig.10b3**). In all cultivars but Apache, θ_{stem} was higher in *WI* treatments meaning that plants orientated their axes towards the inter-row. The orientation was specially marked for Caphorn ($\theta_{stem} = 52^\circ$).
- The mean horizontal distance of leaf tips d_{leaf} showed a general trend to increase under *WI* treatments compared to *NI* treatments, for all cultivars excepted Maxwell. *The result indicates more distant leaves from the plant base (Fig.10b2).*
- The azimuth angle of leaves θ_{leaf} was similar in *WI* and *NI* treatments (**Fig.10b4**), *indicating that plants did not orient preferentially their leaves towards the space between the rows.*

4. DISCUSSION

A common result among the five cultivars was the reduction of tillering under increasing the row spacing. Our data shows that plants reduced their tillering at early stage ($HS \sim 4.8$) when resources were not yet limiting. The maximum density of tillers was reduced by -20% for Apache, Maxwell and Soissons and by -13% for Renan and Caphorn. These findings are in line with [Hiltbrunner et al. \(2005\)](#) who reported a decrease of about 28% of the maximum density of tillers emerged with increasing row space from 0.1875 to 0.3750 m. Later, fewer tillers per square meter had degenerated in *WI* treatments by the time wheat reached maturity; the ear density was reduced in the range of -3% to -10%, and the yield remains unchanged. [Hiltbrunner et al. \(2005\)](#) did not find differences on the ear density and [Johnson et al. \(1988\)](#) reported a mean decrease of ear density of about -21%. So, during the mortality phase of tillers, plants under wide row spacing, having produced fewer tillers compared to *NI* treatment, find themselves in a more comfortable condition with less competition between their axes. Later, they produced similar yield with a slightly reduced number of ears. Yield compensation probably occurred by increasing the number of kernels per ear and the thousand kernel weight as reported by some authors ([Lafond, 1994](#); [Hiltbrunner et al., 2005](#), [Johnson, 1988](#)). In the other hand, under non limiting condition, the reduced

intra-plant competition may explain the increase of protein quality noted by [Hiltbrunner *et al.* \(2005\)](#).

The vertical ground cover under *WI* treatments showed different pattern among cultivars. Increasing row spacing did not impact the ground cover of Caphorn and Renan. Besides, it was slightly reduced for the other cultivars. In the other hand, the plant area index was reduced under *WI* treatments during the early phases of crop cycle which is consistent with the reduction of tillering. At flowering, the plant area index was not reduced, as the lower ear density was compensated by the larger size of upper leaves. Besides, no effect on collars height was observed. Plants under wide row spacing were slightly advanced in their development (lower phyllochron for two cultivars, earlier stems extension for the five cultivars) and produced a slightly higher number of leaves.

The geometry of plants showed a slight change under wide row spacing with differences among cultivars. Plants under *WI* treatment showed a change of their geometrical response during the crop cycle. At early stages, their pseudo-stems were mostly more erected and closer to the plant base may be because plants under wide row spacing had fewer tillers at this stage compared to narrow row spacing (it was reported that the inclination of axes decreased with increasing the number of shoot in the plant [Gibson *et al.*, 1992](#)). No trend was observed on the azimuth angle of plant organs, meaning that plants did not orient their stems and/or leaves towards the free space between rows. At the end of cycle, stems were mostly further from the plant base, with a high variability of response among cultivars ranging from no difference for Renan to an increase of +51 % in Soissons: the range of variation of d_{stem} was larger than the inter-plant distances. When stems were further from the plant base, a slight trend to an orientation towards the free space between rows was observed. The azimuth angle of leaves θ_{leaf} was not changed but leaves presented a higher insertion angle i_{leaf} (more planophyll).

The reduction of the number of tillers emerged and the advanced development of plants under wide row spacing are similar to plant responses under high densities, suggesting a shade avoidance reaction. Plants in *WI* showed sensitivity to the presence of their neighbours in the row rather than to the free space between the rows, they reacted as if plant density was higher. Plants stopped to produce new tiller at early stage (HS~4.6) for which resources were likely not limiting. Such behaviour may have been triggered by phytochrome signalling ([Ballaré *et al.*, 1993](#)). However, plants didn't show any tendency at prospecting the interrow distance at this early stage.

After the start elongation of stems, plants showed a change of behaviour by producing bigger blades, which compensated the reduction of tillering. This response was common for all our cultivars; besides, most cultivars adapted the disposition of their organs in order to prospect more the space. Around flowering, the adaptations differed according to cultivars: (i) stems grew more obliquely in Soissons and Apache (ii) stems oriented toward the free space between rows in Caphorn and (iii) leaves had a higher insertion angle in Soissons, Apache and Maxwell (may be more planophile). Interestingly, the azimuth angle of leaves was not affected, contrary to what is widely reported for maize (eg [Drouet *et al.*,1997](#)).

Our findings concerning yield and tillering responses are on line with what was reported in the literature. Our study provides new information on the degrees of freedom that plants involve to adapt their architecture in response to the location of their neighbours. Representing these behaviours in 3D models would allow to investigate their adaptative value for light capture.

5. Literature cited

- o Abichou M., Fournier C., Dornbusch T., Chambon C., Baccar R., Bertheloot J., ... & Andrieu B. (2013, June). Re-parametrisation of Adel-wheat allows reducing the experimental effort to simulate the 3D development of winter wheat. In 7th International Conference on Functional-Structural Plant Models (pp. 304-306).
- o Abichou M., Dornbusch T., Chambon C., Gouache D, de Solan B, Andrieu B. Parametrizing wheat leaf and tiller dynamics for structural plant models. *Submitted 16-07-2016 to Annals of Botany Journal*
- o Ballaré C. L.,(1994). Light Gaps: Sensing the light opportunities in highly dynamic canopy environments. in: Exploitation of Environmental Heterogeneity by Plants, Caldwell M., Pearcy R (Eds.), Academic Press. London.
- o Ballaré, C. L., & Casal, J. J. (2000). Light signals perceived by crop and weed plants. *Field Crops Research*, 67(2), 149-160.
- o Crabtree, R. J., & Rupp, R. N. (1980). Double and monocropped wheat and soybeans under different tillage and row spacings. *Agronomy Journal*, 72(3), 445-448.
- o Dornbusch, T., & Andrieu, B. (2010). Lamina2Shape-An image processing tool for an explicit description of lamina shape tested on winter wheat (*Triticum aestivum* L.). *Computers and Electronics in Agriculture*, 70(1), 217-224.
- o Drouet, J. L., & Moulia, B. (1997). Spatial re-orientation of maize leaves affected by initial plant orientation and density. *Agricultural and Forest meteorology*, 88(1), 85-100.
- o Evers, J. B., Vos, J. A. N., Andrieu, B., & Struik, P. C. (2006). Cessation of tillering in spring wheat in relation to light interception and red: far-red ratio. *Annals of Botany*, 97(4), 649-658.
- o Epplin, F. M., Allread, V. K., Solie, J. B., Peeper, T. F., & Koscelny, J. A. (1992). Economics of ultranarrow row planting for hard red winter wheat production in Oklahoma. *Journal of production agriculture*, 5(4), 427-431.
- o Freeze, D. M., & Bacon, R. K. (1990). Row-spacing and seeding-rate effects on wheat yields in the Mid-South. *Journal of Production Agriculture*, 3(3), 345-348.
- o Hiltbrunner, J., Liedgens, M., Stamp, P., & Streit, B. (2005). Effects of row spacing and liquid manure on directly drilled winter wheat in organic farming. *European Journal of Agronomy*, 22(4), 441-447.
- o Joseph, K. D. S. M., Alley, M. M., Brann, D. E., & Gravelle, W. D. (1985). Row spacing and seeding rate effects on yield and yield components of soft red winter wheat. *Agronomy Journal*, 77(2), 211-214.
- o Johnson, J. W., Hargrove, W. L., & Moss, R. B. (1988). Optimizing row spacing and seeding rate for soft red winter wheat. *Agronomy Journal*, 80(2), 164-166.
- o Kirby, E. J. M., & Faris, D. G. (1972). The effect of plant density on tiller growth and morphology in barley. *The Journal of Agricultural Science*, 78(02), 281-288.).
- o Maddonni, G. A., Otegui, M. E., & Cirilo, A. G. (2001). Plant population density, row spacing and hybrid effects on maize canopy architecture and light attenuation. *Field Crops Research*, 71(3), 183-193.

- o Marshall, G. C., & Ohm, H. W. (1987). Yield responses of 16 winter wheat cultivars to row spacing and seeding rate. *Agronomy Journal*, 79(6), 1027-1030.
- o Teich, A. H., Welacky, T., Hamill, A., & Smid, A. (1993). Row-spacing and seed-rate effects on winter wheat in Ontario. *Canadian Journal of Plant Science*, 73(1), 31-35.
- o Lafond, G. P. (1994). Effects of row spacing, seeding rate and nitrogen on yield of barley and wheat under zero-till management. *Canadian journal of plant science*, 74(4), 703-711.
- o Lafond, G. P., & Gan, Y. (1999). Row spacing and seeding rate studies in no-till winter wheat for the Northern Great Plains. *Journal of production agriculture*, 12(4), 624-629.

6. Supplementary data

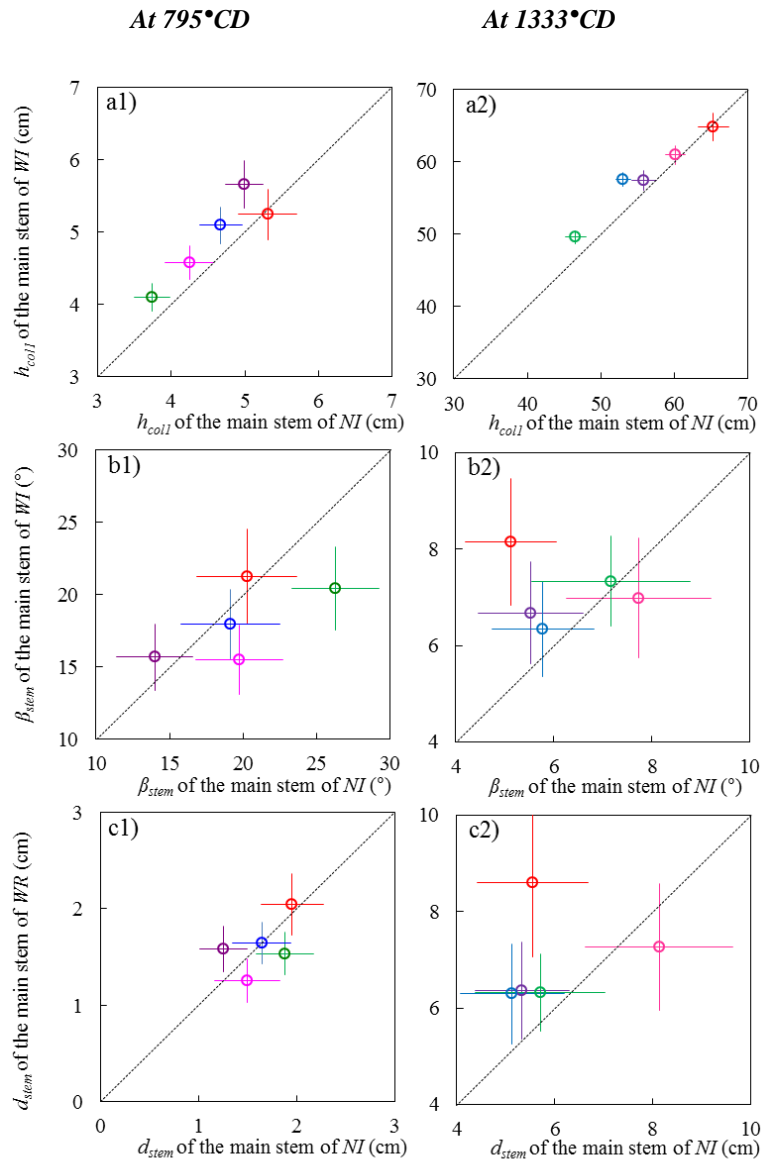



Figure S1: Height , inclination angle and horizontal distance of the upper collar of the main stem (h_{coll} , β_{stem} , d_{stem}) of the wide row spacing (WI) vs. the narrow row spacing (NI). Figures in the left (a1,b1,c1) represent data collected around 795°Cd and those in the right (a2,b2,c2) at 1333°Cd . Symbols represent the mean values measured on 45 to 55 tagged plants per treatment. Each color represents a cultivar as shown in the legend of *figure3a*. Each Error bars marks the 95% confidence intervals of mean estimates. The dotted line represents the line 1:1.



CHAPTER 4: Dynamics of the inclination angle of leaves and stems of winter wheat crop

This chapter is the base of a journal paper by:

Mariam Abichou, Benoit de Solan, Bruno Andrieu

RESUME

Contexte et objectifs. L'architecture 3D des plantes joue un rôle déterminant dans l'interaction avec l'environnement et joue un rôle important dans l'acquisition des ressources, l'exposition des stress et dans les transferts physiques à l'échelle de la plante et du peuplement. Pour ces raisons, la description de la géométrie des plantes est un aspect important dans les modèles « structure-fonction » de plante. Dans ce travail, on s'est intéressé à la caractérisation de l'évolution au cours du temps de : l'angle d'inclinaison des feuilles de chaque rang foliaire et de la pseudo-tige (cylindre incluant les gaines et entrenœuds) de brin maître et des talles.

Matériels & Méthodes. Deux expérimentations ont été menées en 2012/2013 (E1) et en 2013/2014 (E2) avec une sélection de génotypes de blé d'hiver à port contrasté (erectophile et planophile). L'expérimentation (E1) a été conduite au champ avec une densité de semis de 200p/m². Des mesures destructives ont été réalisées une fois par semaine afin de caractériser l'évolution de l'angle d'insertion de chaque feuille du brin maître. Dans l'expérience (E2), les plantes ont été conduites dans des boxes installés en plein air avec deux densités de population (70p/m² et 200p/m²). Des suivis ont été réalisés de façon hebdomadaire afin de suivre l'évolution au cours du temps de la géométrie des plantes. La méthode de digitalisation 3D avec Polhemus a été appliquée. Les variables suivies sont l'angle d'inclinaison de la tige (ou pseudo-tige) de tous les axes des plantes, l'angle d'inclinaison et l'angle d'insertion des feuilles du brin maître. Le nombre et les longueurs de feuilles du brin maître ont été aussi mesurés afin d'estimer l'âge des plantes et des organes.

Résultats. Le résultat marquant de cette étude concerne l'identification d'un pattern de mouvement stable pour les tiges et pour les feuilles. Pour les axes, mes données montrent que l'inclinaison de la pseudo-tige suit une dynamique claire, répétitive et facile à interpréter : les tiges présentent d'abord une inclinaison croissante qui se stabilise à l'arrêt de tallage, ensuite elles se redressent pour atteindre une position verticale tardive autour de la ligulation de la feuille drapeau. Cette progression a été observée à la fois sur le brin maître et sur les talles. La synchronisation observée entre le début de redressement des axes et l'arrêt de tallage suggère que le redressement résulte aussi d'une réaction d'évitement de l'ombre. D'autre part, nos données montrent que l'inclinaison par rapport à la verticale des feuilles à leur point d'insertion varie en fonction de l'âge de la feuille. La progression est claire pour les feuilles inférieures et pour les feuilles supérieures, qui s'inclinent progressivement avec le temps. Les feuilles intermédiaires montrent un mouvement plus complexe, difficile à caractériser. Toutefois lorsqu'on considère l'angle que fait la feuille par rapport à son axe porteur, un schéma unique de progression se trace : on observe une inclinaison progressive jusqu'à une position quasi-stable pour laquelle l'angle avec l'axe diffère généralement fortement entre les feuilles juvéniles et les feuilles adultes.

Conclusion. Les dynamiques du port des feuilles et encore plus des axes ont été très peu étudiées. L'originalité de cette étude consiste à identifier des patterns d'inclinaison des tiges et des feuilles qui sont clairs et répétitifs; ce qui permettra une meilleure représentation de la géométrie dans les modèles FSPM et SPM.

ABSTRACT

Context and aims. The 3D structure of plants is an important aspect of plant-interface with the environment, involved in the capture of resources, the exposition to stresses and physical transfers both within the plant and at canopy level. For these reasons describing plants in 3D is an important aspect of functional structural plant modelling. Despite of this, the representation of plants in FSPM pays little attention to the dynamic aspects of geometry. This work analyses the evolution of the inclination angle of leaves and stems or pseudo-stems (cylinder including sheaths and internodes) during the full crop cycle.

Methods. Two experiments were conducted on 2012/2013 (E1) and on 2013/2014 (E2) exploring five commercial winter wheat cultivars of contrasted stature (erectophile and planophile). Experiment (E1) was conducted in field with a plant density of 200p/m². Destructive measurements were performed at seven dates to characterize leaf curvature and the angle of insertion of individual leaf δ_{leaf} (angle relative to the stem) on the main stems. In experiment (E2), plants were grown in compartments installed outdoor at population densities of 70p/m² and 200p/m². Plant axes and main stem leaves were digitized weekly with a Polhemus digitizer allowing to characterize the evolution over time of: (i) the inclination angle (angle relative to the vertical) of the stem of all plant axes and (ii) the insertion (angle with respect to the vertical) and inclination angle (angle relative to the stem of their bearing axis) of individual leaf rank of the main stem. Measurements on both E1 and E2 were conducted on tagged plants to ensure leaf and tiller rank. In addition to geometrical measurements, we recorded the number and the length (green and senescent) of emerged leaves on the main stem used to compute the age of the plant and the age and the state (green or senescent) of the individual leaf rank.

Results. For the commercial cultivars investigated here, both main stems and tillers stems showed double movement: they started by increasing progressively their stems to attend a maximal inclination close to the time of tillering cessation; then, they straightening to reach a vertical position only close to the time of flag leaf ligulation. This result suggests that the inclination of plant stems is triggered by ontogenic factors. In the other hand, the dynamic of the leaf inclination angle θ_{leaf} with leaf age depended on leaf position: lower and higher leaves showed a progressive droop down with rates and range gradually changing with leaf position and varying between genotypes, intermediate leaves (L6, L7 and L8) showed a complex pattern with a transient straightening due to the movement of the bearing stem during their elongation. Moreover, the dynamic of the leaf insertion angle δ_{leaf} with leaf age showed similarity of pattern among leaf rank. All leaves showed a progressive droop down with rates depending to: (i) the leaf nature (juvenile or adult), (ii) plant density (more erected leaf under high density), and (iii) cultivars.

Conclusion. Our works brings a comprehensive view of leaf and stem movements and highlights the gradual stem inclination and straightening that is of high importance to understand leaf position and orientation. We expect from that work to improve the simulations of plant-environment interactions.

1. INTRODUCTION

The 3D structure of plants is an important aspect of plant-interface with the environment, involved in the capture of resources, the exposition to stresses and physical transfers both within the plant and at canopy level (Saint-Jean *et al.*, 2008; Robert *et al.*, 2008). For these reasons describing plants in 3D is an important aspect of functional structural plant modelling. Functional–structural plant models (FSPM), or virtual plant models, describe explicitly the development over time of the 3D architecture of plants as governed by physiological processes which, in turn, depend on environmental factors (Vos *et al.*, 2010). The explicit representation of the architecture allows describing in details plant-environment interactions and the individual based character makes this approach promising for simulating plant to plant interactions in complex canopies (Barillot, 2014). These models are also used to simulate the signals perceived by sensors and thus improve phenotyping methods (Liu *et al.*, 2016). While visually impressive, the representation of the geometrical aspects of plants in existing models is based on mostly statistical techniques that use collections of measured shapes or measured distributions of parameters (e.g. ADELwheat model of Fournier *et al.*, 2003). Real plants modulate non-randomly the orientation and inclination of their leaves and stems, with implication on light capture, shadowing of competitors and stresses avoidance. For grass, many studies focused on the mature curvature of leaves and their implication in the capture of light (Ledent *et al.*, 1978a,b; Wang *et al.*, 2007; Abreu *et al.*, 2008 ; Prévot *et al.*, 1991). However, no studies, in our knowledge, analysed in detail the dynamic aspects of the geometry of stems and leaves of plants.

In this work, we characterized the evolution during plant lifespan of: (i) stem or pseudo-stem angle with respect to the vertical of both main stem and tillers, (ii) leaf angle with respect to the vertical of individual leaf rank (i.e. leaf inclination angle), and (iii) the leaf insertion angle relative to the direction of the stem of the bearing axis. We characterized these dynamics in plants from five commercial cultivars of winter wheat crop sown under different densities.

2. MATERIALS AND METHODS

2.1. Experimental design and treatments

Experiments was conducted in 2012/2013 and in 2013/2014, at the INRA campus of Thiverval-Grignon (48°51 N, 1°58 E), with a maritime influenced climate and a deep loamy soil. In 2012/2013 (E1), an experiment was conducted in field conditions with five cultivars of winter wheat *Triticum aestivum* (Maxwell, Apache, Caphorn, Renan, and Soissons) sown at a density of 200 seeds m⁻² on 02 October 2012. In 2013/2014, an experiment (E2) was conducted in containers placed outdoors with three cultivars (Apache, Renan and Caphorn) sown by hand on 3 November 2013 at a density of 70 seeds m⁻² for the three cultivars and a density of 200 seeds/m² for Caphorn. Each treatment was sown in two outdoors containers (length 1.20m; width 1.00m; depth 1.2m) each including five rows with an inter-row distance of 0.175m. Eight measured plants per container (16 plants per treatment) are selected from the third or the fourth row to minimise the edge effects.

Nitrogen fertilization followed the standard scheme with one dose at tillering stage and one dose brought shortly before stem elongation. Weeds were controlled by herbicide application

at sowing and during the crop cycle. Air temperature at 2 m was recorded from a nearby meteorological station. Thermal time was computed from plant emergence on an hourly basis, assuming a linear response to temperature with a base temperature of 0°C.



Figure 1: The outdoor containers of experiment E2. Three cultivars (Apache, Renan and Caphorn) were sown by hand on 3 November 2013 at a density of 70 seeds/m² for the three cultivars and at a density of 200 seeds/m² for Caphorn.

2.2. Measurements

In both experiments the number of visible and ligulated main stem leaves and their lengths were measured during the full crop cycle on 10-16 tagged plants per treatment to characterise the Haun stage dynamics (e.g. dynamic of leaf appearance). The percentage of senescence of individual leaf rank was also measured. To compute plant and leaf age during the full crop cycle, we estimated the phyllochron (the inverse of the rate of ligulation). It was defined by adjusting a linear model between the Haun stage and the thermal time. In experiment E2, the number and the order of tillers was followed. The upper tiller to appear was T₅ in low density treatments D70 (Caphorn, Apache and Renan) and T₃ in D200 (Caphorn). Given the coordination of tiller emergence with Haun stage (Abichou *et al.*, 2016a), the Haun stage at cessation of tillering was estimated as HS = 6.9 for D70 and HS = 5.5 for D200.

In experiments E1, destructive measurements were conducted to follow the evolution of the leaf curvature of upper leaves: leaf 7 to flag leaf. About 30 main stems per treatment were collected and photographed weekly from start stem elongation (960°Cd; Haun stage ~8.7) to full senescence (2009°Cd). Stems and leaf midrib were digitized manually from photographs using the POPCORN software (<https://www6.paca.inra.fr/emmah/Production-Documentation/Outils-et-modeles/>). From digitalized data, we calculated the angle of insertion δ_{leaf} of each leaf relative to the bearing stem (see *Fig.1*).

Experiments E2 aimed at analysing the evolution of the plant geometry during the full crop cycle. For this, 16 tagged plants per treatments were followed weekly from the emergence of the 4th leaf of the main stem (counted acropetally) to the full plant senescence. Polhemus digitizer was used to digitalize the pseudo-stems (cylinder including sheaths and internodes) of all tillers and the midrib of all main stem leaves. From digitalized data, a set of variables was calculated as shown in *Fig.2*. These variables are: (i) the inclination angle of the pseudo-stem θ_{stem} (i.e. the angle with respect to the vertical) of all plant axes (main stem and tillers), (ii) the inclination angle θ_{leaf} of the individual leaf rank of the main stem, (iii) the insertion angle δ_{leaf} of individual leaf rank with respect of the direction of the bearing stem.

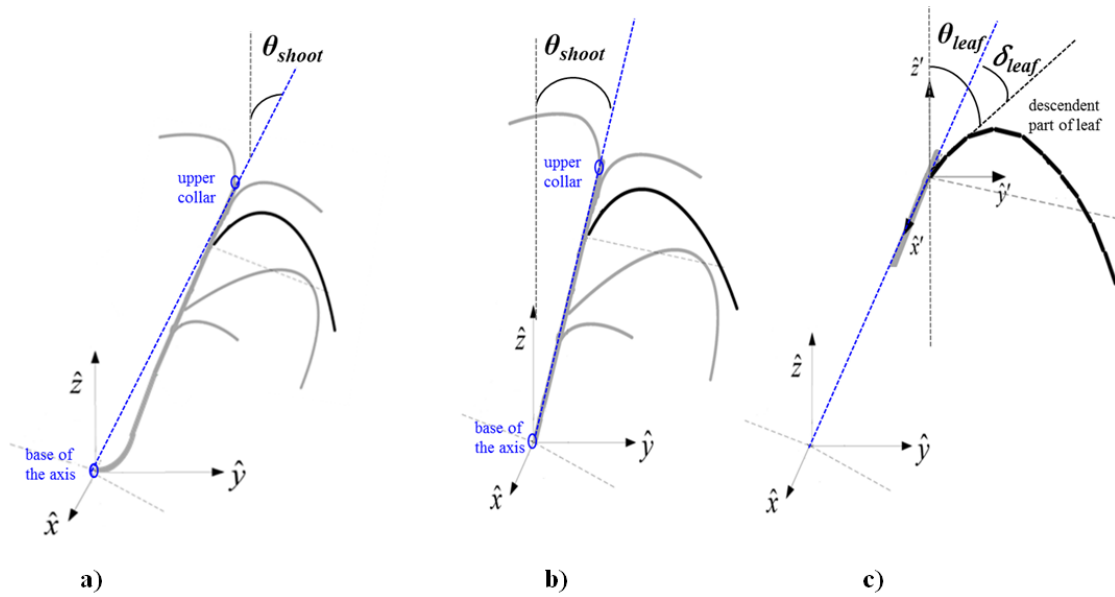


Figure 2: Scheme illustrating the architectural plant variables analyzed:

- $\delta_{leaf(n)}$: The angle of insertion of the leaf at rank 'n' on the main stem; this angle is between the stem and the leaf midrib at the base of the blade
- $\theta_{leaf(n)}$: The inclination of the leaf at the rank 'n' on the main stem. This is the angle between the vertical and the leaf midrib at the base of the blade.
- $\theta_{stem(j)}$: The inclination angle of the stem or pseudostem of the axis 'j'; this angle is between the vertical and the line of stem axis defined as the line between the base of the axis and the upper collar on that axis.

3. RESULTS AND DISCUSSION

3.1. Dynamic of the inclination angle of stems: similarity of patterns between axes triggered by ontogenic factors

The inclination angle of the pseudo-stem (θ_{stem}) vs the phyllochronic plant age is shown in [figure3](#) and [figure4](#).

For the main stems, the [figure3](#) shows a clear pattern with three phases: first, the axes emerged vertical and inclined progressively and reached a maximal inclination that depends to plant density; second, the axes straightened to reach a stable position only close to the time of flag leaf ligulation; then the axes position remained stable. For Caphorn cultivar sown under two densities (D70 and D200), the progress of the inclination angle before the tillering cessation of D200 treatment showed similar patterns, but later, the stem inclination stops for D200 and continued for D70 (e.i. the maximum θ_{stem} was 57° for D70 and 40° for D200). In the other hand, the treatments Caphorn/D70 and Renan/D70 sowing under low density showed similar patterns, but different to Apache/D70 pattern which underline an important cultivar effect. For the treatment sowing under higher density (D200), the maximum inclination was reached at Haun stage of 5.3. Besides, the maximal inclination was reached around a Haun stage of 7 to 7.8 for the cultivars sowing under low density (D70). When axes reached their maximal inclination, the plant stage was very close to the time of tillering cessation for all treatments (D70 and D200).

Concerning tillers, the [figure4](#) shows that tillers follow a similar pattern to that of the main stem: the maximal inclination angle was reached synchronously for all axes and tillers stems reached also a stable angle close to the flag ligulation. The patterns of tiller stems showed hierarchy with tiller rank: T_1 and T_2 had the highest inclination and T_4 and T_5 had the lowest one.

At the end of cycle, we checked by dissection the shape of the stems and we noted that nodes presented a deformed side which underlines their role in correcting stems posture. [Clore \(2013\)](#) reported that the correction of stem position was insured by pulvini which are regions of tissue that are apical to each node and collectively return a reoriented stem to a more vertical position. However, for the early phases we don't know which regions are implicated to drop down of axes.

The correlation between the straightening of plant stems and tillering cessation suggests that the two processes are responses of the same signal. It has been largely proposed that cessation of tillering is a shade avoidance response related to the early detection of neighbours which is mainly sensed by plants through the R:FR ratio ([Casal, 2013](#); [Franklin, 2005](#); [Evers et al., 2007](#)). It seems possible that the straightening is another plant strategy to avoid shade of surrounding plants triggered by light quality signal.

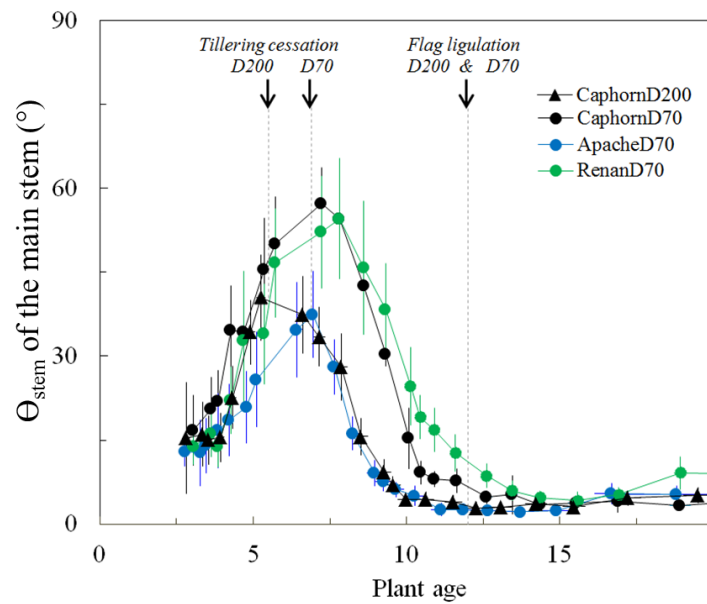


Figure 3: The inclination angle of the main stems vs. the phyllochronic plant age in experiment E2 (Y2013/2014). Treatments consisted in cultivars Apache, and Renan sown at 70plt/m² (D70) and cultivar Caphorn sown at 70plt/m² and 200plt/m² (D200). Each symbol represents the mean value of stem inclination angle calculated over 16 tagged plants. Error bars mark the 95% confidence intervals of mean estimates. Dashed lines show the stage when the plants stopped tillering and the time when flag leaves were ligulated.

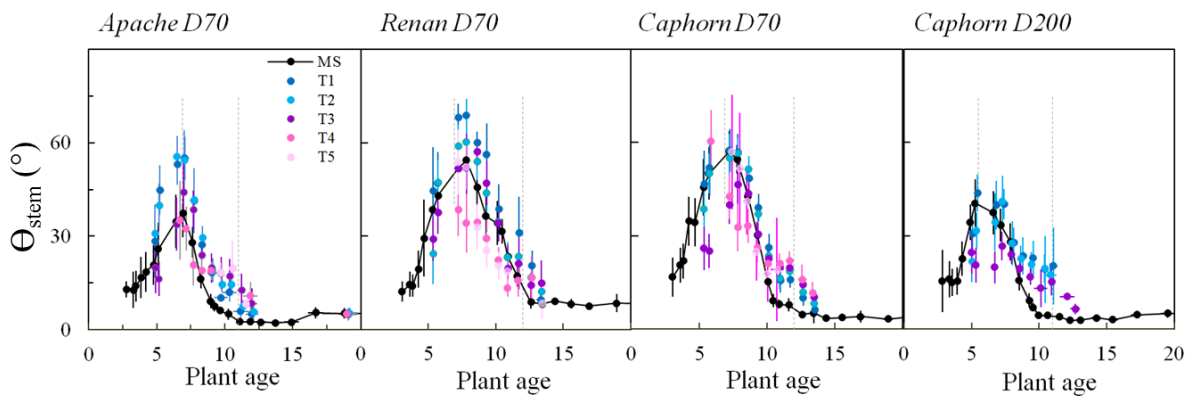


Figure 4: The inclination angle of the plant stems vs. the phyllochronic plant age from emergence for the four treatments from experiment E2 (Y2013/2014). Treatments covered the two cultivars (Apache, Renan) sowing under low density (D70plt/m²) and one cultivar (Caphorn) sowing under two densities (D70plt/m² and D200plt/m²). Figures show data relative to both main stem (black) and all primary tillers emerged. Black symbols represent data relative to the main stem and colored symbols represent the different tiller rank as shown in the legend of the first figure in the left. Each symbol represents the mean value calculated over 16 tagged plants per treatments followed weekly. Error bars mark the 95% confidence intervals of mean estimates. Dashed lines represent the stage when the plants stop tillering and the time when their flag leaf of the main stem is ligulated.

3.2. Dynamic of the inclination angle of leaves: similarity of patterns among leaf ranks

Leaves showed a progressive downward movement for all leaf ranks. The **figure 4** shows the evolution of the leaf inclination angle θ_{leaf} of main stem leaves with the progress of leaf age measured on the four treatments (Apache D70, Renan D70, Caphorn D70 and Caphorn D200) from experiment E2. The dynamic of the leaf inclination angle θ_{leaf} with leaf age depended on leaf position: lower and higher leaves showed a progressive droop down, with rates and ranges gradually changing with leaf position and varying between genotypes; intermediate leaves (L6, L7 and L8) showed a complex pattern with a transient straightening due to the movement of their bearing stems after tillering cessation.

To study the movement of leaves separately from the movement of stems, we analysed δ_{leaf} , the angle of insertion of leaves relative to their bearing axis. This dynamics is presented in **figure 6 and 7**. The progress of δ_{leaf} with leaf age showed a pattern which was similar in all treatments and among all leaf ranks. The δ_{leaf} dynamics consisted in a first phase of increase, then a phase of relative stability. The rates of change of δ_{leaf} depended on the rank of leaves. Juveniles leaves (L2 to L6) showed a rapid increase of δ_{leaf} with almost the same rate for all leaf ranks. Adults leaves (L7 to flag leaf) showed a slower increase of δ_{leaf} , with similar rates for all adult leaves in Apache, but a noticeable decrease of rate with higher leaf rank in Caphorn. The angle of insertion was impacted by plant density: in Caphorn, the leaves in the D200 treatment stayed much more erect compared to those in the low density treatment. Taken together these results show a strong Genotype * Environment interactions in the behaviour of leaf inclination. It would be interesting to study the factors responsible for more erectophile leaves and stems under high density (e.g. light quantity or quality).

4. CONCLUSION

Our work brings a comprehensive view of leaf and stems movements and highlights the gradual stems inclination and straightening that is of high importance to understand leaf position and orientation. We expect from that work to improve the simulations of plant-environment interactions.

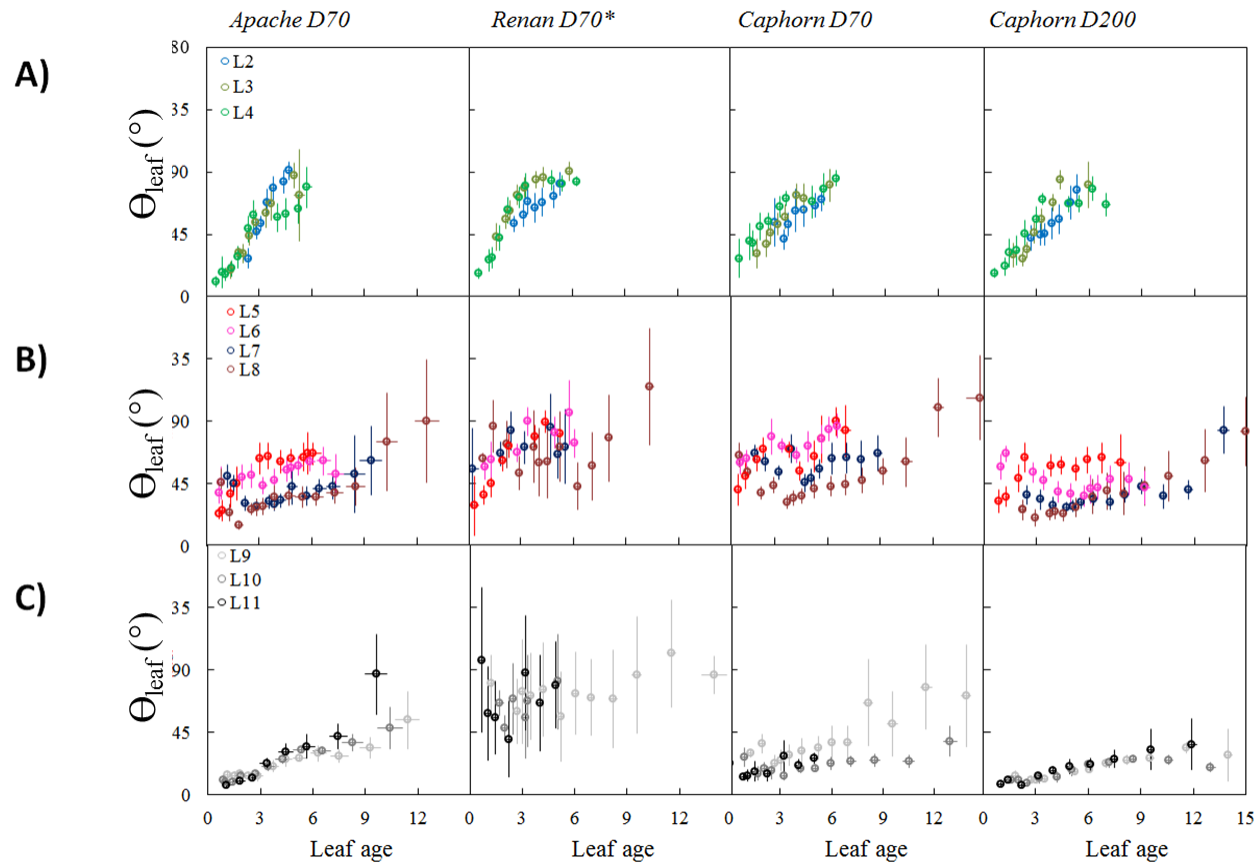


Figure 5: The inclination angle of individual leaf rank of the main stem vs. phyllochronic leaf age from their appearance (i.e. the appearance of a leaf is the moment when their tip emerge above the collar of the previous leaf). Data shows data from experiment E2 as presented in the figure 2. Figures show data of different leaf grouped per leaf ranks: in (A) leaf 2 to leaf 6 (juveniles leaves) and in (B) leaf 7 to flag leaf (adult leaves). Colored symbols represent the different leaf rank as shown in the legend of the left figures. Each symbol represents the mean value calculated over 16 tagged plants per treatments followed weekly. Error bars mark the 95% confidence intervals of mean estimates. **Some bugs were identified in the digit file for the Renan treatment that could explain the large error bars observed; verification is ongoing.*

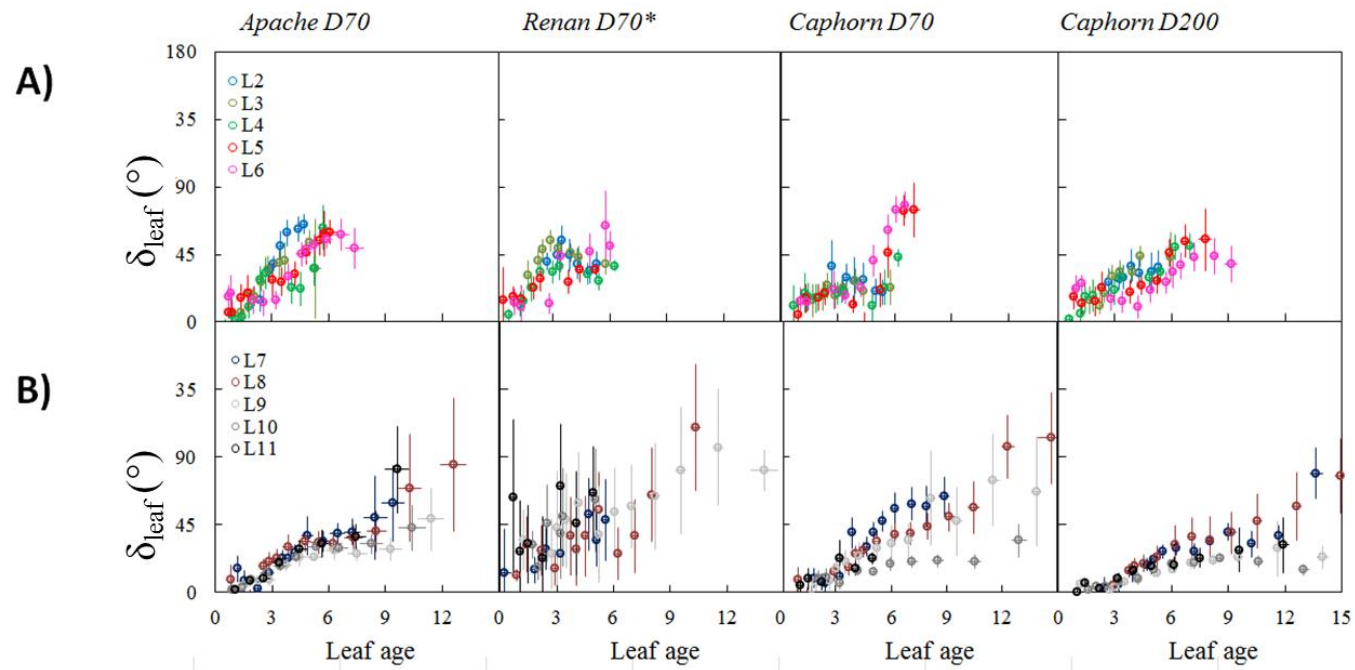


Figure 6: The angle of insertion of individual leaf rank of the main stem vs. phyllochronic leaf age from their appearance (i.e. the appearance of a leaf is the moment when their tip emerge above the collar of the previous leaf). . Data shows data from experiment E2 as presented in the figure 2. Leaf ranks are grouped into two groups: figures (A) represent juveniles leaves (L2 to L6) and figures (B) shows adult leaves (L7 to flag leaf). Colored symbols represent the different leaf rank as shown in the legend of the up-left figures. Each symbol represents the mean value calculated over 16 tagged plants per treatments followed weekly. Error bars mark the 95% confidence intervals of mean estimates. **Some bugs were identified in the estimation of the inclination angle of Renan leaves because leaves shows more complex curvature that explain the large error bars observed; verification ongoing.*

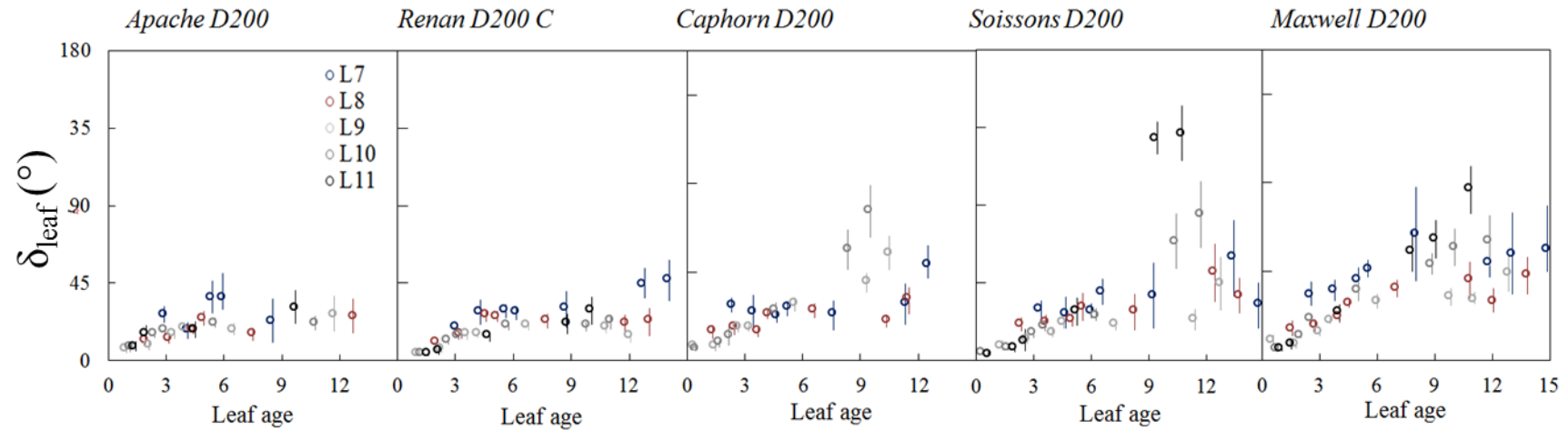


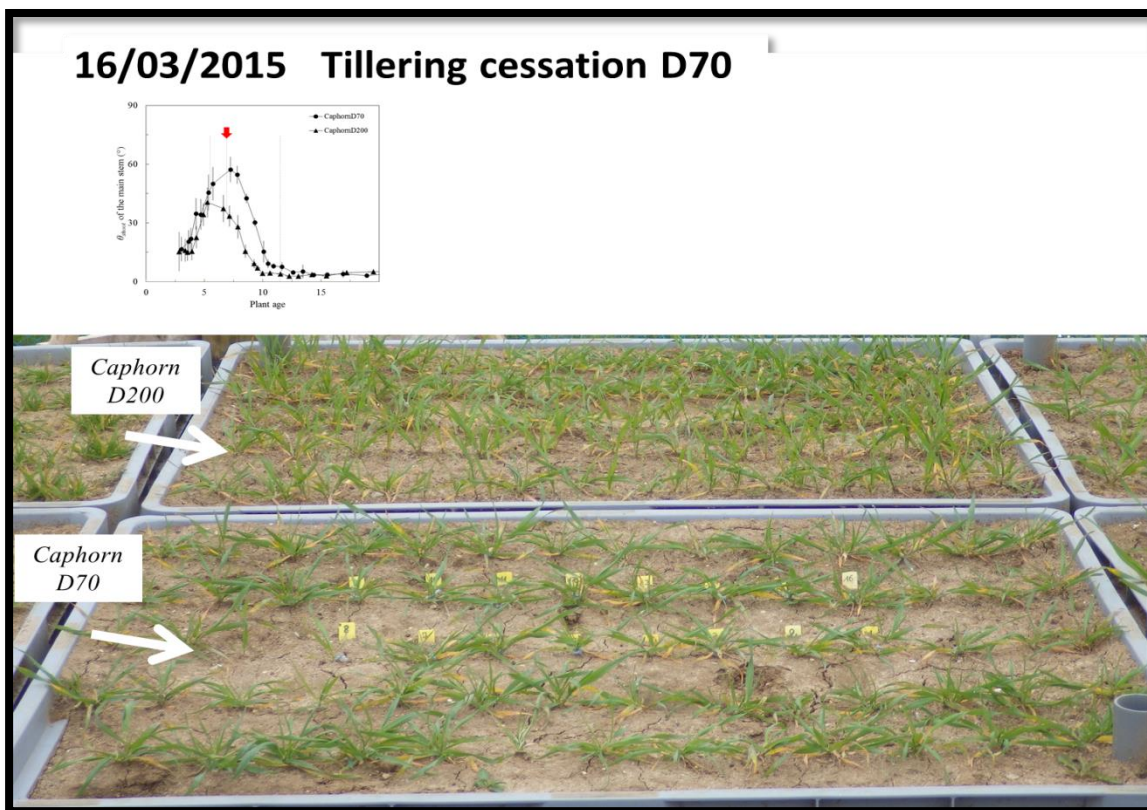
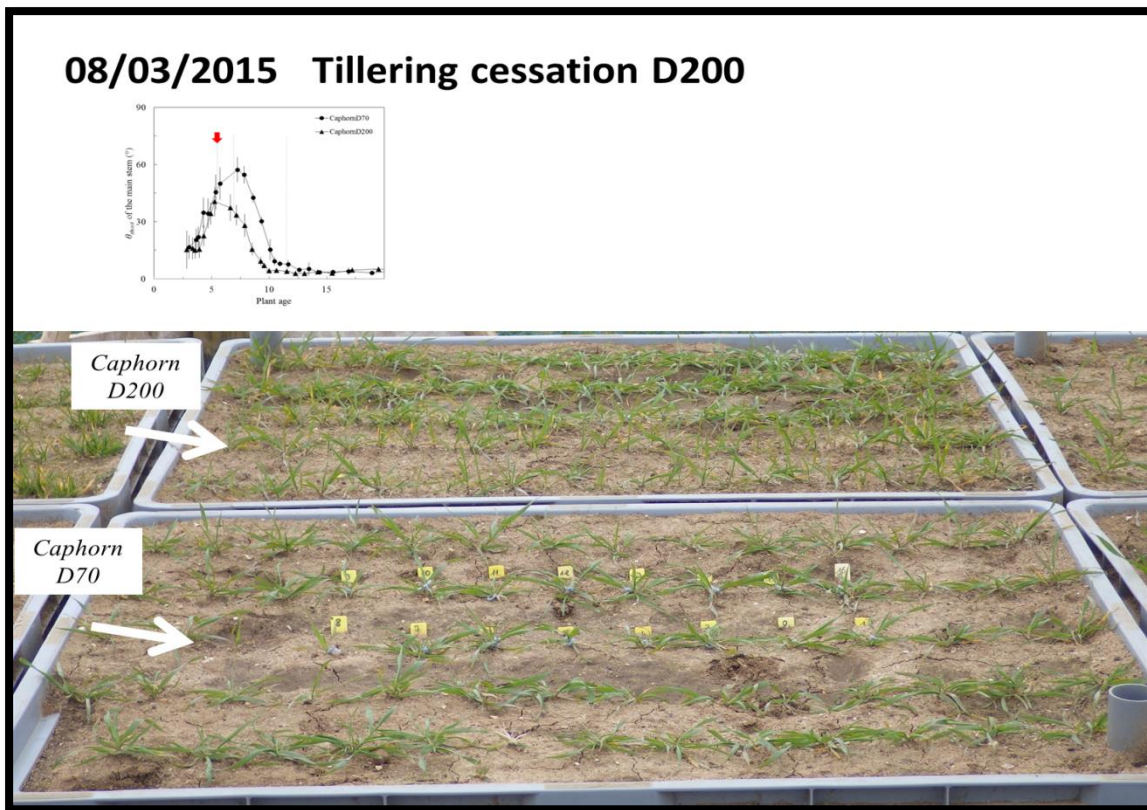
Figure 7: The angle of insertion of individual leaf rank of the main stem vs. phyllochronic leaf age from their appearance (i.e. the appearance of a leaf is the moment when their tip emerge above the collar of the previous leaf). Data are from experiments E1 (Y2012/2013) including five cultivars sowing under standard density D200plt/m². In each figure, each colored symbol represents one leaf rank from leaf 7 to leaf 11 (adult leaves) (see legend of the up-left figure). Seven destructive measurements were carried out to measure the leaf curvature. Each symbol represents the mean value calculated over 20 to 30 plants per treatments. Error bars mark the 95% confidence intervals of mean estimates.

5. Literature cited

- Abichou, M., Fournier, C., Dornbusch, T., Chambon, C., Baccar, R., Bertheloot, J., ... & Andrieu, B. (2013, June). Re-parametrisation of Adel-wheat allows reducing the experimental effort to simulate the 3D development of winter wheat. In 7th International Conference on Functional-Structural Plant Models (pp. 304-306).
- Abreu ME, Munne-Bosch S. 2008. Hyponastic leaf growth decreases the photoprotective demand, prevents damage to photosystem II and delays leaf senescence in *Salvia broussonetii* plants. *Physiologia Plantarum* 134: 369-379.
- Birch, C. J., Andrieu, B., Fournier, C., Vos, J., & Room, P. (2003). Modelling kinetics of plant canopy architecture—concepts and applications. *European Journal of Agronomy*, 19(4), 519-533.
- Casal, J. J. (2013). Canopy light signals and crop yield in sickness and in health. *ISRN Agronomy*, 2013.
- Clore, A. M. (2013). Cereal grass pulvini: Agronomically significant models for studying gravitropism signaling and tissue polarity. *American journal of botany*, 100(1), 101-110.
- Dornbusch, T. (2007). Development and application of a three-dimensional architectural model to describe morphological traits of spring barley (*Hordeum vulgare* L.) stands. Phd thesis, Der Andere Verlag.
- Dornbusch, T., & Andrieu, B. (2010). Lamina2Shape—An image processing tool for an explicit description of lamina shape tested on winter wheat (*Triticum aestivum* L.). *Computers and Electronics in Agriculture*, 70(1), 217-224.
- Evers JB, Vos J, Andrieu B, Struik PC. 2006. Cessation of tillering in spring wheat in relation to light interception and red:far-red ratio. *Annals of Botany* 97: 649-658.
- Evers JB, Vos J, Chelle M, Andrieu B, Fournier C, Struik PC. 2007a. Simulating the effects of localized red:far-red ratio on tillering in spring wheat (*Triticum aestivum*) using a three-dimensional virtual plant model. *New Phytology* 176: 325-336.
- Fournier C, Andrieu B, Ljutovac S, Saint-Jean S. 2003. ADEL-wheat: a 3D architectural model of wheat development. Pages 54-63 in Hu B-G, Jaeger M, eds. *Plant Growth Modeling and Applications*. Beijing, CHN Tsinghua University Press - Springer Verlag.
- Franklin O., Ågren G. I., 2002. Leaf senescence and resorption as mechanisms of maximizing photosynthetic production during canopy development at N limitation. *Functional Ecology*, 16(6), 727-733.
- Franklin, K. A., & Whitelam, G. C. (2005). Phytochromes and shade-avoidance responses in plants. *Annals of Botany*, 96(2), 169-175.
- Ledent J. F., 1978a. Beam light interception by leaves with undulating edges—a simulation of maize leaf sections. *Agricultural Meteorology*, 19(5), 399-410.
- Ledent J. F., 1978. Mechanisms Determining leaf movement and leaf angle in wheat (*Triticum aestivum* L.). *Annals of Botany*, 42(2), 345-351.
- Liu S., Baret F., Abichou M., Boudon F., Zhao K., Fournier C., Andrieu B., Kamran I., Hemmerlé M., de Solan B. Estimating wheat Green area index from ground-based LiDAR measurement through 3D ADEL-Wheat model. *Submitted 19-09-2016 to Agriculture and Forest Meteorology*.
- Wang W.M., Li Z.L., Su H.B., 2007. Comparison of leaf angle distribution functions: Effects on extinction coefficient and fraction of sunlit foliage. *Agricultural and Forest Meteorology* 143:106-122.
- Zhang, W., Tang, L., Yang, X., Liu, L., Cao, W., & Zhu, Y. (2015). A simulation model for predicting canopy structure and light distribution in wheat. *European Journal of Agronomy*, 67, 1-11.

6. Appendix

Supplementary illustration: photographs of plants at tillering cessation which corresponded to stage of maximum stem inclination in all axes.





DISCUSSION GENERALE

1. Rappel du contexte et objectifs

Les modèles architecturaux (*SPM*) sont fondés sur une description botanique et géométrique réaliste de la plante. Ils s'appuient sur des descripteurs morphologiques, qui sont définis par des fonctions paramétriques, empiriques ou statistiques calées sur des mesures expérimentales. Ces modèles peuvent être couplés à des modèles d'interaction avec l'environnement et permettent alors d'analyser comment l'architecture des plantes représentée, à l'échelle fine de l'organe, affectent ces interactions. Dans le cadre d'Arvalis et de l'Unité ECOSYS, les principaux domaines d'intérêt qui ont motivé mon travail sont les suivants :

- En **épidémiologie**, la simulation d'interactions plante-particule, et particulièrement le rôle de la structure du couvert dans l'interception de spores de pathogènes ou de pesticides.
- Pour le **fonctionnement** des plantes, la simulation du phylloclimat, et notamment la distribution du rayonnement lumineux au sein des couverts, pour l'étude de conséquences liées à la quantité et la qualité spectrale du rayonnement.
- En **phénotypage**, la simulation des signaux perçus par des capteurs, qui s'appuie sur le couplage de modèle de plante, de modèle de transfert radiatifs et de modèles de capteurs.

L'objectif appliqué que je me suis fixé était de développer un modèle opérationnel permettant de simuler l'architecture 3D de peuplements de blé pour les applications citées plus haut. Les qualités recherchées pour ce modèle étaient les suivantes:

- Générer des reconstructions *dynamiques*, couvrant l'ensemble du cycle de la culture, de l'émergence jusqu'à la récolte.
- Pouvoir reproduire l'architecture de peuplements *spécifiques*, de façon fidèle aux observations dont on dispose. Si l'on considère un peuplement réel, le modèle doit être capable de simuler d'une façon réaliste les caractéristiques spécifiques de ce peuplement.
- Utiliser un *nombre réduit de paramètres* qui soient faciles à interpréter et à acquérir sur le terrain.
- Pouvoir représenter des peuplements issus d'une *gamme importante* de conditions de culture et de génotypes. Le « domaine » que l'on souhaite pouvoir représenter correspond à une gamme large de densité de semis, de date de semis et de fertilisation azotée. Les peuplements diffèrent également en fonction des conditions météorologiques rencontrées au cours de la croissance. Pouvoir représenter la plasticité de l'architecture était donc une composante majeure de notre travail. En matière de génotypes, je me suis toutefois focalisée sur des variétés commerciales de type « élite ».

2. Axes de travail

Au stade actuel des connaissances, des approches mécanistes ne permettraient pas de simuler avec une grande précision des expérimentations particulières. J'ai choisi une approche paramétrique qui s'appuie sur des observations. Un effort particulier a été consacré à la définition de l'ensemble des fonctions paramétriques nécessaires pour décrire la morphologie des plantes de blé, sa plasticité et son évolution au cours du temps. Les principaux axes de travail ont été les suivants :

- J'ai analysé une **grande base de données** avec une gamme large de conditions de croissance et de cultivars. Ces données proviennent d'expérimentations menées personnellement au cours de cette thèse (15 traitements), mais également de la compilation de données préexistantes dans l'équipe (36 traitements). Les données décrivent la structure botanique des plantes individuelles avec une description des propriétés de **chaque phytomère** (nombre, dimensions, état) sur un nombre important de plantes (entre 15 à 60 par traitement). Ces données sont acquises à plusieurs dates, de façon à décrire la **dynamique** du développement des plantes au cours du temps. Cette base de données est **inédite** à la fois par la gamme des conditions de culture qu'elle couvre et par le niveau de détails qu'elle caractérise.

- J'ai mené des expérimentations dédiées au suivi de la **dynamique** de la **géométrie** des **organes** au cours du temps. Les données acquises caractérisent chaque rang foliaire et chaque tige sur un nombre important de plantes, afin d'assurer une bonne représentativité des mesures et d'analyser les gradients en fonction de la position des feuilles sur les axes. Ceci a été possible en combinant une grande diversité de méthodes d'acquisition et de traitements de données, cela inclut l'expérimentation des nouvelles méthodes (photogrammétrie 3D). Ces données sont **inédites** à la fois par le nombre de traitements qu'elles couvrent, par leur niveau de finesse et de complétude et par leur aspect dynamique.

- Un effort important a été mené dans la définition des fonctions permettant de décrire la dynamique complète de la structure des plantes et dans l'ajustement des paramètres. Compte tenu du couplage avec le modèle ADELwheat, les points auxquels je me suis attachés concernent cinq aspects qui sont nécessaires et suffisants pour représenter les plantes de la levée à la récolte :

- 1) *Dynamique d'apparition des feuilles*
- 2) *Dynamique de tallage : apparition et mortalité*
- 3) *Dynamique de nombre de feuilles vertes et sénescences le long d'un axe*
- 4) *Nombre final de phytomères sur un axe*
- 5) *Dimensions des organes matures (limbes, gaines, entrenœuds, épis)*
- 6) *Géométrie des plantes au cours du temps*

Sur ce dernier point, je n'ai pas pu aller jusqu'à définir une paramétrisation des aspects géométriques. Toutefois nos résultats ont permis d'obtenir une vue synthétique de l'évolution de cette géométrie au cours du développement de la plante.

- J'ai intégré l'ensemble de ces fonctions dans une routine, appelé « **Plantgen** ». Cette routine est couplée au modèle ADELwheat qui effectue la représentation 3D. J'ai

développé également des routines de « *post-processing* » des reconstructions 3D pour calculer des variables caractéristiques à l'échelle du peuplement, elles ont été utilisées notamment pour évaluer la qualité des peuplements simulés. Toutes ces routines sont mises à la disposition de la communauté scientifique sous l'interface OpenAlea et elles sont utilisées dans plusieurs applications.

- J'ai défini un **protocole de mesures** assurant l'obtention de l'ensemble des variables nécessaires pour estimer les paramètres de Plantgen avec un effort expérimental raisonnable.

3. Synthèse des principaux résultats

3.1. Éléments de connaissances et points d'originalité

Ce travail a produit des connaissances concernant la dynamique de l'architecture aérienne chez le blé. Dans cette section, je récapitule les résultats qui me paraissent les plus marquants. J'aborderai quatre points : (i) mortalité des talles, (ii) sénescence des feuille (iii) notion du numéro relatif de phytomère, et (iv) géométrie des tiges et des feuilles.

a) Mortalité des talles. Le tallage est un critère de plasticité important chez les céréales. Il permet aux plantes d'adapter leur croissance en fonction des ressources disponibles. La mortalité des talles est généralement comprise comme une conséquence des compétitions entre les axes d'une même plante pour les ressources, compétition dont l'intensité est maximale pendant la montaison et qui s'arrête autour de la floraison, lorsque le développement végétatif des axes est achevé (Borràs-Gelonch *et al.*, 2012; Sparkes *et al.*, 2006; Davidson et Chevalier, 1990). Toutefois, les auteurs (Alzueta *et al.*, 2012) qui ont caractérisé précisément le moment du début de mortalité, observent que celui-ci peut correspondre à des stades de développement similaires pour des peuplements disposant de niveau de ressources contrastés, contrairement à ce qui serait attendu pour un comportement simplement régulé par les relations offre-demande. Une des difficultés pour évaluer la portée de ces observations est que les critères retenus pour définir la mortalité d'un axe et le début de la mortalité à l'échelle du peuplement étaient peu précisément décrits.

Dans mon travail, j'ai caractérisé la mort d'un axe comme l'arrêt de l'extension des jeunes feuilles ; j'ai suivi la dynamique du nombre d'axes actifs tout le long du cycle de culture et ainsi analysé la mortalité des talles pour des traitements, couvrant une gamme variée de conditions de ressources (état azoté, état hydrique, lumière). En comparant des traitements pour lesquels les plantes avaient produit un nombre de feuilles final très proche, le stade de développement au moment de début de la mortalité était stable, alors que l'indice foliaire variait beaucoup entre les traitements (de 0.8 à 2.9). Sur l'ensemble de nos traitements, le stade de développement des plantes au moment du début de *mortalité des talles* était corrélé au nombre final des feuilles de l'axe principal (FLN^{MS}), lequel variait entre 8 à 14 feuilles ($R^2=0.62$, chapitre1 *Fig.9*) selon les traitements. Ces résultats suggèrent qu'il existe bien un moment qui caractérise le début d'une phase de mortalité et que FLN^{MS} semble être un bon indicateur pour prédire ce moment. D'autre part, nos résultats montrent que la *mortalité des talles se termine* aussi à un stade stable de développement qui est proche de la ligulation de la feuille drapeau du brin maître, malgré des conditions de ressources contrastées ($R^2=0.78$,

chapitre1 **Fig.10**). Malgré la stabilité du stade de développement à l'arrêt de mortalité, le nombre d'épis variait beaucoup (1.4 à 5 épis par plante). Ces résultats suggèrent qu'il existe bien un moment qui caractérise l'arrêt de mortalité et qu'il peut être prédit par FLN^{MS} . Les conditions de ressources semblent avoir peu d'effet sur ce timing, mais sûrement un effet important sur la proportion des talles qui meurent.

L'hypothèse que nous formulons sur la base de ces résultats est qu' « Il existe une phase de mortalité des talles ; son début et sa fin sont pilotés par l'ontogénie de la plante et sont étroitement associés au nombre de feuilles final produit par le brin maitre. Les relations ressources-puits détermineraient la vitesse de mortalité au sein de cette phase, mais pas le moment du début et de la fin ». Cette hypothèse permet de concilier les avis controversés présentés au début, et si elle se confirme, elle sera simple à implémenter dans les modèles.

b) Sénescence des feuilles. La sénescence est définie ici comme étant le passage des tissus d'un état de turgescence à un état nécrotique et desséché. Ce processus impacte fortement l'évolution de l'indice foliaire au cours du temps et une description réaliste de la progression de la sénescence à l'échelle de la feuille, d'un axe et de la plante entière est nécessaire pour les applications des modèles FSPM ou SPM évoquées en introduction. Les mécanismes responsables de la sénescence et de la mort des tissus sont complexes et mal compris. Certains auteurs ont proposé des modèles dans lesquels la vitesse de sénescence des feuilles est égale la vitesse d'apparition de nouvelles feuilles, supposant ainsi une stabilité de nombre de feuilles vertes (McMaster *et al.*, 1991). Toutefois, les auteurs (Hillier *et al.*, 2007; Baccar *et al.*, (2011), qui ont caractérisé plus finement l'évolution de la sénescence des feuilles tout le long du cycle du brin maitre, observent un comportement plus complexe dans lequel le rythme de sénescence n'est pas constant au cours du temps.

Dans mon travail, j'ai analysé **la cinétique de sénescence** pour une gamme large de conditions de croissance, incluant des données que j'avais collectées au cours de cette thèse mais également les données préexistantes dans l'équipe, incluant celles de J. Hillier et R. Baccar, cités plus haut. Sur cette base, j'ai défini une paramétrisation décrivant la progression de la sénescence le long d'un axe et qui tient compte des **différents axes** de la plante (brin maitre et talles). Pour décrire la progression de la sénescence, j'ai choisi de paramétrer **l'évolution du nombre décimal de feuilles vertes** (G_l) dont le pattern temporel était plus clair que celui du nombre de feuilles sénescentes. Contrairement à ce qui été proposé par McMaster (1991), nos données montrent que le nombre de feuilles vertes varie au cours de la période préfloraison. Sur l'ensemble des traitements analysés, l'évolution suit un même pattern stable avec des **moments de ruptures qui correspondent aussi à des stades** du développement de la plante tels que : un début de sénescence de feuille 1 à la ligulation de la feuille 4 ou 5; un minimum de G_l au début de montaison (ligulation de la 4^{ème} feuille depuis le haut) et une troisième rupture à la ligulation de feuille drapeau. Cette paramétrisation est **originale** et présente une **formulation simple et assez robuste**. Elle permet de décrire la progression de la sénescence pour tous les axes de la plante et sur l'ensemble du cycle de culture. Pour la calibrer, il suffit de mesurer le nombre de feuilles vertes G_l à un nombre limité de dates. L'expression de la progression de sénescence en termes de nombre de feuilles vertes est **d'un usage** simple comparé à d'autres approches qui utilisent des surfaces foliaires et elle peut être facilement intégrée dans les modèles SPM.

L'intégration de cette paramétrisation dans les modèles SPM permet de simuler de façon réaliste la progression de la sénescence au cours du temps. Ceci est bien sûr nécessaire pour les calculs d'interaction plante-environnement, mais fournit aussi un **outil potentiellement intéressant pour la validation des modèles** fondés sur des hypothèses fonctionnelles. Ces approches fonctionnelles sont par exemples : (1) l'approche de l'« optimisation » qui suppose que la plante ajuste son nombre de feuilles vertes de manière à maximiser la photosynthèse lumière (Franklin and Agren, 2002; Hikosaka, 2005) ; (2) l'approche de l'« equilibrium » qui suppose que la sénescence est induite dans le cas d'un déséquilibre des teneurs en carbone et azote dans la feuille (Lee and Chen, 2002; Thomas et al., 2003; Weaver et Amasino, 2001) ; (3) l'approche de « seuil » qui suppose que la mort des tissus d'un limbe se produit quand leur masse d'azote surfacique, dépendante de lumière interceptée, devient inférieure à un certain seuil empirique qui varie en fonction de la nutrition azotée (Gabrielle et al., 1998; Bertheloot et al., 2009). Il serait par exemple intéressant de **vérifier si le pattern observé de G_1 est une propriété émergente** prédite par ces modèles. Des modèles 3D réalistes couplés à des modèles de rayonnement permettent également de simuler de façon précise le rayonnement lumineux incident sur chaque feuille, ce qui est l'un des composants des calculs d'optimisation.

c) **Numéro relatif de phytomère.** Chez les graminées la morphologie des talles présente de fortes similarités avec celle du brin-maitre. Ceci peut se comprendre par la similarité des processus qui les construisent et la similarité des conditions dans lesquelles ces processus se déroulent. Chez le blé, le riz et l'orge, plusieurs auteurs ont observé que les dimensions des phytomères supérieurs des talles présentent le même pattern d'évolution en fonction de la position sur l'axe que ceux du brin maitre, à condition qu'un décalage ou un « shift » propre à chaque talle soit pris en compte pour la numérotation des phytomères (Fournier et al., 2003; Evers et al., 2005; Tivet et al., 2001; Buck-Sorlin, 2002). Dans mon travail, j'ai utilisé ce concept de « numéro relatif de phytomère » pour déduire les longueurs des organes sur les talles à partir de celles sur le brin maitre, en considérant un « shift décimal » dont la valeur dépend de la position botanique de la talle. L'originalité de notre travail a été d'approfondir les conditions de validité de cette approche : j'ai estimé séparément les valeurs des shifts pour chacun des composants des phytomères (limbes, gaines et entrenœuds) et montré que les valeurs obtenues étaient très proches. J'ai évalué l'approche sur une large gamme de conditions de croissance (17 traitements qui couvrent 10 génotypes, 3 dates de semis, 3 densités et 2 niveaux de fertilisation N) et montré que la valeur de shift à prendre en compte ne dépendait pas du traitement. Un autre résultat marquant est que les valeurs estimées de ces shifts étaient très proches du Haun stage du brin maitre au moment de l'émergence de la talle (ces valeurs du Haun stage ont été mesurées indépendamment). Ceci supporte l'idée que les organes qui poussent simultanément atteignent les mêmes longueurs. J'ai montré que l'utilisation de ce shift ne permettait toutefois pas de bien estimer les longueurs des feuilles sur les phytomères inférieurs, c'est-à-dire ceux portés par des entrenœuds courts. Pour ceux-ci, une formulation alternative a été proposée. Enfin, j'ai montré que les largeurs des limbes et les diamètres des gaines et des entre-nœuds des talles présentaient des dimensions souvent inférieures comparés au brin maitre. Une explication possible est peut-être liée à la taille réduite des méristèmes pour les talles. Pour ces dernières, en plus de l'utilisation du shift, j'ai

appliqué des facteurs de réduction par ordre de taille. Au final, le travail réalisé fourni un ensemble de relations qui permet de formaliser les similarités entre brin maître et talles, en démontrant leur stabilité sur une large gamme de traitements et de génotypes, mais en cernant également de façon plus complète les caractéristiques morphométriques pour lesquelles elles sont valides. Dans ce travail, je me suis focalisée sur les similarités entre brin-maitre et talle. Je n'ai pas cherché à formaliser les patterns de dimensions le long du brin-maitre, considérant que leur dépendance aux conditions de croissance impliquait de mesurer directement ces valeurs si l'on souhaitait simuler des peuplements correspondant à des conditions de croissance spécifiques. Nos mesures montrent toutefois des fortes corrélations entre les dimensions des différents composants du phytomères (exemple : relation entre longueur gaine et longueur limbe) ou entre les dimensions d'organes successives (exemple : relation entre longueur feuille n et longueur feuille n+1). *Ceci n'a pas été intégré dans la paramétrisation actuelle. L'intégration de ces types de relations représente une voie intéressante d'amélioration qui permettra de réduire le nombre de mesures nécessaires pour calibrer le modèle.*

d) La géométrie des tiges et des feuilles. Les plantes s'adaptent à leur environnement par une plasticité de leur structure et également de leur géométrie. L'adaptation des plantes en termes d'orientation et de port foliaire, et de disposition spatiale des axes n'est pas bien comprise, et la variabilité génotypique dans ces comportements est mal connue, alors que les conséquences sur les interactions entre les plantes et leur environnement sont potentiellement importantes.

Concernant **l'orientation des feuilles** dans le plan horizontal par exemple, le petit nombre de travaux disponibles montre que le positionnement dans l'espace implique des processus actifs (e.g. comportement d'évitement des plantes voisines (Madonni *et al.*, 2002 ; Mullen *et al.*, 2006), avec une variabilité génotypique de comportement importante. Le **port foliaire** et l'inclinaison foliaire ont fait l'objet de plus d'études. On distingue classiquement 3 distributions types pour l'inclinaison foliaire (Wit, 1965) : distributions planophile, plagiophile et érectophile, dont l'importance fonctionnelle est bien reconnue (Wang *et al.*, 2007 ; Abreu *et al.*, 2008 ; Prévot *et al.*, 1991). Toutefois chez des espèces comme le blé, il existe une évolution du port foliaire au cours du développement de la plante (différence de port entre les feuilles émergeant avant et après transition florale) mais aussi tout au long de la vie de la feuille (Ledent *et al.*, 1978a,b). L'évolution - très importante sur certains génotypes - du port après la ligulation n'est pas prise en compte dans les modèles alors que les ordres de grandeur mesurés indiquent qu'elle impacte l'accès au rayonnement, mais aussi l'exposition à la pluie et aux fongicides dans les strates basses du couvert. Concernant la géométrie des axes, il est connu que **l'angle d'inclinaison des axes** constitue une variable clés qui définit la prospection de l'espace, avec une variabilité génotypique de comportement importante (**Fig.1**). L'angle des talles a fait l'objet de très peu de travaux chez le blé alors que c'est un trait reconnu d'importance majeure chez le riz (Yu *et al.*, 2007 ; Yang *et al.*, 2008 ; Jin *et al.*, 2008). Pour le blé, l'image usuelle - et qu'on retrouve souvent dans les modèles actuels de plante virtuelle - est que « les tiges des talles s'écartent plus au moins fortement d'une tige principale orientée verticalement ». Finalement, pour le blé, la vue sur ce processus est fragmentaire. Je n'ai trouvé aucun travail qui quantifie cette variable et sa dynamique au cours

du temps, alors que leur implications sont probablement importantes dans l'efficacité d'interception du rayonnement et la compétitivité vis-à-vis d'adventices (Drews *et al.*, 2004) ou d'espèces cultivées en association.

Mon travail apporte des résultats originaux qui clarifient l'image que l'on a de la géométrie des axes et des feuilles. J'ai caractérisé l'**angle d'inclinaison des tiges et des feuilles** et son **évolution au cours du temps** pour une sélection de géotypes à port contrasté sous deux densités de population.

Pour les feuilles, mes données montrent que l'inclinaison par rapport à la verticale des feuilles à leur point d'insertion varie en fonction de l'âge de la feuille. La progression est claire pour les feuilles inférieures et pour les feuilles supérieures, qui s'inclinent progressivement avec le temps. Les feuilles intermédiaires montrent un mouvement plus complexe et difficile à caractériser. Toutefois lorsqu'on considère l'angle que fait la feuille par rapport à son axe porteur, un schéma unique de progression se trace : on observe une inclinaison progressive jusqu'à une position quasi-stable pour laquelle l'angle avec l'axe diffère généralement fortement entre les feuilles juvéniles et les feuilles adultes (*Chapitre 4, Fig.5 et Fig.6*). La complexité du comportement observé pour les feuilles intermédiaires disparaît, car elle résultait du mouvement de l'axe porteur.

Pour les axes, mes données montrent que l'inclinaison de la pseudo-tige (cylindre incluant les gaines et entrenœuds) suit une dynamique claire, répétitive et facile à interpréter : les tiges présentent d'abord une inclinaison croissante qui se stabilise à l'arrêt de tallage, ensuite elles se redressent pour atteindre une position verticale stable autour de la ligulation de la feuille drapeau. Cette progression a été observée à la fois sur le brin maître et sur les talles (*Chapitre 4, Fig.4*). La synchronisation observée entre le début de redressement des axes et l'arrêt de tallage suggère que le redressement résulte aussi d'une réaction d'évitement de l'ombre « shade avoidance » lié à une sensibilité à la qualité de lumière (ratio rouge clair : rouge sombre) (Evers *et al.*, 2006).

Ces résultats sont originaux car la dynamique du port des feuilles et encore plus des axes a été très peu étudiée. J'ai montré que les patterns d'inclinaison des axes et des feuilles sont clairs et répétitifs, ce qui devrait permettre de les représenter de façon précise dans des modèles. L'ampleur des mouvements observés soulève la question de l'impact de ces mouvements en termes d'adaptation fonctionnelle des plantes et de transferts au sein des peuplements. Il serait intéressant également d'identifier quels facteurs environnementaux (exemple: lumière ; état hydrique) modulent ces dynamiques et les différences génotypiques qui existent. Ce travail a permis de 'décortiquer' certaines composantes importantes de la géométrie, toutefois d'autres composantes (courbure des feuilles, azimuth des feuilles et des axes) restent à analyser, en vue d'une représentation fidèle de la géométrie dans les modèles de plantes virtuelles.

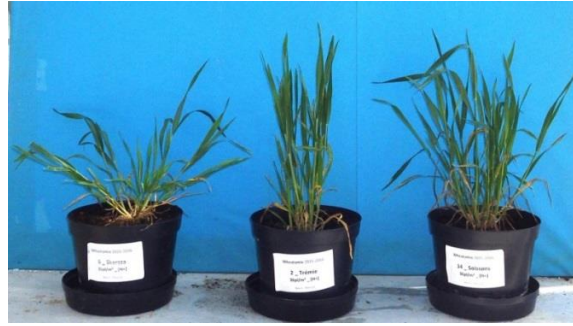


Figure 1: Port des axes des plantes isolées. Chaque pot comporte une seule plante : à gauche la variété *Skerzzo*, au milieu la variété *Trémie* et à droite la variété *Soissons*. La figure illustre la variabilité génotypique du port des tiges et de leurs angles d'inclinaison (données personnelles).

3.2. Méthode de reconstruction de l'architecture : routine opérationnelle et protocole de mesure à effort réduit

Une ***routine opérationnelle*** qui intègre l'ensemble des fonctions paramétriques, présentées dans le premier et le deuxième chapitre, a été développée. Cette routine appelée « Plantgen », permet de décrire l'évolution de l'architecture pour tout le cycle de culture. Cette application permet de générer une collection de plantes avec les caractéristiques morphologiques et dynamiques fondées sur les observations, et incluant une variabilité inter-plantes sur quelques traits majeurs de la structure. Le passage de cet ensemble de fonctions à une application qui les intègre pour générer une description détaillée de chaque plante, dès son émergence jusqu'à sa maturité, a représenté un effort important et coûteux en temps. L'implémentation, le test et la documentation de « Plantgen » ont mobilisé plusieurs personnes (moi-même, Camille Chambon, Tiphaine Vidal et Bruno Andrieu). Cette application n'inclut pas de description de la géométrie. Pour représenter en 3D les plantes, Plantgen est couplé à ***ADELwheat*** pour utiliser ses modules géométriques.

En parallèle, un ***protocole de mesure*** a été défini. Le suivi de celui-ci assure l'obtention de l'ensemble des paramètres nécessaires à la calibration du modèle « Plantgen-ADELwheat ». Une description de ce protocole expérimental, ainsi que du modèle couplé « Plantgen-ADELwheat » avec un guide d'utilisation qui présente l'ensemble de paramètres et la procédure à suivre pour la reconstruction 4D d'un couvert, sont présentés dans les ***annexes 1 et 2***. Avec l'aide de Camille Chambon, j'ai développé une ***interface graphique conviviale*** de la routine « Plantgen » afin de faciliter son utilisation ; elle est disponible en libre accès sur la plateforme OpenAlea. L'intégration dans cette plateforme permet de l'utiliser de façon conjointe avec d'autres outils disponibles sur la plateforme, comme le modèle de radiativité Caribu ou le modèle de maladie Septo3d. La qualité des reconstructions du « Plantgen-ADELwheat » a été évaluée en utilisant des mesures indépendantes représentant des variables intégratives à l'échelle du peuplement: il s'agit principalement de la dynamique d'indice foliaire (LAI et GAI) vert et total et de la dynamique de taux de couverture en visée verticale et inclinée (0° et 57.5°). Par manque de temps, les résultats de cette évaluation n'ont pas été présentés dans ce rapport, toutefois, nous avons les éléments nécessaires pour un article. La synthèse de l'***évaluation du modèle « Plantgen-ADELwheat »*** est la suivante: (1) il existe une bonne adéquation entre les mesures et les simulations de la dynamique d'indice foliaire vert et total ; (2) les simulations de la dynamique du taux de couverture du sol en visée

incliné sont très proches des mesures, toutefois, en visée verticale des écarts importants existent (pour plus de détails lire l'annexe 1.5). Ce résultat signifie que la représentation de la morphologie et de sa dynamique, présentée dans « Plantgen » est satisfaisante. Les défauts des simulations du taux de couverture en visée verticale s'expliquent principalement par des défauts dans la représentation de la géométrie des plantes. Les résultats présentés dans les chapitres 3 et 4 concernant le port foliaire et l'inclinaison des axes ne sont pas intégrés dans la version actuelle d'« ADELwheat; de ce fait certains aspects de géométrie ne sont pas pris en compte (modification de l'inclinaison des feuilles avec l'âge) ou mal caractérisés (inclinaison des axes). Les conséquences observées pour la simulation du taux de couverture du sol suggèrent fortement que les limites actuelles dans la représentation de la géométrie impactent aussi la qualité de simulation des autres transferts qui suivent une direction proche de la verticale, comme l'interception des pesticides et de la pluie. *Deux pistes d'améliorations sont possibles : (i) une meilleure représentation de la dynamique d'inclinaison de chaque axe (à la fois pour le brin maître et les talles) et (ii) une meilleure représentation de la dynamique d'inclinaison des feuilles (prise en compte de la position et de l'âge de la feuille). Nos résultats du chapitre 4 présentent une caractérisation de ces deux patterns qui peuvent être intégrés dans le modèle.*

Par ailleurs, le travail de thèse a permis de **générer un ensemble de peuplements virtuels**, représentant l'architecture 4D de 23 traitements expérimentaux issus d'une gamme large de géotypes, de dates et de densités de semis. Ces traitements sont répertoriés dans l'*annexe 1.6*. Ces peuplements virtuels pourraient être utilisés pour analyser, par simulation, l'impact des traitements contrastés sur l'interception du rayonnement ou des pesticides ou sur le développement des maladies. Ils peuvent être utilisés aussi comme base pour le calcul des signaux perçus par les capteurs, et ils fournissent ainsi un support d'information intéressant pour l'approche d'inversion en phénotypage haut débit. Plus généralement, la réalisation de cette base de peuplements virtuels démontre par l'exemple notre capacité à simuler d'une façon réaliste des peuplements de blé sur une large gamme de conditions.

3.3.Exemples d'applications mises en œuvre

J'ai contribué à deux projets qui se sont déroulés en parallèle à ma thèse et dans lesquels notre méthode de reconstruction a été mise en œuvre: (i) le projet ECHAP (Robert *et al.*, 2009-2014) qui étudiait l'effet d'architecture sur le développement des maladies et sur l'efficacité d'interception des fongicide et (ii) le projet de thèse de Shouyong Liu qui étudie le rôle de l'architecture dans la formation des signaux en proxidtection. Ci-dessous je décris rapidement ces deux projets et l'intérêt spécifique qu'apportent les reconstructions 4D pour ces deux applications.

L'objectif **du projet ECHAP** est de réduire l'utilisation des pesticides (fréquence et dose) en optimisant les mécanismes naturels d'échappement aux maladies liés à l'architecture du couvert et à l'interception des pesticides par les couverts végétaux. L'architecture des couverts est fortement impliquée dans ces processus et le projet ECHAP abordait différentes questions (Robert *et al.*, 2015 ; Robert *et al.*, 2012): (i) quels sont les traits architecturaux des couverts qui impactent la dispersion des spores par éclaboussure? Y a-t-il des traits à rechercher ou à

éviter pour la progression d'une épidémie ? (ii) Comment se répartissent les particules de pesticides sur les différents étages foliaires et est-ce dépendant de la géométrie et des stades de développement des plantes? Quel est le devenir des pesticides (photodégradation ; lessivages ; co-localisation avec maladie, etc.). Le travail s'appuie sur des travaux de modélisation et d'expérimentations. Des expérimentations au champ avec des architectures variées ont été réalisées et notre protocole de mesure, ainsi que le modèle Plantgen (Abichou *et al.*, 2013) ont été mis en pratique pour reconstruire les peuplements issus de ces expérimentations. Ces simulations ont été intégrées dans des modèles de simulation d'épidémie (Thèse Guillaume Garin 2015, Fournier *et al.*, 2013) et de devenir de pesticides. L'étude a confirmé l'effet de l'architecture sur le développement épidémique (Fig.2) ainsi que son effet sur l'interception des fongicides, qui s'exprime clairement entre les variétés. Le couplage de notre modèle « architecture » avec les modèles d'épidémie et de devenir des fongicides permettra ultérieurement de raisonner des stratégies de traitements.

Les résultats sur l'évolution du port des plantes au cours du temps obtenus durant mon travail ne sont pas pour l'instant pris en compte dans les simulations ; ils pourront améliorer la qualité des simulations et permettront d'explorer si des différences génotypiques dans le positionnement des axes ou la dynamique du port foliaire impactent le comportement du système « architecture–épidémie-fongicide ».

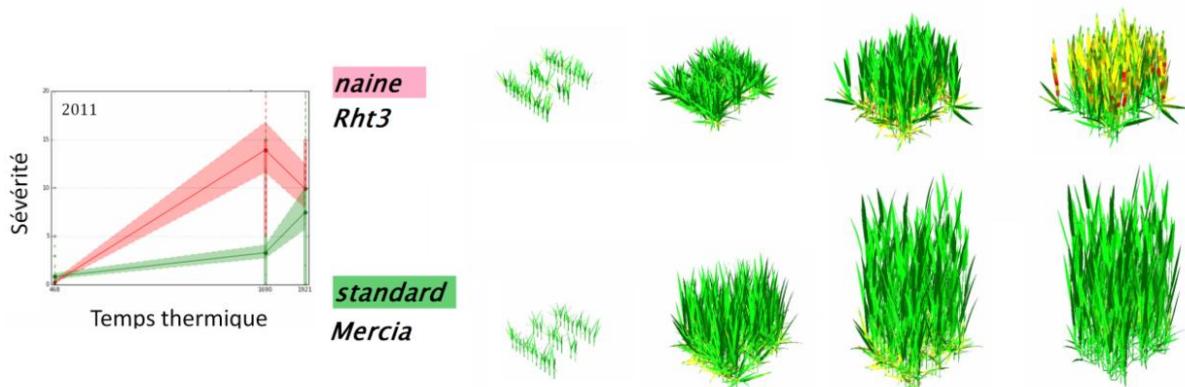


Figure 2 : Evolution de la sévérité d'une épidémie de septoriose pour deux couverts à architecture contrastée (Thèse Guillaume Garin, 2015). Dans ces simulations, la dynamique d'apparition et de sénescence foliaire, la dynamique de tallage et les dimensions finales des organes sont issues de ma paramétrisation « Plantgen ». J'ai aussi participé à l'acquisition des mesures en appliquant le protocole simplifié de mesure que j'avais défini. Des améliorations futures de la représentation géométrique, basées sur mes résultats du chapitre 4, sont désormais possibles.

Le projet de **thèse de Shouyang Liu** a comme objectif d'estimer certaines caractéristiques structurelles et fonctionnelles des couverts végétaux à partir des signaux issus des capteurs LiDAR « *laser detection and ranging* ». Dans ce projet, le modèle « Plantgen-ADELwheat » est couplé à un modèle de simulation du signal LiDAR, ce qui permet de simuler les signaux mesurés pour une gamme d'architectures parfaitement définies. On peut ainsi mettre au point et évaluer « *in silico* » les méthodes d'estimation des caractéristiques structurales du peuplement à partir de ces mesures (Fig.3). Une large gamme de maquettes 3D de blé est simulée. Certaines maquettes sont des reconstructions réalistes de blé obtenues en appliquant notre méthode de reconstruction avec le modèle « Plantgen-ADELwheat » et le protocole de

mesure réduit sur des peuplement réels. Cette base est complétée par des maquettes simulées en faisant varier les paramètres de façon à explorer une large gamme de structures. Sur chaque maquette, on calcule le GAI par les routines de post-traitement et on simule le nuage 3D de points qui serait acquis par un LiDAR. Des algorithmes « Machine Learning » ont été développés pour déterminer des indicateurs permettant d'estimer le GAI à partir des nuages de points de LiDAR. Dans un deuxième temps, la métrique est utilisée sur les nuages de points acquis par un instrument LiDAR au-dessus de peuplements réels, afin d'estimer le GAI des peuplements.

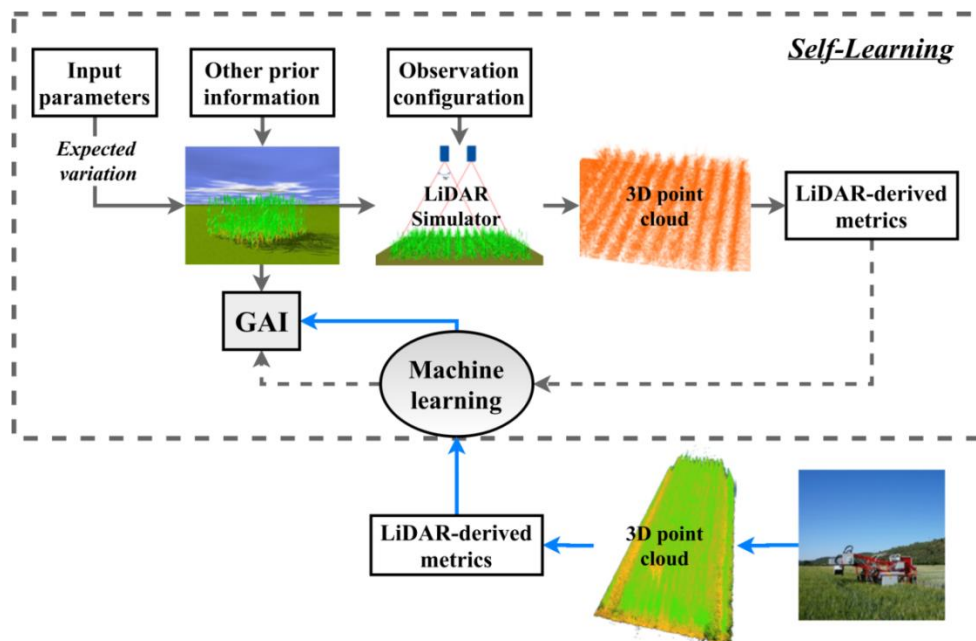


Figure 3: Schéma du principe de la méthode d'auto-apprentissage pour estimer l'indice foliaire global (GAI) avec la technologie LiDAR (Liu *et al.*, 2016)

4. Conclusion

Même si des progrès restent à faire sur le plan de la représentation de la géométrie, et si une marge de progrès existe pour réduire encore l'effort expérimental en simplifiant davantage les paramétrisations, nous pensons que la méthode de reconstruction a acquis un degré de maturité suffisant qui a justifié sa mise en œuvre dans plusieurs applications, comme le couplage avec des modèles d'épidémiologie, l'étude d'interception des pesticides et dans l'étude des caractéristiques spectrales des couverts. Elle peut être utilisée pour tester par simulations la compétition plante-plante et plante-adventice. Elle peut être aussi utilisée pour l'évaluation des hypothèses mécanistes, par la reconstruction d'une expérimentation spécifique permettant de recalculer l'historique d'une variable donnée. L'outil développé peut être utilisé comme un outil de travail pour étudier l'effet des traits architecturaux favorisant l'interception de rayonnement ou l'échappement aux maladies, ce qui guidera les sélectionneurs dans les créations des nouveaux idéotypes. Par ailleurs, les paramétrisations que nous avons définies sur une gamme large de données révèlent des patterns stables et robustes. Ces patterns représentent une bonne base, sur laquelle on peut s'appuyer pour définir des hypothèses mécanistes pour les modèles FSPM. Notre démarche de modélisation est transposable à d'autres céréales : elle fournit un cadre pour comparer les patterns de

morphologie et de développement entre espèces et un outil pour étudier par simulation l'impact des traits architecturaux caractéristiques de chaque espèce.

Enfin, notre modèle est à la fois utile pour la communauté scientifique permettant d'avancer nos connaissances sur la plante et sur d'autres disciplines connexes (pathogène, pesticide, etc). Il peut être aussi un outil d'interface entre la recherche scientifique et la profession pour orienter la sélection de nouveaux idéotypes, ou pour développer des méthodes et outils d'aide à la décision pour une meilleure gestion des cultures.

5. Références bibliographiques

- Abichou, M., Fournier, C., Dornbusch, T., Chambon, C., Baccar, R., Bertheloot, J., ... & Andrieu, B. (2013, June). Re-parametrisation of Adel-wheat allows reducing the experimental effort to simulate the 3D development of winter wheat. In 7th International Conference on Functional-Structural Plant Models (pp. 304-306).
- Abreu ME, Munne-Bosch S. 2008. Hyponastic leaf growth decreases the photoprotective demand, prevents damage to photosystem II and delays leaf senescence in *Salvia broussonetii* plants. *Physiologia Plantarum* 134: 369-379.
- Alzueta I, Abeledo LG, Mignone CM, Miralles DJ. 2012. Differences between wheat and barley in leaf and tillering coordination under contrasting nitrogen and sulfur conditions. *European Journal of Agronomy* 41:92-102.
- Bertheloot J., Andrieu B., Fournier C., Martre P., 2008. A process-based model to simulate nitrogen distribution in wheat (*Triticum aestivum*) during grain-filling. *Functional Plant Biology* 35: 781-796.
- Bertheloot J., 2009. Distribution de l'azote chez le blé (*Triticum aestivum* L.) après la floraison : un modèle dynamique fondé sur une approche structure-fonction. Phd thesis, Paris, Agoparitech.
- Bertheloot J., Abichou M., Fournier C., Andrieu B., (2010, September). Light-nitrogen relationships within plant canopies analysed using in silico reconstruction of wheat crops, 6th International Workshop on Functional-Structural Plant Models (pp. 80-82). USA
- Baccar R, Fournier C, Dornbusch T, Andrieu B, Gouache D, Robert C. 2011. Modelling the effect of wheat canopy architecture as affected by sowing density on *Septoria tritici* epidemics using a coupled epidemic-virtual plant model. *Annals of botany* 108: 1179-1194.
- Borràs-Gelonch G., Rebetzke G. J., Richards R. A., & Romagosa I. , 2012. Genetic control of duration of pre-anthesis phases in wheat (*Triticum aestivum* L.) and relationships to leaf appearance, tillering, and dry matter accumulation. *Journal of experimental botany*, 63(1), 69-89.
- Davidson, D. J., & Chevalier, P. M. (1990). Preanthesis tiller mortality in spring wheat. *Crop Science*, 30(4), 832-836.
- Drews, S., Neuhoff, D., & Köpke, U. (2009). Weed suppression ability of three winter wheat varieties at different row spacing under organic farming conditions. *Weed Research*, 49(5), 526-533.
- De Wit C.T. ,1965. Photosynthesis of Leaf Canopies. Agricultural Research Report, PUDOC, Wageningen, 663, p57.
- De Wit C. T., Van den Bergh J. P., 1965. Competition between herbage plants. *Netherlands Journal of Agricultural Science*, 13(2), 212-221.
- Evers, J. B., Vos, J., Chelle, M., Andrieu, B., Fournier & C., Struik, P. C., 2007. Simulating the effects of localized red: far red ratio on tillering in spring wheat (*Triticum aestivum*) using a three dimensional virtual plant model. *New Phytologist*, 176(2), 325-336.
- Evers JB, Vos J, Andrieu B, Struik PC. 2006. Cessation of tillering in spring wheat in relation to light interception and red:far-red ratio. *Annals of Botany* 97: 649-658.
- Evers JB, Vos J, Chelle M, Andrieu B, Fournier C, Struik PC. 2007a. Simulating the effects of localized red:far-red ratio on tillering in spring wheat (*Triticum aestivum*) using a three-dimensional virtual plant model. *New Phytology* 176: 325-336.
- Evers JB, Vos J, Fournier C, Andrieu B, Chelle M, Struik PC. 2007b. An architectural model of spring wheat: evaluation of the effects of population density and shading on model cohort parameterisation and performance. *Ecological Modelling* 200: 308-320.
- Fournier, C., Pradal, C., Abichou, M., Andrieu, B., Bancal, M. O., Bedos, C., ... & Paveley, N. (2013, June). An integrated and modular model for simulating and evaluating how canopy architecture can help reducing fungicide applications. In 7th International Conference on fonctionnal-structural plant models (pp. p-345).
- Fournier C, Andrieu B, Ljutovac S, Saint-Jean S. 2003. ADEL-wheat: a 3D architectural model of wheat development. Pages 54-63 in Hu B-G, Jaeger M, eds. *Plant Growth Modeling and Applications*. Beijing, CHN Tsinghua University Press - Springer Verlag.

- Franklin O., Ågren G. I., 2002. Leaf senescence and resorption as mechanisms of maximizing photosynthetic production during canopy development at N limitation. *Functional Ecology*, 16(6), 727-733.
- Gabrielle B., Denoroy P., Gosse G., Justes E., Andersen MN (1998b) A model of leaf area development and senescence for winter oilseed rape. *Field Crops Research* 57: 209-222
- Garin G., Fournier C., Abichou M., Houlès V., Pradal C., Robert C. A plant-pathogen model to explore the race between wheat growth and *Zymoseptoria tritici* epidemics. Submitted 21-09-2016 to *Phytopathology Journal*.
- Garin G., 2015. Vers la compréhension des épidémies fongiques foliaires par modélisation multi-échelle dans les couverts architectures. Thèse de doctorat. AgroParisTech, France.
- Hikosaka K., 2005. Leaf canopy as a dynamic system: ecophysiology and optimality in leaf turnover. *Annals of Botany* 95: 521-533.
- Hikosaka K., Ishikawa K., Borjigidai A., Muller O., Onoda, Y., 2006. Temperature acclimation of photosynthesis: mechanisms involved in the changes in temperature dependence of photosynthetic rate. *Journal of experimental botany*, 57(2), 291-302.
- Hillier J., Watt J., Bertheloot J., Lewis P., Fournier C., Andrieu B., 2007. Modelling the time course of senescence in winter wheat at the individual leaf and whole plant level. In: *Horticulture and Food Research Institute of New Zealand, Proceedings of 2007 International Workshop on Functional-Structural Plant Models*. Napier, France: 33.
- Jin J, Huang W, Gao JP, Yang J et al 2008. Genetic control of rice plant architecture under domestication. *Nature Genetics* 40: 1365-1369.
- Ledent J. F., 1978a. Beam light interception by leaves with undulating edges-a simulation of maize leaf sections. *Agricultural Meteorology*, 19(5), 399-410.
- Ledent J. F., 1978. Mechanisms Determining leaf movement and leaf angle in wheat (*Triticum aestivum* L.). *Annals of Botany*, 42(2), 345-351.
- Lee RH, Chen SCG (2002) Programmed cell death during rice leaf senescence is nonapoptotic. *New Phytologist* 155: 25-32.
- Liu S., Baret F., Andrieu B., Abichou M., Allard D., de Solan B., Burger P. (2016a). Modeling the distribution of plants on the row for wheat crops: Consequences on the green fraction at the canopy level. Submitted 16-05-2016 to *Computers and Electronics in Agriculture Journal*.
- Liu S., Baret F., Abichou M., Boudon F., Zhao K., Fournier C., Andrieu B., Kamran I., Hemmerlé M., de Solan B. (2016b). Estimating wheat Green area index from ground-based LiDAR measurement through 3D ADEL-Wheat model. Submitted 19-09-2016 to *Agriculture and Forest Meteorology Journal*.
- Liu S., 2016. Describing the 4D canopy architecture of wheat crops by combining phenotyping observations into the ADEL-Wheat model. Phd thesis, École doctorale 536 « Sciences et agrosociétés », Avignon. France.
- McMaster, G. S., Klepper, B., Rickman, R. W., Wilhelm, W. W., & Willis, W. O. (1991). Simulation of shoot vegetative development and growth of unstressed winter wheat. *Ecological Modelling*, 53, 189-204.
- Maddonni G. A., Otegui M. E., Andrieu B., Chelle M., Casal J. J., 2002. Maize leaves turn away from neighbors. *Plant Physiology*, 130(3), 1181-1189.
- Mullen J.L., Weinig C., Hangarter R.P., 2006. Shade avoidance and the regulation of leaf inclination in *Arabidopsis*. *Plant, Cell and Environment* 29: 1099-1106.
- Robert C., Fournier C., Bedos C., Abichou M., Andrieu B., Perriot B. et al. (2015, may). ECHAP : l'architecture des couverts végétaux: un levier pour réduire l'utilisation des fongicides? 45ème congrès du Groupe Français des Pesticides, Versailles, France.
- Robert, C., Abichou, M., Andrieu, B., et al., 2012. The ECHAP project: Reducing fungicide use by associating optimal treatment strategies and canopies promoting disease escape. In *Plant and Canopy Architecture Impact on Disease Epidemiology and Pest Development*.
- Prévot L., Ariès F., Monestiez P., 1991. Modélisation de la structure géométrique du maïs. *Agronomie*, 11(6), 491-503.

- Sparkes D. L., Holme S. J., Gaju O., 2006. Does light quality initiate tiller death in wheat?. *European Journal of Agronomy*, 24(3), 212-217. Thomas H., Ougham H.J., Wagstaff C., Stead A.D., 2003. Defining senescence and death. *Journal of Experimental Botany* 54: 1127-1132.
- Tivet, F., Pinheiro, B. D. S., Raïssac, M. D., & Dingkuhn, M. (2001). Leaf blade dimensions of rice (*Oryza sativa* L. and *Oryza glaberrima* Steud.). Relationships between tillers and the main stem. *Annals of botany*, 88(3), 507-511.
- Vos J, Evers JB, Buck-Sorlin GH et al., 2010. Functional-structural plant modelling: a new versatile tool in crop science. *Journal of Experimental Botany* 61: 2101-2115.
- Wang W.M., Li Z.L., Su H.B., 2007. Comparison of leaf angle distribution functions: Effects on extinction coefficient and fraction of sunlit foliage. *Agricultural and Forest Meteorology* 143:106-122.
- Weaver L.M., Amasino R.M., 2001. Senescence is induced in individually darkened *Arabidopsis* leaves, but inhibited in whole darkened plants. *Plant Physiology* 127: 876-886
- Yu BS, Lin, ZW, Li HX et al., 2007. TAC1, a major quantitative trait locus controlling tiller angle in rice. *Plant Journal* 52: 891-898.
- Yang XC, Hwa CM. 2008. Genetic modification of plant architecture and variety improvement in rice. *Heredity* 101: 396-404.



ANNEXES

1. *Plantgen-ADELwheat : Application permettant la reconstruction à partir d'un protocole de mesure à effort expérimental réduit*

La routine « Plantgen » est une application qui intègre les fonctions paramétriques présentées dans cette thèse (Chapitres 1 et 2). Elle permet de reconstruction la dynamique de l'architecture d'un couvert de blé pour tout le cycle de culture de l'émergence jusqu'à la maturité. Elle permet de reconstruire une expérimentation bien spécifique à condition que certaines mesures soient réalisées afin d'estimer les paramètres nécessaires pour la calibration. Un protocole expérimental de mesure, considéré aujourd'hui comme minimum, est défini et permet d'assurer l'obtention de l'ensemble des paramètres nécessaires (une marge de progrès existe pour réduire encore l'effort expérimental).

Cette routine a été développée sous OpenAlea et elle était conçue pour faciliter son interfaçage avec ADELwheat. Ainsi, elle génère une description détaillée des caractéristiques d'une collection de plantes (nombre d'axes, d'organes, leurs dimensions et dynamiques) qui sont organisée dans des trois tables compatibles avec le format d'inputs d'ADELwheat. Ce couplage permet principalement d'utiliser les modules géométriques d'ADEL (disposition des plantes, géométrie des feuilles, géométrie des axes) et de reconstruire en 3D les couverts de blé avec les caractéristiques de la structure définies dans « Plantgen ». Nous avons organisé une session de formation de deux jours à Arvalis pour présenter comment utiliser Plantgen-ADELwheat pour générer des maquettes 3D.

Nous décrivons ici les variables et paramètres nécessaires à la reconstruction 3D et montrons comment se présente l'interface utilisateur de l'application. Les principaux éléments du protocole expérimental mis en œuvre pour acquérir ces données sont ensuite présentés. Ce protocole a été mis en œuvre dans le cadre du projet ECHAP et projet de thèse de Shouyang Liu.

1.1. Données d'entrées nécessaires à la reconstruction 3D

Les données nécessaires à la calibration du « Plantgen-ADELwheat » comprennent : (i) le nombre final de feuilles et les dimensions des organes matures du brin maître, (ii) des variables relatives à la phénologie, (iii) des variables relatives au tallage et (iv) une collection de forme de courbure de feuilles. Une description détaillée de ces données est présentée ci-dessous :

* ***Le nombre final de feuilles et les dimensions des organes matures du brin maître.*** Il faut d'abord renseigner le nombre final de feuilles du brin maître, ou même la fréquence de chaque nombre final de feuille si l'on veut distinguer plusieurs cas (les dynamiques dépendront de cette variable). Ensuite, pour chaque phytomère du brin maître, il faut renseigner: longueur et largeur du limbe, longueur et diamètre de la gaine, longueur et diamètre de l'entrenœud. Ces données peuvent être fournies pour différentes catégories de plantes selon le nombre final de feuilles du brin maître. Il est possible aussi de décrire une valeur « moyenne » qui sera alors affectée à toutes les plantes.

* ***Des variables relatives à la phénologie.*** Il est nécessaire de fournir les variables suivantes concernant le brin maître:

- (i) *La date d'émergence de la culture (HS = 0) et le Phyllochrone.* Si le phyllochrone change au cours du cycle: il faut renseigner les deux valeurs de phyllochrone et le moment de la rupture de pente.
- (ii) *La date de montaison, de ligulation feuille drapeau et de floraison du brin maitre.* Par défaut le modèle simule le développement des talles en faisant une estimation standard du délai entre floraison du brin maitre et des talles. Ce délai standard est court. Toutefois nous avons observé dans une expérimentation que la floraison des talles était significativement décalée par rapport au brin maitre. Dans ce cas il est possible à l'utilisateur de donner explicitement le délai en degrés-jours entre floraison du brin maitre et celles des talles.
- (iii) *Le nombre de feuilles vertes à 5 moments du cycle:* au début de la sénescence de la feuille 1, au début montaison, ligulation feuille drapeau, et au moins deux dates après floraison et une date avant la fin de sénescence de la feuille drapeau.
- (iv) *Les données de température.* Les variables de développement (réponses à la température) sont exprimés en temps thermique. Pour calculer le temps thermique, il est possible de fournir les données journalière ou horaire. Il est aussi possible de choisir le type de réponse : soit la réponse linéaire usuelle ($T_{base} = 0^{\circ}C$) ou une réponse non linéaire que nous avons définie (une forme modifiée du modèle de Johnson et Lewin (1946)). La prise en compte de la non-linéarité est importante lorsque les températures se rapprochent de la température optimale.

***Variables permettant de décrire la dynamique de population de talles.** Les variables nécessaires pour décrire la dynamique de tallage (apparition et mortalité) sont: (i) Les probabilités d'apparition de chacun des talles primaires (i.e. leur fréquence au maximum de tallage) et (ii) leur nombre moyen d'épis par plante.

***Un tableau de constantes.** Il contient un petit nombre de valeurs décrivant des allométries (e.g. entre brin maitre et talles) ou relations temporelles (coordinations de développement) au sein de la plante qui sont apparues comme constantes pour l'ensemble des expérimentations disponibles. A priori ces valeurs ne devront pas être changées, sauf éventuellement sur du matériel génétique particulier.

***Une collection de formes de courbure de feuilles.** La collection doit comprendre, pour chaque rang de feuille, un ensemble d'exemple de courbures possibles à différentes dates. Si les données n'ont pas été recueillies pour un cultivar donné, il est possible d'utiliser une collection existante pour un cultivar de port similaire. Pour l'instant nous disposons de collections de formes pour cinq cultivars ayant différents ports (planophyle et érectophyle) issues des expérimentations aux champs à densité standard ($D200\text{plt}/\text{m}^2$) ou faible ($D70\text{plt}/\text{m}^2$) : Soissons, Caphorn, Maxwell, Renan, Apache. A défaut de paramétrisation qui décrit l'évolution de la courbure au cours du temps, un travail sera nécessaire pour déterminer des critères simples à mesurer pour affecter un nouveau cultivar a un élément de la collection.

*** Variables permettant de décrire la géométrie des axes.** La représentation géométrique des axes dans la version actuelle d'ADELwheat répond à une paramétrisation empirique et simplicité non validée avec comme paramètre clé l'écartement final des axes (variable à mesurer à floraison). Toutefois, mes résultats montrent que cette description ne permet pas de décrire d'une façon réaliste la dynamique d'inclinaison des axes. A défaut de paramétrisation validée, nous proposons de mesurer l'angle d'inclinaison du brin maitre à quatre dates: à *Haun stage 4*, à la fin de tallage, *stade 2 nœuds* et *floraison*. Ceci permettra de calibrer le pattern présenté en chapitre 4.

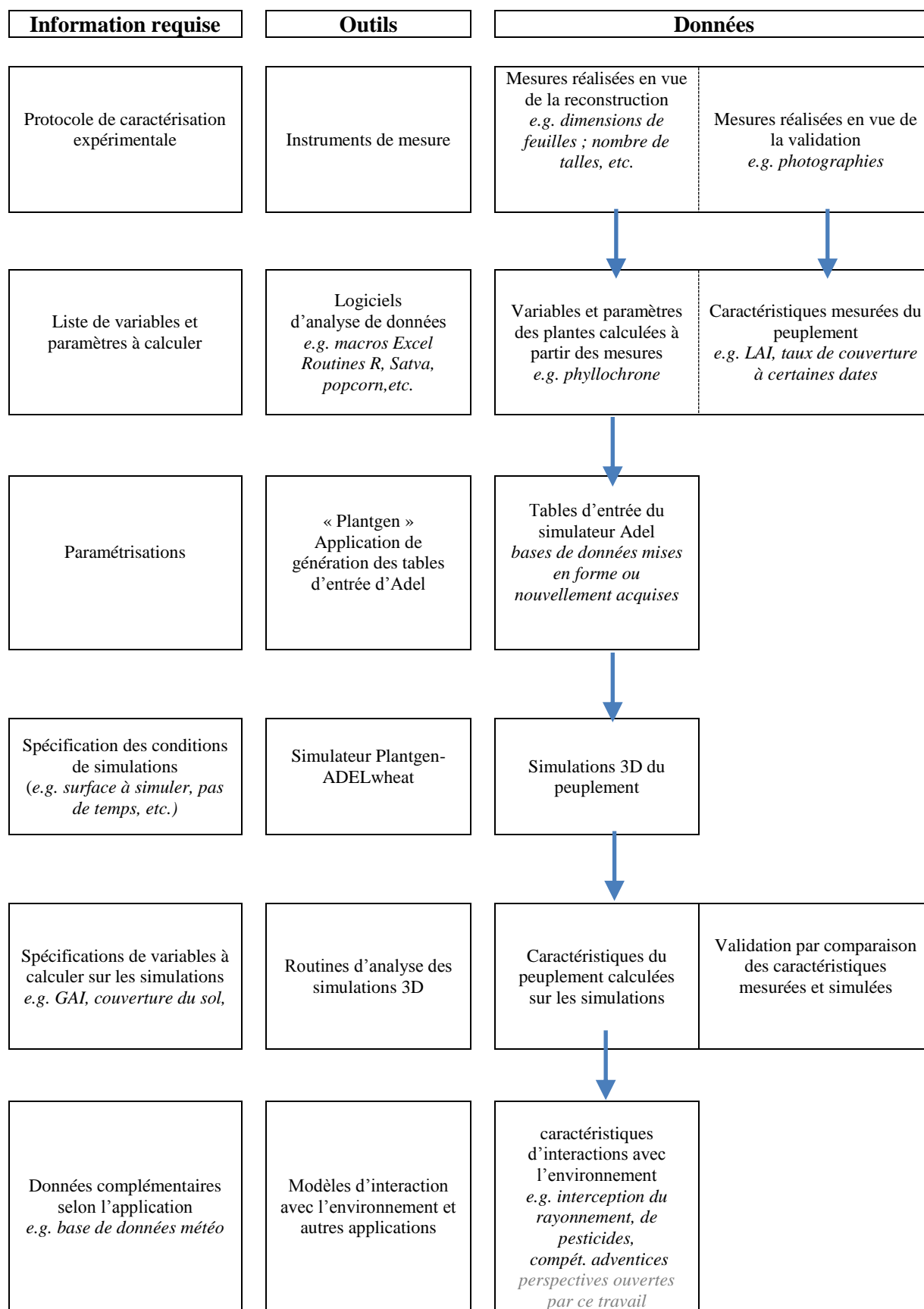


Figure 1: Etapes de l'acquisition des mesures à la reconstruction et à son utilisation, en lien avec les informations requises et outils mis en œuvre.

1.2. Protocole expérimental pour l'acquisition des données nécessaires au calcul des variables d'entrée

Un protocole de mesure complet a été défini afin d'assurer l'acquisition des mesures nécessaires au calcul des paramètres de « Plantgen » décrites dans le précédent paragraphe.

La description détaillée de ce protocole fera l'objet d'une publication. Ici nous présentons les éléments clés de la méthode :

*Nous proposons de taguer 3 répétitions de 15 plantes (**Figure3**) et de réaliser sur les mesures suivantes :

- Le suivi du phyllochrone et du nombre de feuilles vertes du brin maître. Avec au moins 4 points de mesures de Haun stage. Dans le cadre de ce suivi on caractérise les longueurs matures de l'ensemble des limbes.
- Le suivi du nombre de feuilles vertes du brin maître. Avec au moins 6 points de mesures : au début de sénescence de la feuille1, au début montaison, à la ligulation feuille drapeau, à floraison et deux dates avant fin remplissage des grains.
- Le dénombrement des talles primaires pour calculer la probabilité d'émergence pour chaque axe. Pour faciliter les notations il est préférable de faire ces mesures à chaque point de suivi du Haun stage et pas uniquement au moment du maximum de tallage.
- Les mesures des dimensions finales des phytomères supérieurs par scan (**Figure6**) des plantes taguées à floraison. On accède ainsi aux dimensions de tous les entrenœuds et des 4 à 5 gaines et limbes supérieurs (longueur /largeur/surface).
- Les mesures des dimensions finales des limbes et gaines inférieurs (longueur et largeur ou diamètre) par un prélèvement au *stade deux nœuds*. Ce prélèvement permet de calculer des allométries entre limbes et gaines (et entre longueur et largeur limbes). Ainsi les longueurs de limbes mesurées pour les plantes taguées seront utilisées pour calculer l'ensemble des dimensions nécessaires pour compléter la description des plantes taguées.

*Par ailleurs, des mesures de formes de feuilles du brin maître par la méthode des silhouettes sont à prévoir lors des prélèvements : stade 2 nœuds et floraison (**Figure4**).

*En plus, une caractérisation de l'angle d'inclinaison de la tige principale à 4 moments est à prévoir (Haun stage 4, à la fin de tallage stade 2 nœuds et floraison). La mesure peut se faire avec un rapporteur en considérant une ligne droite imaginaire, reliant deux points: la base de la tige le col de la dernière feuille ligulée.

*Il est important de caractériser précisément les dates des stades clefs: levée, début montaison, ligulation de la feuille drapeau (brin maître et talles) ainsi que la densité de plantes (levée, sortie d'hivers, floraison) et le nombre d'axes portant un épi.

*Des mesures supplémentaires peuvent être envisagées pour l'évaluation globale de la qualité des reconstructions 3D. On propose les mesures suivantes : (i) mesures du taux de couverture : photographies en visée verticale et oblique à 57°(**Figure5**), ainsi que (ii) des mesures de LAI (à réaliser au stade 2 nœuds et floraison sur les prélèvements déjà prévues pour l'acquisition des mesures dimensions présenté ci-dessus ; **Figure6**)

Pour caractériser un traitement, l'acquisition des données sur le terrain représente 5 à 6 périodes d'une journée de travail pour une équipe de 2 personnes, suivi chaque fois d'une journée de mesures complémentaires en laboratoire. L'analyse des données en vue de la reconstruction représente environ un mois de travail d'ingénieur. L'effort en termes de temps de travail reste donc important toutefois une part significative correspond aux mesures de taux de couverture et d'indice foliaire nécessaires pour évaluer la qualité des reconstructions.

Le protocole expérimental pourra être allégé. Quelques voies de simplification sont à tester:

- Tester les idées visant à utiliser des relations d'allométries pour estimer les valeurs individuelles de dimensions (gaines/limbes /entrenœuds) à partir de mesures plus simples. Pour une description complète du cycle, il restera toutefois probablement nécessaire d'acquérir des mesures de dimension relatives aux phytomères qui se développent en conditions hivernales puis des phytomères présents à floraison.
- Nous pensons possible de faire l'économie des acquisitions de forme de feuilles et de définir plutôt une paramétrisation qui décrit l'évolution du port foliaire en tenant compte de la position et l'âge issue de mes résultats présentés dans chapitre 4. Dans ce cas, il sera nécessaire de définir des paramètres simples à mesurer pour la calibration de l'angle d'inclinaison. Ensuite, pour définir la forme des feuilles (courbure), on pourra tirer dans les collections existantes une variété de port similaire.
- La photographie en visée oblique (57°) fourni de bonnes estimations des indices foliaires compris entre 0 et 3 (testé et évaluer à plusieurs occasions). Nous pensons possible d'utiliser de façon systématique ce type d'estimation pour le calage de paramètres du modèle.



Figure 3 : Photo d'une plante baguée pour identifier les numéros des feuilles et des talles

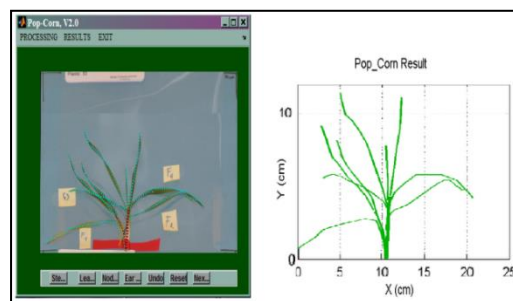


Figure 4 : Résultat de digitalisation des courbures des feuilles par le méthode de silhouette (Logiciel PopCorn)

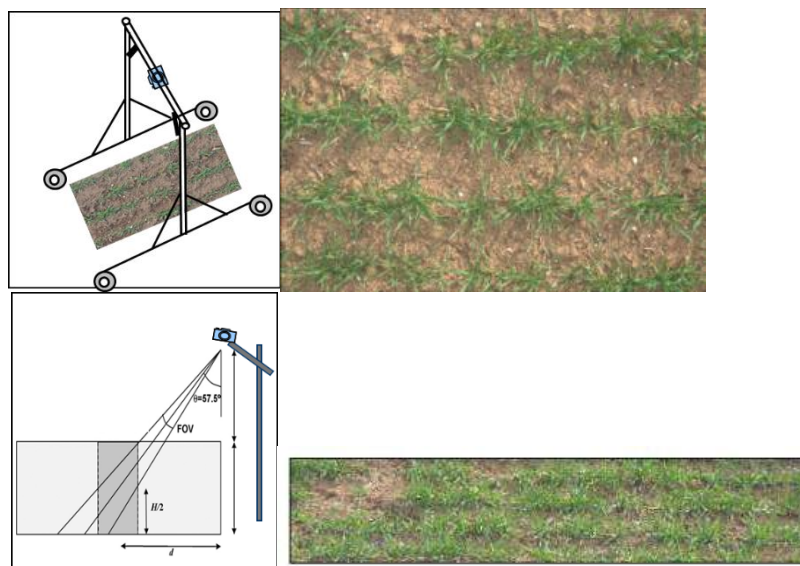


Figure 5 : Schéma illustrant le dispositif utilisé pour acquérir les photos de couverture sur deux angles de vue : visée verticale (0°) en haut et visée oblique (57.5°) en bas.



Figure 6: Scan des organes pour mesurer les dimensions et les surfaces.

1.3.Interface utilisateur

La **figure7** présente le dataflow de l'application « Plantgen » qui génère les tables d'entrées d'ADELwheat. Les boites jaunes renferment les informations nécessaires pour reconstruire d'une façon dynamique un couvert de blé. Ces trois boites sont :

- *Leaf_dynamic_params*. Elle reçoit les variables relatives à la phénologie. Ces données peuvent être contenues dans le fichier « dynT_user.csv » ou être saisies au clavier via des fenêtres interactives (partie en haut à gauche du dataflow).
- *Organ_dimension_params*. Elle reçoit les dimensions des organes du brin maitre (lien vers un fichier dimT_user.csv),
- *Others_params*. Elle reçoit les variables décrivant la densité de plante, la densité d'épi, les probabilités d'apparition des talles primaire, les probabilités de fréquence de nombre de feuilles sur le brin maitre, et les mesures de nombre de feuilles vertes sur le brin maitre apres ligulation feuille drapeau.

Les boites bleues sont l'interface vers les tables d'entrées d'Adel qui ont été remplies par l'application Plantgen (table des axes, table de phénologie, table de dimensions). L'application génère aussi d'autres tables d'enregistrement de valeurs de paramètres, qui permettent une traçabilité des simulations.

Le data flow ne montre pas le module contenant les collections de formes de feuille ou valeurs de paramètres de géométrie des axes, ceux-ci sont directement connecté en entrée d'ADELwheat. Une description de l'interfacage plantgen et Adel est présenté dans la documentation (paragraphe 5).

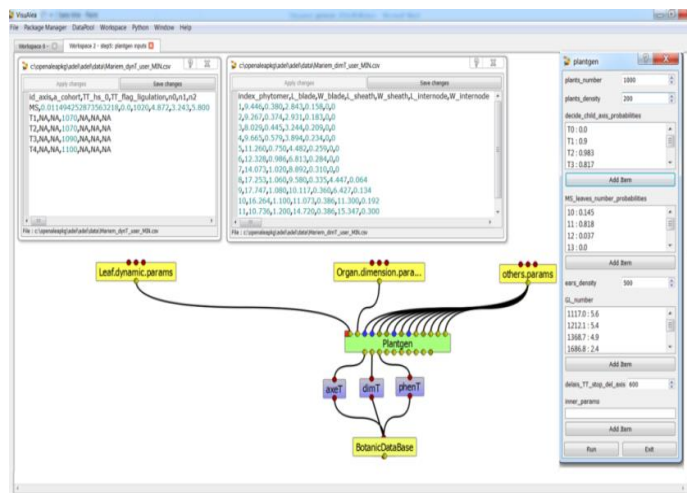


Figure 7: Dataflow de de l'application « Plantgen » disponible sur openAlea

1.4. Routines «Post-processing» : calcul sur les représentations 3D

Le portage du modèle « Plantgen-ADELwheat » sous Open Alea permet l'exploitation des simulations par de nombreux modules informatiques disponibles – ou en cours de développement par la communauté scientifique utilisant cette plateforme. Toutefois leur utilisation est plus ou moins complexe et leur interface utilisateur n'est pas toujours conviviale.

Dans le cadre du projet nous avons agencé les éléments pour :

***La visualisation 3D** (modules utilisés pour les images présentés dans ce manuscrit). La visualisation d'un peuplement peut se faire en simulant la géométrie de vue d'un appareil photographique ; ceci permet d'analyser le pouvoir couvrant qui représente une variable importante utilisée dans l'évaluation des reconstructions. Ces modules sont utilisés pour générer la *figure 7*.

***Affecter un identifiant aux différents modules botaniques (Fig.8)**. Il est possible d'affecter des couleurs spécifiques aux différents modules (gain/limbe/entrenœud), ou aux différents numéros de talles, etc.). Combiné aux modules de visualisation ceci permet d'analyser la part de pouvoir couvrant dues aux différents types d'organes (e.g. limbes, gaines, entrenœuds, etc.).

***Le calcul de variables telles que LAI ou GAI**. Ceci était un des objectifs explicites du projet vue leur importance dans l'évaluation globale du modèle « Plantgen ». En outre il est possible de filtrer les surfaces par types ou état d'organe pour calculer les contributions des gaines, limbes et entrenœuds, ou les contributions des différents types d'axes au GAI global. Ces modules sont utilisés pour générer la *figure 9*.

***La présentation automatisée de graphique d'analyse** (e.g. comparaison de variables simulées et observées, *Fig.10*)

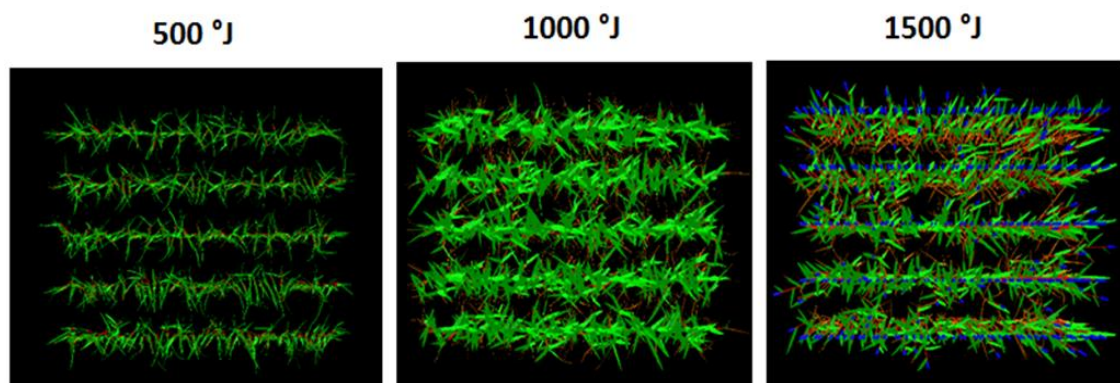


Figure 7 : Simulation d'un peuplement issue de la reconstruction de l'expérimentation (ici c'est l'expérimentation de Bertheloot 2005/2006 ;CapHorn sans fertilisation azoté). La visualisation simule la prise de vue d'un appareil photographique en visée verticale, avec un objectif au format APN de distance focale 50 mm. On a affecté un code couleur par type d'organe : vert : tissus foliaires vert ; marron : tissus foliaires sénescents ; rouge : gaines et tiges ; bleu : épis. La proportion de pixels colorés sur l'image représente donc le taux de couverture du sol. Ainsi le comptage des pixels de chaque couleur donne la contribution de chaque type d'organe au pouvoir couvrant.

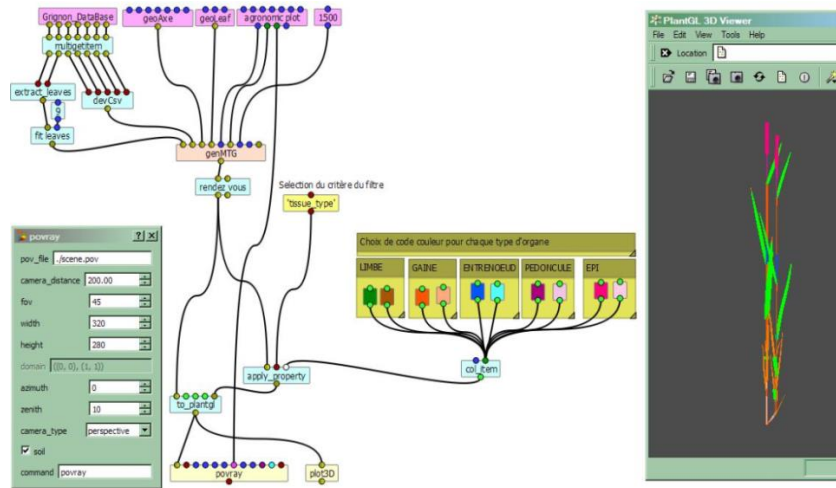


Figure 8 : Ce dataflow illustre l'interface de deux modules d'exploitation des reconstructions : (1) le module permettant d'affecter des couleurs spécifiques aux différents organes. Ici on distingue limbe, gaine entrenœuds, pédoncule et épis et pour chaque organes on distingue selon son l'état (vert ou sénéscent). Une plante ainsi est visualisée à droite ;(2) l'interface du module Povray qui permet la simulation d'une photographie d'un peuplement. On spécifie dans l'interface la hauteur de l'appareil photo, et la direction visée (zénith, azimuth), l'ouverture angulaire de l'objectif, et les dimensions du capteur .Ainsi il est possible de reproduire précisément les conditions de prise de vue lors d'une l'expérimentation.

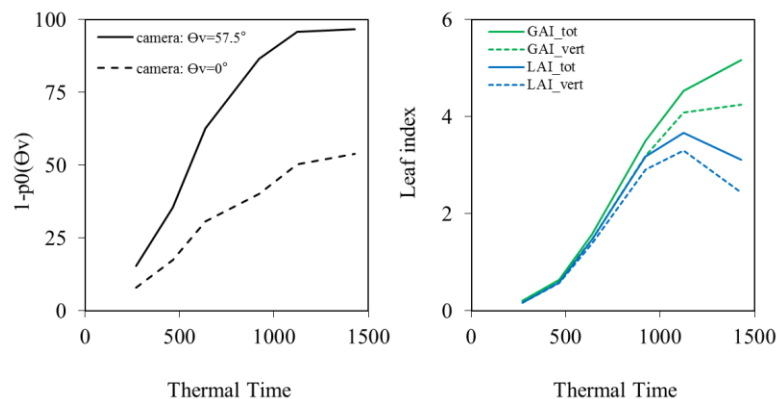


Figure 9 : Figures issues des modules de calcul sur les représentations 3D. La figure à gauche représente les simulations de fréquence de trou sur deux angles de visé calculé sur un peuplement virtuel. La figure à droite représente les simulations de l'indice foliaire vert et total considérant la plante entière GAI (limbe et tiges) ou que les limbes LAI.

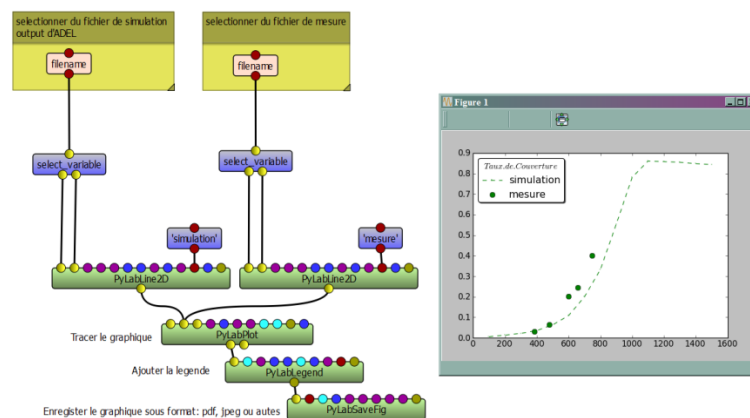


Figure 10 : Data flow de création d'un graphique sous Open Alea. Ici le graphique compare les taux de couverture du sol observés à ceux simulés avec les reconstructions 3D.

1.5. Evaluation qualité de reconstruction

Les reconstructions 4D issues du modèle « Plantgen-ADELwheat » ont été évaluées d'une façon globale en utilisant des jeux de données indépendants. Les critères d'évaluation sont la dynamique d'indice foliaire vert et total (LAI et GAI) et la dynamique de taux de couverture en visé verticale et inclinée. Défaut de temps, le résultat de l'évaluation n'a pas été présenté dans ce rapport. La synthèse de ce travail d'évaluation est la suivante :

- Bonne adéquation entre les mesures et les simulations de la dynamique d'indice foliaire vert (*Figure 11*).

- Certains aspects de géométrie non pris en compte dans le modèle (modification de l'inclinaison des feuilles avec l'âge) ou mal caractérisés (inclinaison des axes) influencent de façon très significative le taux de couverture du sol pour un même indice foliaire.

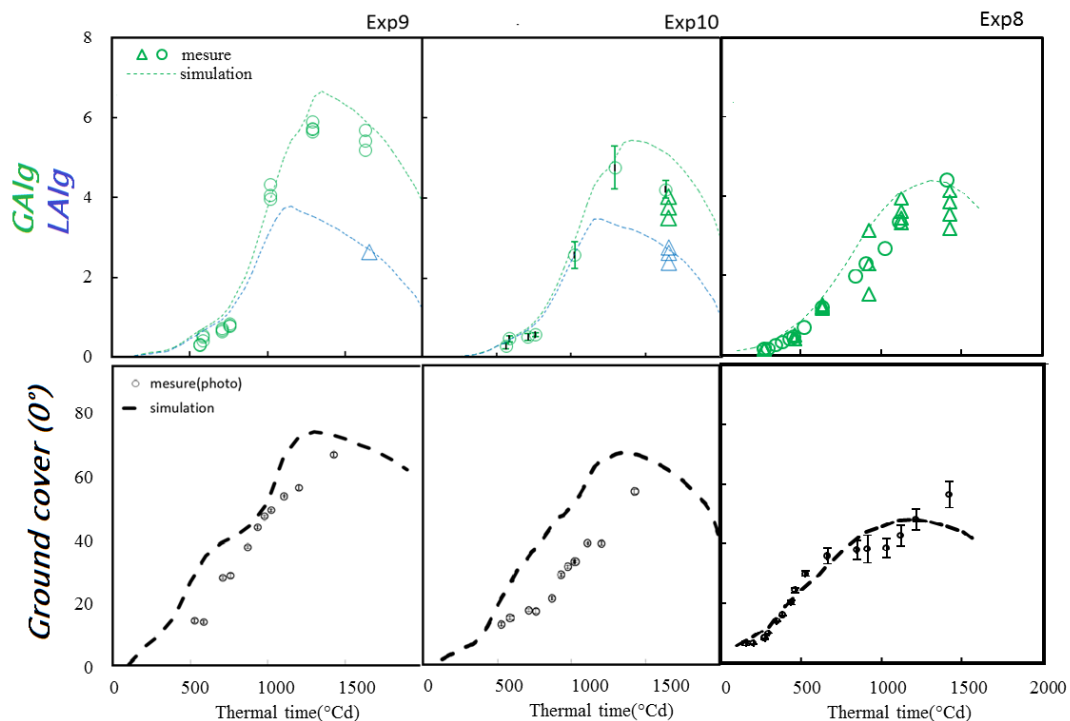


Figure 11: Dynamique d'indice foliaire vert (GAI : global area index ; LAI : leaf area index) et la dynamique de couverture du sol vs. Temps thermique depuis la levée de 3 traitements différents : Soissons Y2012/2013 à gauche, Caphorn Y2012/2013 au milieu et Maxwell Y2010/2011 à droite (informations détaillées sur les traitements est présenté dans le *Tableau 1*). Les symboles représentent les mesures et les lignes représentent les simulations issues du « Plantgen-ADELwheat ».

1.6. Jeu de données simulant différent architecture spécifique.

Un résultat direct de mon travail est de générer des données simulant de façon effective l'architecture 4D d'un ensemble de traitements spécifique. Ces traitements sont présentés dans le *Tableau 1*. La reconstruction 4D de 10 traitements est déjà disponible et la reconstruction est en cours de finalisation pour les 12 autres traitements. Les fichiers de données d'entrées nécessaires à la simulation de ces traitements ont été générés et organisés

dans Open Alea de façon à assurer un archivage pérenne et une utilisation facile (*Fig.12, Fig.13*).

D'autre part, nos données de courbures de feuilles issues de 15 traitements et couvre 5 géotypes seront utilisé pour enrichir la base de données courbe présente dans l'interface du modèle « Plantgen-ADELwheat » ce qui permettra d'améliorer la qualité des simulations. Pour l'instant ce jeu de donnée n'est que partiellement intégré à cette l'interface.

Tableau 1: la liste des traitements qui ont été reconstruit (ou reconstruction en cours) issus des expérimentations sur le campus INRA à Thiverval-Grignon. La liste comporte 23 traitements incluant 5 saisons de culture, 5 cultivars, 2 dates de semis, trois densités, deux distances inter-rangs (IS:17.5cm; ID:35cm) et deux traitements azotés (N+: fertilisation standard ; N0: sans fertilisation).

N° trt.	Year	Cultivar	Sowing date (jj mm)	Sowing Density (pl.m ⁻²)	Nitrogen	Inter-row distance	Referent person	Reconstruction 4D
1	Y05/06	Soissons	S2 (27 Oct.)	D2 (250)	N+	IS	J. Bertheloot	disponible
2	-	Caphorn	S2 (27 Oct.)	D2 (250)	N+	IS	J. Bertheloot	disponible
3	-	Soissons	S2 (27 Oct.)	D2 (250)	N0	IS	J. Bertheloot	disponible
4	-	Caphorn	S2 (27 Oct.)	D2 (250)	N0	IS	J. Bertheloot	disponible
5	Y08/09	Soissons	S3 (17 Nov.)	D1(77)	N+	IS	R. Baccar	disponible
6	-	Soissons	S3 (17 Nov.)	D2(228)	N+	IS	R. Baccar	disponible
7	-	Soissons	S3 (17 Nov.)	D3(514)	N+	IS	R. Baccar	disponible
8	Y10/11	Maxwell	S2 (26 Oct.)	D2(220)	N+	IS	M. Abichou	disponible
9	Y12/13	Soissons	S2 (02 Oct.)	D2 (220)	N+	IS	M. Abichou	disponible
10	-	Caphorn	S2 (02 Oct.)	D2 (220)	N+	IS	M. Abichou	disponible
11	-	Maxwell	S2 (02 Oct.)	D2 (220)	N+	IS	M. Abichou	en cours
12	-	Apache	S2 (02 Oct.)	D2 (220)	N+	IS	M. Abichou	en cours
13	-	Renan	S2 (02 Oct.)	D2 (220)	N+	IS	M. Abichou	en cours
14	-	Maxwell	S2 (02 Oct.)	D2 (220)	N+	ID	M. Abichou	en cours
15	-	Soissons	S2 (02 Oct.)	D2 (220)	N+	ID	M. Abichou	en cours
16	-	Caphorn	S2 (02 Oct.)	D2 (220)	N+	ID	M. Abichou	en cours
17	-	Maxwell	S2 (02 Oct.)	D2 (220)	N+	ID	M. Abichou	en cours
18	-	Apache	S2 (02 Oct.)	D2 (220)	N+	ID	M. Abichou	en cours
19	-	Renan	S2 (02 Oct.)	D2 (220)	N+	ID	M. Abichou	en cours
20	Y13/14	Caphorn	S2 (30 Oct.)	D1(70)	N+	IS	M. Abichou	en cours
21	-	Apache	S2 (30 Oct.)	D1(70)	N+	IS	M. Abichou	en cours
22	-	Renan	S2 (30 Oct.)	D1(70)	N+	IS	M. Abichou	en cours
23	-	Caphorn	S2 (30 Oct.)	D2 (200)	N+	IS	M. Abichou	en cours

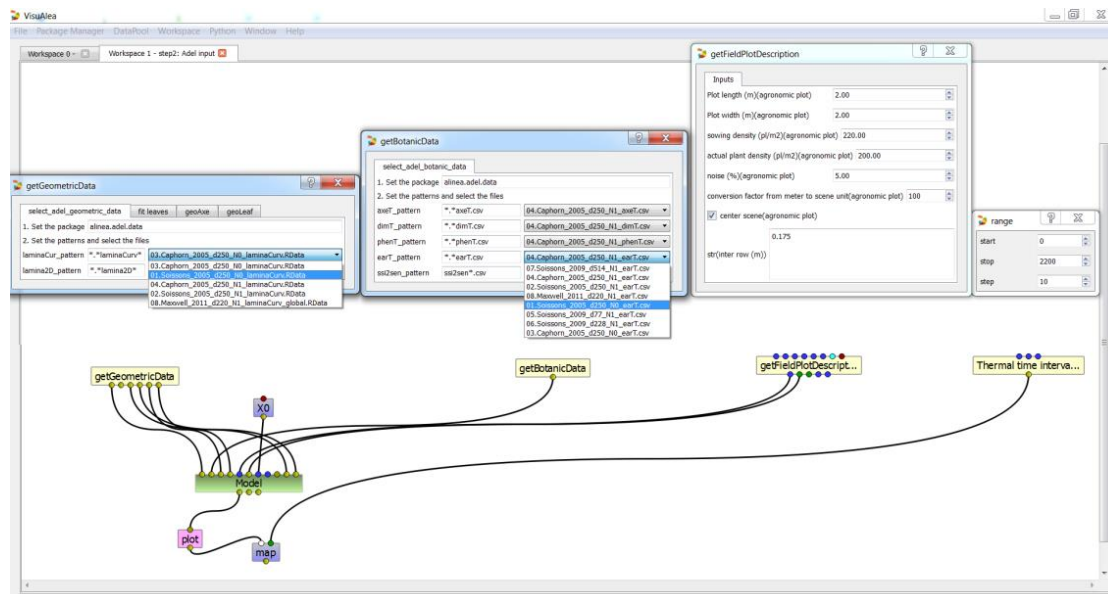


Figure 12 : Représentation de l'interface graphique du modèle « Plantgen-ADELwheat » présentant la possibilité de sélectionner, depuis une liste de traitements disponibles, un traitement spécifique et le reconstruire. Des couverts hybrides peuvent aussi être générés en croisant les fichiers (exemple : structure de Soissons et géométrie de Caphorn).

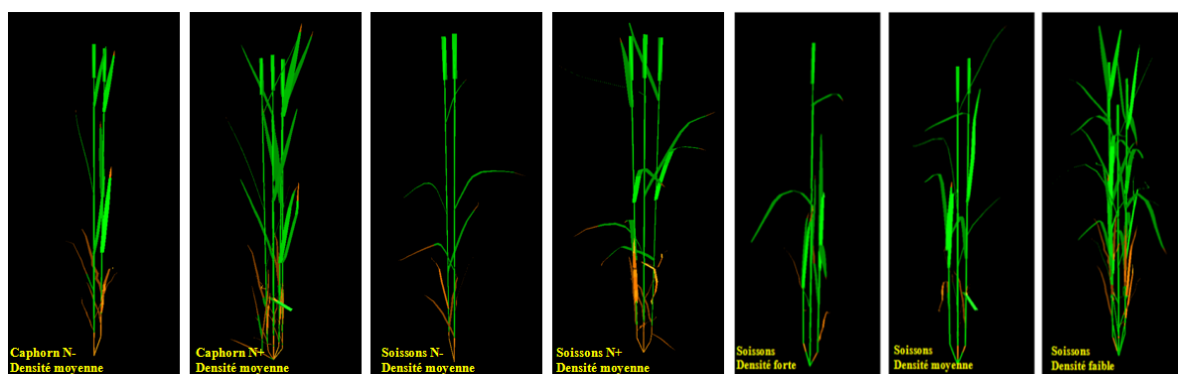


Figure 13 : Simulation de plantes à 1450°Cd après levée pour les traitements numéros 1 à 7 du *Tableau 1*. Chaque traitement est simulé en prenant en compte une variabilité inter-plantes. Ici on a représenté une plante représentant la médiane de chaque peuplement en termes de nombre de tiges et de nombre de feuilles par axe. Les figures illustrent le port plus érigé de Caphorn par rapport à Soissons, et les variations du nombre de tiges en fonctions des traitements. Les tissus sénescents sont représentés ici par la couleur marron.

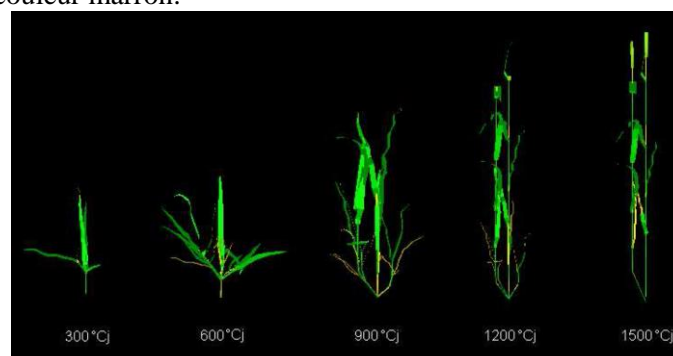


Figure 14 : Simulation de plantes de blé de la variété Caphorn à différents stades de croissance. Les tissus sénescents sont représentés par la couleur marron.

2. Documentation « *Plantgen-ADELwheat* »

La documentation, qui suit, présente le modèle couplé « *Plantgen-ADELwheat* ». Cette documentation est en cours de finalisation elle sera prochainement disponible en ligne sur l'interface OpenAlea à l'adresse suivante:

<http://openalea.gforge.inria.fr/doc/alinea/adel/doc/build/html/user/manual.html>

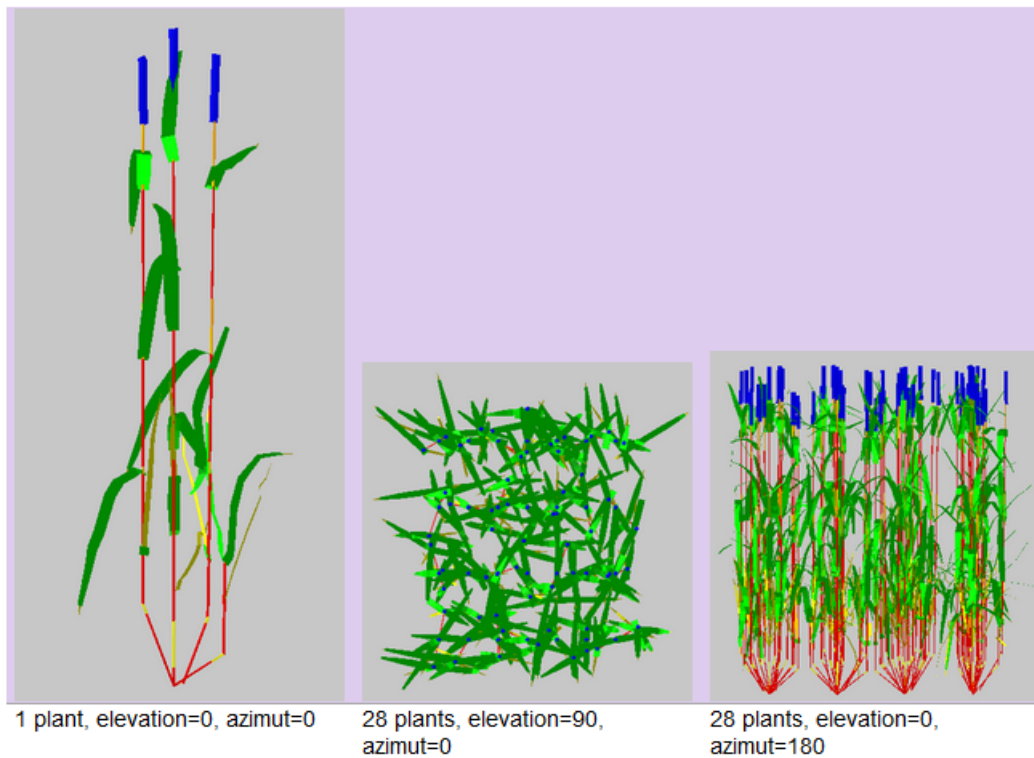
Alinea.PlangenAdel Documentation	Summary
<ul style="list-style-type: none">• General introduction• Description of Adel's inputs<ul style="list-style-type: none">◦ Inputs describing development<ul style="list-style-type: none">▪ <i>axeT</i> : Master table allowing to organize the information plant per plant▪ <i>dimT</i> : description of the dimensions of leaf blades, sheath and internodes▪ <i>phenT</i> : description of phenology of axes▪ <i>earT</i> : description of ear dimension and phenology▪ <i>ssi2sen</i> : description of progression of senescence in upper leaf blades as a function of SSI◦ Inputs describing geometry<ul style="list-style-type: none">▪ How to specify the geometric data◦ Inputs describing simulation◦ Inner options of ADEL<ul style="list-style-type: none">▪ Coordination in organ extension▪ Senescence of sheath and internodes▪ Disappearance of dead tillers• Plantgen model: construction of the input tables<ul style="list-style-type: none">◦ The levels of completeness◦ Construction of Adel input tables using the Python interpreter<ul style="list-style-type: none">▪ The arguments to define by the user▪ Code example◦ Construction of Adel input tables using Visualea◦ Inner parameters for Plantgen model• Description of PlangenAdel's outputs• Appendices<ul style="list-style-type: none">◦ Plantgen model: construction of the input tables<ul style="list-style-type: none">▪ Static view of plantgen▪ Dynamic view of plantgen▪ <i>dynT_user_FULL</i>▪ <i>dynT_user_SHORT</i>▪ <i>dynT_user_MIN</i>▪ <i>dimT_user_FULL</i>▪ <i>dimT_user_SHORT</i>▪ <i>dimT_user_MIN</i>▪ <i>phenT_abs</i>▪ <i>dimT_abs</i>▪ <i>dynT</i>▪ <i>phenT_first</i>▪ <i>HS_GL_SSI_T</i>▪ <i>tilleringT</i>▪ <i>cardinalityT</i>	<ul style="list-style-type: none">Topic: <i>Alinea.PlangenAdel Documentation</i>Release: 0.9Date: février 11, 2015Authors: Mariem ABICHOU, Bruno ANDRIEU and Camille CHAMBONTarget: users

General introduction

ADEL-Wheat (Architectural model of DEvelopment based on L-systems) is designed for simulating the 3D architectural development of the shoots of wheat plants. The model has been coupled with "Plantgen" model that generate botanical and development information of a set of plant. ADEL-Wheat has been also coupled with a light model adapted to field conditions ""Caribu model"", in order to allow calculating the light interception by individual phytoelements during the crop cycle. Applications of such a tool range from the interpretation of remote-sensing signals, to the estimation of crop light use efficiency, or to the assistance in the ecophysiological analysis of plant response to light conditions. The model is based on an analysis of developmental and geometrical similarities that exist among phytomers, to allow a concise parameterisation. Parameterising the model requires using experimental data to document a set of inputs described below.

Beside these user inputs, Adel also make use of constants and of relations (set and 'readable' in Adel.R, but not documented) describing coordination of leaves, dynamics of geometry, computation of visibility and progression of senescence as a function of ssi. See Robert et al (Functional Plant Biology 2008) for description. The next figure shows the global dataflow of Adel:

Simulations are visually realistic. And the model was shown to correctly reproduce important agronomic features such as kinetics of LAI and of plant height. The following table presents simulation of Soissons variety with nitrogen fertilization:



Description of Adel's inputs

Adel requires three kinds of inputs to be provided by the user:

- inputs characterizing the development of plants in the canopy (topology, developmental rate and size of plants)
- inputs characterizing the geometry of axes and of leaves
- inputs characterizing the simulation (time step..) and the plot configuration (number of plants, position)

Units and conventions - Dimension are expressed in cm - Thermal time is expressed in °CD

Position of a phytomer on an axis: Most often (as described below) phytomer position in Adel are counted acropetally and are normalized relatively to the total number of phytomers (leaf 1 relative position is 1/nf and flag leaf relative position is 1). Use of relative positions was chosen to allow sharing data between axes differing by the total number of phytomers. In later versions of Adel the relative phytomer number should be changed by the absolute one. With the convention that 1 is referring to the first true leaf.

Inputs describing development

Development is parameterized in a Rlist containing 3 tables (*axeT*, *dimT* and *phenT*).

These tables have dependencies (cross references). However some may be compatible with others if cross references are maintained. This allows for recombination of parameters.

axeT : Master table allowing to organize the information plant per plant

axeT is the master table that organizes how each plant is described. For each plant, the table contains a few explicit parameters that describe the phenology and the number of modules (eg time of appearance, number of axes and number of leaves on axes) and identifiers that refer to information given in the other tables (*dimT*, *phenT*, *earT*).

All plants to be used for the reconstruction must be listed in *axeT*. If only one plant is given, Adel will clone that plant. To have a correct simulation of tiller dynamics at the plot level, a minimum of 30 plants is recommended.

There is one line per axis. Columns are :

Column	Description
id_plt	Number (int) identifying the plant to which the axe belongs
id_cohort	Number (int) identifying the cohort to which the axe belongs
id_axis	Identifier of the botanical position of the axis on the plant. "MS" refers to the main stem, "T0", "T1", "T2",..., refers to the primary tillers, "T0.0", "T0.1", "T0.2",..., refers to the secondary tillers of the primary tiller "T0", and "T0.0.0", "T0.0.1", "T0.0.2",..., refers to the tertiary tillers of the secondary tiller "T0.0". See <i>Botanical position of the axis on the plant.</i>
N_phytomer_potential	The <i>potential</i> total number of vegetative phytomers formed on the axis. N_phytomer_potential does NOT take account of the regression of some axes.
N_phytomer	The <i>effective</i> total number of vegetative phytomers formed on the axis. N_phytomer does take account of the regression of some axes.

HS_final	The Haun Stage at the end of growth of the axis.
TT_stop_axis	If the axis dyes: thermal time (since crop emergence) of end of growth. If the axis grows up to flowering: <i>NA</i>
TT_del_axe	If the axis dyes: thermal time (since crop emergence) of disappearance. If the axis grows up to flowering: <i>NA</i>
id_dim	key (int) linking to <i>dimT</i> . <i>id_dim</i> allows referring to the data that describe the dimensions of the phytomers of the axis
id_phen	key (int) linking to <i>phenT</i> . <i>id_phen</i> allows referring to the data that describe the phenology of the axis
id_ear	Key (int) linking to <i>earT</i> . <i>id_ear</i> allows referring to the data that describe the ear of the axis. For the regressive axes, <i>id_ear</i> = <i>NA</i> . For the non-regressive axes, <i>id_ear</i> =1.
TT_app_phytomer1	Thermal time (relative to canopy appearance) of tip appearance of the first true leaf (not coleoptile or prophyll)
TT_col_phytomer1	Thermal time (relative to canopy appearance) of collar appearance of the first true leaf
TT_sen_phytomer1	Thermal time (relative to canopy appearance) of full senescence of the first true leaf (this is : thermal time when SSI= 1)
TT_del_phytomer1	Thermal time (relative to canopy appearance) of disappearance of the first true leaf

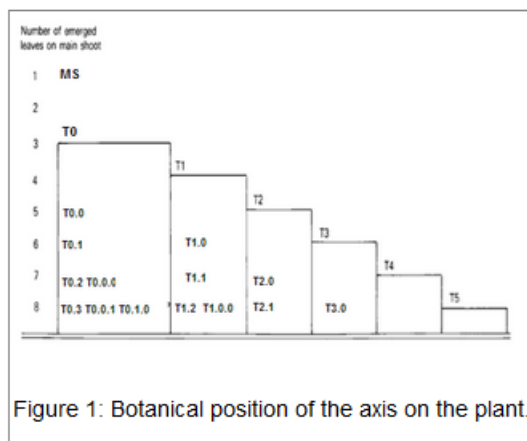


Figure 1: Botanical position of the axis on the plant.

See an example of *axeT*.

dimT : description of the dimensions of leaf blades, sheath and internodes

dimT allows to describe a number of profiles of dimension, each profile being associated to a value of *id_dim*. Dimensions of organs must be given for each of the *id_dim* mentioned in *axeT*.

Positions on an axis are expressed as relative position ($\text{index_rel_phytomer} = \text{phytomer rank}/N_{\text{phytomer}}$);

Use of relative position makes it possible to use a same profile of dimension for axes differing in the final number of phytomers (N_{phytomer}); Use of relative position makes it possible to document a profile with only some the phytomers on an axis: Missing data will be estimated by linear interpolation according to *index_rel_phytomer*;

Actual dimension of the blade, sheath and internode of an axis are hence calculated according to `id_dim` and `N_phytomer`.

There is one line per phytomer documented.

Columns are :

Column	Description
<code>id_dim</code>	the identifier referred to in <i>axeT</i> . By convention, if the current <code>id_dim</code> ends by <code>0</code> (e.g. <code>id_dim=1110</code>), then the current line documents the dimensions of a regressive axis. If the current <code>id_dim</code> ends by <code>1</code> (e.g. <code>id_dim=1111</code>), then the current line documents the dimensions of a non-regressive axis.
<code>index_rel_phytomer</code>	The relative phytomer position : <code>index_rel_phytomer = phytomer rank/N_phytomer</code>
<code>L_blade</code>	length of the mature blade (cm)
<code>W_blade</code>	Maximum width of the mature leaf blade (cm)
<code>L_sheath</code>	Length of a mature sheath (cm)
<code>W_sheath</code>	Diameter of the stem or pseudo stem at the level of sheath (cm)
<code>L_internode</code>	Length of an internode (cm)
<code>W_internode</code>	Diameter of an internode (cm)

See an example of `dimT`.

phenT : description of phenology of axes

phenT controls the dynamics of leaf appearance, ligulation, senescence and disappearance. Internal rules of Adel coordinate sheaths and internodes to the blades so that *phenT* controls indirectly the whole dynamics of plant development.

Positions on an axis are expressed as relative positions.

One timing of development has to be documented for each value taken by `id_phen` in *axeT*; axes sharing a same value of `id_phen` will share the same timing; Use of relative position makes it possible to use a same developmental timing for axes differing in the final number of phytomers; Use of relative position makes it possible to document a developmental timing with a number of value higher than the number of phytomers on an axis: this is required because the dynamics of SSI shows a complex behavior(see below)

Timing of developmental events on a leaf is given relative to the timing of the event on leaf 1 of the axis; Actual timing is computed from *phenT* and the data concerning leaf 1 in *axeT*.

For each `id_phen`, there is one line per value of `index_rel_phytomer` documented. For a smooth description of the dynamics of SSI from crop appearance to maturity, approximately 40 values of `index_rel_phytomer` should be documented (for each value of `id_phen`). More over for each value of `id_phen`, one line should be documented for `index_rel_phytomer = 0`, so as to allow interpolation.

Columns are :

Column	Description
<code>id_phen</code>	the index referred to in <i>axeT</i>
<code>index_rel_phytomer</code>	normalized phytomer position, starting from <code>index_rel_phytomer = 0</code>

dtT_app_phytomer	Thermal time of the appearance of the tip of leaf out of the whorl made by the older blade; expressed as thermal time since TT_app_phytomer1
dtT_col_phytomer	Thermal time of the appearance of collar; expressed as thermal time since TT_col_phytomer1
dtT_sen_phytomer	Thermal time for which SSI = n (where n is the phytomer rank); expressed as thermal time since TT_sen_phytomer1
dtT_del_phytomer	Thermal time after which the leaf blade is destroyed and is not displayed in the 3D mock-up anymore; expressed as thermal time since TT_del_phytomer1

See an example of phenT.

earT : description of ear dimension and phenology

There is one line per ear type (referred by id_ear in *axeT*)

Column	Description
id_ear	the identifier referred to in <i>axeT</i>
dtT_ap_ear	Thermal time interval between flag leaf ligulation and ear appearance (appearance of the tip of highest spike, discounting the awn)
dtT_ap_peduncle	Thermal time interval between flag leaf ligulation and peduncle appearance (appearance of the base of the ear)
TT_z92	Thermal time (relative to canopy emergence) of the end of grain filling (corresponding on z92 on Zadoks scale)
L_peduncle	length of the ear peduncle: from the last node to the base of the ear (cm)
W_peduncle	diameter of the ear peduncle (cm)
L_ear	length of the ear without awns (cm)
A_ear	projected area of ear without awn (cm ²)
L_spike	Total length of the spike : from base of the ear to the top of the awns (cm)

ssi2sen : description of progression of senescence in upper leaf blades as a function of SSI

Adel considers two categories of phytomers for describing the progression of senescence in leaf blades.

- for lower leaves, the senescence progresses linearly as function of SSI and blades sequentially: the senescence of blade at rank n starts when senescence of blade n-1 has finished. This means that the senesced fraction of leaf n is : $1+SSI -n$. It depends only in ssi and there is no need for additional parameters.
- for upper leaves, the progress of senescence is more complex and several leaf blades senesce simultaneously: SSI2senT contains data to calculate the fraction of senesced area of each upper leaves as function of ssi.

The upper leaves correspond approximately to the leaves beard by an elongated internode. The number of lower leaves showing a linear progress of senescence is called Nsenlow; The number of upper leaves showing a complex progress is called Nsenup

All upper leaf blades start to senesce at the same time, that is at $SSI = Nsenlow$; Senescence of each upper leaf blade progresses first at a slow rate, identical for all leaves, then at a fast rate.

The parameter used to describe these kinetics are the value of the slow rate (R_{sen1}), the value of ssi ($dssit1$) at the onset of fast senescence and the value of SSI ($dssit2$) at full senescence for each upper leaf.

The table defines the parameter values for the upper leaves. There is one line per upper leaf and the number of lines of the file must be $Nsenup$. The values d_{SSIt1} and $dssit2$ are specified in term of difference with the ssi at onset of upper leaves senescence ($Nsenlow$)

It should be noted that the present description of progress of senescence is over-parameterized, resulting in a constraint between parameters value. This comes from the fact that at any time the sum of the rate of progress of senescence for all leaves should be one. Complying with this constraint is not straightforward. So a user that do not know precisely the value of parameters in his experiment should probably use the default values to ensure a consistent behavior.

Column	Description
N_senup	Number of leaves that show two phases during senescence (the value is repeated for all lines!)
R_sen1	Rate of progress of senescence during phase 1 (the value is repeated for all lines !)
dssit1	(SSI when the leaf blade starts phase 2) - $Nsenlow$)
dssit2	(SSI when the leaf blade is 100% senesced - $Nsenlow$)

Inputs describing geometry

Input are required to define the geometry of leaves (normalized 2D shape, midrib curvature and azimuth) and the geometry of stems (inclination, azimuth)

Normalized 2D shapes are leaf width variations with distance to the base of the leaf, both axes being normalized so that max values is 1.

Normalized 2D shapes and midrib curvature are stored as collections and Adel will draw an individual leaf by scaling a 2D shape plus taking a midrib curvature from these collections.

The inclination of axes is defined by two parameters $DredT$ and $Tillerinc$. $DredT$ represents the horizontal distance between the main stem and a tiller at flowering. $Tillerinc$ represents the angle of insertion of a tiller at flowering. When a tiller grows, it starts with angle of 3° compared to the vertical. Then, during the period of extension of the lower internode, insertion angle increases up to the value $Tillerinc$. It will keep this value until the top of the stem reaches the distance $DredT$ from the main stem. When this is reach, the two upper visible nodes rotate so that the top of the tillers remains at distance $DredT$. Any internode that elongate later is vertical. Note that when sheath disappear, new node become visible and will become involved in the process.

$genGoeaxe$ (see below) includes a parameter to randomly tilt the main stem of a small value around the vertical. When the main stem is tilted, all the plant follows

How to specify the geometric data

The collections for 2D leaf shape and for leaf curvature should be specified as one list of lists of matrices for 2D shape and one list of matrices for midrib curvature.

How to specify the geometric data

The collections for 2D leaf shape and for leaf curvature should be specified as one list of lists of matrices for 2D shape and one list of matrices for midrib curvature.

- the first level in the list is for collection index
- the second level is for matrix index.

See *alea* for more information.

Besides these collections, R functions should be provided as inputs. A first list of function is for defining the axis geometry; A second list of functions is for selecting shapes in the collections mentioned above.

The first list should provide 3 R functions of axis number (0 = main stem) that return:

- **azT** : the azimuth(deg) of the first leaf of the axis with reference to the azimuth of the parent axes
- **incT** : the inclination (deg) of the base of the tiller compared with main stem
- **dredT** : the distance (at maturity) between tiller and main stem

These functions can be generated by the predefined *genGeoAxe* node or be freely user-defined in a *freeGeoAxe* node.

In *genGeoAxe* The azimuth of a tiller stem is the same as that of the axilling main stem leaf. The azimuth of the first leaf of a primary tiller is with an angle of 75° relatively to that of the axilling main stem leaf. For secondary tillers, the azimuth of the first leaf is also with a fixed angle relatively to that of the parent tiller.

A sample code of "geoAxe" function is:

```
geoAxe <- list(  
  azT = function(a) {  
    ifelse(a == 0, 0, 75 + (runif(1)-0.5)*5)  
  },  
  incT = function(a) {  
    ifelse(a == 0, runif(1) * 5, 82 + (runif(1) - .5) * 5)  
  },  
  dredT = function(a) {  
    ifelse(a == 0, 0, runif(1) * 7)  
  }  
)
```

The second list should provide two Rfunctions for drawing in the collections of leaf shape

Inputs have to be axis number, leaf position, leaf position counted from top, and leaf stage, defined as current length/final length. Returned values have to be :

- **azim** : the azimuth (deg) of the leaf compared to the previous one
- **Lindex** : the index of the collection to use for leaf curvature

These functions can be generated by the predefined *genGeoLeaf* node or be freely user-defined in a *freeGeoLeaf* node:

A sample code for a "geoLeaf" function is be :

```
geoLeaf <- list(  
  Azim = function(a,n,ntop) {0 * runif(1)},  
  Lindex = function(a,n,ntop,stage) {ntop + 1}
```

Inputs describing simulation

Time step is given as a list of values of thermal times for which a mock-up is to be produced. Positions of plants within the plot are given externally from adel to a planter.

Inner options of ADEL

Todo: add reference to C.Fournier's and B.Andrieu's publications which describe the working hypotheses, and remove the following subsections.

This section documents the inner options of ADEL.

Coordination in organ extension

The thermal time of leaf tip appearance and leaf collar appearance given in *phenT* are used to calculate a number of features; - the leaf extension (blade + sheath) is simulated as starting 0,4 phyllochron between tip appearance, and having a constant rate (cm.°C-1.J-1) for a duration of 2 phyllochrons - The model calculate the length of the hidden part of a leaf (whorl length) : at tip emergence, this hidden length is the blade length; at collar emergence this hidden length is taken as the length of sheath n-1; Between it is approximated by linear interpolation. This is used to calculate the length of the visible part of the leaf in the post processing treatments. Note that this calculation is not fully accurate because sheath n-1 stop growing before collar n emerges

The leaf extension is simulated as consisting sequentially of the blade extension, followed by the sheath extension.

The internode extension is simulated as following sequentially the sheath extension, and taking place at a constant rate, for a duration of 1/(stemleaf) phyllochron It is known that in grass, internode fast extension start at collar emergence. However there is no such calculation of collar emergence in the model: it expected that the synchronization with collar emergence will be reasonably well approximated by the synchronization implemented with the end of leaf extension.

The parameters for these coordinations are defined in AdelRunOption, which remained to be documented

Senescence of sheath and internodes

The senescence of sheath n is simulated as being synchronous with the senescence of blade n+2 The disappearance of sheath n is simulated as synchronous with disappearance of blade n+1

There is no senescence implemented for internodes : they stay green. For ear and peduncle : to be documented

On regressing tillers, individual leaf senescence is simulated from SSI with the same pattern as on non-regressing tillers.

Disappearance of dead tillers

A dead tiller can be programmed to disappear some time after it stops growing. Only the blades and sheaths, not the internodes, disappear. This will be changed in further version, so that internode also disappear When this happens, it has priority over the process of disappearance following leaf senescence.

Plantgen model: Construction of the input tables

ADEL requires inputs characterizing the development of plants as described in *Inputs describing development*.

The `plantgen` package allows the user who does not have a complete set of data to estimate the missing inputs. Inside this package, the module `plantgen_interface` is the front-end for the generation of the tables `axeT`, `dimT` and `phenT`. `plantgen_interface` also permits to generate some other tables for debugging purpose. To construct `axeT`, `dimT`, `phenT` and the debugging tables, the module `plantgen_interface` uses the modules `plantgen_core`, `tools` and module `params`. The diagram *static view* describes the dependencies between the different modules of the package `plantgen`.

Todo: add reference to M.Abichou's publication which describes the working hypotheses.

We have considered three possible levels of completeness of data, denoted as MIN, SHORT, and FULL. In the next subsections, we:

- describe the levels of completeness of the data and of the parameters set by the user,
- describe how to construct the inputs of ADEL from a Python interpreter, using the routine `gen_adel_input_data`. This routine can be used whatever the level of completeness of the raw inputs, adapting the processing automatically,
- describe how to construct the inputs of ADEL from the Visualea interface, using the node `plantgen`.

`gen_adel_input_data` belongs to module `plantgen_interface`. `gen_adel_input_data` produces the following tables:

- `axeT`
- `dimT`
- `phenT`
- `phenT_abs`: the equivalent of `phenT`, but with absolute thermal times and absolute positions.
- `dimT_abs`: the equivalent of `dimT`, but with absolute positions.
- `dynT`: the dynamic of the leaves for each type of axis.
- `phenT_first`: a subset of `phenT_abs`, containing only the lines of `phenT_abs` which correspond to the first phytomer of each axis.
- `HS_GL_SSI_T`: the dynamic of Haun stage, green leaves and senescent leaves when thermal time varies, for each cohort.
- `tilleringT`: the dynamic of tillering.
- `cardinalityT`: the theoretical and the simulated cardinalities of each cohort and each axis.

`gen_adel_input_data` also produces a dictionary which stores the values of the arguments of `gen_adel_input_data`. This dictionary is aimed to log the configuration used for the construction.

The diagram *dynamic view* describes the data flow when the user calls `gen_adel_input_data`.

in `plantgen`. To help the user understanding the dataflow in `plantgen`,

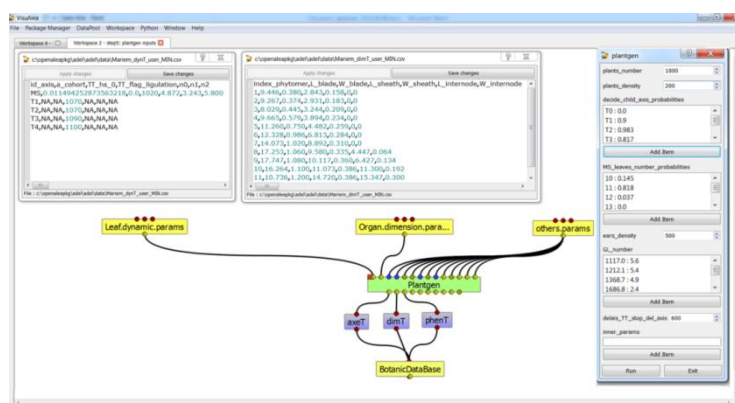
The levels of completeness

The information needed to generate Adel input must be provided in two tables: `dynT_user` and `dimT_user`. `dynT_user` and `dimT_user` can have different levels of completeness: `FULL`, `SHORT` and `MIN`. According to their level of completeness, `dynT_user` and `dimT_user` take different shapes and/or contents.

The table below list the specific designation in `plantgen` for `dynT_user` and `dimT_user` for each level of completeness:

Level of completeness	Description	<code>dynT_user</code>	<code>dimT_user</code>
FULL	the table contains data for <i>at least</i> each most frequent non-regressive axis.	<code>dynT_user_FULL</code>	<code>dimT_user_FULL</code>
SHORT	the table contains data for <i>exactly</i> each most frequent non-regressive axis.	<code>dynT_user_SHORT</code>	<code>dimT_user_SHORT</code>
MIN	the table contains data for the most frequent main stem only.	<code>dynT_user_MIN</code>	<code>dimT_user_MIN</code>

See also: the documentation of `DataCompleteness` in the *Reference guide*.



Construction of Adel input tables using the Python interpreter

`gen_adel_input_data` can be used from Python interpreter.

First we explain the arguments of `gen_adel_input_data` that the user has to define. Second we present a complete code example to use `gen_adel_input_data` from a Python interpreter.

The arguments to define by the user

The arguments to define are:

- *dynT_user*: the leaf dynamic parameters set by the user,
- *dimT_user*: the dimensions of the axes set by the user,
- *plants_number*: the number of plants to be generated,
- *plants_density*: the number of plants that are present after loss due to bad emergence, early death..., per square meter,
- *decide_child_axis_probabilities*: the probability of emergence of an axis when the parent axis is present. *decide_child_axis_probabilities* are set only for axes belonging to primaries tillers.
- *MS_leaves_number_probabilities*: the probability distribution of the final number of main stem leaves,
- *ears_density*: the number of ears per square meter,
- *GL_number*: the thermal times of GL measurements and corresponding values of green leaves number,
- *delais_TT_stop_del_axis*: the thermal time between an axis stop growing and its disappearance,
- *TT_col_break*: the thermal time when the rate of progress Haun Stage vs thermal time is changing. If phyllochron is constant, then *TT_col_break* is 0.0.
- *inner_params*: the values to overwrite the inner parameters with. See *Inner parameters for Plantgen model* for more details.

Important:

- `gen_adel_input_data` checks automatically the validity of these arguments, EXCEPT for *inner_params*. Thus, the user should be sure of what he is doing when setting the *inner_params*.
- only *dynT_user* and *dimT_user* are mandatory. For all other arguments, default value is used if no value is passed by the user.

Code example

Now let's see a complete code example to use `gen_adel_input_data` from a Python interpreter:

```
# import the pandas library. In this example, pandas is used to read and
# write the tables.
import pandas

# read the dynT_user_MIN table. "dynT_user_MIN.csv" must be in the working directory.
dynT_user = pandas.read_csv('dynT_user_MIN.csv')

# read the dimT_user_MIN table. "dimT_user_MIN.csv" must be in the working directory.
dimT_user = pandas.read_csv('dimT_user_MIN.csv')

# define the other arguments
plants_number = 100
plants_density = 250
decide_child_axis_probabilities = {'T0': 0.0, 'T1': 0.900,
                                   'T2': 0.983, 'T3': 0.817,
                                   'T4': 0.117}
MS_leaves_number_probabilities = {'10': 0.145,
                                   '11': 0.818,
                                   '12': 0.037,
                                   '13': 0.0,
                                   '14': 0.0}

ears_density = 500
GL_number = {1117.0: 5.6, 1212.1:5.4,
             1368.7:4.9, 1686.8:2.4,
             1880.0:0.0}
```

Code example

Now let's see a complete code example to use `gen_adel_input_data` from a Python interpreter:

```
# import the pandas library. In this example, pandas is used to read and
# write the tables.
import pandas

# read the dynT_user_MIN table. "dynT_user_MIN.csv" must be in the working directory.
dynT_user = pandas.read_csv('dynT_user_MIN.csv')

# read the dimT_user_MIN table. "dimT_user_MIN.csv" must be in the working directory.
dimT_user = pandas.read_csv('dimT_user_MIN.csv')

# define the other arguments
plants_number = 100
plants_density = 250
decide_child_axis_probabilities = {'T0': 0.0, 'T1': 0.900,
                                   'T2': 0.988, 'T3': 0.817,
                                   'T4': 0.117}
MS_leaves_number_probabilities = {'10': 0.148,
                                   '11': 0.818,
                                   '12': 0.037,
                                   '13': 0.0,
                                   '14': 0.0}

ears_density = 500
GL_number = {'1117.0: 5.6, 1212.1:5.4,
             1268.7:4.9, 1686.8:2.4,
             1880.0:0.0}
delais_TT_stop_del_axis = 600
TT_col_break = 0.0
inner_params = {'DELAIS_PHYLL_COL_TIP_1ST': 1.0,
                'DELAIS_PHYLL_COL_TIP_NTH': 1.6}

# launch the construction
from alinea.adel.plantgen.plantgen import gen_adel_input_data
(axeT,
 dimT,
 phenT,
 phenT_abs,
 dimT_abs,
 dynT,
 phenT_first,
 HS_GL_SSI_T,
 tilleringT,
 cardinalityT,
 config) = gen_adel_input_data(dynT_user,
                               dimT_user,
                               plants_number,
                               plants_density,
                               decide_child_axis_probabilities,
                               MS_leaves_number_probabilities,
                               ears_density,
                               GL_number,
                               delais_TT_stop_del_axis,
                               TT_col_break,
                               inner_params)

# write axeT, dimT and phenT to csv files in the working directory, replacing
# missing values by 'NA' and ignoring the indexes (the indexes are the labels of
# the lines).
axeT.to_csv('axeT.csv', na_rep='NA', index=False)
dimT.to_csv('dimT.csv', na_rep='NA', index=False)
phenT.to_csv('phenT.csv', na_rep='NA', index=False)

# "axeT.csv", "dimT.csv" and "phenT.csv" are now ready to be used by Adel.
```

Otherwise, the function `read_plantgen_inputs` permits to define the *arguments* by importing a Python module.

Using `read_plantgen_inputs` with the module `plantgen_inputs.py`, the preceding example becomes:

```
from alinea.adel.plantgen.plantgen import read_plantgen_inputs
# "plantgen_inputs_MIN.py" must be in the working directory
(dynT_user,
 dimT_user,
 plants_number,
 plants_density,
 decide_child_axis_probabilities,
 MS_leaves_number_probabilities,
 ears_density,
 GL_number,
 delais_TT_stop_del_axis,
 TT_col_break,
 inner_params) = read_plantgen_inputs('plantgen_inputs_MIN.py')

# launch the construction
from alinea.adel.plantgen.plantgen import gen_adel_input_data
(axeT,
 dimT,
 phenT,
 phenT_abs,
 dimT_abs,
 dynT,
 phenT_first,
 HS_GL_SSI_T,
 tilleringT,
 cardinalityT,
 config) = gen_adel_input_data(dynT_user,
                               dimT_user,
                               plants_number,
                               plants_density,
                               decide_child_axis_probabilities,
                               MS_leaves_number_probabilities,
                               ears_density,
                               GL_number,
                               delais_TT_stop_del_axis,
                               TT_col_break,
                               inner_params)

# write axeT, dimT and phenT to csv files in the working directory, replacing
# missing values by 'NA' and ignoring the indexes (the indexes are the labels of
# the lines).
axeT.to_csv('axeT.csv', na_rep='NA', index=False)
dimT.to_csv('dimT.csv', na_rep='NA', index=False)
phenT.to_csv('phenT.csv', na_rep='NA', index=False)

# "axeT.csv", "dimT.csv" and "phenT.csv" are now ready to be used by Adel.
```

`read_plantgen_inputs` permits the user to store the arguments, so he can reuse them later.

`plantgen` is located in `alinea.adel.plantgen`. You can access to `plantgen` through the package explorer of VisuAlea, or just typing "plantgen" in the Search tab of VisuAlea.

The associated widget, which appears when you open `plantgen`, permits to configure the construction.

Construction of Adel input tables using Visualea

The node `plantgen` allows to construct the inputs of ADEL.

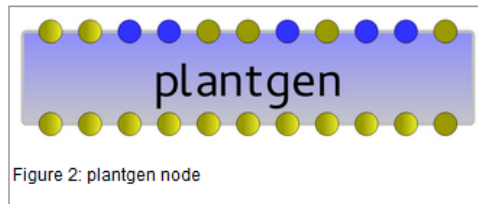
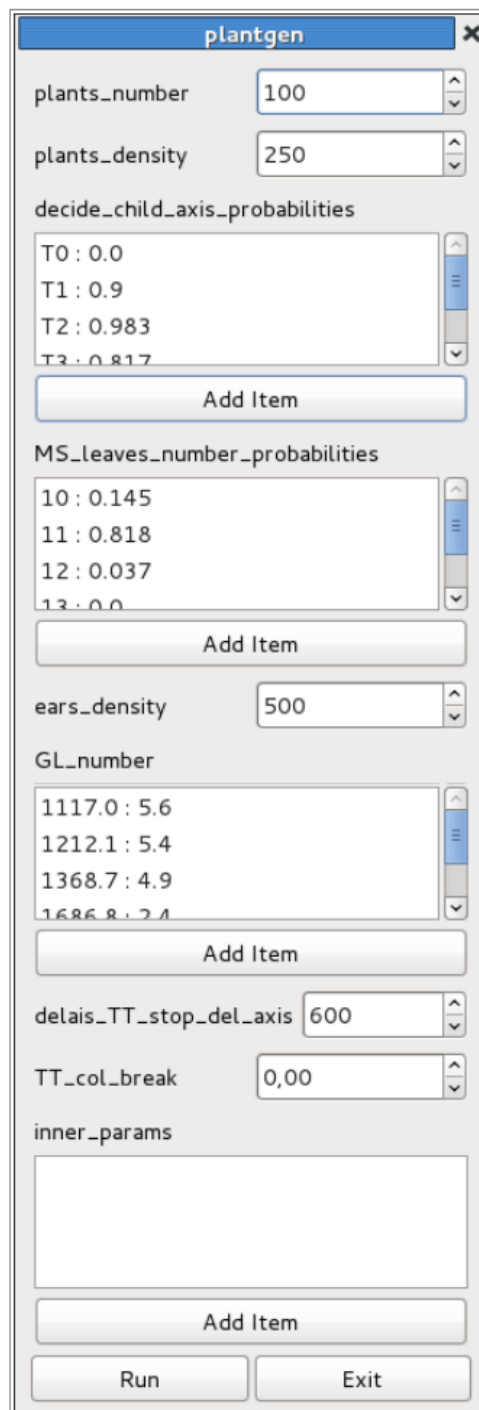


Figure 2: plantgen node

`plantgen` is located in `alinea.adel.plantgen`. You can access to `plantgen` through the package explorer of VisuAlea, or just typing "plantgen" in the Search tab of VisuAlea.

The associated widget, which appears when you open `plantgen`, permits to configure the construction.



plantgen

plants_number 100

plants_density 250

decide_child_axis_probabilities

T0 : 0.0
T1 : 0.9
T2 : 0.983
T3 : 0.817

Add Item

MS_leaves_number_probabilities

10 : 0.145
11 : 0.818
12 : 0.037
13 : 0.0

Add Item

ears_density 500

GL_number

1117.0 : 5.6
1212.1 : 5.4
1368.7 : 4.9
1686.8 : 2.1

Add Item

delais_TT_stop_del_axis 600

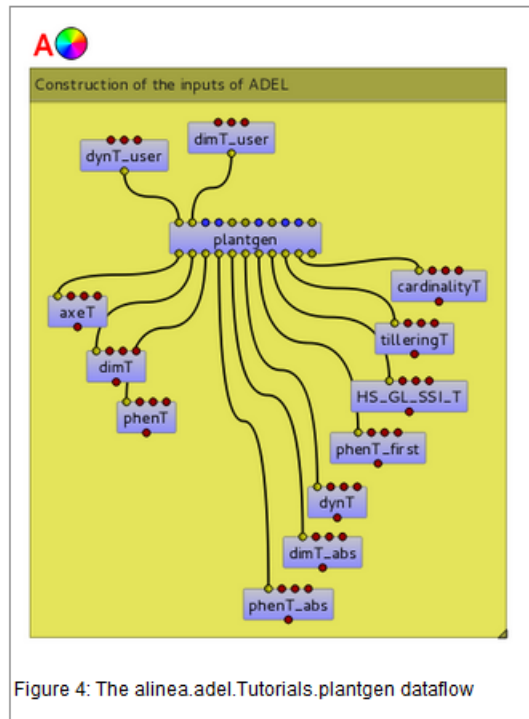
TT_col_break 0,00

inner_params

Add Item

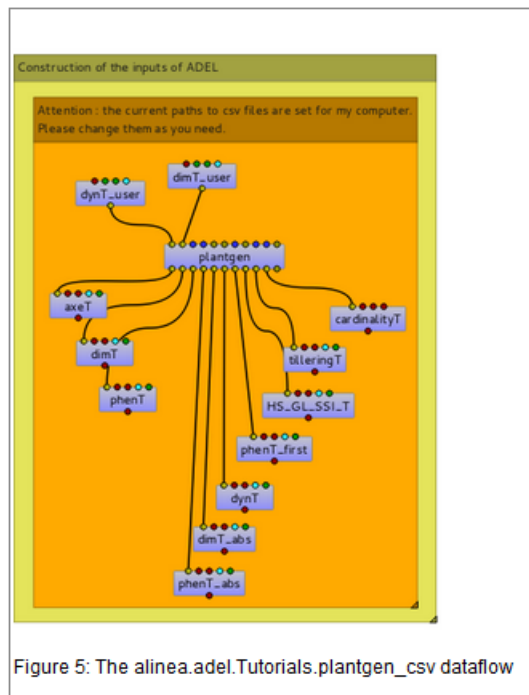
Run Exit

The following dataflow demonstrates how to use `plantgen` through Visualea:



The user must select existing data nodes to set the input and output tables.

The following data-flow demonstrates another way to use `plantgen` through Visualea:



In this case the user must give the paths of csv files for inputs and outputs.

Warning: the paths set in `alinea.adel.Tutorials.plantgen_csv` will not work on your computer. You have to adapt them to your needs.

Finally, the node `read_plantgen_inputs` permits to define the values of the input ports of `plantgen` by importing a Python module. `read_plantgen_inputs` is also located in `alinea.adel.plantgen`.

For example, using `read_plantgen_inputs` with the module `plantgen_inputs.py`, the dataflow becomes:

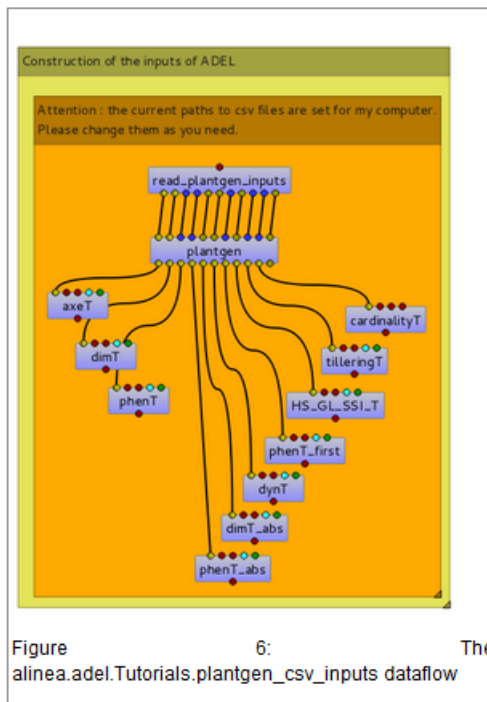


Figure 6: The `alinea.adel.Tutorials.plantgen_csv_inputs` dataflow

`read_plantgen_inputs` permits the user to store the values of the input ports, so he can reuse them later.

Inner parameters for Plantgen model

These parameters are:

- `SECONDARY_STEM_LEAVES_NUMBER_COEFFICIENTS`: the coefficients `a_1` and `a_2` to calculate the final number of leaves on tillers from the final number of leaves on main stem.
- `EMF_1_MS_STANDARD_DEVIATION`: the standard deviation in the thermal of emergence of plants in the plot.
- `LEAF_NUMBER_DELAY_MS_COHORT`: the delays between the emergence of the main stem and the emergence of each cohort.
- `N2_MS_DIV_N2_COHORT`: ratio between the maximum number of green leaves on the tillers and the maximum green leaves on the main stem
- `DELAIS_PHYLL_COL_TIP_1ST`: delay between tip appearance and collar appearance for the first leaf only.
- `DELAIS_PHYLL_COL_TIP_NTH`: delay between tip appearance and collar appearance for all leaves except the first one.
- `DELAIS_PHYLL_SEN_DISP`: the time during which a fully senesced leaf on a non-elongated internode remains on the plant.
- `DELAIS_REG_MONT`: the time between the start of the regression and the bolting.
- `TT_DEL_THAUT`: the thermal time at which leaves on elongated internode disappear.
- `FIRST_CHILD_DELAY`: the delay between a parent cohort and its first possible child cohort
- `REGRESSION_OF_DIMENSIONS`: the regression of the dimensions for the last 3 phytomers of each organ.

These parameters can be set by the user through the input argument *inner_parameters* of the function `gen_adel_input_data`, or set directly in the module `params`. They permit a finer parameterization of the construction.

See [documentation of params](#) for more information.

Description of Adel's outputs

The function `RunAdel` permits to simulate 3D architectural development of the shoots of wheat plants, according to a list of dates (thermal times) and Adel's inputs (see [Description of Adel's inputs](#)).

`RunAdel` returns a Python dictionary. Each key of the dictionary represents an output. The following table describes each of these outputs.

Output of RunAdel	Description
<code>refplant_id</code>	plant id
<code>axe_id</code>	axe id
<code>ms_insertion</code>	phytomer insertion position, starting from the base (not normalized)
<code>nff</code>	final number of leaves produced by the axe
<code>HS_final</code>	final haun stage reached by the axe (determine regression or not)
<code>numphy</code>	phytomer position (from bottom)
<code>ntop</code>	phytomer position (from top)
<code>L_shape</code>	lamina length (cm)
<code>Lw_shape</code>	lamina width (cm)
<code>LsenShrink</code>	shrink in lamina width due to senescence. Width is the remaining width proportional to the blade width before senecened
<code>LcType</code>	selector for first level in leaf database (ntop). First level is the leaf type indexed by the phytomer position (ntop).
<code>LcIndex</code>	index for selecting the leaf geometry from the replicates of the same phytomer (LcType)
<code>Linc</code>	inclination of the base of the lamina relatively to the sheath (deg)
<code>Laz</code>	azimuth relative to the previous leaf (<code>Laz[1] = azT</code> , <code>Laz[2:end] = azim</code>) (<code>azT</code> refers to the the azimuth(deg) of the first leaf of the axis with reference to the azimuth of the parent axe. <code>azim</code> refers to the azimuth (deg) of the leaf compared to the previous one. <code>azT</code> and <code>azim</code> are defined in the user-defined function, <code>geoAxe</code> and <code>geoLeaf</code> , respectively.)
<code>Lpo</code>	proportion of green tissue in the lamina (on a length basis)
<code>Lpos</code>	proportion of senescent tissue in the lamina (on a length basis)
<code>Gd</code>	apparent diameter of the sheath
<code>Ginc</code>	inclination relative to of the previous sheath
<code>Gpo</code>	proportion of green tissue in the sheath (on a length basis)
<code>Gpos</code>	proportion of senescent tissue in the sheath (on a length basis)
<code>Ed</code>	diameter of the internode in cm
<code>Einc</code>	inclination relative to of the previous internode
<code>Epo</code>	proportion of green tissue in the internode (on a length basis)
<code>Epos</code>	proportion of senescent tissue in the internode (on a length basis)
<code>rph</code>	normalized phytomer position (= <code>numphy/nff</code>) ?? to be confirmed
<code>rssi</code>	relative senescence index (<code>ssi - numphy</code>)
<code>rhs</code>	relative haun stage (<code>haun stage - numphy</code>)

Then, the function `mtg_factory` permits to construct a MTG from the output of `RunAdel`.

Finally, the function `mtg_interpreter` permits to add a geometry to the MTG computed by `mtg_factory`.

The resulting MTG has the following properties:

Scale	Label	Properties (up to date 26/09/2014; may change)	Comments
1	plant*	azimuth, edge_type, label, position, replant_id	*number of plants
2	MS/T*	HS_final, edge_type, label, nff, timetable	MS: main stem; * the order of tillers
3	metamer*	L_shape, edge_type, label	*the position of metamer (numphy)
4	internode	azimuth, diameter, edge_type, inclination, label, length, ntop, senesced_length, visible_length	
4	sheath	azimuth, diameter, edge_type, inclination, label, length, ntop, senesced_length, visible_length	
5	StemElement	area, azimuth, edge_type, geometry, green_area, green_length, inclination, is_green, label, length, offset, senesced_area, senesced_length	
5	blade	diameter, edge_type, inclination, label, length, n_sect, ntop, rolled_length, senesced_length, shape_mature_length, shape_max_width, shape_xysr, visible_length	
5	LeafElement1	area, edge_type, geometry, green_area, green_length, is_green, label, length, position_senescence, senesced_area, senesced_length, srb, srl	

Appendices

The appendices describe the data used by Adel for pre and post-processings. The appendices also contains static and dynamic view of the system, to help the user understanding hwo it works.

Plantgen model: construction of the input tables

In this section we first present internal views of the package `plantgen`:

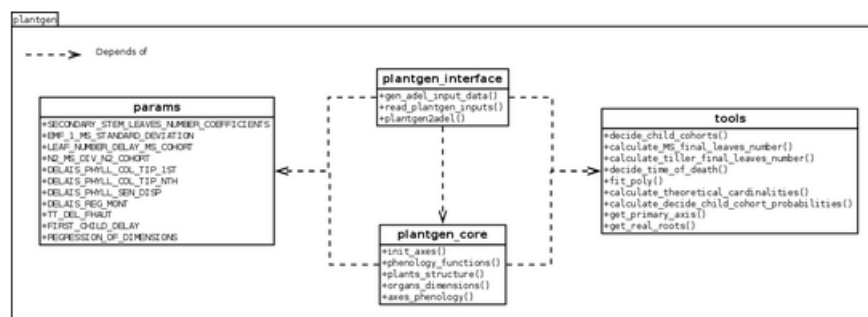
- a *static view* to describe the dependencies between the different modules of `plantgen`,
- a *dynamic view* to describe the data flow when the user calls `gen_adel_input_data`.

Then, we describe the data used in Plantgen for the construction of the input tables of Adel:

- *dynT_user_FULL*: the dynamic of the Haun stage of **at least** the most frequent non-regressive axes.
- *dynT_user_SHORT*: for each *id_axis*, the dynamic of the Haun stage of **exactly** the most frequent non-regressive axes.
- *dynT_user_MIN*: the dynamic of the Haun stage of the most frequent main stem, and, for each primary axis, the thermal time when Haun Stage is equal to the final number of phytomers.
- *dimT_user_FULL*: the dimensions of **at least** the most frequent non-regressive axes.
- *dimT_user_SHORT*: the dimensions of **exactly** the most frequent non-regressive axes.
- *dimT_user_MIN*: the dimensions of the most frequent main stem.
- *phenT_abs*: the equivalent of *phenT*, but with absolute thermal times and absolute phytomer ranks.
- *dimT_abs*: the equivalent of *dimT*, but with absolute phytomer ranks.
- *dynT*: the dynamic of the Haun stage for each axis.
- *phenT_first*: a subset of *phenT_abs*, containing only the lines of *phenT_abs* which correspond to the first phytomer of each cohort.
- *HS_GL_SSI_T*: the dynamic of Haun stage, green leaves and senescent leaves when thermal time varies, for each cohort.
- *tilleringT*: the dynamic of tillering.
- *cardinalityT*: the theoretical and the simulated cardinalities of each cohort and each axis.

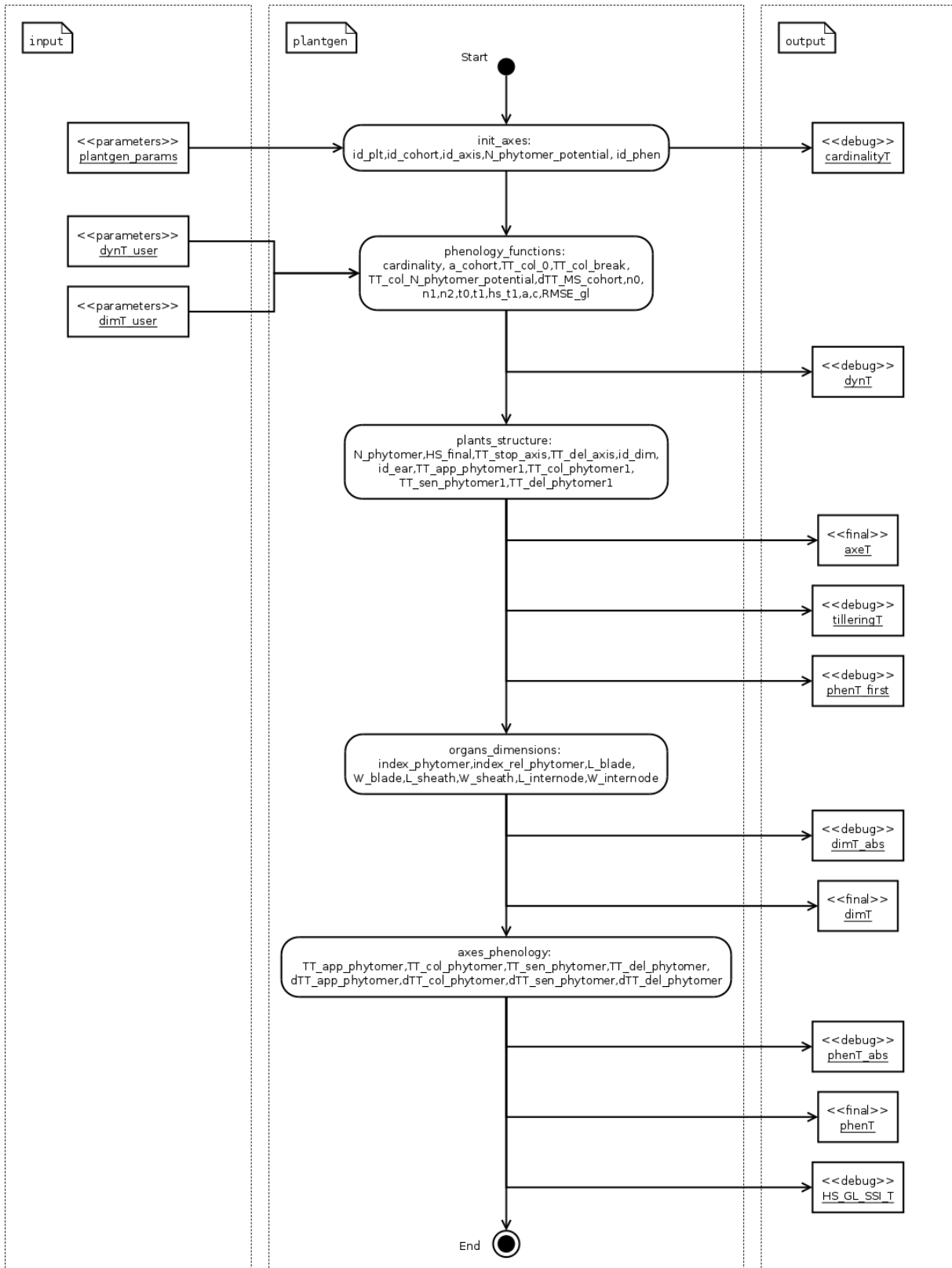
Static view of plantgen

This diagram describes the dependencies between the different modules of `plantgen`.



Dynamic view of plantgen

This diagram describes the data flow when the user calls `gen_ade1_input_data`.



`<<type of data>>`
`my_data`

Data involved in the data flow.
The type of data can be either:
- "parameters": input data,
- "debug": output data used for debugging,
- "final": output data used by Adel.

`my_routine:`
output 1, output 2, ...

A routine uses to compute variables
"output 1", "output 2", ...

→ A transition

dynT_user_FULL

dynT_user_FULL is a table which describes the dynamic of the Haun stage of **at least** the most frequent non-regressive axes. The most frequent axes are the axes which have the most frequent number of phytomers.

dynT_user_FULL contains a line of data for **at least** each couple (*id_axis*, most frequent *N_phytomer_potential*), where *id_axis* and *N_phytomer_potential* are defined in *axeT*.

Each line contains the following data: *id_axis*, *N_phytomer_potential*, *a_cohort*, *TT_col_0*, *TT_col_N_phytomer_potential*, *n0*, *n1* and *n2*. See *dynT* for the meaning of these parameters.

See an example of *dynT_user_FULL*.

dynT_user_SHORT

dynT_user_SHORT is a table which describes the dynamic of the Haun stage of **exactly** the most frequent non-regressive axes. The most frequent axes are the axes which have the most frequent number of phytomers.

dynT_user_SHORT contains a line of data for **exactly** each couple (*id_axis*, most frequent *N_phytomer_potential*), where *id_axis* and *N_phytomer_potential* are defined in *axeT*. The couples (*id_axis*, **NOT** most frequent *N_phytomer_potential*) are not documented in *dynT_user_SHORT*.

Each line contains the following data *id_axis*, *a_cohort*, *TT_col_0*, *TT_col_N_phytomer_potential*, *n0*, *n1* and *n2*. See *dynT* for a description of these parameters.

See an example of *dynT_user_SHORT*.

dynT_user_MIN

dynT_user_MIN is a table which describes the dynamic of the Haun stage of the most frequent main stem. The most frequent main stem is the main stem which has the most frequent number of phytomers. *dynT_user_MIN* also contains, for each primary axis, the thermal time when Haun Stage is equal to the final number of phytomers.

The first line contains the following data: *id_axis*, *a_cohort*, *TT_col_0*, *TT_col_N_phytomer_potential*, *n0*, *n1* and *n2*. In the other lines, only *id_axis* and *TT_col_N_phytomer_potential* are documented: *a_cohort*, *TT_col_0*, *n0*, *n1* and *n2* are NA (i.e. Not Available).

See *dynT* for a description of these parameters.

See an example of *dynT_user_MIN*.

dimT_user_FULL

dimT_user_FULL is a table which documents the dimensions of **at least** the most frequent non-regressive axes. The most frequent axes are the axes which have the most frequent number of phytomers.

dimT_user_FULL contains a line of data for **at least** each couple (*id_axis*, most frequent *N_phytomer_potential*), where *id_axis* and *N_phytomer_potential* are defined in *axeT*.

Each line contains the following data: *id_axis*, *N_phytomer_potential*, *index_phytomer*, *L_blade*, *W_blade*, *L_sheath*, *W_sheath*, *L_internode* and *W_internode*. *id_axis* are the botanical positions (see *Botanical position of the axis on the plant*). *N_phytomer_potential* are the final number of phytomers. The other data are the same as the ones in *dimT_abs*.

See an example of *dimT_user_FULL*.

dimT_user_SHORT

dimT_user_SHORT is a table which documents the dimensions of **exactly** the most frequent non-regressive axes. The most frequent axes are the axes which have the most frequent number of phytomers.

dimT_user_SHORT contains a line of data for **exactly** each couple (*id_axis*, most frequent *N_phytomer_potential*), where *id_axis* and *N_phytomer_potential* are defined in *axeT*. The couples (*id_axis*, **NOT** most frequent *N_phytomer_potential*) are not documented in *dimT_user_SHORT*.

Each line contains the following data: *id_axis*, *index_phytomer*, *L_blade*, *W_blade*, *L_sheath*, *W_sheath*, *L_internode* and *W_internode*. *id_axis* are the botanical positions (see *Botanical position of the axis on the plant*). *N_phytomer_potential* are the final number of phytomers. The other data are the same as the ones in *dimT_abs*.

dimT_user_MIN

dimT_user_MIN is a table which documents the dimensions of each phytomer of the most frequent main stem. The most frequent main stem is the main stem which has the most frequent number of phytomers. Each line contains the following data: *index_phytomer*, *L_blade*, *W_blade*, *L_sheath*, *W_sheath*, *L_internode* and *W_internode*. See *dimT_abs* for a description of these data.

See an example of *dimT_user_MIN*.

phenT_abs

phenT_abs is an intermediate table used to construct *phenT*. This table is not an input of Adel. Thus the user normally needn't it. This table can be useful for debugging.

phenT_abs is the same as *phenT*, except that

- the positions of the phytomers are not normalized,
- the thermal times of developmental events are absolute.

See an example of *phenT_abs*.

dimT_abs

dimT_abs is an intermediate table used to construct *dimT*. This table is not an input of Adel. Thus the user normally needn't it. This table can be useful for debugging.

dimT_abs is the same as *dimT*, except that the positions of the phytomers are not normalized.

See an example of *dimT_abs*.

dynT

dynT is an intermediate table used to construct the input of Adel. This table is not an input of Adel. Thus the user normally needn't it. This table can be useful for debugging.

dynT is a table which describes the dynamic of the Haun stage of all non-regressive axes. For each couple (*id_axis*, *N_phytomer_potential*) in *axeT*, *dynT* contains a line with the following data:

Column	Description
id_axis	the botanical position (see <i>Botanical position of the axis on the plant.</i>) of the axis
id_cohort	the cohort to which belongs the axis
cardinality	the cardinality of the couple (<i>id_axis</i> , <i>N_phytomer_potential</i>) in <i>axeT</i>
N_phytomer_potential	the final number of phytomers of the axis
a_cohort	the rate of Haun Stage vs Thermal time. This is the rate of the first phase in case of bilinear behavior.
TT_col_0	the thermal time for Haun Stage equal to 0
TT_col_break	the thermal time when the rate of phytomers emergence is changing
TT_col_N_phytomer_potential	the thermal time when Haun Stage is equal to <i>N_phytomer_potential</i>
n0	number of green leaves at <i>t0</i>
n1	number of green leaves at <i>t1</i>
n2	number of green leaves at <i>TT_col_N_phytomer_potential</i>
t0	the thermal time at the start of leaf senescence
t1	the thermal time at which the senescence starts
hs_t1	the Haun Stage at <i>t1</i>
a	the coefficient of the 3rd order term of the polynomial describing the dynamics of the number of green leaves after flowering
c	the coefficient of the 1st order term of the polynomial describing the dynamics of the number of green leaves after flowering
RMSE_gl	the RMSE for the dynamic of the number of green leaves after estimation of parameter <i>a</i> .

The lines are ordered first by **id_axis** in ascending order, then by **cardinality** in descending order.

See an example of *dynT*.

phenT_first

phenT_first is an intermediate table used to construct *phenT* and *axeT*. This table is not an input of Adel. Thus the user normally needn't it. This table can be useful for debugging.

phenT_first is a subset of *phenT_abs*, and contains only the lines of *phenT_abs* which correspond to the first phytomer of each non-regressive axis, i.e. *index_phytomer* equal to 1.

See an example of *phenT_first*.

HS_GL_SSI_T

HS_GL_SSI_T is constructed for debugging purpose.

HS_GL_SSI_T describes, for each cohort, the dynamic of Haun stage, Green leaves and leaf senescence index when *TT* varies.

For each couple (*id_cohort*, *N_phytomer_potential*) in *axeT* and for each *TT*, *dynT* contains a line with the following data:

Column	Description
id_phen	the concatenation of <i>id_cohort</i> and <i>N_phytomer_potential</i> . For example, if <i>*id_cohort*==4</i> and <i>*N_phytomer_potential*==8</i> , then <i>*id_phen*==408</i> .
TT	the thermal time.
HS	the Haun Stage.
GL	the number of green leaves.
SSI	the number of senescent leaves.

Note: For each axis, *TT* varies from 0 to `alinea.edel.plantgen.params.TT_DEL_FRAUT`.

See an example of *HS_GL_SSI_T*.

tilleringT

tilleringT is constructed for debugging purpose.

tilleringT describes the dynamic of tillering. It stores the number of axes per square meter at important thermal times: the start of growth, the thermal time of the bolting, and the thermal time of the flowering.

Column	Description
TT	the thermal time.
axes_density	the number of axes per square meter.

See an example of *tilleringT*.

cardinalityT

cardinalityT is constructed for debugging purpose.

cardinalityT describes the theoretical and the simulated cardinalities of each cohort and each axis. It permits the user to validate the simulated cardinalities against the theoretical ones. Both cardinalities are calculated from the probabilities of emergence of an axis when the parent axis is present. These probabilities are given by the user. Theoretical cardinalities are calculated globally without randomness.

Column	Description
id_cohort	the index of the cohort
id_axis	the index of the axis
theoretical_cohort_cardinality	the theoretical cardinality of the cohort
simulated_cohort_cardinality	the simulated cardinality of the cohort
theoretical_axis_cardinality	the theoretical cardinality of the axis
simulated_axis_cardinality	the simulated cardinality of the axis

See an example of *cardinalityT*.

Titre : Modélisation de l'architecture 4D du blé : Identification des patterns dans la morphologie, la senescence et le positionnement spatial des organes pour une large gamme de situations de croissance.

Mots clés : blé virtuel, modélisation, architecture, morphologie, géométrie, développement.

Résumé: La simulation de l'architecture des plantes est devenue un front de recherche très actif, en raison de son importance pour la compréhension du fonctionnement des plantes et de leurs interactions avec l'environnement. Pouvoir simuler l'architecture d'un peuplement avec une fidélité suffisante pour représenter les traits spécifiques issus d'une expérimentation présente un grand intérêt dans l'analyse de cette expérimentation.

Dans ce contexte, l'objectif de mon projet de thèse a été de développer un modèle opérationnel permettant de reproduire par simulation l'architecture 4D d'un peuplement pour tout le cycle de culture et de façon fidèle aux observations. Notre démarche s'appuie sur la caractérisation expérimentale d'une gamme de cultivars commerciaux cultivés dans la région parisienne. Ces données représentent une gamme large de séquences climatiques, dates et densités de semis et de fertilisation azotée.

L'analyse de ces données a permis d'identifier des fonctions stables et robustes décrivant les dynamiques d'apparition et de mortalité, ainsi que

les patterns de dimensions des différentes composantes de la plante. Nous apportons aussi des informations originales sur leur géométrie et leur positionnement spatial au cours du temps. Ces fonctions ont été regroupées dans une routine permettant de décrire la dynamique complète de l'architecture d'une collection de plantes de l'émergence jusqu'à la maturité.

Notre méthode de reconstruction a permis de générer les reconstructions 4D d'une part importante de nos traitements expérimentaux; elle a également été mise en œuvre dans plusieurs projets menés parallèlement à mon travail.

Notre modèle peut être aussi utilisé pour explorer des architectures potentielles en vue de proposer des nouveaux ideotypes.

Finalement, notre démarche de modélisation est transposable à d'autres céréales : elle fournit un cadre pour comparer les patterns de morphologie et de développement entre espèces et un outil pour étudier par simulation l'impact des traits architecturaux caractéristiques de chaque espèce.

Title: Modelling of the 4D architecture of wheat: identifying patterns describing the morphology, the senescence and the spatial orientation of organs under a high range of growth conditions.

Keywords: virtual wheat, modelling, architecture, morphology, geometry, development.

Abstract: The simulation of plant architecture has become a very active front of research because of its importance for understanding the functioning of plants and their interactions with the environment.

When analysing observations of experimental treatments, it is of a great interest to be able to simulate the architecture of the crop with sufficient fidelity to represent the specific traits resulting from the experiment.

In this context, the objective of the thesis project was to develop an operational model allowing to simulate the 4D architecture of a collection of individual plants for the whole crop cycle and in a way faithful to the observations. Our approach builds on the experimental characterization of a range of commercial cultivars cultivated in the Paris region. These data represent a wide range of climatic sequences, sowing dates, densities of seedlings and nitrogen fertilization.

The data analysis allowed us to identify stable and robust functions that describe the dynamics of appearance and mortality and the final dimensions

of the different components of the plant. Our work brings also novel information on the evolution of their geometry and spatial organisation over time. These functions were coded into a model that describes the dynamics of the architecture of a collection of plants from their emergence to their full maturity.

Our reconstruction method allowed us to generate 4D reconstructions for a large part of our experimental treatments; it has also been used in several projects carried out in parallel with this work.

Our model can also be used to explore potential architectures traits in order to propose new ideotypes.

Finally, our modelling approach can be applied to other cereals: it provides a framework for comparing patterns of morphology and development between species and provides a tool to study, by simulation, the impact of the architectural traits of each species.

